ISTANBUL TECHNICAL UNIVERSITY ★ GRADUATE SCHOOL OF SCIENCE ENGINEERING AND TECHNOLOGY

PRODUCTION AND CHARACTERIZATION OF WHITE LIGHT BASED ON ENERGY UP CONVERSION MECHANISMS IN Yb^{3+}, Nd^{3+},Tm^{3+} RARE EARTH IONS DOPED Y_2O_3-SiO_2 NANO-PHOSPHOR MATERIALS

Ph.D. THESIS

Hatun ÇINKAYA YILMAZ

Department of Physics Engineering

Physics Engineering Programme

NOVEMBER 2019

ISTANBUL TECHNICAL UNIVERSITY ★ GRADUATE SCHOOL OF SCIENCE ENGINEERING AND TECHNOLOGY

PRODUCTION AND CHARACTERIZATION OF WHITE LIGHT BASED ON ENERGY UP CONVERSION MECHANISMS IN Yb^{3+}, Nd^{3+}, Tm^{3+} RARE EARTH IONS DOPED Y_2O_3-SiO_2 NANO-PHOSPHOR MATERIALS

Ph.D. THESIS

Hatun ÇINKAYA YILMAZ
(509112110)

Department of Physics Engineering

Physics Engineering Programme

Thesis Advisor: Prof. Dr. Gönül ERYÜREK

NOVEMBER 2019

İSTANBUL TEKNİK ÜNİVERSİTESİ ★ FEN BİLİMLERİ ENSTİTÜSÜ

Yb^{+3}, Nd^{+3}, Tm^{+3} NADİR TOPRAK İYON KATKILI Y_2O_3-SiO_2 NANOFOSFOR MALZEMELERDE ÜST ENERJİ DÖNÜŞÜM MEKANİZMASINA DAYALI BEYAZ IŞIK ÜRETİMİ VE KARAKTERİZASYONU

DOKTORA TEZİ

Hatun ÇINKAYA YILMAZ
(509112110)

Fizik Mühendisliği Anabilim Dalı

Fizik Mühendisliği Programı

Tez Danışmanı: Prof. Dr. Gönül ERYÜREK

KASIM 2019

Hatun ÇINKAYA YILMAZ, a Ph.D. student of ITU Graduate School of Science Engineering and Technology student ID 509112110, successfully defended the thesis/dissertation entitled "PRODUCTION AND CHARACTERIZATION OF WHITE LIGHT BASED ON ENERGY UP CONVERSION MECHANISMS IN Yb^{3+}, Nd^{3+}, Tm^{3+} RARE EARTH IONS DOPED Y_2O_3-SiO_2 NANO-PHOSPHOR MATERIALS", which she prepared after fulfilling the requirements specified in the associated legislations, before the jury whose signatures are below.

Thesis Advisor : **Prof. Dr. Gönül ERYÜREK** .....
İstanbul Technical University

Jury Members : **Prof. Dr. Uğur YAHŞİ** .....
Marmara University

Prof. Dr. Gönül BAŞAR .....
Istanbul University

Assoc. Prof. Dr. Şaziye UĞUR .....
Istanbul Technical University

Assoc. Prof. Dr. Sevim İŞÇİ TURUTOĞLU .....
Istanbul Technical University

Date of Submission : 26 July 2019
Date of Defense : 1 November 2019

In memory of my mother Arife ÇINKAYA and my father Ahmet ÇINKAYA,

FOREWORD

I would like to express my gratitude and respect to my supervisor, Prof. Dr. Gönül ERYÜREK. I am thankful to her since she provided me a free working atmosphere with her guidance during my thesis work.

I am also grateful to Prof. Dr. Baldassare Di BARTOLO who gave me an opportunity to work with him in the Spectroscopy Laboratory of Boston College. During one year, I spent in the U.S.A; he guided me with his knowledge and experiences to complete my works. I would like to thank Prof. Dr. John COLLINS for his help with using the experimental set up of Spectroscopy Laboratory of Boston College and his friendship. I am also thankful to Boston College Physics Department for making all department facilities available to me.

I would express my thanks to members of our laboratory group at Istanbul Technical University; Assoc. Prof. Dr. Gökhan BİLİR and Assoc. Prof. Dr. Murat ERDEM. I thank Dr. Sevcan TABANLI for her valuable discussions with me about our studies and her friendship. I want also thank the members of the Physics Engineering Department of Istanbul Technical University and my all friends. I wish to express my sincere gratitude to my thesis committee members, Prof. Dr. Uğur YAHŞİ and Assoc. Prof. Dr. Şaziye UĞUR for their valuable time for me. I respectfully remember my jury member Prof. Dr. Ayhan MERGEN who died during my doctorate study.

I would like to thank the Scientific and Technological Research Council of Turkey (TUBITAK) for funding this thesis with the 1002-Short Term R&D Funding Program (with the project number 114F491) and 2214-International Research Fellowship Programme (for Ph.D. Students). I am also thankful to Istanbul Technical University Scientific Research Projects Department (ITU BAP-Project# 38542) for funding this work. Let me further thank all persons and organizations, which I may have forgotten to mention here, for their contributions.

I would like to express my sincere gratitude to my dear family; Filiz ÇINKAYA CİVELEK, Fatma ÇINKAYA GİDİK, Engin CİVELEK, Ada CİVELEK, Duru GİDİK and Kemal GİDİK who always supported me even though I neglected them most of the time. I would also like to thank Havva YILMAZ and Mümin YILMAZ for their supporting me to complete the writing the thesis in the last one year.

My most special thanks to Recep YILMAZ who is my dearest for his giving more value to my career than his own. I am especially thankful to him with his support and patience during the time we spent in the USA. And, I would like to thank my little sunshine Deniz YILMAZ who is my source of motivation this year.

Last but not least, I would like to express my deepest gratitude to my deceased mother and father, who are great heroes, for their efforts in our education despite their all impossibilities. I dedicate this thesis to their memories.

July 2019 Hatun ÇINKAYA YILMAZ
(Physicist)

TABLE OF CONTENTS

Page

ABBREVIATIONS

RE : Rare Earth
UC : Upconversion
Nd^{3+} : Neodymium (III)
Yb^{3+} : Ytterbium (III)
Tm^{3+} : Thulium (III)
OH : Hydrate
Y_2O_3: SiO_2 : Yttrium oxide and Silicon dioxide
Eu^{3+} : Europium (III)
Dy^{3+} : Dysprosium (III)
Er^{3+} : Erbium (III)
$Y_2Si_2O_7$: yttrium disilicate
Y_2SiO_5 : yttrium orthosilicate
UV : ultraviolet
NIR : Near Infrared region
VIS : visible
CT : Charge Transfer
L : ligand
RGB : Red-Green-Blue
CIE : the Commission Internationale de l'Éclairage
HSB : Hue, Saturation, Brightness
LED : Light Emitting Diode
HCI : Hydrochloric acid
XRD : X-ray Diffraction
SEM : Scanning Electron Microscopy
TEM : Transmission Electron Microscopy
EDS : Energy Dispersive X-ray spectroscopy
FTIR : Fourier Transform Infra-Red Spectroscopy
FWHM : Full Width Half Maximum
kV : kilo Volt
mA : milli Ampere
JCPDS : Joint Committee for Powder Diffraction Data
CCT : Correlated Colour Temperature
CRI : Color Rendering Index
WL : White Light
PA : Photon Avalanche
ESA : Energy State Absorption
ET : Energy Transfer
CR : Cross Relaxation
CUC : Cooperative Upconversion
EMU : Energy Migration-mediated Upconversion

SYMBOLS

D : grain size
δ2θ : width at half maximum of the XRD peak
O : oxygen
Si : silicon
HT1 : 0.5% Tm^{3+} doped yttrium silicate
HT2 : 1% Tm^{3+} doped yttrium silicate
HT3 : 0.25% Tm^{3+} doped yttrium silicate
HY : bulk form of 10% doped Yb^{3+} sample
HY1250 : powder form of 10% doped Yb^{3+} sample
SY1250 : undoped yttrium silicate
HTY1_1250 : 0.5% Tm^{3+}/ 10%Yb^{3+}codoped yttrium silicate
HTY2_1250 : %0.25 Tm^{3+}/10% Yb^{3+} codoped yttrium silicate
HTY3_1250 : %1.0 Tm^{3+}/10% Yb^{3+}codoped yttrium silicate
HNTY1_1250 : %10 Yb^{3+} , %1 Nd^{3+}, %0.5 Tm^{3+} triply doped yttrium silicate
HNTY2_1250 : %10 Yb^{3+}, %0.5 Nd^{3+}, %0.25 Tm^{3+} triply doped yttrium silicate
HNTY3_1250 : %2 Yb^{3+}, %0.25 Nd^{3+}, %0.5 Tm^{3+} triply doped yttrium silicate
HNTY4_1250 : %2 Yb^{3+}, %0.5 Nd^{3+}, %0.25 Tm^{3+} triply doped yttrium silicate
HNTY5_1250 : %10 Yb^{3+}, %0.25 Nd^{3+}, %0.5 Tm^{3+} triply doped yttrium silicate
TEOS : tetraethyl orthosilicate
$Y(NO_3)_3.6H_2O$: Yttrium Nitrate Hexahydrate
$Yb(NO_3)_3.5H_2O$: Ytterbium Nitrate Pentahydrate
$Nd(NO3)_3.6H_2O$: Neodymium Nitrate Hexahydrate
HNO_3 : Nitric acid
Ψ : wavefunction
I_{em} : emitted intensity
I_0 : incident intensity
I : final intensity
η : luminescence efficiency (quantum efficiency)
n : number of the photons
P : pumping power

LIST OF TABLES

Page

LIST OF FIGURES

Page

PRODUCTION AND CHARACTERIZATION OF WHITE LIGHT BASED ON ENERGY UP CONVERSION MECHANISMS IN Yb^{3+}, Nd^{3+}, Tm^{3+} RARE EARTH IONS DOPED Y_2O_3-SiO_2 NANO-PHOSPHOR MATERIALS

SUMMARY

Rare earth (RE) doped nanophosphors are used in a wide range application from scientific areas to photonic applications due to their unique and diverse luminescence characteristics. Most of these applications depend strongly on the size and structure of the material. The principle strategies for obtaining new luminescent materials involve the variation of host lattice and luminescent ions. The rare earth ions have unique electronic configurations and this structure distinguishes them from other optically active ions such as transition metals. The optically active electrons in rare earth are shielded from the local Coulombic environment, and the energy levels remain quite constant. Since the 4f electrons are shielded from the environment by the outer-filled shells of 5s and 5p electrons, the 4f electrons do not participate in the chemical bonding. This non-bonding property is responsible for the chemical similarity of different rare earth ions. The shielded character of 4f electrons affects the spectroscopic properties of the rare earth ions. Since the rare earth ions have sharp emission lines, strong absorption band, and less sensibility, they are the most desirable candidates as laser materials.

The overall objective of this thesis is to synthesize yttrium silicate (Y_2O_3-SiO_2) host doped with Yb^{3+}, Nd^{3+} and Tm^{3+} rare earth ions that called as the nanophosphors materials and to obtain white emission based on upconversion mechanisms from the triply doped samples. For this purpose, the structural and optical properties of Tm^{3+}, Nd^{3+} or Yb^{3+} single doped, Tm^{3+}/ Nd^{3+}, Yb^{3+}/ Tm^{3+} or Nd^{3+}/Yb^{3+} codoped and Yb^{3+}/ Nd^{3+} /Tm^{3+} triply doped yttrium silicate samples were systematically investigated by various experimental methods. The most important aspects of the study are the generation of white light, investigating the effects of upconversion (UC) energy mechanisms, the influence of the various synthesis techniques on the luminescence properties, and examining the mechanisms responsible for the generation of white light. Many physical parameters such as pumping powers, ambient pressure, temperature, excitation wavelength, and annealing temperature of the sample affect the optical properties of materials. For these reasons, investigating the luminescence characteristics of the RE doped nanomaterials depending on various physical parameters is very important to improve the quality and application area of the luminescent materials.

Nanostructured materials are typically defined with the particle diameters or grain sizes of 100 nm or less. The nanosize enhances structural, electronic, thermal and optical properties when compared with their single-crystal form. Therefore, the reduction to the nano size of such materials aims to investigate the issue of how the optical properties affected, and thus to further extend the use of these materials in optics. Up to now, these mechanisms are not completely understood and one aim of this thesis is to bring new improvements to literature with experimental results.

Light in different colors for various laser applications has been obtained using the rare earth ion doped nanophosphors until now. The white light produced by a broadband emission or multiphoton excitation processes from different materials doped with RE's were studied, however, it is still not clear that white light appears only depends on certain physical conditions, or it is only revealed due to type of material being used. Therefore, even if the physical mechanism of white light generation cannot be explained completely, investigating the emission characteristics of new types of materials at different physical conditions is very important to understand the mechanism of white light generation. The results of the thesis obtained from different kinds and portions of rare earth ions, various pumping power, and pressure, in different temperatures range and different excitation wavelengths of laser diode will contribute to design new kinds of materials to generate white light for photonic and industrial applications. The results of the thesis can contribute certainly to research and development activities about white light.

Yb^{+3}, Nd^{+3}, Tm^{+3} NADİR TOPRAK İYON KATKILI Y_2O_3-SiO_2 NANOFOSFOR MALZEMELERDE ÜST ENERJİ DÖNÜŞÜM MEKANİZMASINA DAYALI BEYAZ IŞIK ÜRETİMİ VE KARAKTERİZASYONU

ÖZET

Nadir toprak (RE) iyon katkılı nanofosforlar kendilerine has ve çeşitli lüminesans özelliklerinden dolayı bilimsel alandan fotonik uygulamalara kadar geniş bir alanda kullanılmaktadırlar. Bu uygulamaların çoğu malzemenin boyutuna ve yapısına bağlıdır. Yeni tür lüminesans malzemeleri elde etmek için ana strateji çeşitli host latisler ve lüminesans iyonlar kullanmaktır. Nadir toprak iyonları kendilerine has özel elektronik biçimlere sahiptir ve bu yapıları onları geçiş metalleri gibi diğer optik olarak aktif iyonlardan ayırmaktadır. Nadir topraklardaki optik olarak aktif elektronlar yerel Coulomb çevresi tarafından perdelenmekte ve enerji seviyeleri neredeyse sabit şekilde kalmaktadır. 4f elektronları çevreden dış yörüngeleri dolu 5s ve 5p elektronları ile perdelenmektedirler ve sonuç olarak, 4f elektronları kimyasal bağa katılmamaktadır. Farklı nadir toprak iyonlarının kimyasal yapılarının benzer olma sebebi budur.

4f elektronlarının perdelenme karakteri nadir toprak iyonlarının spektroskopi özelliklerini etkilemektedir. Bu iyonlar keskin lüminesans çizgilere, güçlü soğurma bandlarına sahip olduklarından lazer malzemeleri olarak en çok istenen adaylardır. Fosfor olarak adlandırdığımız malzemeler ise kristal formda, inorganik ve yalıtkandırlar. Nadir toprak iyonları katkılandırıldığında bu malzemelerin ışık yayınlama özellikleri etkilenmektedir ve katkılı nanoparçacıklar düşük enerjili olan kızılötesi fotonları soğurarak daha yüksek enerjili foton yayılımını sağlayabilirler. Bu özellikleri onları optik ve fotonik alanlarında çok kullanışlı malzemeler haline getirmekte ve uygulama alanları görüntüleme teknolojilerinden biyolojik uygulamalara kadar çok geniş bir yelpazeyi kapsamaktadır.

Nadir toprak (RE) iyonları katkılı nanofosforlarda, düşük frekanslı fononlar luminesansın fonon destekli durulmasına güçlü bir şekilde katkı verirler ve bu modların konumsal olarak sınırlanmasından dolayı nanofosforların optik özellikleri bulk haldeki fosforlardan farklıdır. RE katkılanmış nanofosforların optik özellikleriyle ilgili diğer bazı etkili faktörler; kristal alan etkileri, 4f elektronlarının spin-orbit çiftlenimi ve nanoyapılı malzemelerin birim hacim başına yüzey oranlarının geniş olmasıdır. Nadir toprak iyon katkılı fosfor malzemeler ince film veya toz formda çeşitli yöntemlerle üretilebilir. Fakat görüntü keskinliğin azalması ve ışık yayma etkisinin kısıtlanması sebebiyle bu tür malzemelerin ince film olarak kullanılması tercih edilir değildir. Bu sebeple toz formda üretmek ve boyutu nano mertebesinde tutmak kullanımını daha verimli hale getirmektedir. Nanofosforların luminesans özellikleri üzerine yapılan çalışmalar, nanofosforlarda nadir toprak iyon konsantrasyonu arttığında bulk hale göre lüminesans şiddetinin arttığını ve daha yüksek ışık elde edildiğini göstermiştir. Bunun yanısıra nano boyutta fosforların, ekran çözünürlüğünü arttırdığı, ışığın kararlı bir şekilde bozulmadan yayılmasını sağladığı ve biyo-uygunluk

özelliklerine sahip olduğu görülmüştür. Öte yandan nadir toprak iyon katkılı inorganik katı fosfor malzemeler termal radyasyonu elektrik enerjisine çevirebilmeleri özelliklerinden dolayı beyaz ışık yayan diyot yapımında da kullanılmıştır. Üst dönüşüm işlemini gerçekleştirebilmeleri bu tür malzemeleri optik ve fotonik alanlarında çok kullanışlı hale getirmiştir. Üst dönüşüm (UC) diğer adıyla anti-Stokes işlemi bir sistemin iki veya daha fazla fotonun enerjilerini soğurarak daha yüksek enerjili bir foton yaymasıdır. Bu mekanizma incelenirken aktivatör olarak kullanılan iyon ve konsantrasyonu, konak malzeme (katkı yapılan malzeme) ve nano boyut olmak üzere üç temel faktör dikkate alınır.

Nadir toprak iyon katkılı malzemeleri üretmek için en kullanışlı ve kolay sentez yöntemlerinden biri sol-jel metotudur. Sol-jel metodu düşük maliyet, düşük çalışma sıcaklığı ve kolaylıkla yapılabilir basamaklar gerektirmesinden dolayı bu tür malzemeleri üretmek için çok uygun bir yöntemdir. Genel olarak sol-jel sürecinde sistem sıvı fazdan (sol) katı faza (jel) geçiş yapar. Bu süreçte ana malzeme bir seri hidroliz ve polimerizasyon tepkimeleri ile ′sol'e dönüşür. Devam eden süreç sonunda da jel meydana gelir. Sol-jel yönteminin içerdiği genel kimyasal reaksiyonlar, uygun tasarımın yapılması ve kararlı fazın üretimi için başlangıç materyalinde son materyale kadar tüm işlem boyunca kontrole imkân verdiğinden büyük öneme sahiptir. Sol-jel yönteminin birçok avantajı vardır. Bu yöntemde kullanılan alet ve malzemeler basittir. Hem materyallerin oksit bileşimlerine olanak sağlar hem de yeni hibrit organik-inorganik materyallerin üretimine izin verir. Malzemelerin termal bozunma riskinin bu yöntemle minimize edilebileceği, yüksek saflık ve stokiometrinin elde edilebileceği gösterilmiştir. Sol-jel işleminin düşük sıcaklığı, çoğunlukla oksit materyallerin kristalizasyon sıcaklığının altındadır ve böylece nadir amorf malzeme üretimine izin verir. Enerji tasarrufu, yüksek homojenliğe sahip malzeme sentezi, malzemelerin mikro yapısının kontrol edilebilirliği ve yöntemde oluşabilecek kirliliklerin örgü içine girememesi, sol-jel yönteminin diğer avantajlarındandır. Bu sebeplerle bu tezde incelenen numuneler (Yb^{+3}, Nd^{+3}, Tm^{+3} katkılı itriyum silikat malzemeler) sol-jel yöntemi kullanılarak sentezlenmiştir.

Bu tezin genel amacı, nanofosfor malzemeler olarak adlandırılan Yb^{+3}, Nd^{+3} ve Tm^{+3} nadir toprak iyonları katkılı itriyum silikat (Y_2O_3-SiO_2) malzemelerini sentezlemek ve bu örneklerden üst dönüşüm mekanizmalarına dayalı beyaz ışık emisyonu elde etmektir. Bu amaçla, tekli Tm^{+3}, Nd^{+3} veya Yb^{+3}, ikili Tm^{+3}/ Nd^{+3}, Yb^{+3}/ Tm^{+3}, ve Nd^{+3}/Yb^{+3} ile üçlü Yb^{+3}/ Nd^{+3}/Tm^{+3} katkılı itriyum silikat malzemeler sistematik olarak sol-jel metoduyla sentezlenmiştir. Burada Nd^{+3} ve Tm^{+3} iyonları, fotonları ~800 nm'de soğurmada rol oynamaktadır. Yb^{+3} iyonları ise Nd^{+3} iyonundan Tm^{+3} iyonuna veya tam tersi enerji transferi gerçekleştiren bir köprü görevi görmektedir. Nd^{+3} iyonu yakın kızılötesi bölgede (NIR) optik olarak aktif bir iyondur ve 800 nm' de güçlü bir soğurmaya sahiptir. Nd^{+3} daha düşük bir seviyeye geçince durulabilir ve taban durumdaki Yb^{+3} iyonunu resonans enerji transferiyle hassaslaştırır. Cam, seramik ve bulk kristal malzemelerde yapılan ölçümlerde üst dönüşüm prosesi 800 nm'de sağlanabilmiştir. Fakat boyutun etkisiyle kontrol edilemeyen morfoloji, düşük üst dönüşüm verimi ve yüzey kimyasından dolayı cam, seramik ya da bulk malzemeler biyolojik uygulamalar başta olmak üzere pek çok uygulamada problem yaratmıştır. Bu sebeple nano boyutta üçlü katkılandırmayla yapılan malzemeler üzerinde çalışılmıştır. Klasik olarak ikili nadir iyon katkı yapılmış üst dönüşümlü nanoparçacıkların 980 nm ile uyarımıyla karşılaştırıldığında, 800 nm'de aynı üst dönüşüm luminesans yayılım şiddetinde uyarılan üçlü katkılı sistemlerde, daha düşük ısı etkileri ortaya çıkmıştır. Üçlü sistemler üzerinde beyaz ışık araştırmaları yapılmış ve beyaz ışık eldesinde

uyarımın yapıldığı güç yoğunluğunun yanısıra konak malzeme seçimi, katkılanan nadir toprak iyon oranları, tavlama sıcaklığının da çok önemli olduğu gösterilmiştir. Üçlü olarak nadir toprak iyonlarıyla katkılanmış üst dönüşümlü nano parçacıklar üzerine yapılan çalışmalarla, alışılagelmiş ikili nadir iyon katkı yapılmış malzemeler için uygulamada karşılaşılan problemler aşılmaya çalışılmaktadır.

Nadir toprak iyonları katkılandırılmış luminesans özellik gösteren malzemelerin yapısal analizlerinin dikkatlice yapılması gerekmektedir. Çünkü lüminesans özellikler atom veya moleküllerin farklı enerji durumlarındaki geçişleriyle ilgilenmektedir ve bu olaylar malzemelerin yapısal özellikleriyle yakından ilişkilidir. Özellikle bu enerji geçişleriyle ışımasız enerji kayıpları oluşuyorsa yani latis elektron etkileşmeleri gerçekleşiyorsa mekanizmaların değerlendirilmesinde malzemenin yapısal özellikleri çok önemli bir rol oynar. Tez kapsamında üretilen malzemelerin yapısal ve optik özellikleri farklı analitik yöntemler kullanılarak analiz edilmiştir. Malzemelerin yapısal özelliklerini incelemek için X-Işını Kırınım yöntemi (XRD), Taramalı Elektron mikroskobu (SEM), Geçirimli elektron mikroskobu (TEM), Enerji Dağılımı X-ışını Spektroskopisi (EDS) ve Fourier Dönüşüm Kızılötesi (FTIR) Spektroskopisi gibi teknikler kullanılmıştır.

Tez çalışmasında önce konu hakkında genel bir bilgi verilip ardından konu kapsamındaki fiziksel mekanizmalar anlatılmıştır. Malzemelerin sentezi, yapısal analizler için çalışılan teknikler ile deneysel ekipmanlar kısaca tanıtılmıştır. Sırasıyla nadir iyon katkısı yapılmayan konak malzemenin, tekli Nd^{+3}, Tm^{+3}veya Yb^{+3} katkılı, ikili Nd^{+3}/ Yb^{+3}, Nd^{+3}/Tm^{+3}ve Tm^{+3}/Yb^{+3} katkılı, üçlü Nd^{+3}/Tm^{+3}/Yb^{+3} katkılı itriyum silikat malzemelerin yapısal ve optik özellikleri incelenmiştir. Sonrasında bulk yani tavlanmamış haldeki %20 Yb^{+3} katkılı malzemenin emisyon özelliklerine yer verilmiştir. Tezin sonraki kısımlarında beyaz ışığın sıcaklığa ve basınç değişimlerine göre nasıl değiştiği gösterilmiştir.

Çalışmanın en önemli yönleri, beyaz ışığın oluşumunu, üst dönüşüm (UC) enerji mekanizmalarının beyaz ışık oluşumundaki etkilerini, çeşitli sentez tekniklerinin ışıma özellikleri üzerindeki etkisini araştırmak ve beyaz ışığın oluşumunda sorumlu mekanizmaları incelemektir. Bunlardan başka, pompalama gücü, ortam basıncı, sıcaklık, uyarma dalga boyu, numunenin tavlama sıcaklığı gibi birçok fiziksel parametre malzemelerin optik özelliklerini etkiler. Bu nedenlerden dolayı, RE katkılı nano malzemelerin çeşitli fiziksel parametrelere bağlı olarak emisyon özelliklerini araştırmak, ışıyan malzemelerin kalitesini ve uygulama alanını geliştirmek için çok önemlidir. Bu tür malzemelerin nano boyutuna indirgenmesi, optik özelliklerin nasıl etkilendiği konusunu araştırmayı ve böylece bu malzemelerin optikte kullanımını daha da genişletmeyi amaçlamaktadır. Fosfor boyutlarının nano aralığa indirgenmesi, tek kristalli formlarıyla karşılaştırıldığında malzemelerin termal ve optik özelliklerini iyileştirir. Bu mekanizmalar şimdiye kadar tam olarak anlaşılamamıştır ve bu tez deneysel sonuçlarla konuyla ilgili literatüre katkı sağlamayı amaçlamaktadır.

Nano boyutlu fosfor malzemelerin görüntüleme ve fotonik endüstrisinde kullanılmaya çalışılması önemli gelişmeleri de beraberinde getirmiştir. Fakat nanoboyutun ışımasız enerji kayıplarının ana kaynağı olan latis elektron etkileşmesine yani fonon enerji durum yoğunluğuna etkisi konusunda çalışmalar yeterli düzeyde değildir. Fosfor malzemelerin boyutlarının nano mertebesine indirilmesiyle termal ve optik özelliklerin tek kristal formlarına göre daha iyi biçimde geliştiği görülmüştür. Bu sebeple çeşitli sentezleme tekniklerinin boyuta etkisi ve boyutun bu nano malzemelerin optik ve termal özelliklerini nasıl etkilediği, fotonik alanı için temel

araştırma konularındandır. Bugüne kadar nadir toprak iyon katkılı nanofosforlar üzerinde yapılan çalışmalarda çeşitli lazer uygulamaları altında farklı renklerde ışıklar elde edilmiştir. Bu tezde, üst dönüşüm enerji mekanizması esasına dayalı ya da termal beyaz ışık üretimi elde etme konusunda sınırlı olan çalışmalara katkı sağlanacaktır. Beyaz ışığın sadece belirli fiziksel koşullara bağlı olarak mı oluştuğu yoksa sadece beyaz ışığı oluşturmak için kullanılan malzemenin yapısıyla mı ilgili olduğu net değildir. Bu nedenle, beyaz ışık oluşumunun fiziksel mekanizması tam olarak açıklanamasa bile, farklı fiziksel koşullardaki yeni malzeme türlerinin emisyon özelliklerini araştırmak, beyaz ışık oluşum mekanizmasını anlamak için çok önemlidir. Tez kapsamındaki deneylerden çıkan sonuçlar, farklı tür ve konsantrasyonlardaki nadir toprak iyonlarından, çeşitli pompalama gücü ve ortam basınçlarından, farklı sıcaklık aralıklarında lazer diyodunun iki farklı (975/808 nm) uyarma dalga boyundan elde edilmiştir; bu fiziksel ve endüstriyel uygulamalar için beyaz ışık üreten yeni tür malzemelerin tasarlanmasına katkı sağlayacaktır. Tez sonuçları, beyaz ışığın elde edilmesine yönelik araştırma ve geliştirme faaliyetlerine kesinlikle katkıda bulunacaktır.

1. INTRODUCTION

The materials doped with the rare earth (lanthanide- RE) ions are extremely quite interesting systems in the scientific area due to their excellent optical properties. In some circumstances, since these materials show the upconversion and multiphoton absorption luminescence characteristics, they have been investigated for many applications such as optical sensing photovoltaics, data storage, nonlinear imaging, biosensors, multiphoton confocal microscopy, and photodynamic therapy, etc. [1-6]. The materials doped with the rare earth ions (such as Nd^{3+}, Tm^{3+}, Yb^{3+}) can convert near infrared emission to the visible light that process is known as upconversion (UC). Upconversion is the process where one or more photons are absorbed by a material and re-emitted with a higher energy photon. Materials can show this effect is known as upconverters. These materials can respond to near IR energy for example; with ~980 nm or ~800 nm diode lasers, and emit a range of photon energies at visible wavelengths. A major type of up converter is based on rare earth (RE) doped salts of various metals, usually fluorides, and silicates in solid crystal or glass matrices [7-9]. The photons with energies below the material bandgap cannot excite an electron into the conduction band. However, by upconversion process, the photons go up to conduction band by lower energy and this mechanism is used for many optical applications. In cooperative emission that is a kind of upconversion two interacting ions in the excited state return to their ground state simultaneously. They emit one photon with the sum of energies of single ion transitions. Cooperative emission has been observed from Yb^{3+} pairs in this thesis.

RE ions generally appear in a trivalent state and 4f electron shell determines the optical properties of them. Since 4f electron shell is shielded by 5s and 5p electron shells, it is almost insensitive to the surrounding atom of the host environment. This is the reason for weak interaction between optical centers and the crystalline field (weak electron–phonon coupling). The rare earth doped nanostructures are the ideal systems to investigate the dependence of electrical, optical, and mechanical properties of

materials on size and dimensionality. RE compounds have been demonstrated in a wide range application such as luminescence materials and catalysts, and most of these applications depend strongly on the size and structure. Therefore, the luminescence characteristics and energy transfer mechanisms in rare earth doped materials have been studied to improve their optical properties. Since the interesting properties of rare earth ions, they are used to fabricate upconverted luminescent materials. In this thesis, Nd^{3+}, Tm^{3+} and Yb^{3+} were used as rare earth ions. Nd^{3+} and Tm^{3+} ions can be excited by using ~800 nm diode laser excitation while Yb^{3+} ion can be excited by 975 nm diode laser. The luminescence properties of all samples were studied by 975 nm and/or 808 nm excitation corresponding to suitable excitation wavelength for each one. Yb^{3+} may transfer its energy to other ions when it is excited at 975 nm. It is well known that Yb^{3+} ion generally leads to being a bridge for energy transition between the ions. Nd^{3+} ion also has a sensitizer property, however, studying the Nd^{3+} ion doped system is more difficult due to its very complex electronic transitions.

The trivalent RE ions can be replaced with some ions with similar atomic radius in the host matrix and this substitution causes a distortion of crystal field around them. Therefore, some spectral changes are possible in luminescence spectra and at this point, the selection of the host matrix is very effective on luminescence characteristics. The host materials should have high chemical stability and a high refractive index. Besides the hosts preferably should have low phonon energy to decrease multi-phonon relaxations between electronic energy levels of RE ions. Although electronic energy levels are almost independent of the host materials, the phonon energy of host, so lattice vibrations directly affect non-radiative transition probabilities. Yttrium silicates (Y_2O_3-SiO_2) are suitable to be host materials for RE elements because of their high thermal and chemical stabilities [10-14].

Luminescence properties of materials depend on some parameters such as types and concentration of host materials or rare earth ions, synthesis procedure, sample environment, etc. The different dopants give different absorption and radiation energies in the host. In addition, the influence of various synthesis techniques on the size and the effect of the size of those nanomaterials on the optical and thermal properties are basic research areas for various photonic device design and their developments. The selection of host material changes the luminescent effects on the emission properties such as obtaining different colors in emitted light. It is vital to

choose the kinds of host material and dopants such as Yb^{3+}, Tm^{3+} and Nd^{3+}, and concentrations of them for luminescence properties. Many studies have been performed to investigate the luminescence properties of rare earth doped materials and generation of white emission obtained from different host materials doping with a single rare earth ion such as Eu^{3+}, Dy^{3+} [15], Nd^{3+} [16, 17,18], or Yb^{3+} [19, 20] etc. as well as co-doped or triple doped ones.

In this thesis, luminescent emission properties and white light produced by thermally or upconversion energy transfer mechanism have been investigated for yttrium silicate (Y_2O_3-SiO_2) host material doped with various proportions of Yb^{3+}, Nd^{3+} and Tm^{3+} rare earth ions. The possible transition energies due to the rare earth ions were investigated depending on changing the concentration and kinds of the chemicals, excitation pumping powers, excitation wavelengths, annealing temperature, ambient pressure, temperature, etc. The effects of dopant concentrations on spectral features and the luminescence profile were investigated at atmospheric pressure and vacuum. The temperature (between 4K - 780 K) dependence of emission was studied, in detail. In addition, the color quality parameters were determined at each condition with the corresponding photos of emitted samples. The luminescence dynamics of samples at various physical conditions were also investigated by measuring the decay and rise patterns.

In this thesis, we summarized the structural analyses and luminescence results about sol-gel synthesized undoped, single rare earth ions (Nd^{3+}, Tm^{3+} or Yb^{3+}) doped, codoped (Nd^{3+}/ Tm^{3+}, Nd^{3+}/ Yb^{3+}or Tm^{3+}/Yb^{3+}), triply doped (Nd^{3+}/ Tm^{3+} /Yb^{3+}) yttrium silicate nanophosphors and bulk sample. For the structural and morphological properties, several analysis techniques were carried out and the results were discussed to get an idea about their effects on luminescence spectra. X-ray Diffraction (XRD), Scanning Electron Microscopy (SEM), Transmission Electron Microscopy (TEM), Energy Dispersive X-Ray Spectroscopy (EDS) and Fourier Transform Infra-Red (FTIR) Spectroscopy methods were performed to determine the structural and morphological properties of the samples. The effects of several physical parameters such as pumping powers, an excitation wavelength of the laser beam, sample environment (pressure and temperature), concentrations of ions, and annealing temperature of samples on luminescence properties were investigated, in detail.

The observed UC emissions of various color and white light based on both upconversion and thermal processes were investigated at various physical conditions. In Chapter 2, we have explained some basic concepts about the study and introduced host material and dopant ions used in the thesis. The devices, experimental setup and the synthesis method have been described in Chapter 3. In Chapter 4, we have explained the structural analyzes and luminescence properties of undoped yttrium silicate sample. We have discussed power dependent luminescence properties of undoped sample under both vacuum and atmospheric pressure at 808 and 975 nm excitation wavelengths. In Chapter 5, we have examined the structural properties and luminescence behavior of Nd^{3+}, Tm^{3+} or Yb^{3+} doped yttrium silicate samples at different excitation wavelengths depending on pumping power and pressure. In Chapter 6, the structural properties of codoped samples (Nd^{3+}/Tm^{3+}, Yb^{3+}/ Nd^{3+}, or Tm^{3+} / Yb^{3+} doped yttrium silicate samples) and their power dependent upconversion properties have been examined at 808 nm or 975 nm excitations and various pressures. In Chapter 7, structural analyzes of triply doped yttrium silicates ($Nd^{3+}/Tm^{3+}/Yb^{3+}$ doped samples) have been performed and how luminescence properties change in different wavelength excitations depending on power. Chapter 8 has described the white light obtained from un annealed (bulk) Yb^{3+} doped sample at atmospheric conditions. In Chapter 9, the effects of ambient temperature on luminescence properties and white light have been investigated at some powers. In addition, we have studied the power dependence of white emission at some special temperature values. Chapter 10 examined power dependence of upconversion emission at various pressures and described the influence of pressure and pumping power on luminescent properties. The conclusions and contributions of the thesis, also recommendations for future works were given in Chapter 11.

2. THEORETICAL BACKGROUND

Trivalent RE ions doped materials are very interesting and desirable materials for optical applications since they can convert near-infrared photons into visible emission. In addition, they have high luminescence efficiencies, excellent mechanical and thermal stabilities. The upconversion emission and white light production from these kinds of materials have been studied for many years [21-24]. Luminescence characteristics depend on both the energy levels of rare earth ions and the host material properties. Since light-emitting materials or phosphors can absorb light and emit them in visible range on the electromagnetic spectrum, these materials are used for industrial and photonic applications such as lightning and display technologies. Rare earth doped materials are mostly in powder form with various size from nanometers to micrometers, however, nanomaterials exhibit very interesting and various structural/optical properties as compared to those in the bulk form. In other words, the luminescence properties are strongly dependent on the size [25, 26].

2.1 Fundamentals of Luminescence

Luminescence materials can absorb energy due to their special electronic structures when they are excited by a laser. These excitations to ground level are achieved either by the non-radiative excitation (the heat emission at vibrational energy levels) or by radiative emission (corresponding to the emission of a photon). This phenomenon is called as luminescence. If the absorbed energy is high enough, an electron can be excited from its ground state in an upper electronic state. It is well known that the energy of emitted photons is given by:

$$\Delta E\ (eV)\ =\ h\nu = \frac{\mathrm{hc}}{\lambda(\mathrm{nm})} \sim \frac{1240}{\lambda(\mathrm{nm})} \qquad (2.\ 1)$$

There are some categories of luminescence and if the excitation source is photonic, it is called as photoluminescence. The emission spectrum, absorption spectrum,

excitation spectrum and lifetime determine the luminescence characteristics of the materials. The emission spectrum is the intensity of photon emission versus wavelength at particular excitation energy and it gives information about the energies. The absorption spectrum means the intensity of absorption as a function of wavelength.

We know that an atom in higher energy state from its initial state wants to fall lower state due to the law of entropy from thermodynamics. The jumping from the high energy level to low, photons are generated with energy, which is the difference between the levels. This is called emission. If the transition is larger, photons that are more energetic are appeared, for example, blue and red color. The luminescence can be classified into two kinds due to emission properties. These are the radiative transition and nonradiative transition. Luminescence is created by the radiative transitions between two states of atoms or molecules. When an electron in an atom is excited to higher energy level and then turn into its lower energy state, light occurs and this transition is called radiative transition. In other words, if the energy appears as photons, the transition is radiative transition. The electronic transition occurs from the lowest excited of singlet or triplet state to ground state in the radiative luminescence. Another transition is nonradiative transitions where the energy is lost without emission of radiation such as heat. During the radiative transition process, the energy must be conserved and there is an energy difference between higher and lower energy states. This difference appears either a photon of emitted light or energy transferred to another energy state.

2.1.1 Luminescent Efficiency

In photoluminecence process, the material absorbs light. The incident and final intensities of light are not the same due to the passing of the light through the material and the emitted intensity must be proportional to the absorbed intensity, given by:

$$I_{em} \propto \eta (I_0 - I) \tag{2.2}$$

where I_{em} is emitted, I_0 is incident and I is the final intensities which are given in photons per second. The proportionality constant η is known as luminescent efficiency or quantum efficiency. This constant is also the ratio of the number of the emitted and absorbed photons and vary from 0 to 1.

The performance of phosphors is described as quantum efficiency by the following expression:

$$\text{Quantum Efficiency} \quad \eta_{\text{int}}(\lambda) = \frac{\text{number of emitted photons}}{\text{number of absorbed photons}} \tag{2.3}$$

2.1.2 Stokes and Anti-Stokes Shifts

The emission spectrum is shifted to lower energies when it is compared with the absorption spectrum. It is called a Stokes shift. The part of the absorbed energy that is not emitted transfer to the crystal lattice as phonons (heat). If the photon energies are higher than the absorbed photon energy, this process is called anti-Stokes or upconversion luminescence.

2.2 Upconversion Phenomena

Up conversion (UC) or anti Stoke process is an optical process in which high-energy photons through sequential absorption of two or more low energy photons. Up conversion process, generate one high-energy photon out of two or more low energy photons. The photons with energies below the material band gap cannot excite an electron into the conduction band. However, by up conversion process, the photons go up to conduction band by lower energy and this mechanism is used for many optical applications.

2.2.1 Upconversion mechanisms

There are some UC mechanisms and they can occur either alone or a combination of processes in a system. These UC mechanisms are Excited State Absorption (ESA), Energy Transfer Upconversion (ETU), Photon Avalanche (PA), Cooperative Upconversion (CUC), and Energy Migration-mediated Upconversion (EMU) processes.

2.2.1.1 Excited State Absorption (ESA)

Excited state absorption (ESA) process occurs when one or more low energy photons were excited from ground state to intermediate state. Then, they populate the intermediate state; by way of upconversion, emission occurs. ESA can occur only after an electron has already been excited to the lower excited state. The lower excited state has higher energy than the ground state level and the higher excited state is higher in

energy than the lower excited state. ESA process was generally observed at low doping concentration (<1%) of the activator ions since the high doping concentration can reduce the UC emission via nonradiative relaxation processes.

2.2.1.2 Energy Transfer Upconversion (ETU)

The Energy Transfer Upconversion (ETU) process is more efficient than ESA and it involves sensitizer and activator ions. When the sensitizer ion is excited, it transfers its energy to the nearest activator ion and upconversion emission is obtained from the activator when it goes back to lower excited state or ground state.

2.2.1.3 Photon Avalanche (PA)

The Photon Avalanche (PA) process is a more complex process than other UC mechanisms. The photon avalanche process occurs only at a critical level of pumping power (threshold power). If the pump power is high enough, a nonresonant ground state absorption process initially fills the intermediate reservoir level of many ions, and resonant ESA or ETU were occurred from another exciting ion to populate the UC emitting level. Then, some cross relaxations take place between excited and ground state ions. Therefore, the population of the reservoir level and the UC emitting level increase. This causes an "avalanche' effect of generating more ions that are excited with the feedback looping.

2.2.1.4 Cooperative Upconversion (CUC)

The Cooperative Upconversion CUC process is similar to ETU process and includes two types of luminescent centers sensitizer and activator. In CUC process, two interacting ions in the excited state return to the ground state simultaneously, emitting one photon with the sum of energies of the single ion transitions. Cooperative emission has been observed for Yb^{3+} pairs in many studies [30, 31]. The efficiency of CUC is lower than that of the ETU.

2.2.1.5 Energy Migration Mediated Upconversion (EMU)

The Energy Migration Mediated Upconversion EMU process was first proposed in 2011 [32]. The EMU process involves sensitizer, accumulator, migrators, and activator. In this process, the sensitizer is excited by ground state absorption and then transfers its energy to an accumulator. This upgraded it to a higher excited state. Then,

energy migration takes place from higher excited state of the accumulator to migrator, and this process followed by migration of excitation energy through the migrators via core-shell interface. The migrated energy is trapped by an activator in the shell and so emits UC luminescence [33].

2.2.2 Power dependence of upconversion

The dependence of emission intensities on pump powers for the samples is determined by the formula,

$$I \sim P^n \tag{2.4}$$

where n is the number of photons required to absorbed for a particular UC emission. The means of n is the photon number required for UC excitation process, which can be obtained from the slope of the emission intensity versus excitation powers in a log-log plot. In addition, the electronic structure of RE ions and so UC mechanism has a key role to determine the emission characteristics.

2.3 Host Lattice: Yttrium Silicates

As mentioned before, the host materials should have good optical, mechanical and thermal properties. In most cases, the rare earth ions replace other ions of similar size and same charge state in the host matrix. For rare earth doped yttrium silicate samples, the dopant ions are replaced by the Y^{3+} ions randomly. The selection of the host material changes the emission properties. Among the nanocrystalline materials, the Y_2O_3-SiO_2 host matrix is very suitable for doping with RE ions due to its high mechanical properties, low phonon energy and easily synthesis [34-36]. Because of their excellent chemical and thermal stability, similarity in ionic radius of Y^{3+} in yttrium silicate and rare earth (RE) ions, they are well suited host materials. The host lattice determines the structure of system such as distance between the dopant ions, atomic interactions between host and dopant ions, and the type of ions surrounding the dopant. UC emission efficiency depends strongly on host phonon energy, multi-phonon relaxation processes depressed, and efficiency enhanced in low phonon energy hosts. Although the yttrium silicate has many advantages as a host material, the crystal structures of Y_2SiO_5 and $Y_2Si_2O_7$ are very complicated. In the phase diagram of Y_2O_3-SiO_2, a region exists where the 1:1 and 1:2 compositions coexist [37].

2.4 Rare Earth Ions

The elements are called as rare earths (RE) or lanthanides with the atomic numbers 57 through 71 in periodic table that are lanthanum (La), Cerium (Ce), Praseodymium (Pr), Neodymium (Nd), Promethium(Pm), Samarium(Sm), Europium (Eu), Gadolinium (Gd), Terbium (Tb), Dysprosium (Dy), Holmium (Ho), Erbium (Er), Thulium (Tm), Ytterbium (Yb) and Lutetium (Lu). Rare earth elements are commonly used as luminescent centers or activators in the host lattices. As we mentioned before, they have a wide application area due to their unique optical properties, high quantum efficiency, and good stabilities. The studies on rare earth doped materials have a great interest by researchers since industrial and photonic applications are developing by investigating the new and efficient nanophosphors. In this study, three different rare earth ions, Nd^{3+}, Tm^{3+} and Yb^{3+}, were used as doping elements.

Neodymium(III) (Nd^{3+}) ion is very suitable for optical pumping in the broadband optical region from UV to NIR for photonic applications. It has a wide absorption band with the large absorption cross-section at ~800 nm and emits by an emission transition in the $4f^n$ configuration. For optical pumping, using ~800 nm wavelength laser provides to obtain efficient emissions from Nd^{3+}. The energy levels of Nd^{3+} ions are very complicated according to Dieke diagram and to assign the energy levels of Nd^{3+} may be very difficult due to thermal effects and overlapping of the energy levels of Nd^{3+} ions in host materials [38, 39]. Therefore, investigating the new doping systems for near infrared (NIR) diode laser applications to Nd^{3+} doped ions may provide researchers to develop the optical properties of the materials.

Thulium(III)(Tm^{3+}) ion is an attractive activator for solid-state lasers [40]. When the $^3H_4$ state of Tm^{3+} ion is excited by near 800 nm light from a diode laser, Tm^{3+} ion is used for infrared laser oscillation in the 1.8–2.2 mm range with the $^3F_4 \rightarrow {}^3H_6$ transition. In addition, Tm^{3+} ion emits light in the blue region due to the $^1G_4 \rightarrow {}^3H_6$ transition of it.

Ytterbium (III) (Yb^{3+}) is the fourteenth element in the lanthanide series. Among the rare earth ions, ytterbium (III) has important properties for near infrared lasers applications because of providing diode laser pumped media and having very simple electronic structure (only two level $^2F_{7/2}$ ground state and $^2F_{5/2}$ excited state). Excited Yb^{3+} ions exhibit long lifetimes (of the order of 1 ms or s) and allow storing large

energies in the excited state [41]. The trivalent ytterbium ion absorbs light in near infrared range of wavelengths and shows emission at the infrared range (~1000 nm).

2.4.1 Electronic structure of rare earth ions

The inner atomic orbitals of rare earth ions that are called 4f orbitals have a gradual filling. The atomic number of rare earth ions family ranging from 58 (Ce) to 71 (Lu) where the 4f orbitals are gradually filled from 1 to 14. There are very important properties of the electronic structure of rare earth. One of the most important ones is that 4f electrons wave functions have a highly localized nature. They do not overlap with the other neighboring atoms, and they are shielded by the 5s and 5p electrons. The 4f electrons are closer to the nucleus than 5s, 5p, and 6s electrons and so, they are embedded into the electronic cloud. Consequently, rare earth ions in solid form tend to have the same electronic structure as the free ions. So, 4f electrons are isolated from the effect of the ligands (L) and the crystal field. This property affects the optical and magnetic properties [42, 43].

The 4f electrons have quantum numbers n= 4 and l=3, m_l and m_s can take the values of 3, 2, 1, 0, -1, -2, -3 and 1/2, -1/2, respectively. So, each of the seven 4f orbitals contains two electrons. If those orbitals are empty, they have the same energy and called as degenerated. If the orbitals are partially filled, the degeneracy increases. To classify the 4f energy levels is very complex since there are 3432 energy levels for the f electrons [42, 43]. In addition, the optical properties of them are extremely rich. Since there are seven 4f orbitals, the splitting of electronic levels quite complex for rare earth ions and the abundance of electronic levels is important for the development of luminescent materials. The electronic transitions between the levels emit photons and these photons have a different energy. The peaks on an emission spectrum express these electronic transitions. If the electron in a rare earth atom is represented by a wave function (Ψ), Schrödinger equation is

$$H\Psi = E\Psi \tag{2.5}$$

where E is the electron energy and H is Hamiltonian that is the sum of the all interactions due to the electron.

$$H = H_0 + H_{e-e} + H_{SO} + H_{cf} \tag{2.6}$$

Hamiltonian is the sum of these four terms. H_0 is the attractive Coulomb interaction between the electrons and the nuclei; H_{e-e} is the repulsive Coulomb interaction between electrons. H_{so} is the interaction between magnetic field and the magnetic moment of electron and it is called spin-orbit coupling. The last term H_{cf} represents the crystal field effect [43].

The rare earth elements have the electronic configuration [Xe] $6s^2 5d^1 4f^n$. When they are ionized, the electrons of 6s and 5d layers are disappeared and this configuration becomes to [Xe]$4f^n$ with n varying from 1 (Ce^{3+}) to 14 (Lu^{3+}) for trivalent cations. The transitions of f-electrons are responsible for the interesting photo physical properties of lanthanide ions such as sharp absorption and emission lines. The physical mechanism of electron-electron interactions and spin orbit coupling are helpful to the determination of spectroscopic levels. Dieke and co-workers [39] have investigated the energy levels of 4f electrons of Ln^{3+} ions and the standard reference for rare earth luminescence is known as Dieke diagram.

2.4.2 Optical transitions among rare earth ions

The main optical transitions among rare earth based materials are intraconfigurational electronic transition between 4f levels: $4f^n \rightarrow 4f^n$, interconfigurational electronic transition between 4f and 5d (4f 5d) ($4f^n \rightarrow 4f^{n-1}\text{-}5d^1$) and charge transfer (CT) electronic transition between 4f and ligand (L): transition $4f^n\text{-}L \rightarrow 4f^{n+1}\text{-}L^{n-1}$. The emission peaks in which one indicates a special electronic transition generally sharp due to the shielding of 4f-4f transitions. The sharp peaks indicate that the crystal field effect is negligible. The optical properties due to the 4f-4f transitions are almost independent of the host matrix. On the contrary, if there are 4f-5d transitions, the spectra contain large bands.

4f-4f transitions; for the $4f^n \rightarrow 4f^n$ transitions, the interaction with the phonons is very low and the peaks are very sharp in the spectrum. In special rare earth, the energy of a certain 4f-4f transition is the same and independent from the host matrix. The only difference is their intensities that are changed since the crystalline field does not affect very much the positioning of 4f energy level [43].

4f-5d transitions (interconfigurational transitions); the absorption and emission spectra of 4f-5d or 5d-4f transitions always have a broadband and the crystal field effect is dominant, in other words, coupling with the phonons is strong. In addition,

the chemical structure of the host is effective on the wavelengths of 4f-5d transitions [43].

Charge transfer transitions (interconfigurational transition); the charge transfer (CT) transition is important in the absorption mechanism of many phosphors. In the charge transfer mechanism, the light is not absorbed by a modification of the electronic distribution between rare earth and ligand, e.g., oxygen and the energy is then transferred to rare earth. Charge-transfer bands are related to excitations of a ligand electron into a 4f orbital [43].

2.5 Crystal Field Effects

In a solid, charges of neighboring ions generate a perturbation and this perturbation can have the crystal field effect. 4f orbitals were not largely affected by these perturbations due to the shielding from their environment. The crystal field effects are very important in the optical properties of rare earth ions. Unlike, 5d orbitals are extremely affected by their environment and they are filled after the excitation of 4f configuration with only one electron. These effects are the symmetry of the site, the nature of the ligand (oxygen, sulfide...), the vibrations of host lattice and the structural disorder [42, 44]. The 4f-4f transitions are sharp, but optical transitions between 4f-5d have broad emission energies. The host matrix is investigated by the properties of neighboring atoms and symmetry of sites, coordination, etc. These parameters affect the position of energy levels. Due to the crystal field of host materials, the energy levels of rare earth ions split into several Stark levels and selection of host material changes the luminescence effects of the emission.

2.6 Absorption Spectra

Since RE ions have an internal partially filled 4f electron shell, this property gives various electron transitions in UV, visible and IR regions of the electromagnetic spectrum. Energy transfer can play an important role in luminescent materials, so phosphors. The luminescence efficiency of a phosphor can be increased by codoping it with the second kind of donor. Then, an energy transfer from donor to acceptor occurs and direct or indirect energy transfer to the acceptor can relax the exciting centre. These mechanisms can be determined by using absorption spectra. In the direct

mechanism, the energy transfers occur directly from the donor to the acceptor by an interaction [43].

2.7 Light and Color

The colors which can be obtained by combining a given set of three primary colors (RGB) (blue, green and red) are represented on the chromaticity diagram by a triangle contained the coordinates of the three colors and two color coordinates x and y. Three dimensional color space CIE XYZ is the basis for all color management systems. The two-dimensional CIE chromaticity diagram shows a special projection of three-dimensional CIE color space XYZ. The definition of a color base on the values known as tristimulus values for photometry: Hue, Saturation, Brightness (HSB). In physical optics, the dominant wavelength is Hue, the power of light is intensity per Saturation, and luminescence value is the Luminance per Brightness. International Color Standards CIE 1931 RGB is shown in Figure 2.1.

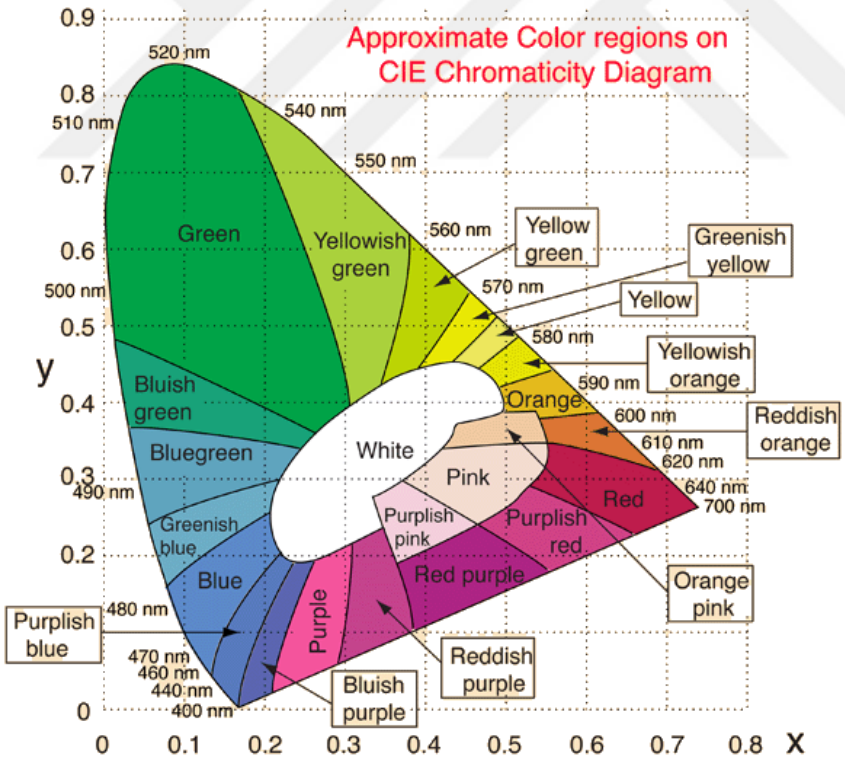

Figure 2.1 : Approximate color regions on CIE chromaticity diagram [45].

White light is defined as the complete mixture of all wavelengths of visible range. White light can be generated by a variety of sources both in space and of artificial sources on earth. For example, sun and other stars are sources of white light.

Fluorescent light bulbs and white LEDs produce artificial white light. The white coordinate is shown as x=0.33, and y=0.33 on CIE Chromaticity diagram.

2.7.1 Correlated Color Temperature (CCT)

Correlated Color Temperature (CCT) is the temperature of an ideal blackbody radiator whose chromaticity most nearly resembles that of light and CCT is a characteristic of visible light. Color temperature is expressed in Kelvins. Low CCT (below 3200K) indicates that the light is warmer, so more yellow-red; on the other hand, high color temperature (above 4000K) means colder or bluer light [46].

2.7.2 Commission International de I'Eclairage (CIE)

Commission International de I'Eclairage (CIE) is the international method to describe the composition of any color denoted by X, Y, Z, also called tristimulus values, in terms of three primaries (red–green–blue). The x, y, z, are the ratios of X, Y, Z of the light to the sum of the three tristimulus values, and they are called as chromaticity coordinates. We use the (x, y) donation to represent a color.

2.7.3 Color Rendering Index (CRI)

The Color Rendering Index (CRI) is a quantitative measure of the ability of a light source to show the colors of various objects by comparing it with a natural light source. The CRI is determined from the spectrum of a light source and it can take the value from zero to 100. Any color of light can be of combining two line emissions. At least three spectral colors are needed to obtain a two-dimensional gamut of colors [47].

3. MATERIALS, METHODS, AND INSTRUMENTS

There are some requirements for obtaining good phosphor materials such as the choices of host and dopants. The luminescence properties are strongly affected by choosing them also controlling many other physical parameters such as the size of particles, minimizing the defects, synthesis technique, sensitivity of equipment etc. Therefore, fabrication of the materials and experimental techniques for determining structural and optical properties are very important.

In the thesis, the sol-gel method is used to synthesize the luminescent yttrium silicate (Y_2O_3-SiO_2) host materials doped with Yb^{3+}, Nd^{3+}, Tm^{3+} rare-earth ions in different concentrations. The synthesized samples were annealed at 1150^0C or 1250 ^{0}C for 12 hours. After the annealing process, the powder samples have been obtained by using an agate mortar. The structural and optical properties of these nanophosphors were determined by various techniques and analyses. The emission properties of samples were investigated depending on kinds of dopants, concentration, excitation pumping powers, sample environments such as pressure and temperature, excitation wavelength, and annealing temperature of the samples.

3.1 Material Synthesis: Sol-Gel

In the study, to fabricate undoped and RE doped yttrium silicate nanophosphors (Y_2O_3-SiO_2 doped with Yb^{3+}, Nd^{3+}, Tm^{3+}), the high purity Yttrium(III) nitrate hexahydrate (99.9%), Ytterbium(III) nitrate pentahydrate (99.9 %), Neodymium(III) nitrate hexahydrate (99.9%), Thulium(III) nitrate pentahydrate powder (99.9%) salts and tetraethyl orthosilicate (TEOS, 99.9%) were purchased from Sigma-Aldrich. In addition, HCI, HNO_3, distillate water, and ethanol were used for preparing the solutions.

$$Y_2O_3\text{-}SiO_2: Yb^{3+}: Nd^{3+}: Tm^{3+} \quad (3.1)$$

The synthesis technique is one of the most important parameters that affect the optical and structural properties of luminescent materials. The sol-gel method is used for preparing Y_2O_3: SiO_2 nanocomposites since the technique has many advantages such

as needed low temperature, minimizing thermal decomposition, easy to control of the process [48].

In general, in the sol-gel process, the system passes from the liquid phase (sol) to solid phase (gel). The sol-gel process generally consists of some basic steps; hydrolysis of the initiator, sol-gel condensation (the active species of alcohol or water condensation), gelation, aging, drying, and high temperature operation. General chemical reactions contained in the sol-gel method have great significance because the technique allows the controlling process during all steps. The devices and materials used in the sol-gel technique are very simple. It provides both combining the materials as oxides compounds and producing new hybrid organic-inorganic materials. The working temperature of the sol-gel process is extremely low; it is often below the crystallization temperature. The risk of thermal decomposition of the materials was minimized by this method and it is shown that high purity and stoichiometry are obtained by many experiments [47-49]. Aging and drying conditions can be controlled by controlling mechanical strength and pore size. Energy saving, the synthesis of materials with high homogeneity, the controllability of the microstructure of the material and not entering the pollution to the lattice are other advantages of the sol-gel method.

A representative sol-gel procedure for all samples can be summarized for the case of undoped and 10% Yb^{3+} doped yttrium silicate nanophosphors in detail, as follows. The ratio of TEOS: Y $(NO_3)_3.6H_2O$ and TEOS: Y $(NO_3)_3$. $6H_2O$: Yb $(NO_3)_3$. $5H_2O$ were 0.53:0.47 and 0.477, 0.423, 0.1 to produce undoped and Yb^{3+} yttrium disilicate glass, respectively. 5 ml ethanol and 5 ml distillate water were used for solving both the rare earth salts and Y $(NO_3)_3$. $6H_2O$ by using a magnetic stirrer separately at room temperature. Then, those solutions were stirred by adding 1N 1cc HNO_3 as a catalyst, separately at 70 ^{0}C for 45 minutes. For Y $(NO_3)_3$. $6H_2O$ solution 10 ml distillate water and 20 ml ethanol were used together. In addition, TEOS, 5 ml distillate water, 5 ml ethanol and 1N 1cc HCI solution were stirred at room temperature separately. Y $(NO_3)_3.6H_2O$ and rare earth solutions were added and mixed at 70 ^{0}C for 40 minutes. Then, we waited for the temperature of all solutions to reach the room temperature. TEOS solution was added to the solution and all the solution is mixed for 2.5 h continuously at room temperature. The gel sample poured into petri dishes and left in a desiccator at least ~8 weeks to obtain glassy form. The powder forms of samples were obtained after the heat treatment of gel-like samples in a laboratory furnace at

1150 ^{0}C or 1250 ^{0}C for 12 h. The samples were grinded in an agate mortar to produce nano-crystalline yttrium silicate powders. These procedures were applied for all samples with various concentrations of rare earth ions salts to fabricate nanophosphor powders. The molar ratio of Y_2O_3-SiO_2 was at 1.127 for all samples.

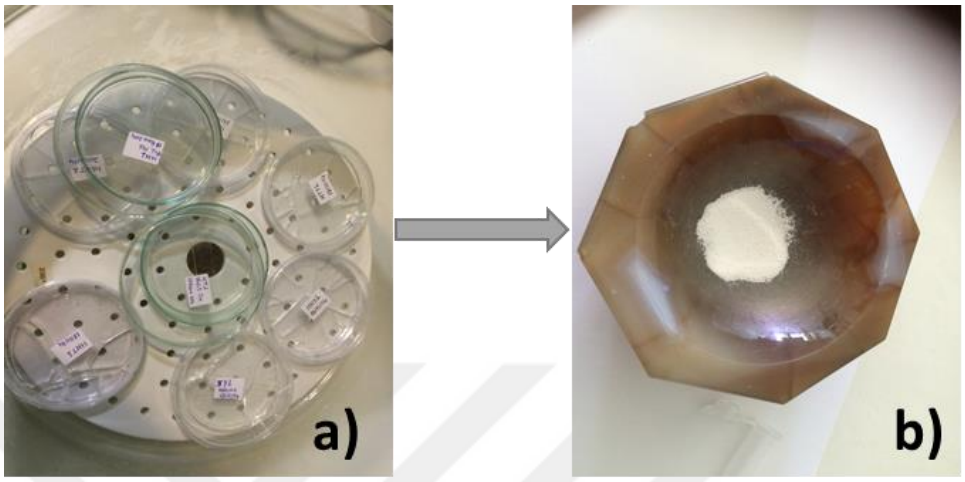

Figure 3.1 : The representative photos of the fabricated a) glassy samples doped with rare earths (Yb^{3+}, Tm^{3+} and Nd^{3+}) and b) nanopowder sample after the heat treatment.

The heating rate in the furnace for annealing procedure was arranged as follows; heating continued for 6 hours until target temperature, the temperature stayed at the target temperature for 12 hours, temperature has fallen to room temperature for 6 hours, total annealing time for each sample was 24 hours. Picture 1.b shows the representative photo of the powder sample after the annealing process.

3.2 Structural Analysis

To develop and study the nanomaterials, structural analyses are very necessary and the appropriate devices should be used for characterizations. Both understanding the structural and surface properties lead us to develop the new nanomaterials for various applications.

For the studies in this thesis, the structural characteristics of sol-gel synthesized nanomaterials were investigated by various techniques such as X-ray Diffraction (XRD), Scanning Tunneling Microscopy (SEM), Transmission Electron Microscopy

(TEM), Energy Dispersive X-ray Spectrometry (EDS) and Fourier Transform Infrared Spectroscopy (FTIR).

3.2.1 X-ray Diffraction (XRD)

The X-ray diffraction (XRD) technique is a powerful technique to determine the structure of crystalline materials. The crystalline phases of samples can be determined by analyzing diffraction patterns. The shape and place of the diffraction lines such as width can give an idea for size, size distribution or defects in nanomaterials. The line width of the pattern is broadened when the size of the nanomaterials decreases and the line width of the XRD pattern can be used for determining the grain size of the sample by Debye Scherrer equation:

$$D = \frac{K\lambda}{\delta 2\theta \cos\theta} \tag{3.2}$$

where grain size (D), K is the constant between 0 and 1 (for spherical particles 0.89), $\delta 2\theta$ the full width at half maximum of the XRD peak of a specific lattice plane (h k l) in radians (FWHM), λ is the wavelength of the incident X-ray beam, and θ is the diffraction angle [50].

The X-ray diffraction (XRD) measurements were taken by the model Bruker D2 Phaser Model (Cu-Kα radiation) diffractometer at 30 kV and 10 mA setting in the 2θ range from 10^0 to 70^0 or 50^0 with scanning steps of 0.002 with the wavelength k=1.5418 Å. The crystalline phases of samples were determined according to JCPDS (Joint Committee for Powder Diffraction Data) by using XRD results.

3.2.2 Scanning Electron Microscopy (SEM)

Scanning Electron Microscopy (SEM) is a very useful technique to determine the surface properties of materials. The limit of the spatial resolution of an optical microscope is usually the order of a few hundred nanometers because of the diffraction limit of light. For many applications and investigations of nanomaterials, the higher resolution is necessary and SEM technique has the extremely good resolution that is down to ~1 nm. The SEM images give information about the surface topology, morphology, and chemical composition. The efficiency of the emission depends on some properties of the surface such as geometry, chemical characteristics, and composition. Therefore, it is important that SEM images provide us getting

information about surface of the sample. The morphological properties of powder samples were investigated with an FEI-Quanta FEG 250 model Scanning Electron Microscope taking the images at low (100000×) and high magnifications (200000×).

3.2.3 Fourier Transform Infrared Spectroscopy (FTIR)

Fourier Transform Infrared Spectroscopy (FTIR) is a technique used to obtain an infrared spectrum of absorption or emission of materials. FTIR spectrometers collect high spectral resolution data for all wavelengths simultaneously in a wide spectral range. FTIR measurements give information about chemical bonding and vibrational bands in the samples optically. FTIR results are used to identify and characterize the structure of samples, determine the contamination, and decomposition in the structure. In the thesis, the FTIR measurements were taken by using a Perkin Elmer Spectrum One spectrometer.

3.2.4 Transmission Electron Microscopy (TEM) and Energy-Dispersive X-ray spectroscopy (EDS)

Transmission electron microscopy (TEM) has a high spatial resolution and is used to perform structural and chemical characterization. The TEM can image the atoms in crystalline specimens at resolutions close to 0.1 nm. It also allows quantitative chemical analysis. TEM is used for getting information about particle size, shape, and crystallinity. The specimen should be thin enough because electrons transmit through the sample.

Energy-dispersive X-ray spectroscopy (EDS) is also an analytical technique used for the elemental analysis of a sample. The main principle in EDS, there is an interaction between the X-ray excitation source and a sample. In EDS analysis, each element has a unique atomic structure allowing a unique set of peaks on its electromagnetic emission spectrum.

In the thesis, Transmission electron microscopy (TEM) measurements were carried out in JEOL 2010F model transmission electron microscope equipped with an energy dispersive X-ray spectroscopy (EDS). The specimen was prepared by dispersing the powder in ethanol, followed by ultrasonic agitation, and then deposition on a lacey carbon film on a 400 mesh copper grid.

3.3 Optical Analyses

The optical characterization of the synthesized phosphors was studied with the absorption, diffusive reflectance, luminescence spectroscopies, also rise and decay patterns measurements under atmospheric conditions and vacuum. The various color and white emissions properties, the energy transfer mechanisms were investigated depending on various physical parameters as mentioned before.

3.3.1 Luminescence spectroscopy; components of the optical set-up

The upconversion and white light emission properties of rare earth doped and undoped yttrium silicate nanopowders have been measured by a near infrared cw laser excitation of the LDI-820 laser diode with 808 nm and/or 975 nm wavelength. The measurements were performed using a Mc Phearson Inc. Model 2051 monochromator. The optical signal was detected by Hamamatsu R1387 photomultiplier tube and sent to EG&G Model 5210 lock-in amplifier. To avoid scattering of the emitted light and avoid the second harmonic generation of laser excitation 975 nm, a short pass 900 nm cut-off filter was used for measurements. For the excitation of 808 nm of laser diode measurements, a 775 nm short pass filter was also used. An Allied Scientific Pro ASP-MK350 Model illuminance meter was used for determining the color quality parameters. All the output power values of the laser beam were measured by Power Max 500D (Molectron) power meter. The measurements of decay and rise patterns at atmospheric pressure and vacuum were carried out using a shutter to interrupt the laser beam and a Tektronix model TDS 3052B oscilloscope. The spectral properties of the phosphor materials have been found to depend on several physical parameters. The main components for the experimental set up are introduced as follows:

- *Monochromator*

The monochromator is a fundamental optical device for luminescence measurements. It is used to separate different components of the laser light beam. It generally converts the polychromatic beam to a monochromatic beam. A simple monochromator consists of an entrance slit, mirrors, a dispersive element such as prism or diffraction grating. The measurements in this thesis were performed by using a McPherson model 2051 one-meter scanning monochromator. The device has a 600 groove/mm grating and blazed at 1.25 μm. The device has a resolution and wavelength resetability of 0.1 Å with repeatability of +/- 0.05 Å.

- *Light detector (photomultiplier tube)*

A photomultiplier tube (PMT) detects very weak signals and absorption of photon results in the emission of an electron in a PMT. It consists of photocathode and an electron multiplication system. The photocathode converts photons to electrons and the multiplication system amplifies the electric signal.

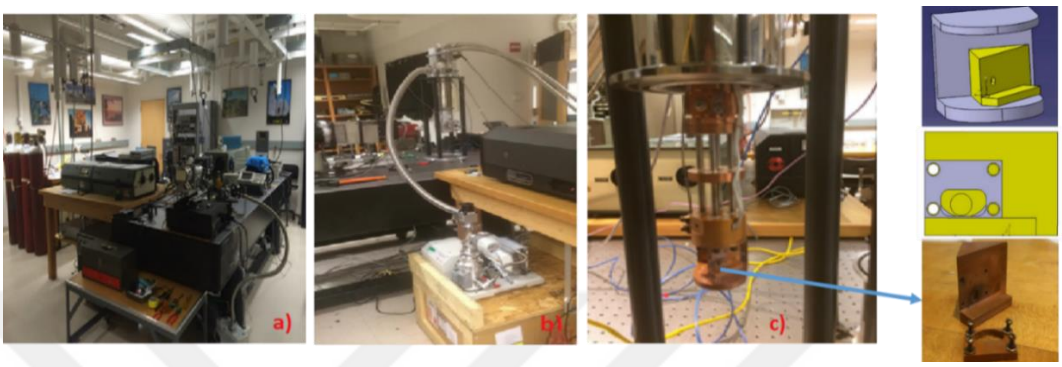

Figure 3.2 : The experimental setup; a) the whole picture of the setup b) the vacuum system c) the sample holder.

In the experiments, Hamamatsu type R1387 photomultiplier tube was used and the best spectral response was the range from 350 to 850 nm.

- *Signal processing apparatus*

Lock-in Amplifier is used to amplify the AC signal of the Photomultiplier tube. In the set-up, we used the EG&G Model 5206 as a lock-in amplifier. A chopper is used to carry the frequency of the optical signal and operated at 250 Hz in the set up during experiments. It is placed at the entrance of the monocromator. It removes the DC biases due to the instrumentation and amplifiers.

- *Collecting data*

The box-car averager takes place in the experimental setup and integrates signals during a sampling window and then stores it. The boxcar averager is connected to the computer and data received from the boxcar is sent to computer. The computer is programmed to show the plots of intensity vs. wavelength. The program is LabVIEW from National Instruments.

- *Vacuum and Temperature system*

For the vacuum experiments, two experimental set up were used and Janis manufactured both. The system used a Janis Research Model RD dewar connected

with a Leybold Model RW2 compressor in the old system. In the new system, T-Station vacuum system was used which is a small automatic pumping system that is suitable for a wide range of vacuum applications. It uses an EXT75DX turbomolecular pump. The pump provides the vacuum up to 10^{-6} mbar. The temperature dependence on luminescence properties has been investigated by using JANIS model Temperature System. The sample was mounted on the cold finger of a closed cycle Helium refrigerator for temperature measurements. The temperature range was from ~4K to ~800 K and temperature was controlled by the Lake Shore Model 335 Temperature controller. The experimental set up for temperature measurements consists of a refrigerated chamber with RDK 205 J 4K cold head, SRDK 205 series cryocooler, and wide range gauge. During temperature measurements, the enthalpy of materials used for constructing cryostats drops rapidly when the temperature was decreased. The helium transfer must start at a very low rate, and is maintained at that rate until the entire contents of the helium reservoir are cooled below 20K. Model 335 Temperature controller provides to control temperature by using the heater during measurements and arrange the temperature ramp rate. When a sample is attached on a cold finger, it is necessary to establish good thermal contact, and also reduce the heat load into the sample as much as possible.

3.3.2 Absorption measurements setup

The device known as spectrophotometer is used for absorption measurements. Generally, it consists of a light source, a monochromator, a sample holder, a light detector and a computer. The light source is usually a tungsten lamp for visible and infrared ranges, a deuterium lamp for the ultraviolet range. The monochromator is used for selecting wavelength by the light source and scans it in the desired range. The light detector that is generally photomultiplier tube for UV-VIS range and SPb cell for IR range measures the light intensity passing through the sample. A computer displays the absorption spectrum and records it. The spectrophotometer can be operated at different modes, for example, optical density, absorbance or transmittance. The absorption measurements in the study were recorded with Varian Cary 5000 UV/VIS/NIR spectrophotometer between 350 and 1200 nm.

3.3.3 Diffusive reflectance measurements setup

The reflectivity spectra give complementary information for absorption results for the powder form of samples. Reflectivity and absorption spectra are related to each other by using Kramers- Kronig relations. Reflectivity is:

$$R = \frac{I_R}{I_0} \tag{3.3}$$

where I_0 is incident intensity and I_R is the reflected intensity. Reflectivity spectra can be in two modes that are direct or diffuse reflectivity. The diffusive reflectance data was taken by using the Perkin Elmer Model Lambda 35 UV –Vis spectrometer in the range of 400 nm-1100 nm at room temperature to identify the absorption lines.

4. STRUCTURAL AND LUMINESCENCE PROPERTIES OF UNDOPED YTTRIUM SILICATE(Y_2O_3: SiO_2) NANO PHOSPHOR

Yttrium silicate (Y_2O_3: SiO_2) is one of the most suitable hosts for luminescence applications as mentioned in Chapter 2. Depending on the phonon energies of the host medium, some of the lifetime's level can be strongly quenched by multi-phonon transitions. Therefore, the hosts should have low phonon energy to decrease the multi-phonon relaxations between electronic energy levels of RE ions [51, 52].

In this part of the thesis, the studies about undoped yttrium silicate samples (without doping rare earth ions) will be explained.

4.1 Structural Analyses of Undoped Y_2O_3-SiO_2 Sample

For the structural analyses of undoped powder sample, X-Ray Diffraction (XRD), Fourier Transform Infrared Spectroscopy (FTIR), Scanning Electron Microscopy (SEM), Transmission Electron Microscopy (TEM) and Energy-dispersive X-ray spectroscopy (EDS) measurements were carried out at room temperature.

XRD patterns of the undoped sample are shown in Figure 4.1. The average particle size of the sample is estimated as ~86 nm by using the Scherer equation and the structure of the sample was found to be α-$Y_2Si_2O_7$ with card number 38-0223 according to Joint Committee for Powder Diffraction Data (JCPDS) [53].

For TEM measurement, the specimen was prepared by dispersing the powder in ethanol, followed by ultrasonic agitation for 2 hours, and then deposition on a lacey carbon film on a 400 mesh copper grid. TEM measurement and EDS images are shown in Figure 4.2a and 4.2b, respectively. Figure 4.2a shows that the sample has a crystalline structure and it is a good agreement with XRD result as indicated in Figure 4.1. The signals and numerical values obtained from the EDS image show the presence of Y (18.8 atomic %), Si (21.23 atomic %) and O (59.98 atomic %).

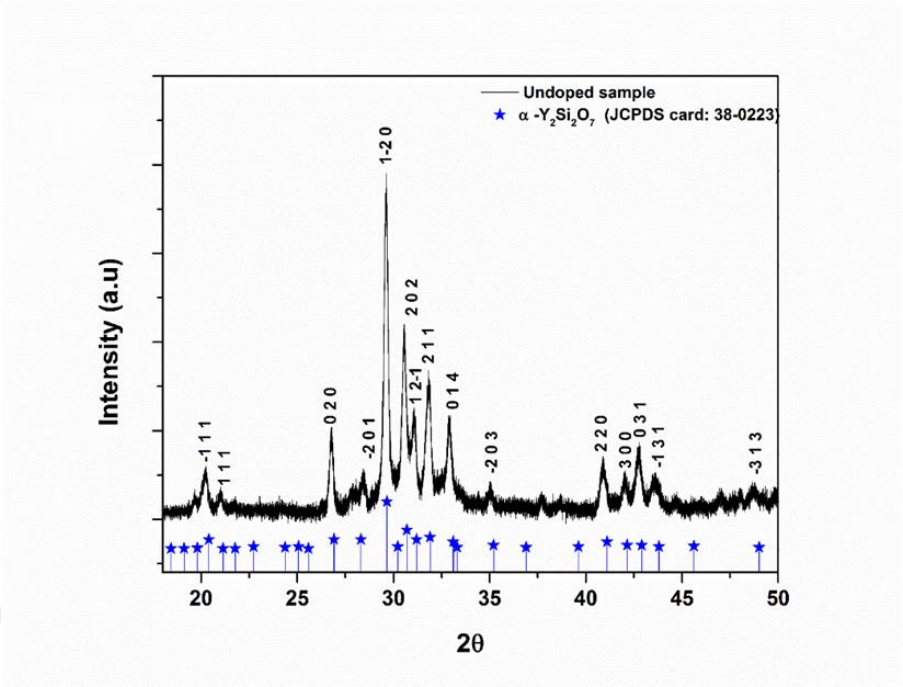

Figure 4.1 : XRD patterns of undoped yttrium silicate powder.

The other peaks in the spectra indicate C and Cu and they are due to carbon-copper grids used for measurement (Figure 4.2b).

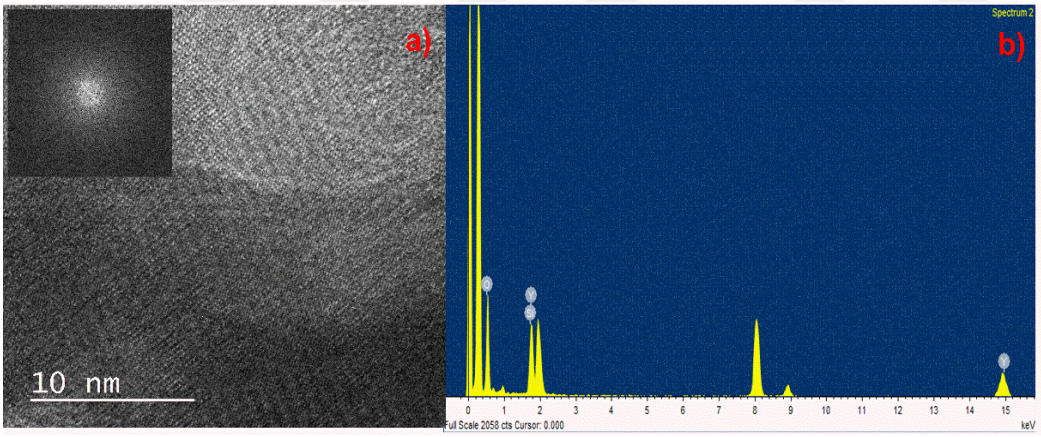

Figure 4.2 : a) TEM and b) EDS images of undoped yttrium silicate.

The SEM images are shown in Figure 4.3. As seen from the figure, undoped α-$Y_2Si_2O_7$ particles were observed as granular-like nanoparticles, with the particle diameters ranging from 69 to 128 nm [19]. Figure 4.4 shows Fourier Transform Infrared Spectroscopy (FTIR) results and Table 4.1 summarizes the peaks corresponding bonds [54, 55]. 800-1000 cm^{-1} domain corresponds to Si-O stretching vibration involving non-bridging oxygen. The band situated at around 843 cm^{-1} is ascribed to multiple Si-

O stretching in which all oxygen and silicon atoms of silicate groups participate in the vibration.

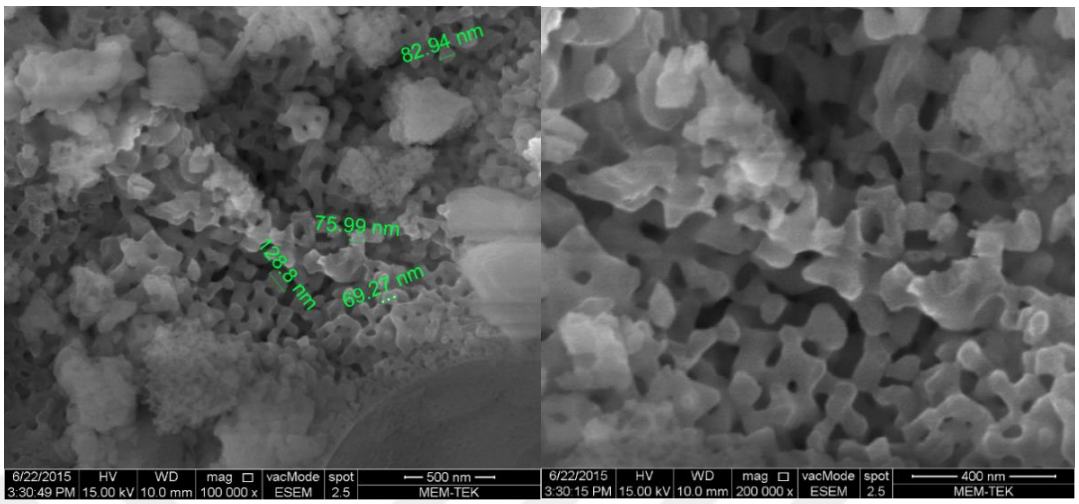

Figure 4.3 : The SEM images of undoped powder annealed at 1250^{o}C for 12h.

FTIR results showed that 600-1200 cm^{-1} domain corresponds to Si-O and Y-O stretching vibration involving non-bridging oxygen.

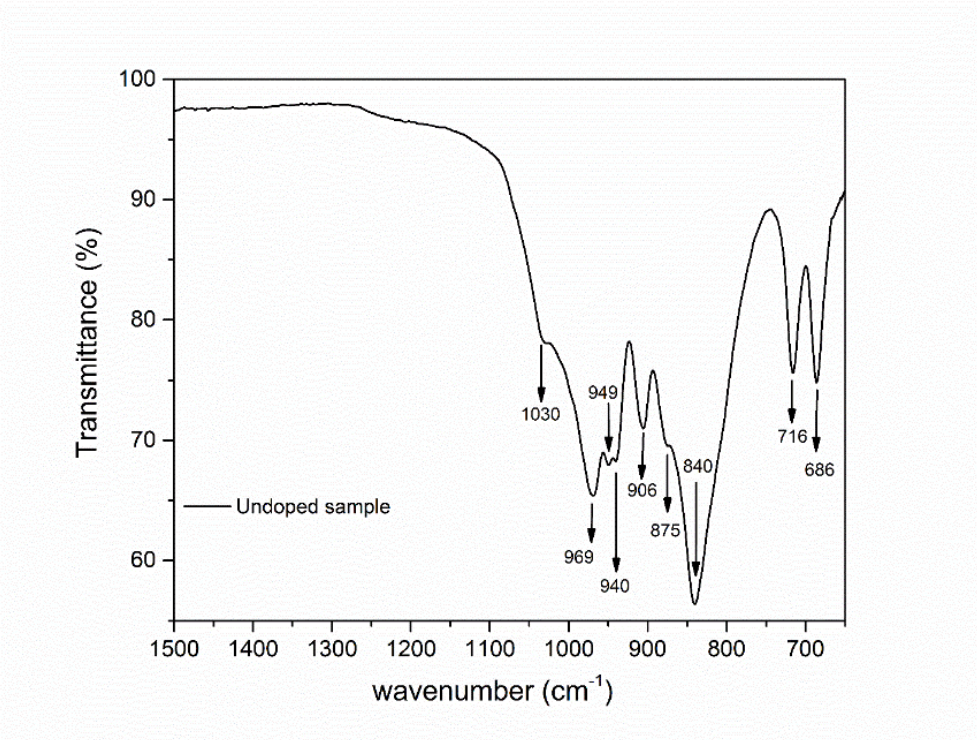

Figure 4.4 : The FTIR result of undoped powder annealed at 1250^{0}C for 12h.

In this domain, to characterize the vibrational bands are difficult because single Y-O and Si-O vibrations co-exist in similar spectral ranges. 4000–3000 cm^{-1} where OH stretching vibrations of water and OH groups appear and 400–1100 cm^{-1} where the

Si–O and Y–O vibrations occur [55]. 1000 -1200 cm^{-1} domain for stretching vibrations of silicon atoms are against oxygen atoms in Si-O-Si bonds. The slight broadband in the range 1000-1100 cm^{-1} is due to the presence of silicon as precursors and this band is assigned to asymmetric (Si-O-Si) vibration. The peak at 1030 cm^{-1} may correspond to the superposition of rocking Si-O vibrations and Y-O bond vibrations. The broad bands above 800 cm^{-1} are assigned to Si-O and Y-O vibrations. The frequency shifts and broadening of yttrium silicate samples may be due to combined effects of the transfer of electron density from the yttrium to the Si-O bond and a wider distribution of Si-O bond angles available in silicates. FTIR results for all samples in this thesis are the same, so the result of the undoped sample was given as a representative example in Figure 4.4.

Table 4.1 : The summary of the FTIR results for undoped yttrium silicate.

wavenumber(cm^{-1})	bonding
1030	Si-O-Si asymmetric stretching vibration
969	C-O stretching
949	Si-O or Y-O vibration
940	O-H bending or asymmetric vibration of Si-OH
906	O-H bend or Y-O vibration or Si-O vibration
875	C-H bend or Y-O vibration or Si-O vibration
840	C-H bend or Y-O vibration or Si-O vibration
716	C-H bend or Y-O vibration or Si-O stretching

4.2 Absorption and Luminescence Measurements of α - $Y_2Si_2O_7$ sample

For optical analyses, absorption measurement was recorded with Varian Cary 5000 UV/VIS/NIR spectrophotometer between 350 and 1200 nm for the bulk sample before the annealing process. The luminescence spectra of annealed sample were measured by using a diode laser LDI-820 with both 975 and 808 nm excitations and using Mc Phearson Inc. Model 2051 monochromator. The short pass 900 nm and 775 nm cutoff filters were used to avoid scattering of emitted light and avoid the second harmonic generation of laser excitation 975nm and 808 nm, respectively. The color quality parameters and the decay/rise patterns measurements were carried out at atmospheric pressure and vacuum.

4.2.1 Absorption spectra of undoped sample

Figure 4.5 shows a representative absorption spectrum for undoped yttrium silicate sample before annealing, there are two peaks at 978 nm and 1171 nm and they can be attributed to water absorbance [56]. It is expected that there was not any peak in the absorption spectra for the host sample. However, we have observed the peaks belonging to water.

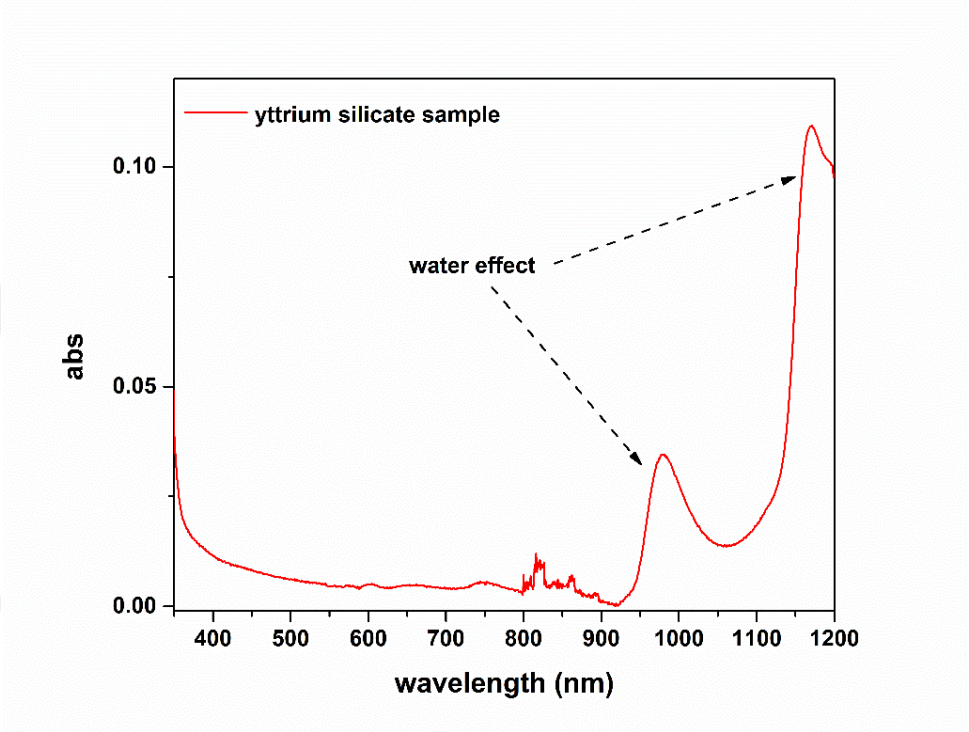

Figure 4.5 : The absorption spectra of the un-annealed undoped bulk yttrium silicate.

4.2.2 Luminescence properties of α-$Y_2Si_2O_7$ sample at 975 nm excitation

The luminescence spectra of the undoped sample are shown in Figure 4.6 at atmospheric conditions under diode laser excitation of 975 nm. The broadband white light spectra were obtained at high powers of output laser. The white light of undoped $Y_2Si_2O_7$ was not very strong at atmospheric pressure when we compare it with the vacuum case (Figure 4.6 and Figure 4.7). It can be expected that obtaining white light can be possible by upconversion energy transfer mechanisms between the rare earth ions for the nanophosphor system. However, we obtained white emission from the host sample. Therefore, it is also proved that the generation of white light is related to the structure of the host sample.

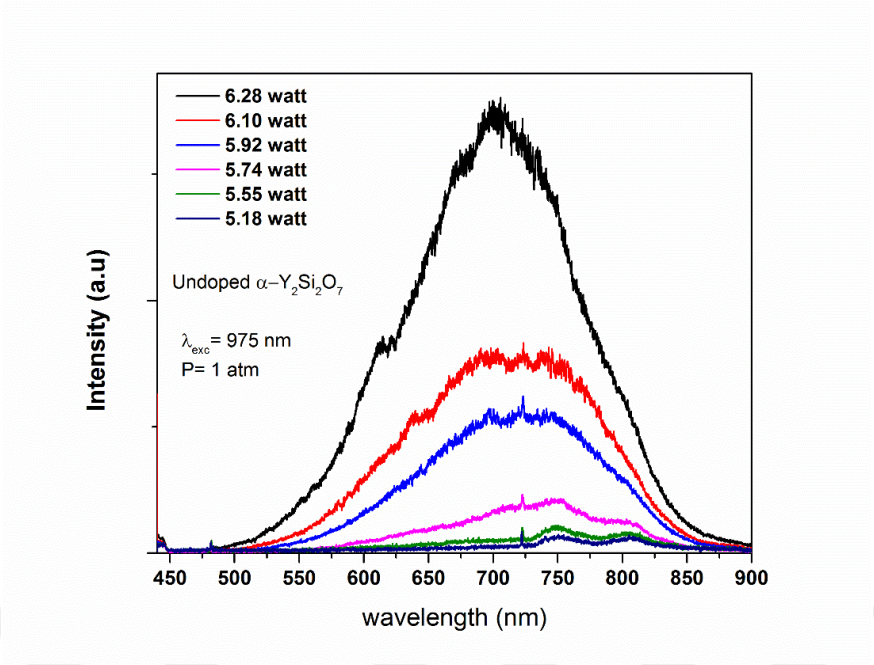

Figure 4.6 : White light spectra of α- $Y_2Si_2O_7$ at atmospheric pressure depending on pumping powers.

If we have a suitable host structure, we can observe the white emission thermally from host [57, 58]. In addition, white emission was observed from the undoped $Y_2Si_2O_7$ sample under vacuum at least 1.45 W as shown in Figure 4.7.

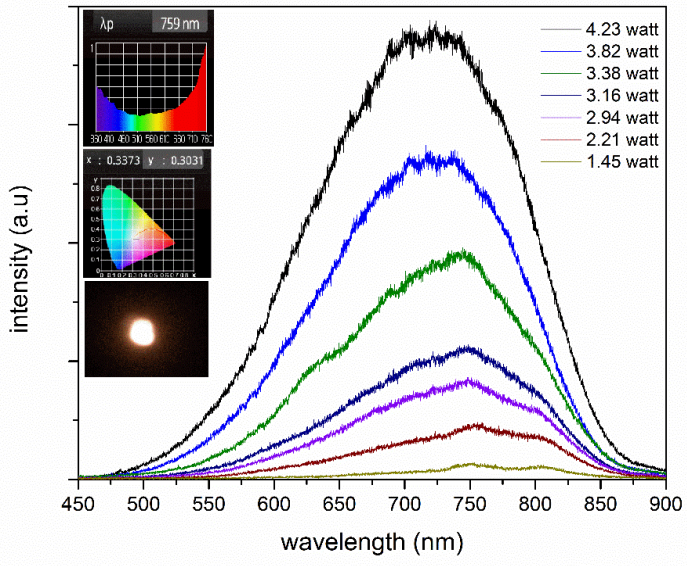

Figure 4.7 : White light spectra of α- $Y_2Si_2O_7$ at vacuum (0.01 mbar), chromaticity diagram and photo of the sample at 3.38 W.

The peak position of white light is ~745 nm below 3.38 W. Above 3.38 W, the maximum intensity is centered at ~716 nm with a broad range. There is shifting to a

high energy region that is from ~742 nm at ~1.96 W to ~711 nm at ~4W and it indicates that these shiftings are in good agreement with Wien's displacement law resulted from blackbody radiation [59,60]. Figures 4.8 and 4.9 show the number of photons involved in the population process at atmospheric pressure and vacuum, respectively.

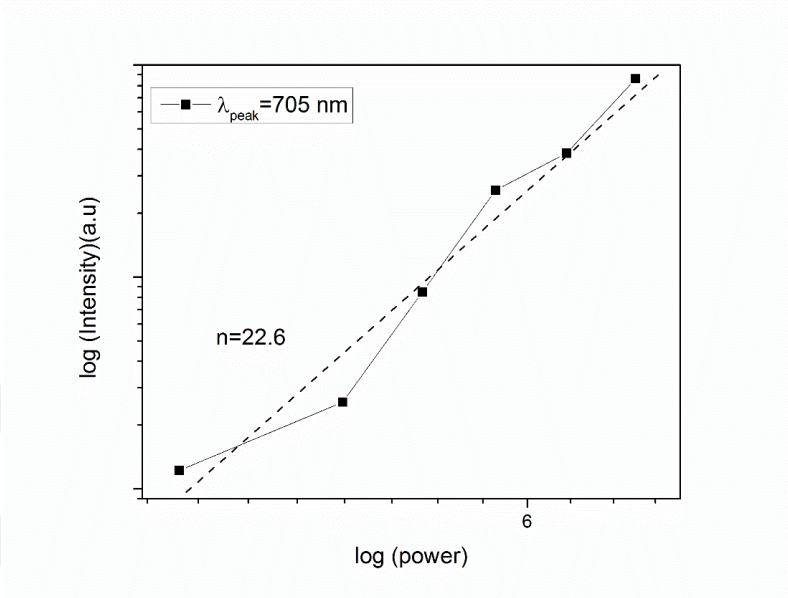

Figure 4.8 : Double logarithmic plot of Intensity versus Power for white light spectra from undoped α- $Y_2Si_2O_7$ sample at atmospheric pressure.

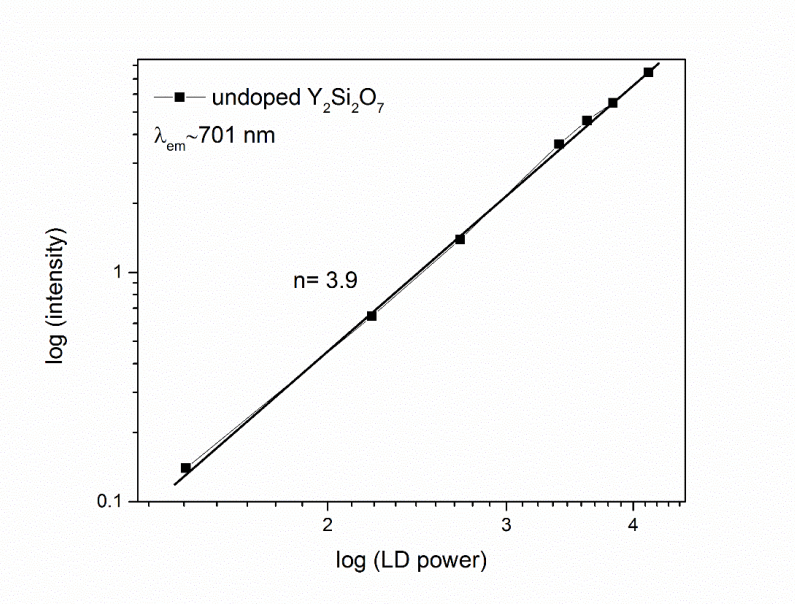

Figure 4.9 : Double logarithmic plot of Intensity versus Power for white light spectra from undoped α- $Y_2Si_2O_7$ sample at vacuum.

The slope values indicate that thermal processes for white light generation are more effective at atmospheric conditions than that is in vacuum. The white emission was

observed from the undoped $Y_2Si_2O_7$ sample at least for 1.45W and 5W pumping powers under vacuum and atmospheric pressure, respectively.

Thermal processes are responsible for white light generation for the undoped sample. The decay/rise patterns are also evidence for occurring of thermal processes due to taking a long time in several seconds. This behavior can be seen in Figure 4.10. The decay and rise patterns for the undoped sample are shown in Figures 4.10a and 4.10b, respectively, under vacuum with 975 nm excitation at 701 nm emission wavelength.

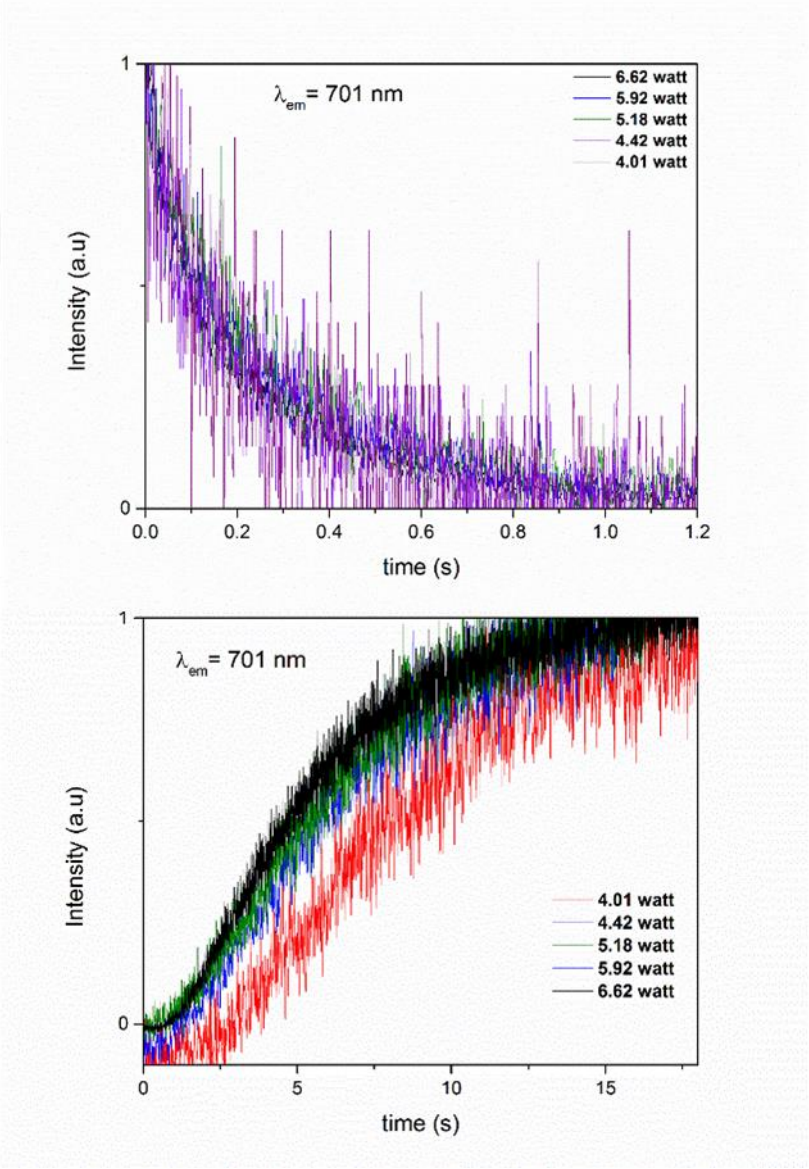

Figure 4.10 : Decay and rise patterns for 701 nm depending on power from undoped α- $Y_2Si_2O_7$ at vacuum (0.01 mbar).

The decay patterns haven't strong dependence on pumping power, however, rise patterns are sensitive to pumping powers. The rising pattern is faster at low output laser powers and decreased when the power is increased.

4.2.3 Luminescence properties of α-$Y_2Si_2O_7$ sample at 808 nm excitation

The luminescence behavior of the yttrium silicate sample was investigated at a diode laser excitation of 808 nm. Figure 4.11 shows the thermal white light spectra obtained from the sample. Below ~4.9 W, the emission was very weak and could not be detected at atmospheric conditions. The inset figure indicates that thermal processes and photon avalanche mechanisms are effective for white emission due to the high value of n (n~14). This emission from α-$Y_2Si_2O_7$ sample at vacuum conditions was stronger and the threshold power is lower than that of atmospheric conditions at 808 nm excitation. We observed the same behavior at 975 nm excitation.

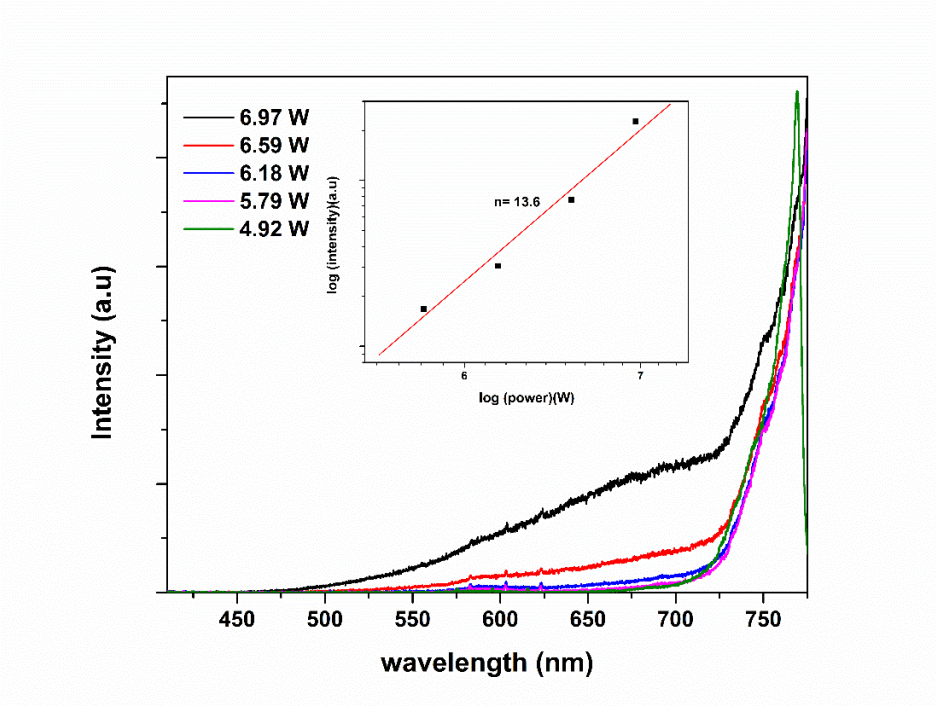

Figure 4.11 : The luminescence spectra of the α-$Y_2Si_2O_7$ depending on power at atmospheric pressure.

Figure 4.12 shows the luminescence spectra at vacuum conditions under 808 nm excitation. The emission was observed in a wide range of excitation powers from 6.97 W to 0.84 W. The inset figure shows double log representation of the intensity versus pumping powers and two different slopes regions were obtained for the sample that is similar to our another work [61].

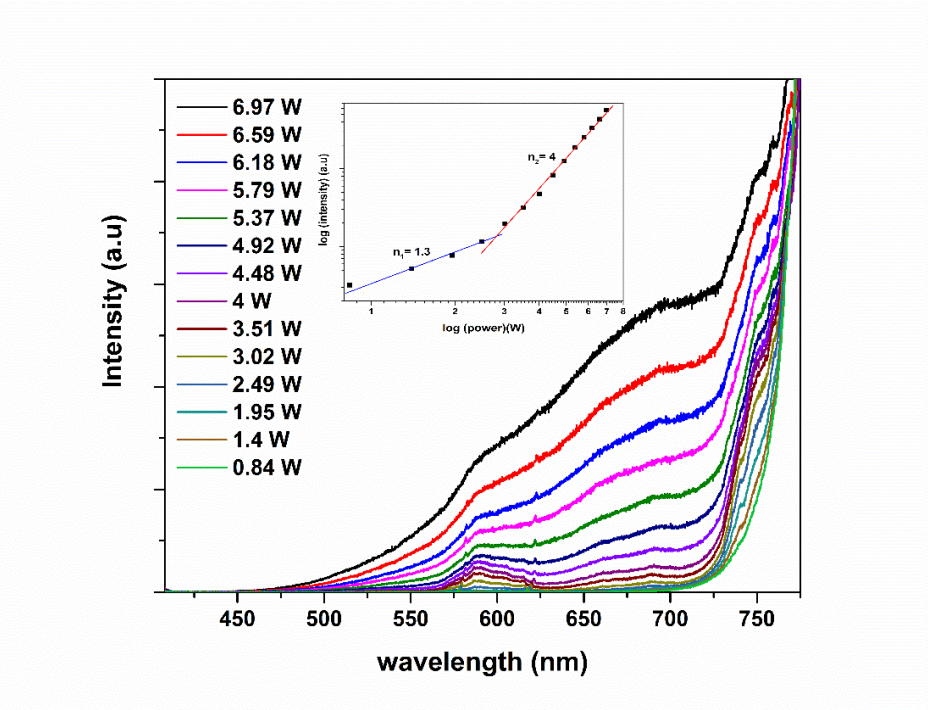

Figure 4.12 : The luminescence spectra of the α-$Y_2Si_2O_7$ depending on pumping powers at vacuum (0.01 mbar).

The results at 808 nm excitation show that thermal effects are more effective at atmospheric conditions. The weak shoulder centered near 580 nm may be due to the impurities and defects in the yttrium silicate host. The excitation energy can be transported to crystal defects where non-radiative decay occurs.

The illuminance meter results were listed in Table 4.2 for both atmospheric pressure and vacuum cases at 808 nm excitation. It is seen that CIE 1934, x and y values are increasing with pumping power. In addition, CRI values are increasing while CCT values are decreasing with increasing pumping powers at atmospheric pressure. The chromaticity values (x, y) are increasing and CCT is decreasing with increasing pumping powers at vacuum. The CRI values are kept a constant value (~87) for vacuum conditions at 808 nm excitation.

Table 4.2 : Illuminance meter results and photos of undoped yttrium silicate sample at 808 nm excitation.

Undoped yttrium silicate at 808 nm excitation (under atmospheric pressure)

Power (W)	CIE 1931 coordinates (x, y)	CCT(K)	CRI(Ra)	Illuminance meter spectrum	Image of the emission
6.97	(0.4559, 0.3729)	2448	91	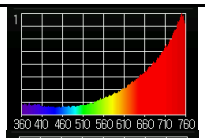	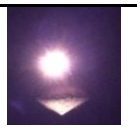
6.18	(0.3606, 0.3214)	4194	85	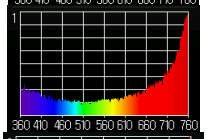	
4.92	(0.3431, 0.3177)	4947	86	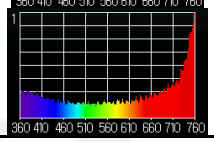	

Undoped yttrium silicate at 808 nm excitation (under vacuum)

Power (W)	CIE 1931 coordinates (x, y)	CCT(K)	CRI(Ra)	Illuminance meter spectrum	Image of the emission
6.97	(0.3655, 0.3248)	4032	87	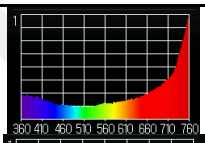	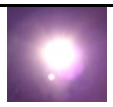
6.18	(0.3586, 0.3222)	4284	87	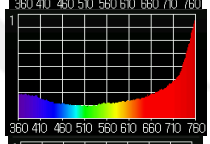	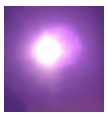
4.92	(0.3496, 0.3191)	4647	87	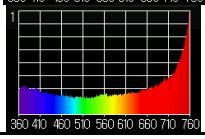	

5. STRUCTURAL AND LUMINESCENCE PROPERTIES OF SINGLE RARE EARTH DOPED YTTRIUM SILICATE (Y_2O_3: SiO_2) NANO PHOSPHORS

5.1 Nd^{3+} doped Yttrium Silicate Nano Powders

The investigation of the new source of visible light is an interesting field of research and we are presenting a new and relevant addition to the scientific literature in this field, a contribution based on NIR excitation of a nanopowder of yttrium silicate doped with Nd^{3+} ions. The electronic structure of the rare earth ions and thus upconversion mechanism play an important role to determine the emission characteristics. For this purpose, in literature, Nd^{3+} doped systems have been investigated in various hosts such as glasses, transparent glass-ceramics, polymers and crystals [62- 64].

Until now, there are very limited studies about luminescence properties including the white emissions of Nd^{3+} doped nanopowders. In this part of the thesis, white light production from 1% Nd^{3+} doped Y_2O_3:SiO_2 because of blue, green, orange and red color emissions and thermal processes were analyzed both in the vacuum (0.01 mbar) and atmospheric pressures. In order to investigate its optical properties, the sample was excited by 808 nm beam of a laser diode. The emission was found to be a function of output powers of laser and the pressure of the sample's environment. Emission for upconverted white light mainly due to the transitions of Nd^{3+} ions was obtained below ~5.79 W of the laser beam power at atmospheric pressure. For powers exceeding ~5.79 W, the powder emitted a thermal white light (WL) due to the photon avalanche mechanism together with thermal processes. The threshold power to obtain thermal white light with the transitions of Nd^{3+} ions was decreased at vacuum conditions. These processes were investigated in detail by studying the spectral differences of the rise and decay patterns at atmospheric pressure and vacuum conditions.

5.1.1 Material synthesis

1% Nd^{3+} doped yttrium silicate nanophosphor was synthesized by the sol-gel method as described in Chapter 3. The ratio of Y_2O_3: SiO_2 was kept as 1.127. The obtained gel sample was annealed at 1250 ^{0}C for 12h to obtain its powders form.

5.1.2 Crystalline structure

The structural analysis of the powder sample was investigated with X-Ray Diffraction analysis (XRD) by using Bruker D2 Phaser Model (Cu-Kα radiation, λ=1.54184A˚) diffractometer with scanning steps of 0.002^0/2θ from 15^0 to 65^0. The result is shown in Figure 5.1. The diffraction pattern can be indexed to monoclinic phase X_1-Y_2SiO_5, space group P21/c (JCPDS card number 00-52-1810) [65].

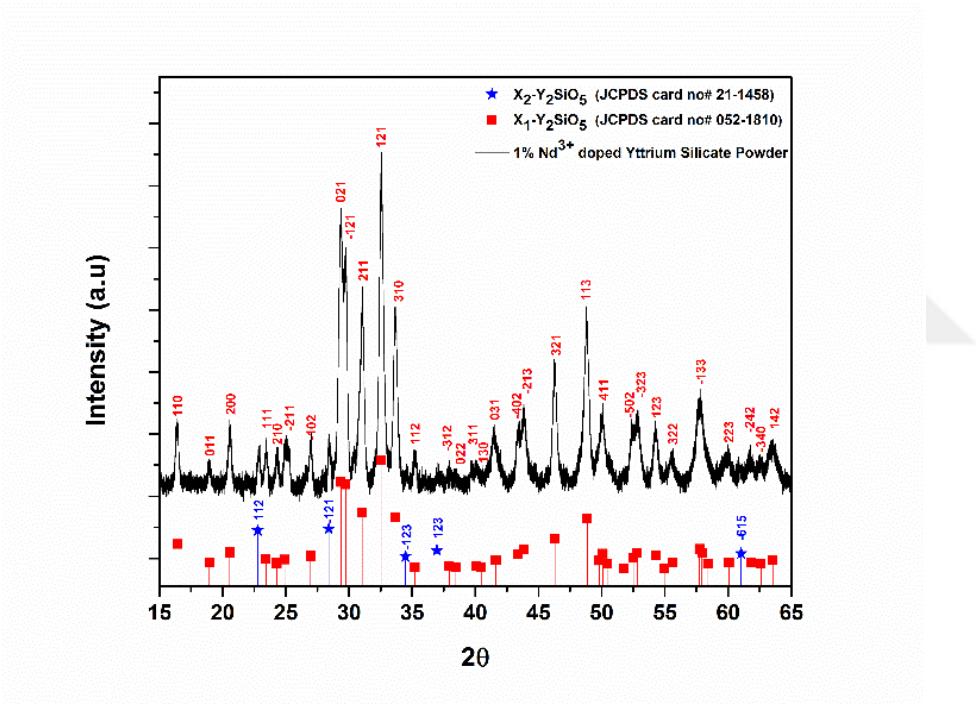

Figure 5.1 : XRD patterns 1% per mole Nd^{3+} doped monoclinic X_1-Y_2SiO_5 nanopowder with the very small amount of impurity peaks of monoclinic X_2-Y_2SiO_5 annealed at 1250 °C for 12 h.

The dominant peak was observed at 2θ= ~32.50 and the corresponding lattice plane is indexed as (121) for monoclinic X_1-Y_2SiO_5. The very small amount of impurity peaks was detected and they may be attributed to monoclinic X_2-Y_2SiO_5 (JCPDS card number PDF#21-1458) [66]. The weight of the very weak X_2-Y_2SiO_5 phase was determined to be ~3.6 % wt. by the reference intensity ratio (RIR) method [67, 68]. The average particle size was calculated to be about 51 nm by using the Scherer

equation [50]. Y_2SiO_5 has polymorphic structure and can be in the monoclinic X_1- or X_2-type at different synthesis temperature. There may be incomplete polymorph transformation between the X_1-Y_2SiO_5 and X_2-Y_2SiO_5 phases [69]. It is clearly found that the sample has a single-phase state (Y_2SiO_5) with main phase X_1-Y_2SiO_5 and very little additional X_2-Y_2SiO_5 phase, thus confirming successful synthesis. The rare earth ion (Nd^{3+}) may be substituted for yttrium (Y^{3+}) in this host lattice since they have similar ionic radii.

A diode laser LDI-820 with 808 nm excitation wavelength was used to measure the luminescence spectra of the sample. A short pass 775 nm cut-off filter was used to avoid the scattering and the second harmonics of laser excitation during the measurements. An Allied Scientific Pro ASP-MK350 Model illuminance meter was used for determining the color quality parameters. The room temperature decay and rise profiles were also obtained at both atmospheric pressure and vacuum conditions.

5.1.3 Luminescence properties at atmospheric conditions

Figure 5.2 shows the luminescence spectra of the sample at atmospheric conditions. The emission bands appeared due to upconversion processes between the electronic states of Nd^{3+} ions are much broader than those observed in the crystals. This is mainly due to the nanosize of the particles [18, 61]. In Figure 5.2, the observed blue emission bands were very weak when we compare them with green, orange and red emissions. These blue UC emissions centered at ~440 nm and ~488 nm below 5.79 W may be attributed to $^2P_{1/2}\rightarrow{}^4I_{9/2}$ and $^2G_{9/2}\rightarrow{}^4I_{9/2}$ transitions of Nd^{3+} ion, respectively, and they completely disappear at 5.79 W. The possible energy transitions for green UC band centered at ~542 nm may be $^2G_{7/2}\rightarrow{}^4I_{9/2}$ transition of Nd^{3+} and the band disappeared above 5.79 W output power of laser. Above 5.79 W, the emission at ~568 nm may be due to $^2G_{5/2}\rightarrow{}^4I_{9/2}$ transition. The orange band at ~602 nm due to $^4G_{5/2}+{}^2G_{7/2}\rightarrow{}^4I_{9/2}$ transition starts to appear as a shoulder at 5.79 W with increasing effects of thermal processes. The broader red UC emission centered at ~693 nm, which can be attributed to $^4F_{7/2}+{}^4S_{3/2}\rightarrow{}^4I_{9/2}$ transition of Nd^{3+} ions, shifts to 702 nm for higher excitation power values. The sharp lines between 714 nm and 775 nm (or ~758 nm) may be due to $^4F_{5/2}+{}^2H_{9/2}\rightarrow{}^4I_{9/2}$ transitions for all excitation powers. The visible light for the sample was white light based on upconversion mechanism below laser output power of 5.79

W and the sample emitted very intense candle like a white light with the emissions of Nd^{3+} ion above 5.79 W.

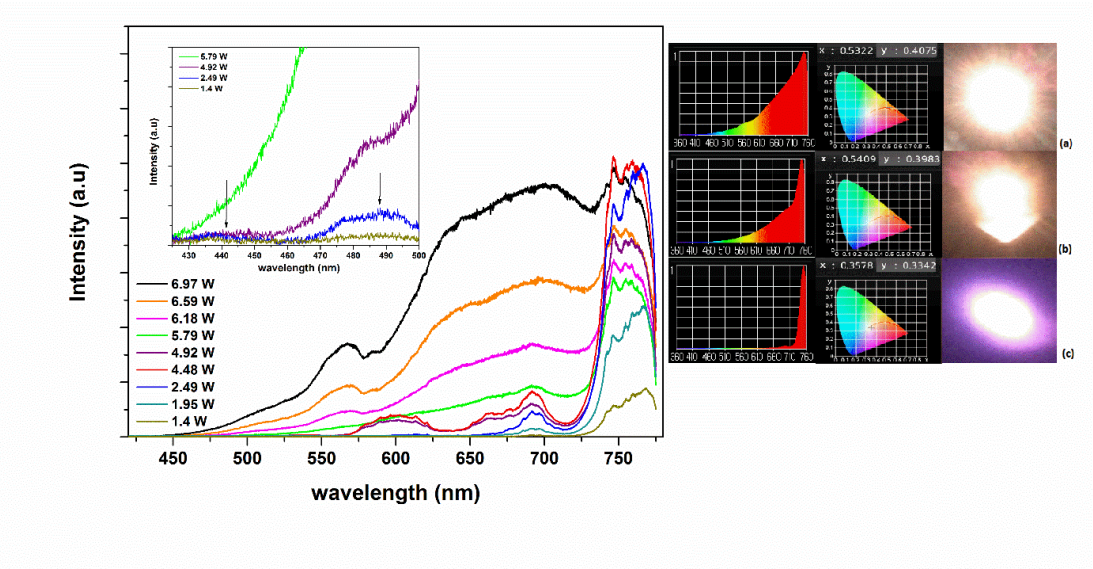

Figure 5.2 : Luminescence spectra of 1% Nd^{3+} doped yttrium silicate nanophosphor depending on power at atmospheric conditions. Chromaticity values (x, y) were given for a) 6.97 W b) 5.79 and c) 1.4 W.

For the luminescence characteristics, host matrix, defects, and dopant ions are very important and from Figure 5.2, it is shown that there is shifting for locations of the maximum emissions intensities with an increasing output power of the laser. Thus, thermal processes become to affect the spectral profile of upconversion emission bands. The main reasons for these shifts may be due to the crystal field effects and the defects. Any changes of the structure of the host material can modify the energy transfer, crystal field strength, color or luminescent intensity [70]. About 585 nm, a broadband emission line instead of discrete energy levels may be mainly due to the thermal effects and defects in the material, especially at high pumping powers.

If the number of the required laser photons (n) for an upconversion emission is much larger than ~2, this illustrates that there may be a photon avalanche mechanism [71, 72]. As seen in Figure 5.3, power dependencies of the emission intensities at atmospheric conditions indicate that there is an ‘n shape’ behavior below output laser power of ~5.79W as reported by some other researches [73, 74]. However, the slope values are larger than expected (n=2) that may indicate that, below 5.79 W, a photon avalanche upconversion mechanism together with thermal processes occur instead of conventional two or three photon absorptions at green ~542 and red ~758 nm bands [75-77].

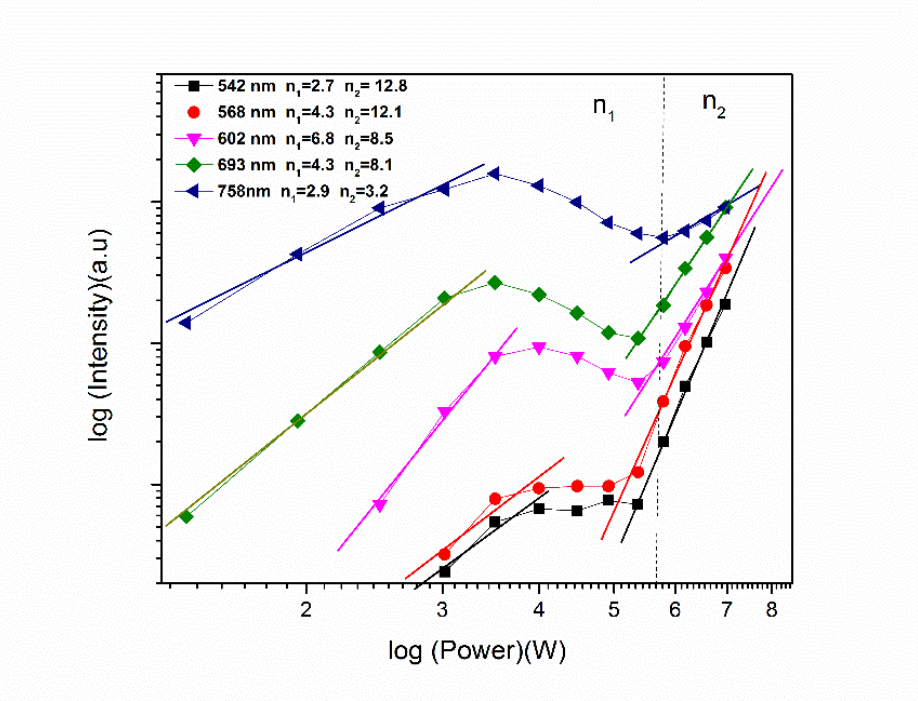

Figure 5.3 : Double logarithmic representation for 1% Nd^{3+} doped yttrium silicate nanopowder at atmospheric conditions.

The broad bands are possibly affected by a photon avalanche population process because of cross-relaxation processes provided that excitation power is high. Five intensive bands centered at ~542, ~568, ~602, ~693 and ~758 nm were reported to be due to multiphoton processes requiring three, four or seven photon absorptions. Apart from these, thermal effects and photon avalanche mechanism due to the combination of ground state absorption, excited state absorption, and cross relaxation processes take longer times [78, 79]. This behavior is in good agreement with long decay and rise patterns at 692 nm, as shown in Figures 5.4a and 5.4b. These patterns give some information about both the thermal nature of the process and emission mechanisms [79, 80]. In Figure 5.4a, it is shown that decay patterns seemed to increase in length with an increasing output power of the laser. The rise patterns measured were found to be very complicated with output powers and they were shorter for higher laser powers (Figure 5.4b). This anomalous behavior at a lower time scale was also observed in several other studies [80-82] and it may be due to being together of photon avalanche upconversion processes and thermal effects to form white light.

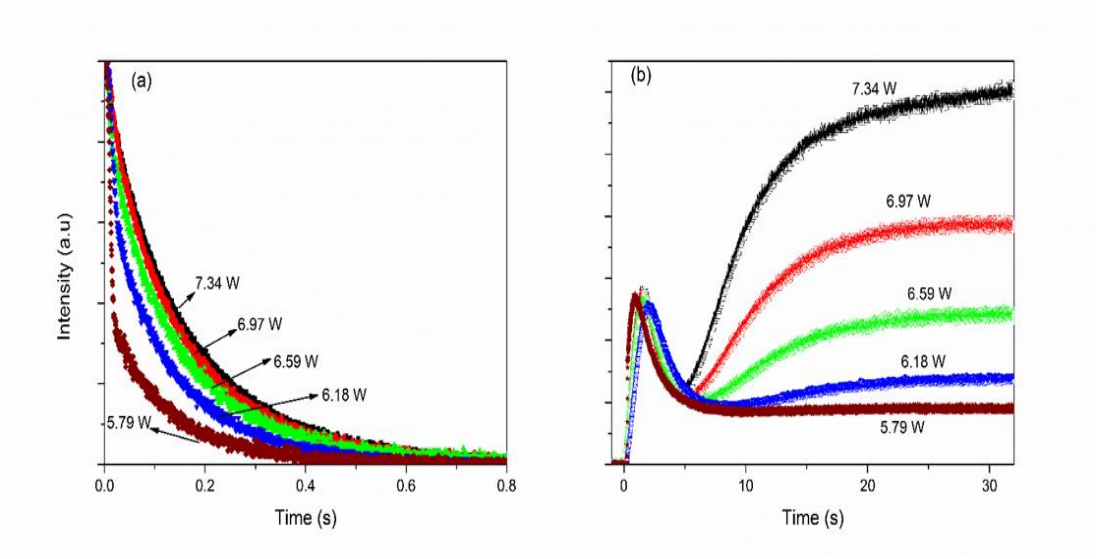

Figure 5.4 : a) Decay; b) Rise patterns at 692 nm for 1% per mole Nd^{3+} doped yttrium silicate nanopowder depending on output power at atmospheric conditions.

5.1.4 Luminescence properties at vacuum conditions

Luminescence properties of the sample were investigated under vacuum (0.01 mbar). In Figure 5.5, white light generation is shown with the emissions of Nd^{3+} ions. The inset figure shows emissions from UC white light to thermal white light at definite pumping powers. The very weak emission centered at ~482 nm due to $^2G_{9/2} \rightarrow {}^4I_{9/2}$ transition starts to disappear above ~3.51 W. The shoulders centered at wavelengths above ~532 nm due to several Nd^{3+} transitions start broadening in-homogeneously above ~4.48 W because of the thermal effects. The broadband peaks at ~605 nm, ~666 nm, and ~748 nm may be due to $^4G_{5/2}+{}^2G_{7/2} \rightarrow {}^4I_{9/2}$, $^4F_{9/2} \rightarrow {}^4I_{9/2}$ and $^4F_{5/2}+{}^4S_{3/2} \rightarrow {}^4I_{9/2}$, transitions of Nd^{3+}, respectively. The pumping power dependence shows that slope values are extremely high (n=5 or 6) and this may indicate that the avalanche mechanism is still occurring (Figure 5.6). The broadband is possibly affected by a photon avalanche population process because of cross-relaxation processes if the excitation power is high. The luminescence dynamics were investigated by measuring the rise and decay intensity patterns in vacuum (Figure 5.7). The decay patterns have similar characteristics at 605 and 666 nm and they were not strongly dependent on output powers of laser in vacuum conditions. However, the rise patterns measured as a function of the output power of laser were found to be very complicated in shape, as they were in atmospheric conditions (Figure 5.4).

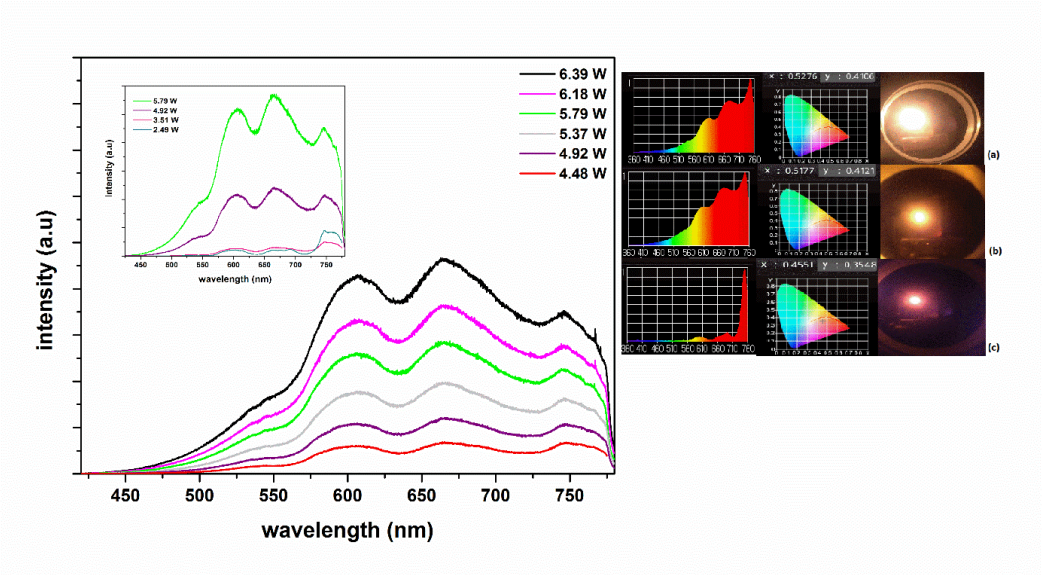

Figure 5.5 : Emission spectra of 1% Nd^{3+} doped yttrium silicate nanophosphor depending on power at 0.01 mbar. Chromaticity values (x, y) were given for a) 5.79 W and b) 3.51 W and c) 1.4 W.

The rise patterns at 605 nm are shorter than that of it is at 666 nm and longer with decreasing output power of the laser. The reason for this unusual characteristic may be due to thermal processes and the effect of superposition of Nd^{3+} emissions.

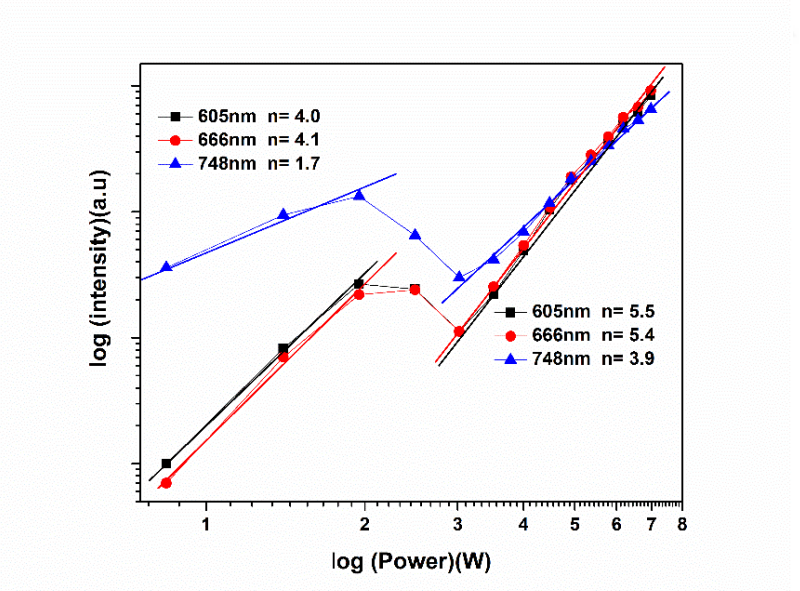

Figure 5.6 : Double logarithmic representation of 1% Nd^{3+} doped yttrium silicate nanopowder at vacuum (0.01 mbar).

The decay and rise patterns last several seconds, and it gives additional evidence for the thermal nature of the process as at atmospheric pressure. It is also seen that the atmospheric condition decay patterns are shorter than those at vacuum conditions

(Figure 5.4 and Figure 5.7). The extraordinary behavior at lower times was also shown at vacuum like measurements in atmospheric conditions.

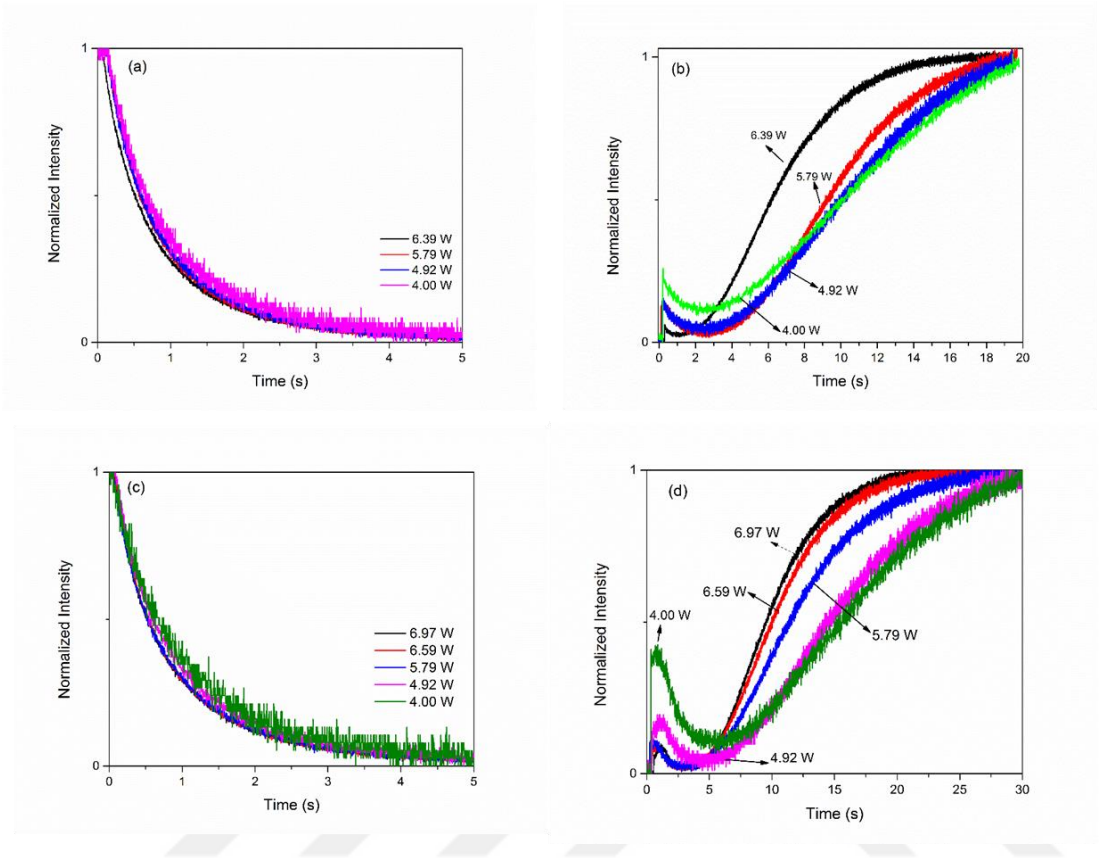

Figure 5.7 : a) Decay; b) rise patterns at 605 nm and c) decay d) rise patterns at 666 nm for 1% per mole Nd^{3+} doped yttrium silicate depending on output power at vacuum.

The illuminance meter measurements show that color temperatures of 1% Nd^{3+} doped sample at both atmospheric and vacuum conditions were candle like white for high output laser powers, as shown in Table 5.1. However, when laser output power was decreased, the Correlated Color Temperature values were generally increased according to CIE 1931. The emitted color by sample converted from candle like 'warm white' to 'incandescent lamp like white' and 'cool white' from high to low output powers of the laser. Accordingly, the Color Rendering Indices (CRI) values show that the emitted light was more stable at vacuum conditions when compared with the atmospheric pressure results.

Table 5.1 : The CIE 1931 (x, y) coordinates for 1% Nd^{3+} doped sample at 808 nm excitation.

At atmospheric Pressure			
Output Power (W)	CCT(K)	CRI(Ra)	CIE coordinates
6.97	1978	95	(0.5264, 0.4093)
6.59	1921	95	(0.5322, 0.4075)
6.18	1855	96	(0.5380, 0.4040)
5.79	1801	96	(0.5409,0.3983)
5.37	1799	94	(0.5319, 0.3869)
4.92	1946	85	(0.5022, 0.3726)
4.48	1984	78	(0.4972,0.3718)
4	1895	75	(0.5101,0.3751)
3.51	1798	74	(0.5255,0.3789)
3.02	1775	76	(0.5296, 0.3800)
2.49	2247	85	(0.4716, 0.3721)
1.95	3522	83	(0.3897, 0.3510)
1.4	4411	88	(0.3578,0.3342)
0.84	4777	89	(0.3477, 0.3261)
At vacuum			
Output Power (W)	CCT(K)	CRI(Ra)	CIE coordinates
6.97	2068	90	(0.5177, 0.4121)
6.59	2027	89	(0.5226, 0.4122)
6.18	2000	88	(0.5253, 0.4116)
5.79	1976	88	(0.5276, 0.4106)
5.37	1947	87	(0.5298, 0.4089)
4.92	1920	87	(0.5310, 0.4059)
4.48	1904	86	(0.5281, 0.3995)
4	1937	87	(0.5173, 0.3910)
3.51	2068	87	(0.4911, 0.3757)
3.02	2484	88	(0.4419, 0.3543)
2.49	2925	87	(0.4097, 0.3408)
1.95	2778	84	(0.4197, 0.3461)
1.4	2307	78	(0.4551, 0.3548)
0.84	3489	85	(0.3832, 0.3305)

When we notice to the results obtained at atmospheric pressure and vacuum, the luminescence profile of Nd^{3+} doped yttrium silicate powder can be affected by the change of pressure. These changes at different pressures are mainly due to the changes in the crystal field, not the energy transitions of the Nd^{3+}. When the Nd^{3+} ion is embedded into the host, the lattice rearrangements occur and perturbations appear between the dopant ion and its neighborhood [83, 84]. The crystal field perturbations depend on the distance between ions, the conformity of the ionic radii between the dopant and host cation, the geometrical configuration of the ions and electronic shielding [84, 85]. The pressure changes affect the distance between ions, the strength,

and the symmetry of the crystal field as well as the crystal field perturbations. Thus, these perturbations may play an important role in the crystal structure and can cause the changes in relative intensities, spectral shifts on the luminescence profile. The previous studies indicated that high pressures can also cause changes in the host structure completely and so luminescence properties [85, 86]. The pressure affects the luminescence properties due to all of these modifications and distortions in the local symmetry in the lattice surrounding the dopant ions.

Table 5.2 summarizes the number of required laser photons (n) for different transitions, as obtained using the slope of the log I versus log P at two different pressures. For the Nd^{3+} doped sample, the green band centered at ~542 nm and green-yellow band centered at ~568 nm, the orange band centered at ~602 nm and red bands at ~693 nm require ~three, four, seven, four photons absorption at atmospheric pressure, respectively. Above ~5.79 W, n values increase due to the effects of growing of photon avalanche with thermal processes. The upconversion mechanism with three-photon absorption is more efficient at the $^4F_{5/2}+^2H_{9/2}\rightarrow{}^4I_{9/2}$ transition (~758 nm). The $^4G_{5/2}+^2G_{7/2}\rightarrow{}^4I_{9/2}$ transition at ~602 nm requires less photon at vacuum conditions as compared with that at atmospheric pressure.

In conclusion, white light based on both UC emission and thermal processes was obtained at atmospheric and vacuum conditions for diode laser excitation of 808 nm. Several emission bands at low pumping powers (below 5.79 W) due to energy levels of the Nd^{3+} doped samples were observed at atmospheric pressure. The photon avalanche mechanism with thermal processes for white light spectra is more effective at high pumping powers. In the vacuum (0.01 mbar), the spectrum consists of a thermal white light above ~3.51 W and presents peaks corresponding to Nd^{3+} transitions. While the emitting light was candle like white light at high powers, it was upconverted white light at low powers for both conditions. The illuminance meter measurements show that color temperatures of the 1% Nd^{3+} doped sample at both atmospheric and vacuum were close to incandescent lamps for high output laser powers. However, these values were increased for low output laser powers according to CIE 1931.

Table 5.2 : The list of the n values for Nd^{3+} doped sample at atmospheric pressure and vacuum under 808 nm excitation.

Atmospheric Condition			
		Power <5.79W	Power >5.79W
λ (nm)	Transition	n_1	n_2
542	$^2G_{7/2}\rightarrow{}^4I_{9/2}$	2.7	12.8
568	$^2G_{5/2}\rightarrow{}^4I_{9/2}$	4.3	12.1
602	$^4G_{5/2}+{}^2G_{7/2}\rightarrow{}^4I_{9/2}$	6.8	8.5
693	$^4F_{7/2}+{}^4S_{3/2}\rightarrow{}^4I_{9/2}$	4.3	8.1
758	$^4F_{5/2}+{}^2H_{9/2}\rightarrow{}^4I_{9/2}$	2.9	3.2
Vacuum Condition			
		Power <3.51W	Power >3.51W
λ (nm)	Transition	n_1	n_2
605	$^4G_{5/2}+{}^2G_{7/2}\rightarrow{}^4I_{9/2}$	4.0	5.5
666	$^4F_{9/2}\rightarrow{}^4I_{9/2}$	4.1	5.4
748	$^4F_{5/2}+{}^4S_{3/2}\rightarrow{}^4I_{9/2}$	1.7	3.9

It is a valuable result that upconverted white light from the blue, green and red region from a single dopant (Nd^{3+}) is obtained below ~5.79 W and ~3.51 W for atmospheric pressure and vacuum, respectively. The long decay and rise patterns gave evidence for the thermal nature of the processes. This compound could be a white light source for usage in many scientific and industrial applications.

5.2 Tm^{3+} Doped Yttrium Silicate Nano-Powders:

Thulium (Tm^{3+}) ion has a strong absorption near 800 nm and exhibits emissions from near infrared to ultraviolet region. It has a wide application area, for example, $^3F_4\rightarrow{}^3H_6$ transition of Tm^{3+} ion has applications in medicine and remote sensing of the atmosphere (LIDAR devices). In addition, $^1D_2\rightarrow{}^3F_4$ and $^3H_4\rightarrow{}^3F_4$ transitions are used for high capacity data storage optical devices and S-band (1460–1530 nm) amplification (TDFAs) in optical telecommunication, respectively [87-88]. Herein, upconversion properties of yttrium silicate (Y_2O_3: SiO_2) nanopowders doped with different concentrations (0.5%, 1% and 0.25 % per mole) of Thulium (III) (Tm^{3+}) rare earth ions have been demonstrated at various pumping powers. The samples were annealed at 1250^0C during 12 h. Luminescence properties of prepared 0.5% per mole Tm^{3+} doped sample (HT1) was investigated at atmospheric and vacuum conditions. In addition, 1% per mole Tm^{3+} doped (HT2) and 0.25% per mole Tm^{3+} doped (HT3) samples were compared with HT1 sample at atmospheric conditions. The emissions

due to the energy transfers of appropriate dopants were observed when the samples were excited by a diode laser excitation of 808 nm.

5.2.1 Structural analyses of the Tm^{3+} doped samples

The phase identification of the obtained samples was performed on X-ray powder diffractometer (XRD). Figure 5.8 shows the XRD patterns of the powders and according to the Joint Committee on Powder Diffraction Data, all powders mostly contain peaks corresponding to the triclinic α-$Y_2Si_2O_7$ phase with the card number 38-0223.

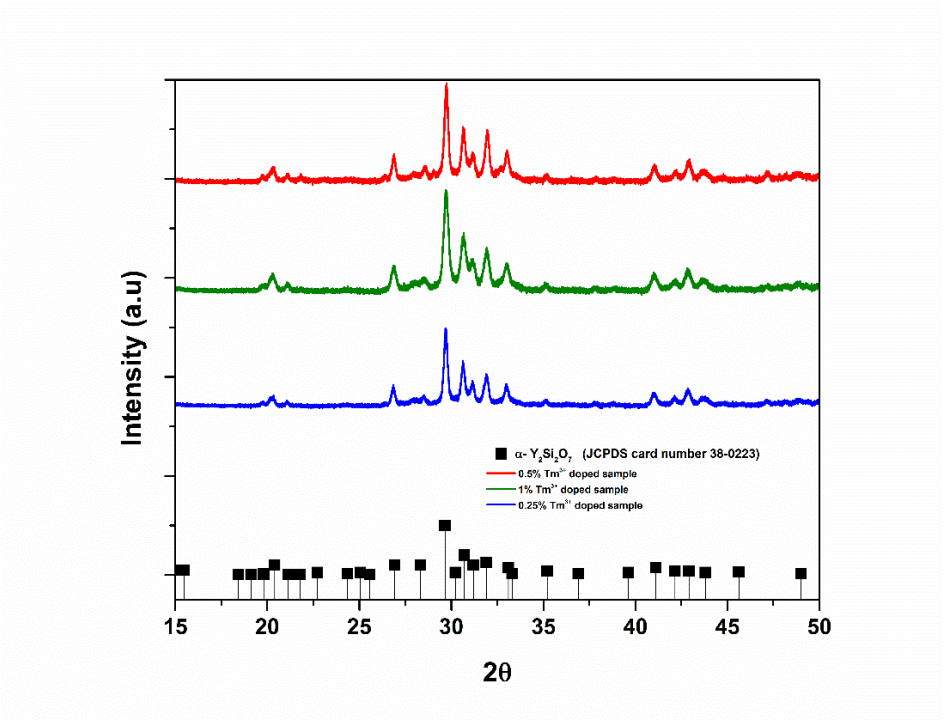

Figure 5.8 : XRD patterns of Tm^{3+} doped α-$Y_2Si_2O_7$ nanophosphors annealed at 1250 °C for 12 h.

Average crystalline sizes were estimated by the Scherer equation and were found to be ~62 nm, ~45 nm, ~59 nm for 0.5%, 1%, 0.25 % Tm^{3+} doped powders, respectively. The representative SEM images for the samples were shown in Figure 5.9 for 1% Tm^{3+} doped sample. It can be seen that the particles were observed as granular-like nanoparticles and the polycrystals formed by agglomeration are shown in Figure 5.9. The role of dopant concentration and excitation wavelength on upconverted luminescence property of Tm^{3+} doped nanocrystals are investigated in literature [89,90], we observed for the low concentration of Tm^{3+} ion that there were no changes for crystal structure.

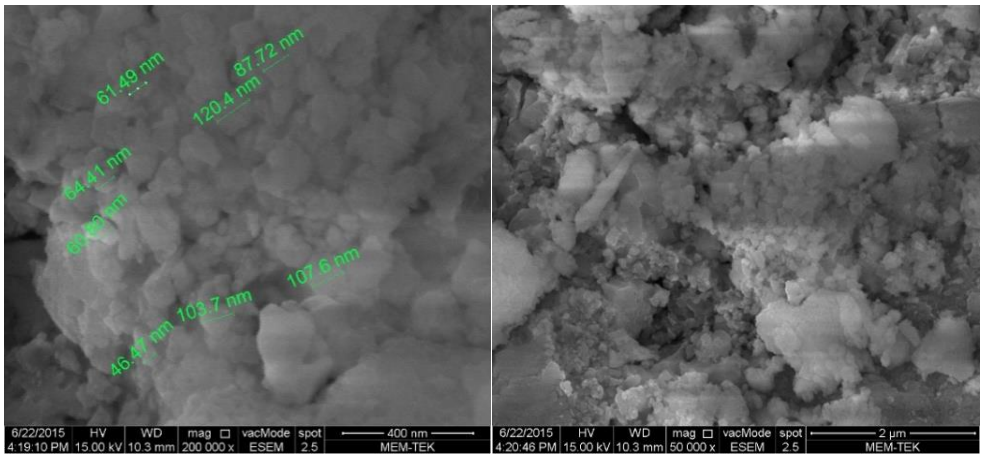

Figure 5.9 : A representative example for Scanning Electron Microscopy images, 1% Tm^{3+} doped nanophosphor.

All the powders are composed of agglomerates of particles of different sizes and shapes forming a highly porous material.

5.2.2 Luminescence properties of Tm^{3+} doped samples

The sol-gel synthesized Tm^{3+} doped yttrium silicate nanophosphors showed the intense upconversion luminescence under excitation by a NIR laser (808 nm). The emission characteristics of all samples are similar with only differences in relative peak intensities. Figure 5.10 shows the luminescence spectra of the 0.5% Tm^{3+} doped sample (HT1) with depending on excitation laser powers at atmospheric conditions.

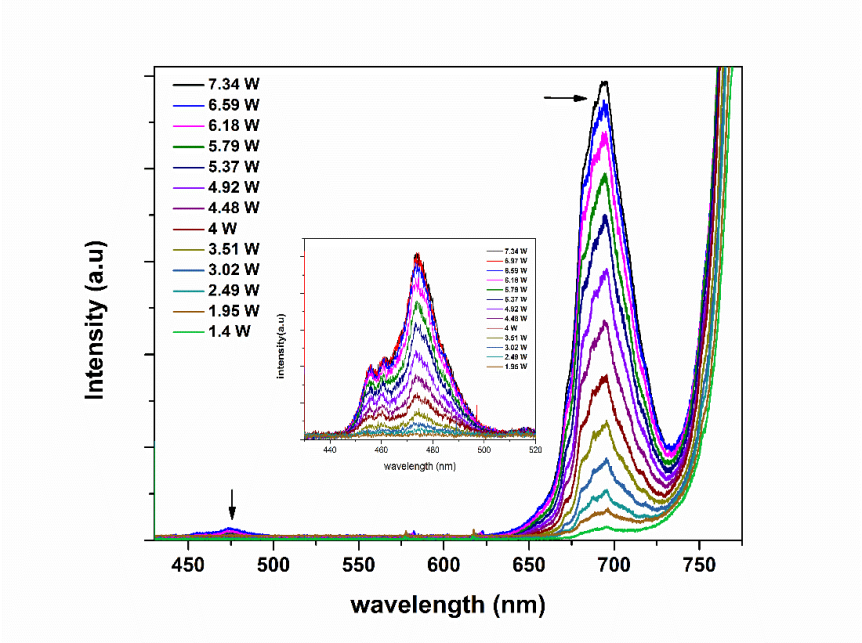

Figure 5.10 : The luminescence profile of the 0.5% per mole Tm^{3+} doped Yttrium silicate sample at atmospheric conditions.

The peaks centered at ~475 nm and ~695 nm may be due to $^1G_4 \rightarrow {}^3H_6$ and $^3F_3 \rightarrow {}^3H_6$ transitions of Tm^{3+} ion, respectively. The pump power dependence of emission bands at 475 and 695 nm was investigated, and the result is shown in Figure 5.11 at atmospheric pressure.

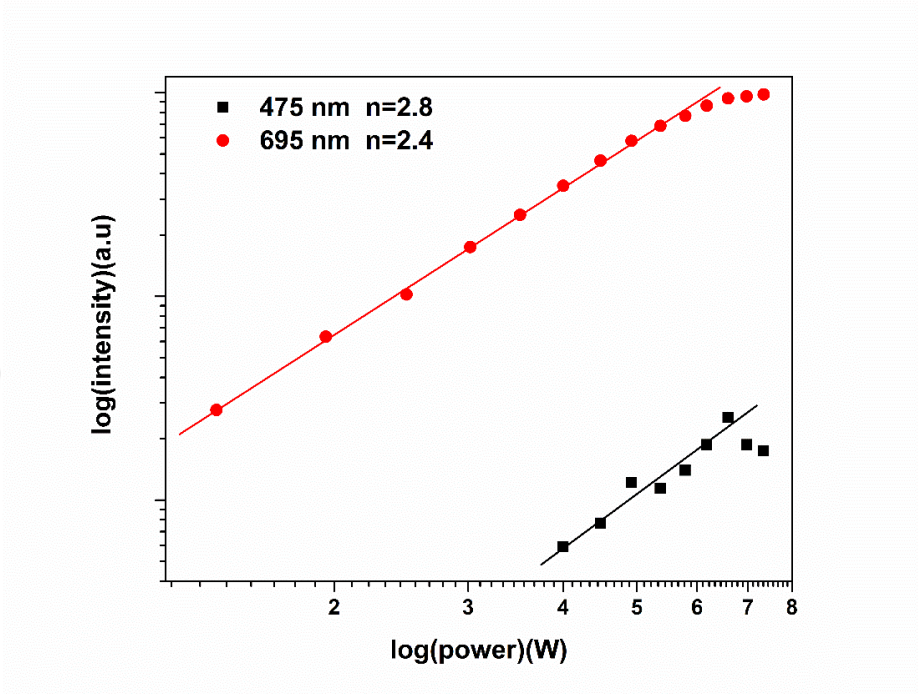

Figure 5.11 : Log-log plot of the 0.5% per mole Tm^{3+} doped Yttrium silicate sample at atmospheric conditions.

The experimental data for these two emission bands have been fitted with a straight line. The slopes were found ~2 which confirms that these emission lines have two-photon absorption processes.

The luminescence spectra for 0.5% Tm^{3+} doped yttrium silicate was also measured at vacuum ($1x10^{-5}$ mbar) and the results were shown in Figure 5.12. The only spectral difference between atmospheric and vacuum case is that there is a wide shoulder between 450 nm and 650 nm at vacuum. The pump power dependence of the emission bands was again analyzed for vacuum case with little shifting wavelengths of peaks (476 and 694 nm) when comparing with the atmospheric pressure case (Figure 5.13).

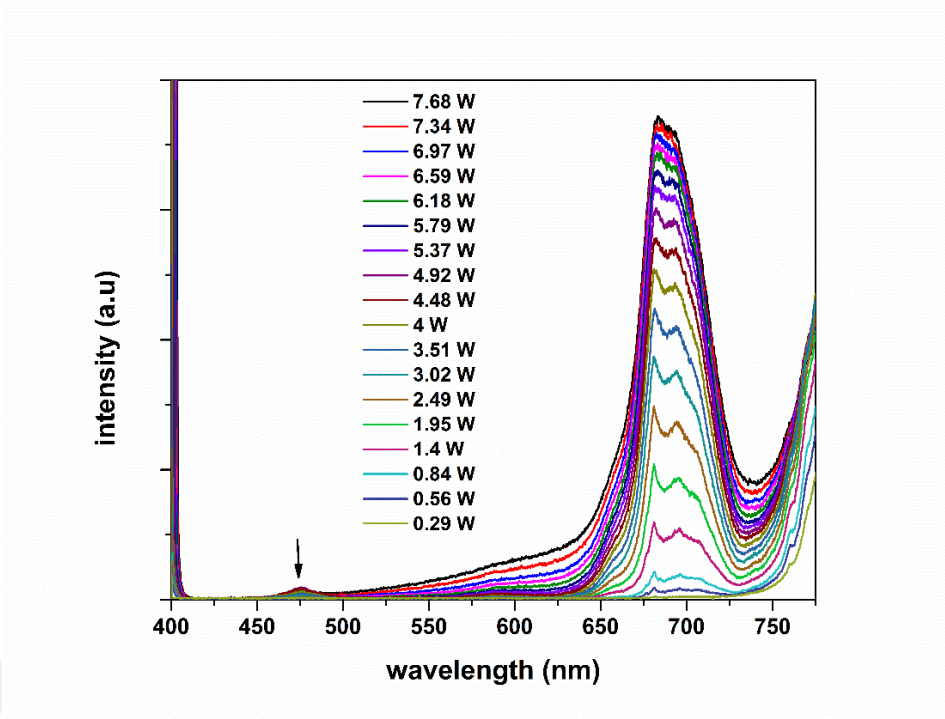

Figure 5.12 : The luminescence profile of the 0.5% per mole Tm^{3+} doped Yttrium silicate sample at vacuum (10^{-5} mbar).

The slope was again near 2. Table 5.3 shows the CIE-1931 chromaticity values of HT1 sample at various pumping powers under vacuum and atmospheric conditions.

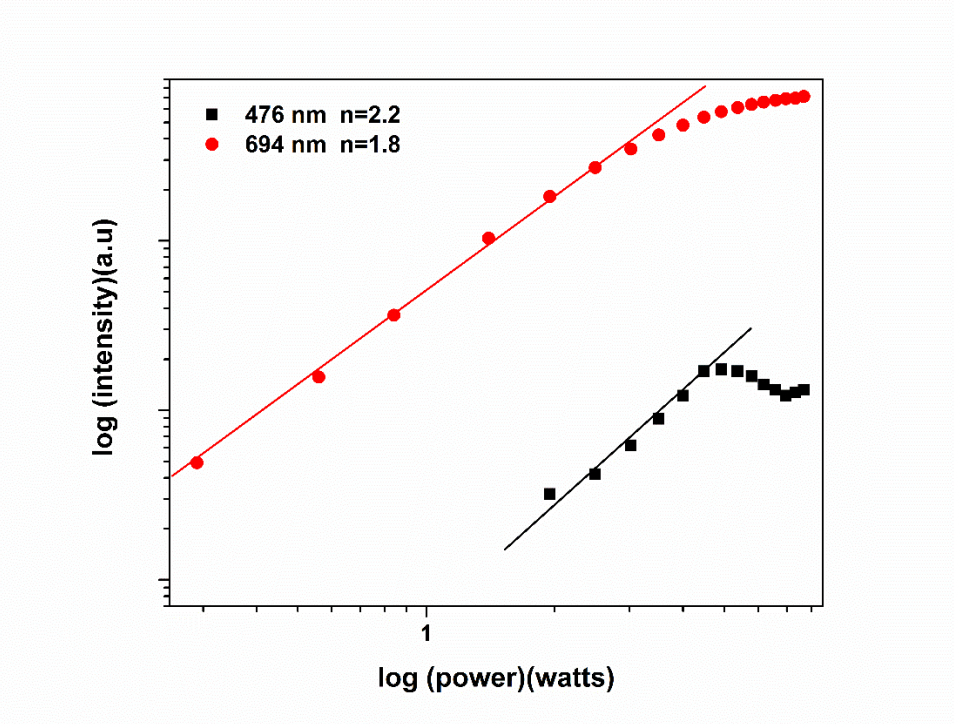

Figure 5.13 : Log-log plot of the 0.5% per mole Tm^{3+} doped Yttrium silicate sample at vacuum.

Figure 5.14 shows the luminescence spectra of HT2 and HT3 samples at atmospheric conditions with the excitation of 808 nm. It is shown that the spectra are very similar to each other. We can say that luminescence behaviors of Tm^{3+} doped yttrium silicate samples are similar when the concentration of Tm^{3+} is low. Upconversion emissions due to the energy transitions of Tm^{3+} ions were obtained for samples at atmospheric conditions under 808 nm excitation.

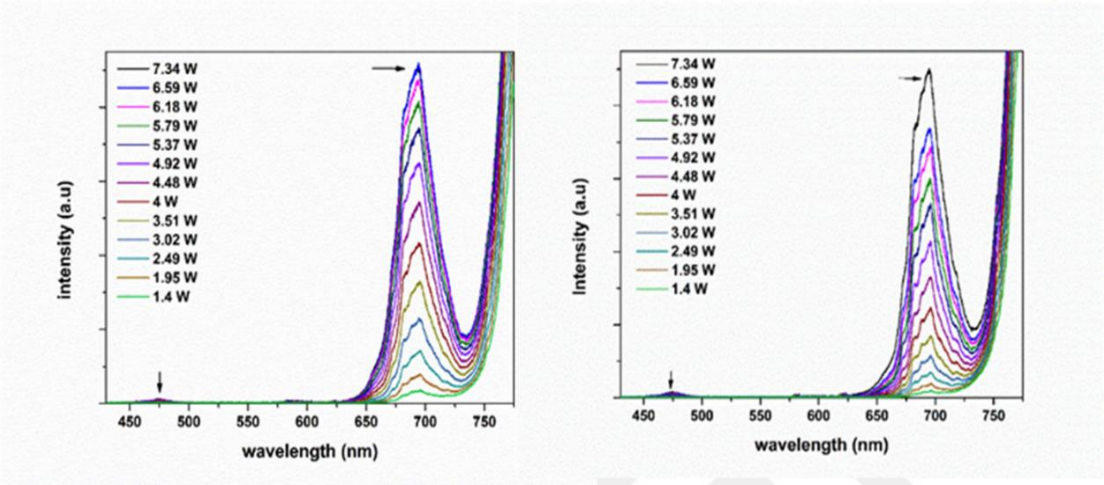

Figure 5.14 : The luminescence profile of the a) 1% per mole Tm^{3+} (HT2) and b) 0.25% per mole Tm^{3+} (HT3) doped yttrium silicate sample at atmospheric condition.

Table 5.3 : The illuminance meter results and the corresponding photos of the emission for the 0.5 % Tm^{3+} doped yttrium silicate sample.

at atmospheric pressure

Power (W)	CIE 1931 coordinates (x, y)	CCT(K)	CRI(Ra)	Illuminance meter spectrum	Image of the emission
7.34	(0.3438, 0.3107)	4876	82	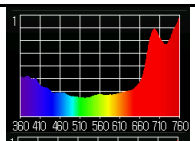	
5.79	(0.3437, 0.3130)	4894	84	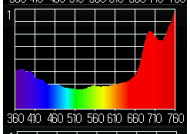	
4.0	(0.3441, 0.3166)	4895	86	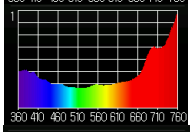	
1.95	(0.3452, 0.3207)	4862	88	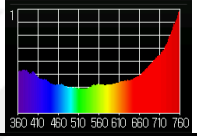	

at vacuum (10^{-5} mbar)

Power (W)	CIE 1931 coordinates (x, y)	CCT(K)	CRI(Ra)	Illuminance meter spectrum	Image of the emission
7.34	(0.4043, 0. 3408)	3044	82	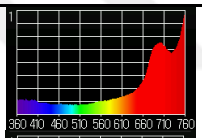	
5.79	(0.3724, 0.3261)	3794	81	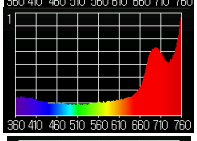	
4.0	(0.3562, 0.3211)	4371	83	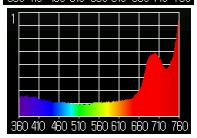	
1.95	(0.3502, 0.3239)	4655	86	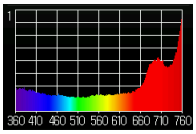	

Double log representation of the intensity-power is also similar for the samples as seen in Figure 5.15.

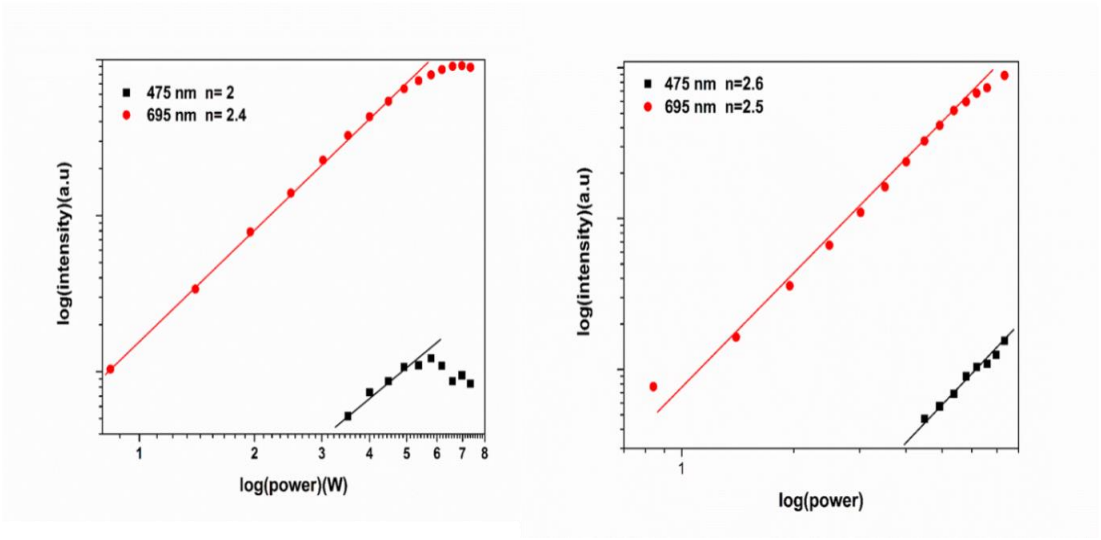

Figure 5.15 : The log plot of the a) 1% per mole Tm^{3+} and b) 0.25% per mole Tm^{3+} doped yttrium silicate sample at atmospheric condition.

Table 5.4 shows the chromaticity coordinates, CCT and CRI values depending on the pumping powers at atmospheric conditions according to CIE 1931.

Table 5.4 : The CIE 1931 (x, y) coordinates for the 1% per mole Tm^{3+} doped (HT2) and 0.25% per mole Tm^{3+} doped (HT3) samples at atmospheric pressure with 808 nm excitation.

HT2			
Output Power (W)	CCT(K)	CRI	CIE coordinates
7.34	4398	81	(0.3553, 0.3195)
6.97	4446	82	(0.3543, 0.3199)
6.59	4471	82	(0.3538, 0.3201)
5.79	4545	83	(0.3521, 0.3204)
4.92	4631	85	(0.3503, 0.3209)
4	4704	86	(0.3489, 0.3225)
3.02	4766	88	(0.3477, 0.3240)
1.95	4788	89	(0.3474, 0.3254)
1.4	4791	89	(0.3474, 0.3256)
HT3			
Output Power (W)	CCT(K)	CRI	CIE coordinates
7.34	4918	75	(0.3420,0.3009)
6.59	4899	76	(0.3424, 0.3019)
5.79	4909	77	(0.3425, 0.3040)
4.92	4957	80	(0.3420, 0.3076)
4	4932	83	(0.3428, 0.3115)
3.02	4908	87	(0.3441, 0.3195)
1.4	4868	88	(0.3452,0.3215)

5.3 Yb^{3+} Doped Yttrium Silicate Nano-Powders

Ytterbium (III) ion is one of the most promising rare earth ions that has been used for photonic applications in different host materials. The Yb^{3+} ion has several advantages for spectroscopic properties due to its simple energy level configurations, no cross relaxation process and suitability of it broad absorption lines for infrared laser diode excitation. In RE systems, Yb^{3+} is generally used as a sensitizer of energy transfer for infrared to visible upconversion lasers, because it has a simple electronic structure with a large energy gap between its ground ($^2F_{7/2}$) and excited ($^2F_{5/2}$) states that splits into the Starks levels when doped in a matrix. The Yb^{3+} ions are used as sensitizers in the upconversion process, which do not necessarily contribute to the overall white light emission [91, 92].

In this part of the thesis, we have reported that white light generation from Yb^{3+} doped yttrium silicates in various concentrations. We observed several emission bands due to Er^{3+} impurities due to technological reasons at low pumping power spectra and many Stark levels also appeared in the spectra because of the local disorder around Yb^{3+} ions in yttrium silicate host. Although Yb^{3+} ions have no emission in visible range according to Dieke diagram, UC mechanism responsible for blue emission is a two-photon absorption process and is ascribed to cooperative luminescence from Yb^{3+}-pairs. Broadband WL generated in samples may be due to thermal emissions. The intensity of WL is highly nonlinear with excitation power. The luminescence characteristics of the samples showed blue-green UC characteristics and transitions of unwanted Er^{3+} impurities at 'low' pumping power values between 0.38 W- 2.94 W, 0.38 W- 2.33 W, 0.12 W- 0.92 W, 0.12 W- 1.06 W for 1%, 2%, 5% and 10% Yb^{3+} doped samples, respectively. When the concentration of Yb^{3+} increases, blue light becomes visible at lower power values. When the pumping power was increased, white light spectra were obtained from all samples. The threshold power to obtain white light spectra decreased by increasing Yb^{3+} concentration and the generation of white light is strongly dependent on Yb^{3+} concentration. We observed that the higher is the dopant concentration; the lower is the power at which white light appears. The increase of Yb^{3+} concentration causes a shift of the peak of white light to a high-energy region.

5.3.1 Structural analyses of the Yb^{3+} doped samples

Structural and morphological analyses of the Yb^{3+} doped samples were performed by using different analytic techniques such as XRD, SEM, FTIR, TEM and EDS. The XRD patterns indicate that all nanopowders contain crystalline phases. Figure 5.16 shows the XRD patterns of 1%, 2%, 5% per mole Yb^{3+} doped and undoped yttrium silicate nanopowders to compare them. The average particle sizes were estimated as ~89 nm, ~102 nm, ~87 nm, ~86 nm for nanopowders, respectively, by using the Scherer equation. Figure 5.17a shows 10% Yb^{3+} doped sample and average particle size is estimated to be ~78 nm. According to JCPDS (Joint Committee for Powder Diffraction Data), the main structure of the samples may be found to be α-$Y_2Si_2O_7$ (triclinic, P-1(2) space group) with card number 38-0223.

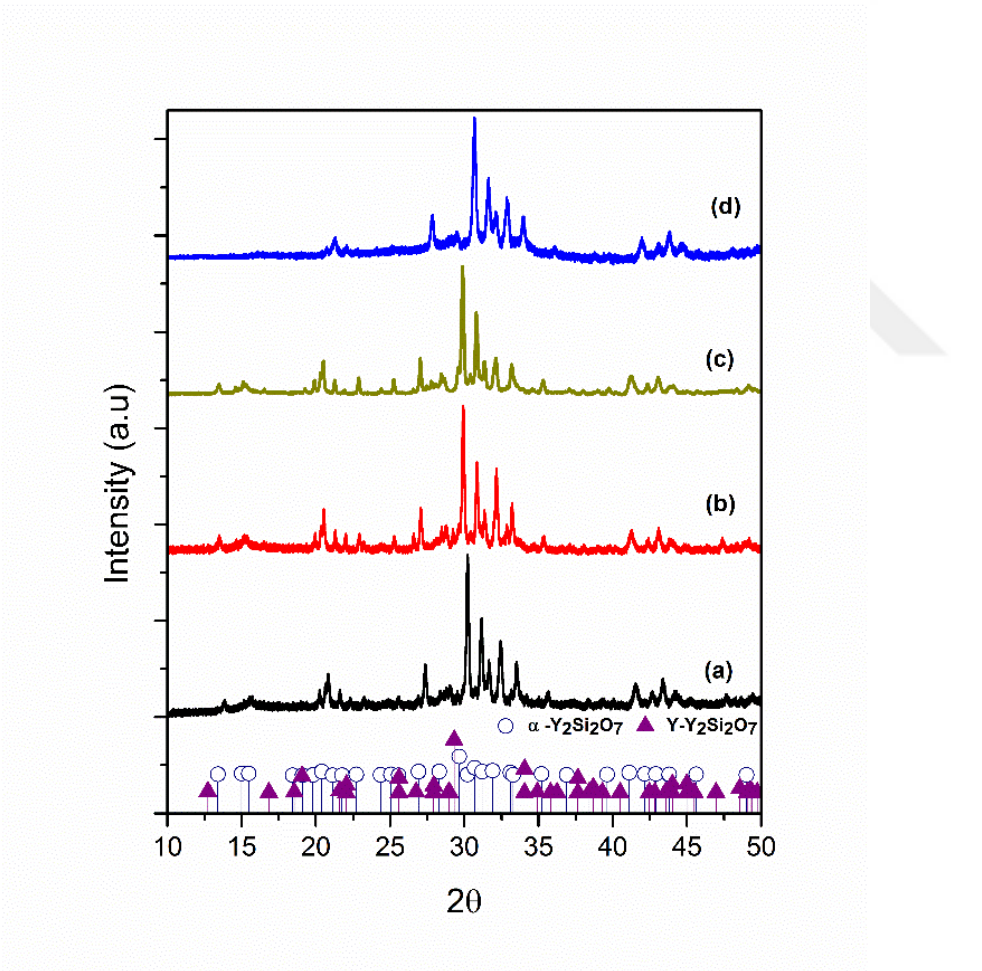

Figure 5.16 : XRD patterns of the (a) 1% per mole (b) 2% per mole and (c) 5% per mole Yb^{3+} doped and d) undoped $Y_2Si_2O_7$ nanophosphors annealed at 1250 ^{0}C for 12 h.

The doping ytterbium (1%, 2%, 5% and 10% Yb^{3+} per mole) may cause the additional peaks due to Y-$Y_2Si_2O_7$ phase with card number 74-1994 according to JCPDS. Figure 5.17b shows the XRD patterns of the 20% Yb^{3+} doped sample. The average particle size of 20% per mole Yb^{3+} doped sample was estimated ~129 nm.

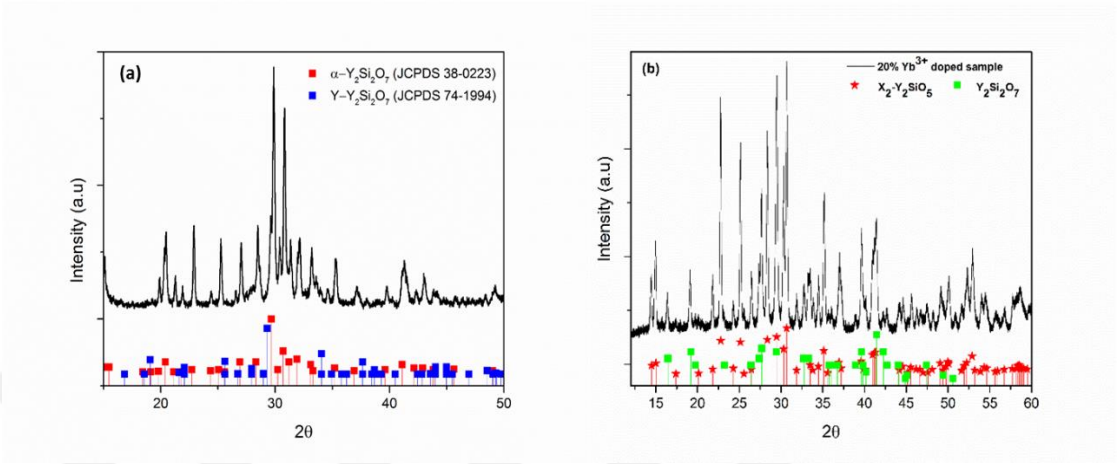

Figure 5.17 : XRD patterns of (a) 1% per mole (b) 2% per mole and (c) 5% per mole Yb^{3+} doped and d) undoped $Y_2Si_2O_7$ nanophosphors annealed at 1250 ^{0}C for 12 h.

The structure of 20% per mole Yb^{3+} doped sample is most likely X_2-Y_2SiO_5 phase with monoclinic structure in P-12(a) space group, (card number 36-1476). 20% per mole Yb^{3+} doped sample may also show Keiviite-(Y)-$Y_2Si_2O_7$ monoclinic phase with the card number 38-0440. In correspondence to 1:1 molar ratio, we can find both phases of yttrium silicate as $Y_2Si_2O_7$ and X_2- Y_2SiO_5 due to the phase diagram of Y_2O_3: SiO_2 [37]. This additional phase was identified as Y-phase of $Y_2Si_2O_7$ (PDF74-1994) and was attributed to the presence of a high concentration of Yb^{3+} ions in the host. The modification in the structure of yttrium silicate powders may cause by the similarity of the atomic radii of Yb^{3+} and the host ion material (Y^{3+} ions). It should be considered as a possible cause of modification for the structure and luminescent properties of yttrium silicate powders [61].

The Transmission Electron Microscopy (TEM) images of 5% Yb^{3+} doped yttrium silicate powder is shown in Figure 5. 18. The average crystallite size determined from TEM image was found to be about ~90 nm for powder, which are in good agreement with those obtained from the XRD spectra using the Scherer equation.

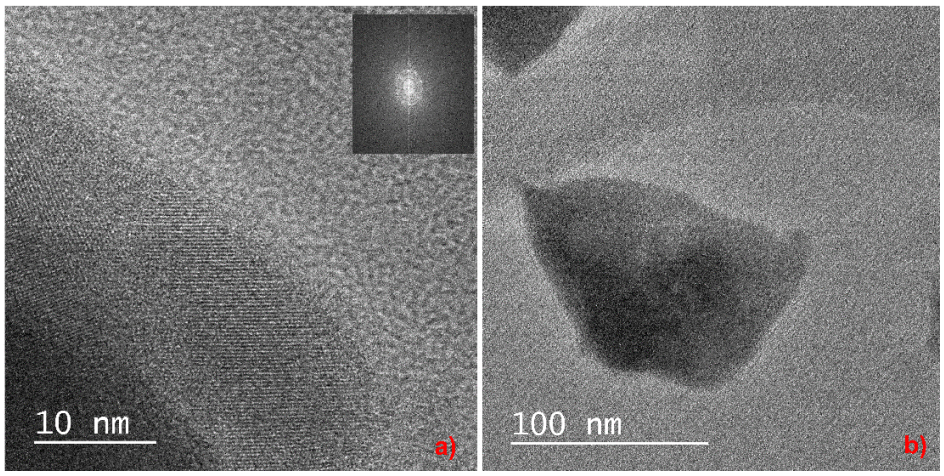

Figure 5.18 : Transmission Electron microscopy images of 5% Yb^{3+} doped $Y_2Si_2O_7$ powder with two different resolutions; a) 10 nm scale and b) 100 nm scale.

SEM images of both undoped and Yb^{3+} doped nanoparticles are presented in Figure 5.19 for comparison with undoped sample. Figure 5.19b shows partially agglomerated crystallites of observed phases from XRD spectra.

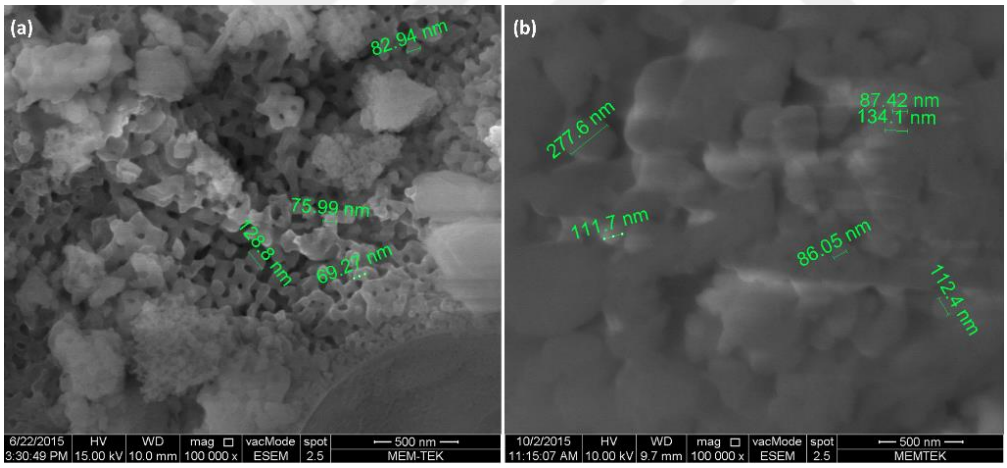

Figure 5.19 : The SEM images of undoped a) and 10%Yb^{3+} doped b) powders annealed at 1250^0C for 12h.

As seen from Figure 5.19a, undoped α-$Y_2Si_2O_7$ particles were observed as granular-like nanoparticles with the diameters of the particles ranging from 69 to 128 nm. As seen from Figure 5.19b, agglomeration increases in the presence of Yb^{3+} with the diameters of the particles range from 86 to 227 nm. The deviation in estimated sizes between the SEM images and the XRD patterns is because calculations from the XRD patterns refer to a single average crystalline size while those determined from the SEM images refer to the size of the polycrystals that are formed by agglomeration.

5.3.2 Diffusive reflectance measurements

Figure 5.20 shows absorption and diffusive reflectance spectra together of un-annealed bulk (HY) and annealed powder (HY1250) samples doped with 10% Yb^{3+}, respectively. The diffusive reflectance measurement shows that 10% Yb^{3+} doped yttrium silicate has an extremely broad spectral band in the range of 800-1100 nm. The reflectance spectral band is increasing when the concentration of Yb^{3+} ion is high in yttrium silicate host matrices.

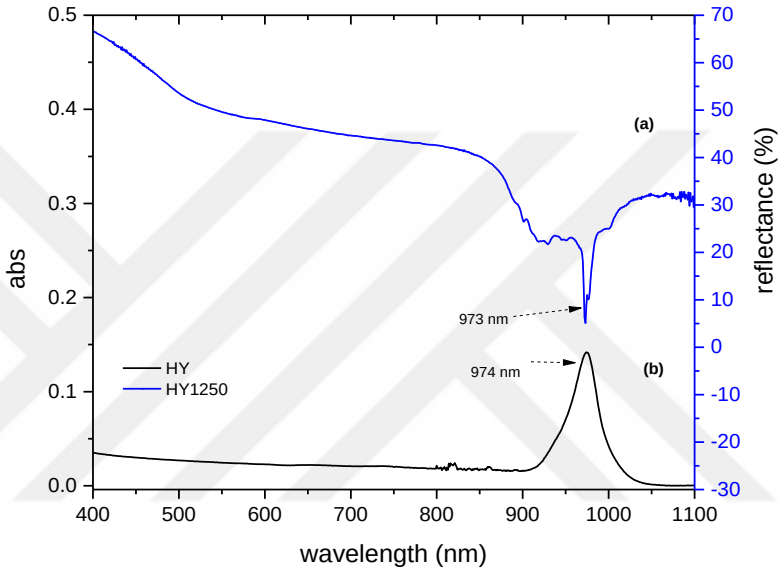

Figure 5.20 : a) The diffusive reflectance spectra of 10% Yb^{3+} doped powder sample and b) the absorption spectra of 10% Yb^{3+} doped bulk sample without heat treatment.

Figure 5.21 gives the diffuse reflectance spectra of both undoped (SY1250) and Yb^{3+} doped annealed yttrium silicate powders for comparison. The main transition is at 973 nm corresponding to $^2F_{7/2} \rightarrow {}^2F_{5/2}$ transition of Yb^{3+} ion. The main transition and Stark splits were only obtained from Yb^{3+} doped sample, not the undoped sample. We may obtain the $^2F_{7/2}$ (0) $\rightarrow {}^2F_{5/2}$ (0) main transition at 973 nm, $^2F_{7/2}$ (0) $\rightarrow {}^2F_{5/2}$ (1) transition at 951 nm and $^2F_{7/2}$ (0) $\rightarrow {}^2F_{5/2}$ (2) at 918 nm may belong to Yb^{3+} as Stark splits are seen in Figure 5.21 b. Moreover, the $^4I_{15/2}(0) \rightarrow {}^4I_{11/2}(0)$ at 1001 nm, $^4I_{15/2}(0) \rightarrow {}^4I_{11/2}(1)$ at 976 nm, $^4I\ 1_{5/2}(0) \rightarrow {}^4I_{11/2}(2)$ at 945 nm and $^4I_{15/2}(0) \rightarrow {}^4I_{11/2}(3)$ at 929 nm transitions of Er^{3+} impurities are also seen in Figure 5.21b.

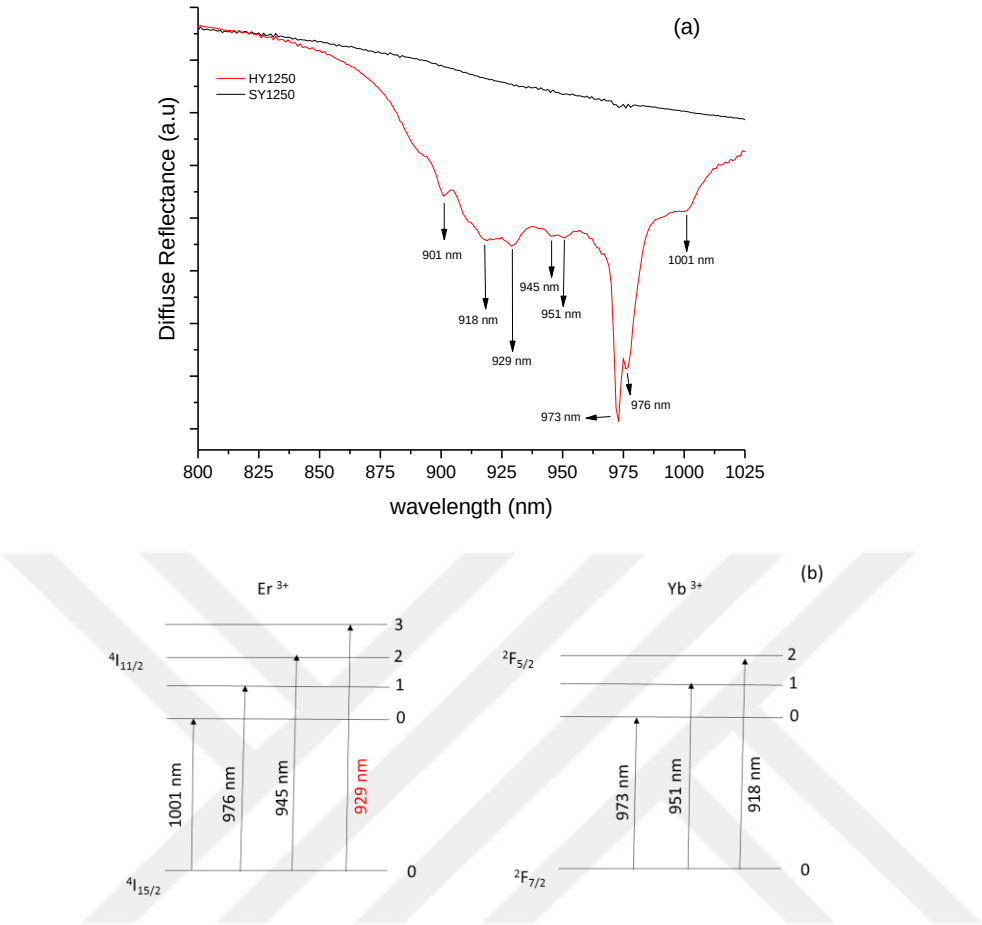

Figure 5.21 : a) The diffuse reflectance spectra of the 10% Yb^{3+} doped powder annealed at 1250 ^{0}C (HY1) and undoped annealed sample(SY1) b) possible transitions corresponding to wavelengths.

5.3.3 Luminescence properties of Yb^{3+} doped samples

The upconversion color and white light emission spectra in various concentrations of Yb^{3+} doped yttrium silicate nanopowders were measured between 450 nm and 900 nm at atmospheric pressure and vacuum (0.01 mbar) with various pumping powers. The slit of the 1 m McPherson monochromator was set at 500 μm for all samples except for 20% Yb^{3+} doped sample. The slit was changed to 20 μm because the emission was very strong and the saturation occurred due to very bright white light.

The spectra of UC are shown for 5% Yb^{3+} doped nanopowder in Figure 5.22 with 975 nm laser excitation at atmospheric pressure. The sample exhibits a luminescence emission in the blue-green region and red domain of visible spectra under the 975 nm excitation. The blue emission is a cooperative emission corresponding to the simultaneous radiative relaxation of $Yb^{3+} \rightarrow Yb^{3+}$ ion pairs around ~475 nm; the green

and red emission are due to ($^2H_{11/2}$, $^4S_{3/2}$) $\rightarrow ^4I_{15/2}$ at ~523 nm and $^4F_{9/2} \rightarrow ^4I_{15/2}$ at ~653 nm energy transitions of unwanted Er^{3+} impurities, respectively.

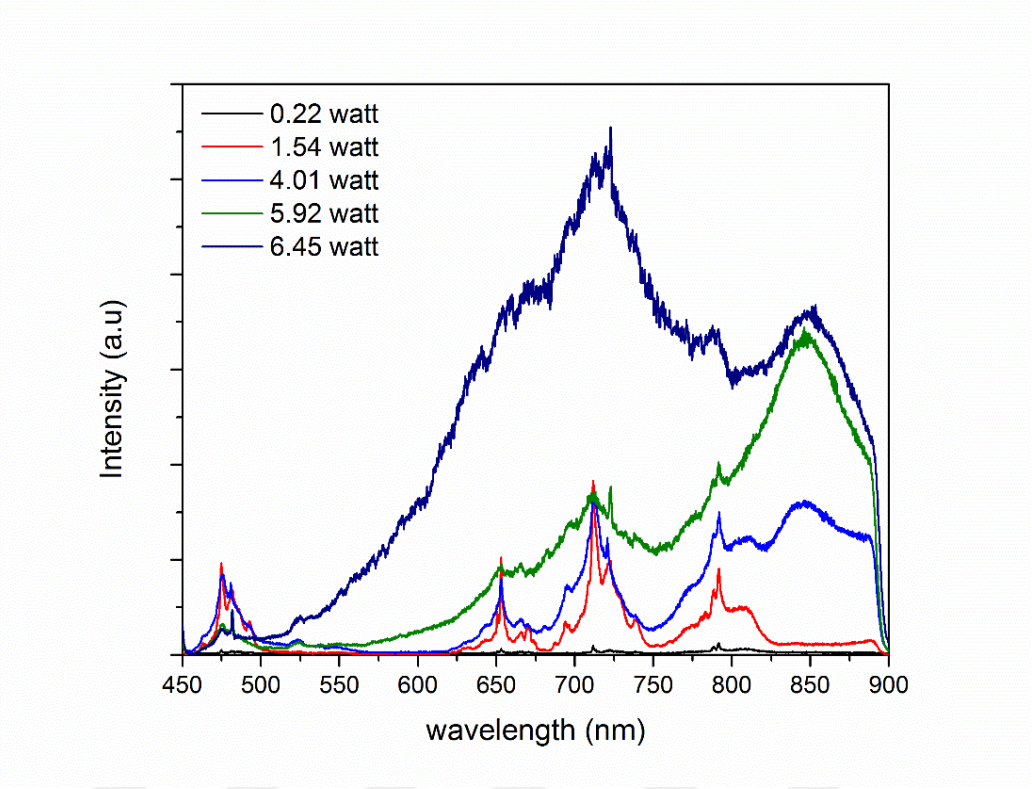

Figure 5.22 : Luminescence spectra of 5% Yb^{3+} doped yttrium silicates at atmospheric pressure.

The appearance of the Er^{3+} luminescence indicates presence of small amount of this ion in the raw materials used for synthesis of the powders (despite the claimed high purity) and, as a result the transfer of energy from Yb^{3+} ions to Er^{3+} impurities is also present for all Yb^{3+} doped samples [19, 58, 61]. The white light was obtained when the pumping power is at least ~1.32 W for 5% Yb^{3+} doped powder under vacuum condition. The white light was obtained when the pumping power is at least ~2.45 W for 5% Yb^{3+} doped sample at vacuum as shown in Figure 5.23. The $^4I_{9/2} \rightarrow ^4I_{15/2}$ energy transition of Er^{3+} impurities around 835 nm becomes weak when the pumping power is increased for the vacuum case. At high pumping powers, red emission is spreading and the spectra begin to turn white light spectra. The luminescence characteristics of 5% Yb^{3+} doped yttrium silicate samples showed blue-green UC characteristics because of the cooperative emissions of two Yb^{3+} ions and transitions of unwanted Er^{3+} impurities at 'low' pumping power values at both atmospheric and vacuum conditions.

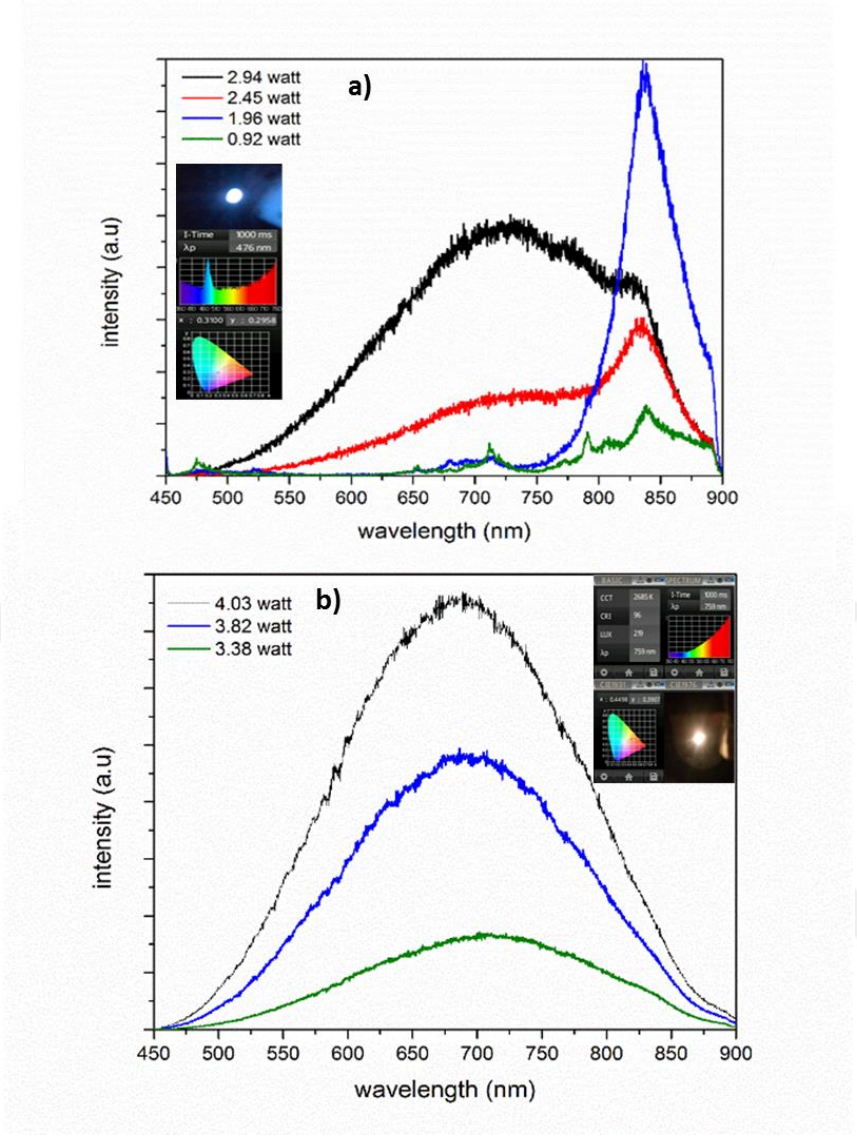

Figure 5.23 : Luminescence spectra of 5% Yb^{3+} doped yttrium silicates at vacuum (0.01 mbar) Illuminasmeter results at low a) (0.92 W) and b) high (3.38 W) powers.

The white light was obtained when the pumping power is at least ~3.0 W and ~1.19 W for 10% Yb^{3+} doped sample under atmospheric and vacuum conditions, respectively (Figure 5.24 and 5.25). A blue UC emission that could easily be seen by the naked eye was observed in Yb^{3+} doped powder at atmospheric conditions. The main peak of white emission of 10% Yb^{3+} doped sample was ~680 nm for atmospheric conditions. The increase of Yb^{3+} concentration causes a shift of the peak of white light to a high-energy region. The white light becomes visible for 10%Yb^{3+} doped powder at least 1.19 W under vacuum conditions (Figure 5.25).

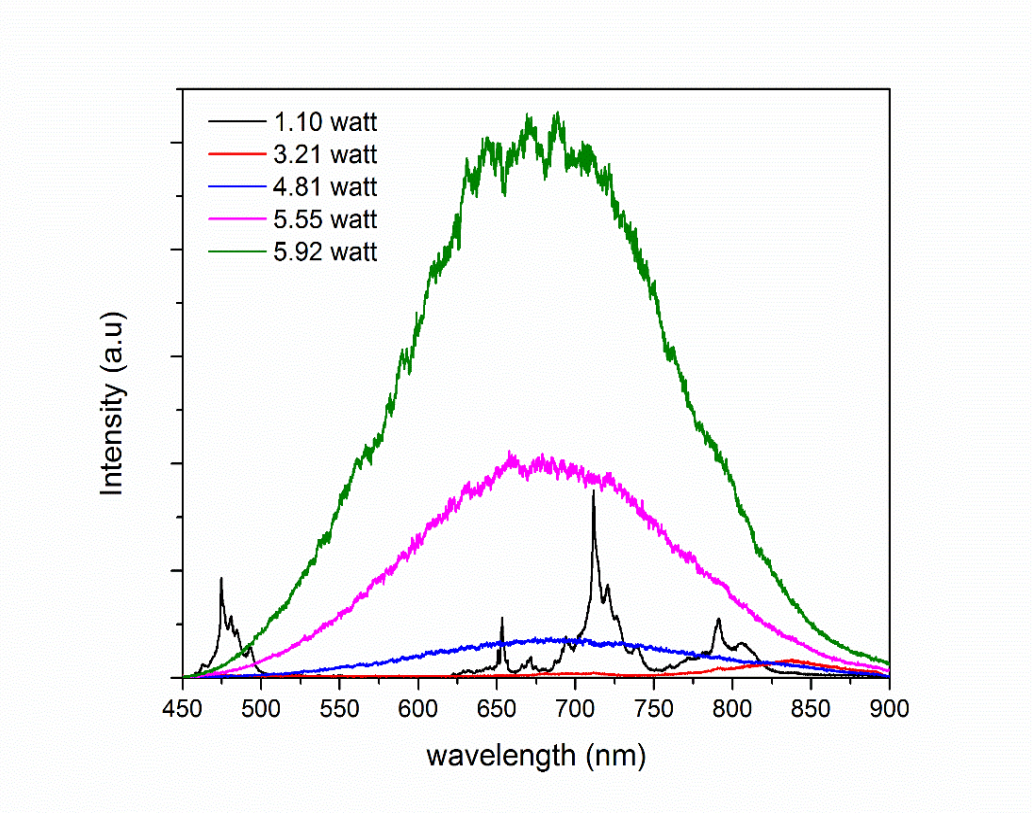

Figure 5.24 : Luminescence spectra from 10% Yb^{3+} yttrium silicate at atmospheric pressure.

WL emission becomes stronger as the UC emission disappears. Namely, at low pumping power levels, the UC emission from the doped sample in the 400 nm to 500 nm region is mainly from the RE ions, but it diminishes when the white light continuum begins to appear with increasing pumping power. The position of the peak of the white light shifts to the lower wavelengths of ~665 nm for 20% Yb^{3+} doped sample. For 20% Yb^{3+} doped yttrium silicate sample, we could not obtain blue, green or red upconversion emission at low power values under 0.01 mbar. The white light becomes visible for 0.92 W for 20% Yb^{3+} doped sample under vacuum. The threshold power to obtain white light spectra decreased by increasing Yb^{3+} concentration and the generation of white light is strongly dependent on Yb^{3+} concentration.

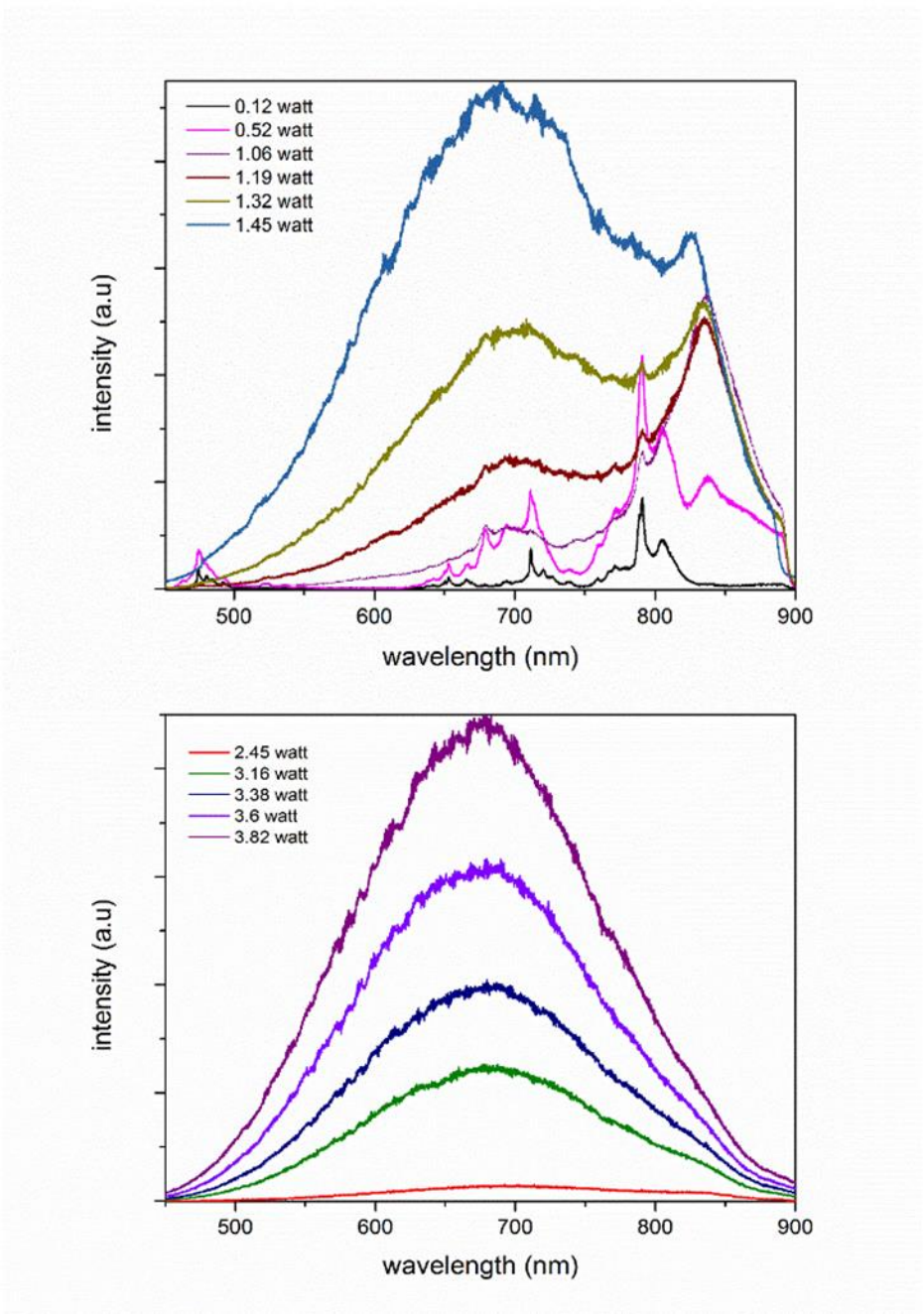

Figure 5.25 : Luminescence spectra from 10% Yb^{3+} yttrium silicate sample at vacuum (0.01 mbar).

The luminescence dynamics decay and rise patterns, of Yb^{3+} doped samples, were investigated depending on pumping power. The decay and rise patterns of low concentration of Yb^{3+} doped samples are not strongly depending on pumping power and the order of time scale shows the thermal processes are effective on the emission mechanism because of taking several seconds. The decay patterns have not strong dependence on pumping power; however, the rising patterns are more sensitive to the

pumping powers. The representative examples at vacuum are shown in Figures 5.26 and Figure 5.27 for 1% and 5% Yb^{3+} doped nanopowders, respectively.

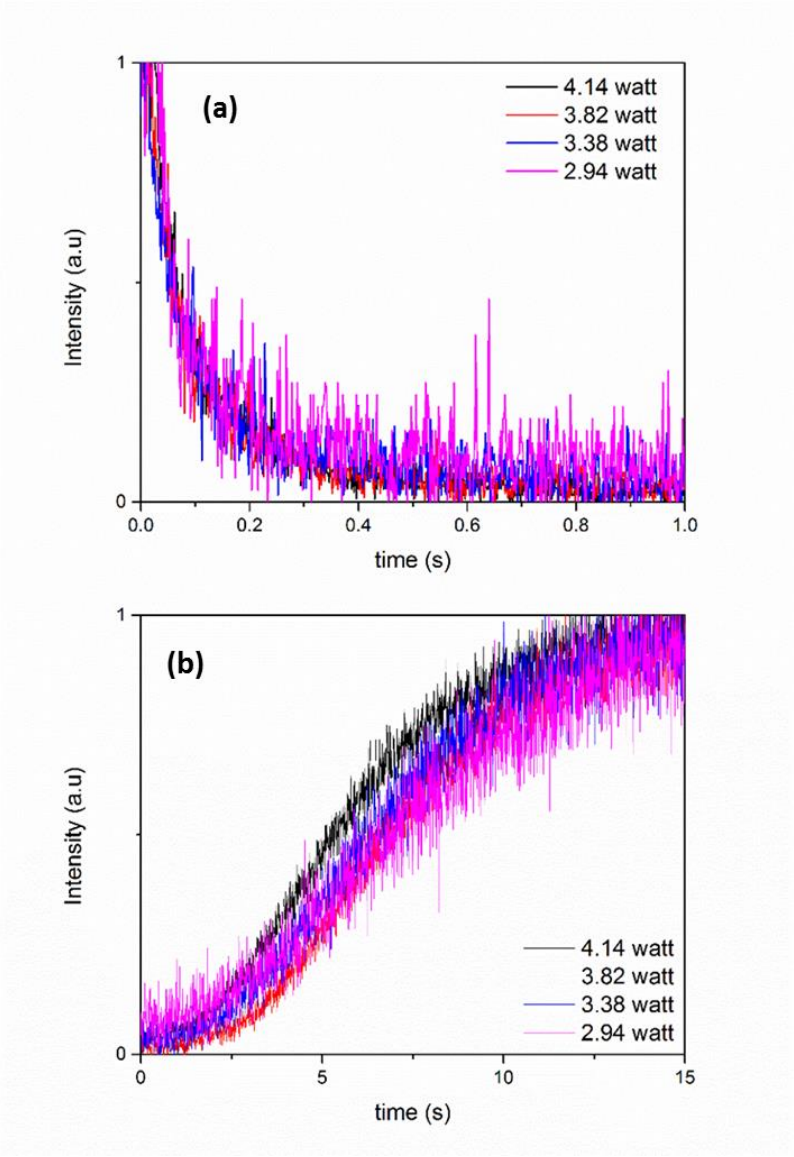

Figure 5.26 : a) Decay and b) rise patterns of 1% Yb^{3+} doped sample at 0.01 mbar under vacuum (0.01 mbar) at 701 nm.

However, the rise patterns of the yttrium silicate samples doped with the higher concentration of Yb^{3+} are strongly dependent on the power as seen in Figure 5.28. Figure 5.28 shows the decay and rise patterns for the 20% Yb^{3+} doped nanopowder. The rise patterns are faster at higher powers and decreased to lower power values.

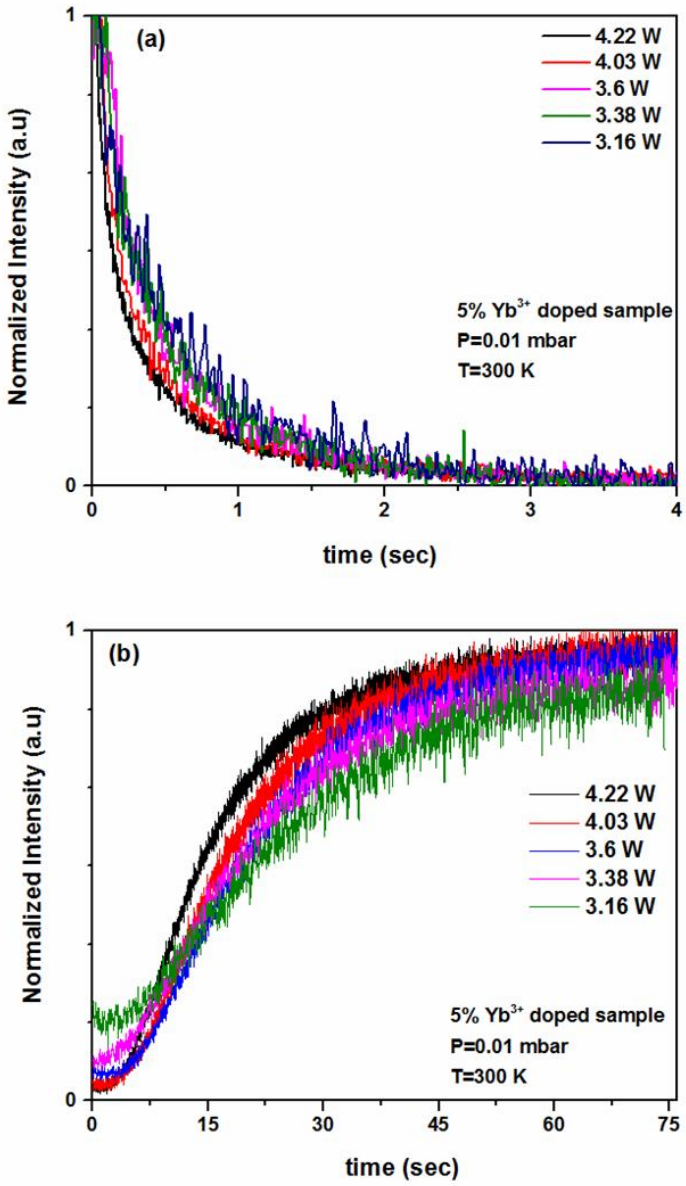

Figure 5.27 : Power dependency of 5% per mole Yb^{3+} doped yttrium silicate (a) decay and, (b) rise curves at various pumping powers at 698 nm.

As seen in Figure 5.28, the rising pattern is very fast at high powers and decreased to low power values gradually for the sample. The rise time patterns are also affected by both pumping power and a high concentration of Yb^{3+} ions.

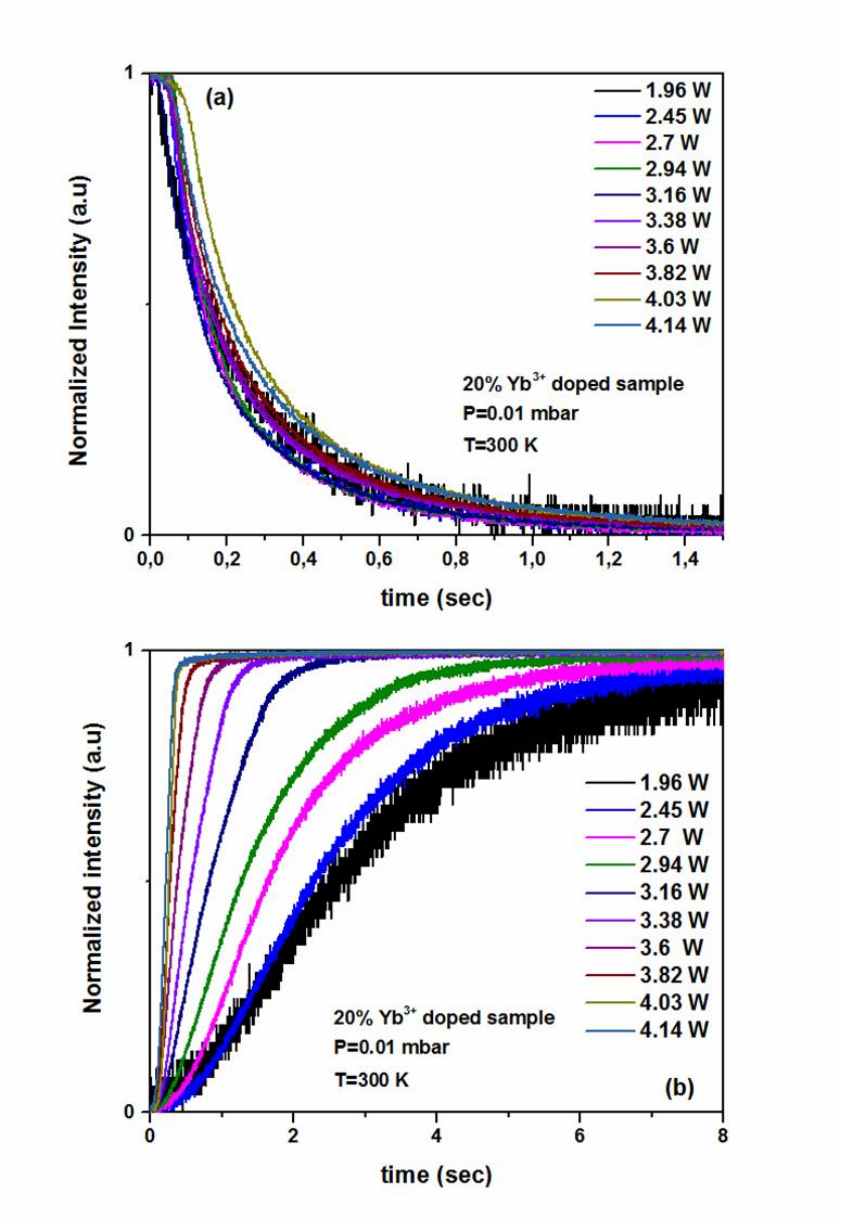

Figure 5.28 : Power dependency of 20 % per mole Yb^{3+} doped yttrium silicate nanopowder (a) decay and, (b) rise patterns at various pumping powers.

We have also investigated the luminescence behavior of the samples depending on the pressure Figure 5.29 and Figure 5.30 show the representative examples of white light generation depending on pressure for 5% and 10% Yb^{3+} doped yttrium silicate nanopowders. The broad emission around ~791 nm, ~ 801 nm and ~ 834 nm can be $^4I_{15/2} \rightarrow {}^4I_{9/2}$ transition of Er^{3+} impurities [97, 98].

Figure 5.30 shows the spectra of 10% Yb^{3+} doped yttrium silicate depending on pressure. The 10% Yb^{3+} doped sample emits blue emission due to Yb^{3+}- Yb^{3+} ion pair at ~475 nm at atmospheric pressure.

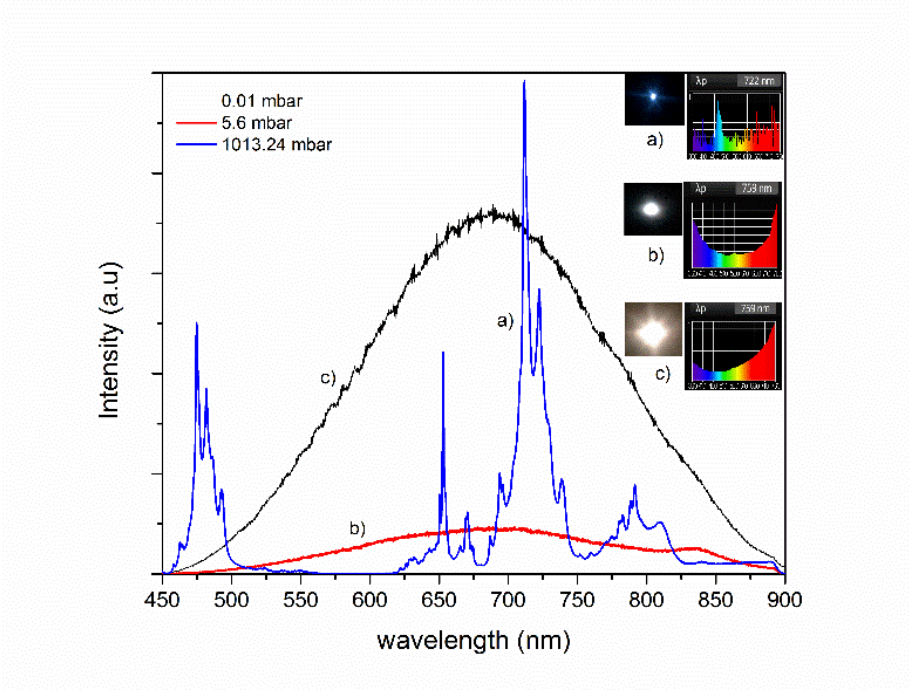

Figure 5.29 : The spectral difference of the 5% per mole Yb^{3+} doped yttrium silicate nanopowder at a) room pressure b) 5.6 mbar c) 0.01mbar by pumping power at 3.38 watts. The insets are the corresponding spectra measured by the illuminance meter.

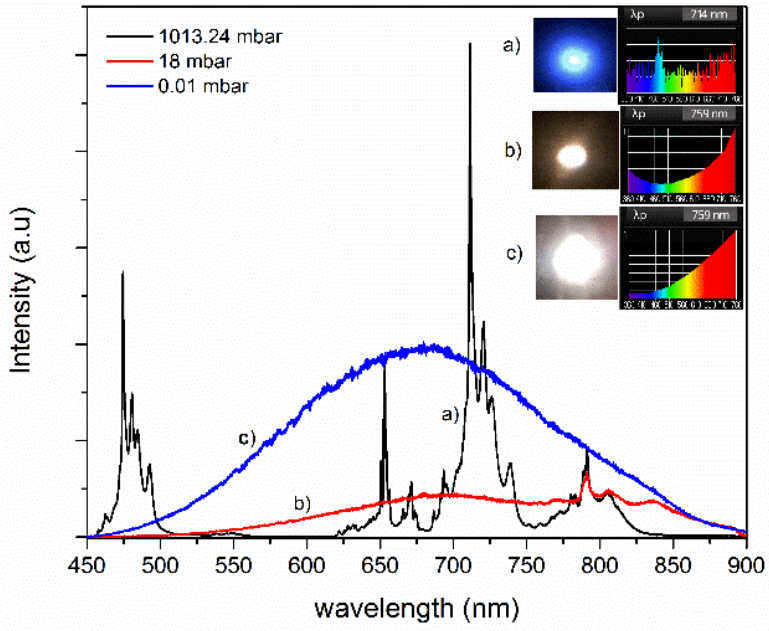

Figure 5.30 : Emission characteristics of 10% per mole Yb^{3+} doped yttrium silicate at 3.38 W pumping power at a) atmospheric pressure b) 18 mbar c) 0.01mbar. The insets are the corresponding spectra measured by the illuminance meter.

In Figure 5.31a, the spectra of 20% Yb^{3+} doped yttrium silicate are shown under atmospheric pressure and 0.01 mbar at 3.38 W.

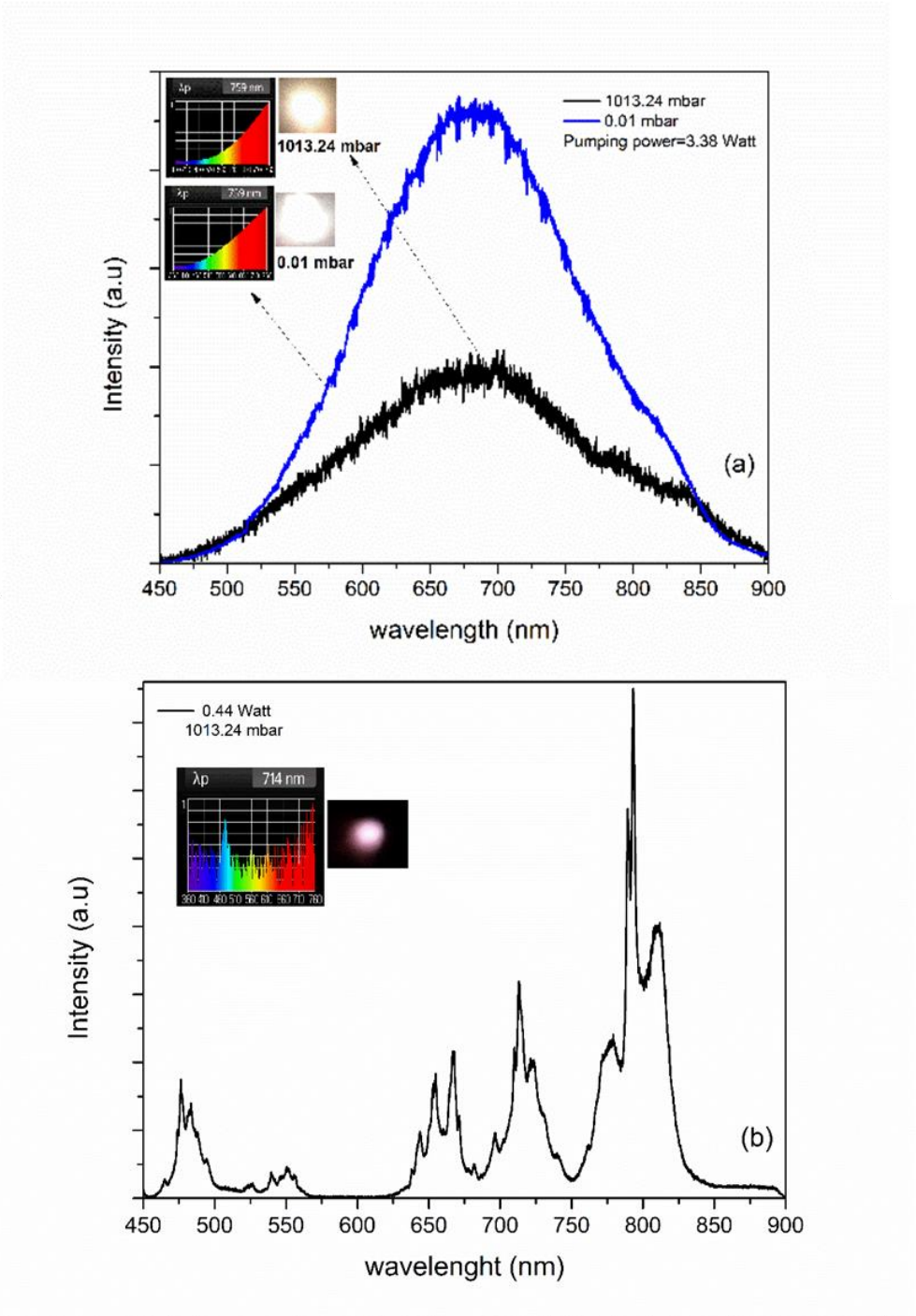

Figure 5.31 : Emission characteristics of 20% Yb^{3+} doped yttrium silicate sample a) at 3.38 W pumping power at 0.01 mbar and atmospheric pressure b) at 0.44 W at atmospheric pressure.

In Figure 5.31b, 20% Yb^{3+} doped sample emits blue emission due to Yb^{3+}-Yb^{3+} ion pair at ~475 nm at atmospheric pressure but low pumping power (0.44 W). The Er^{3+} impurities in the nanopowder cause the red emission band; also energy transfer from

Yb^{3+} to Er^{3+} impurities tend to cause a slight green emission (~521 nm) attributed to the $^4I_{15/2} \rightarrow {}^2H_{11/2}$ transition of Er^{3+} (Figure 5.31b). In addition, the rising and decaying time patterns were measured depending on pressure as seen in Figure 5.32.

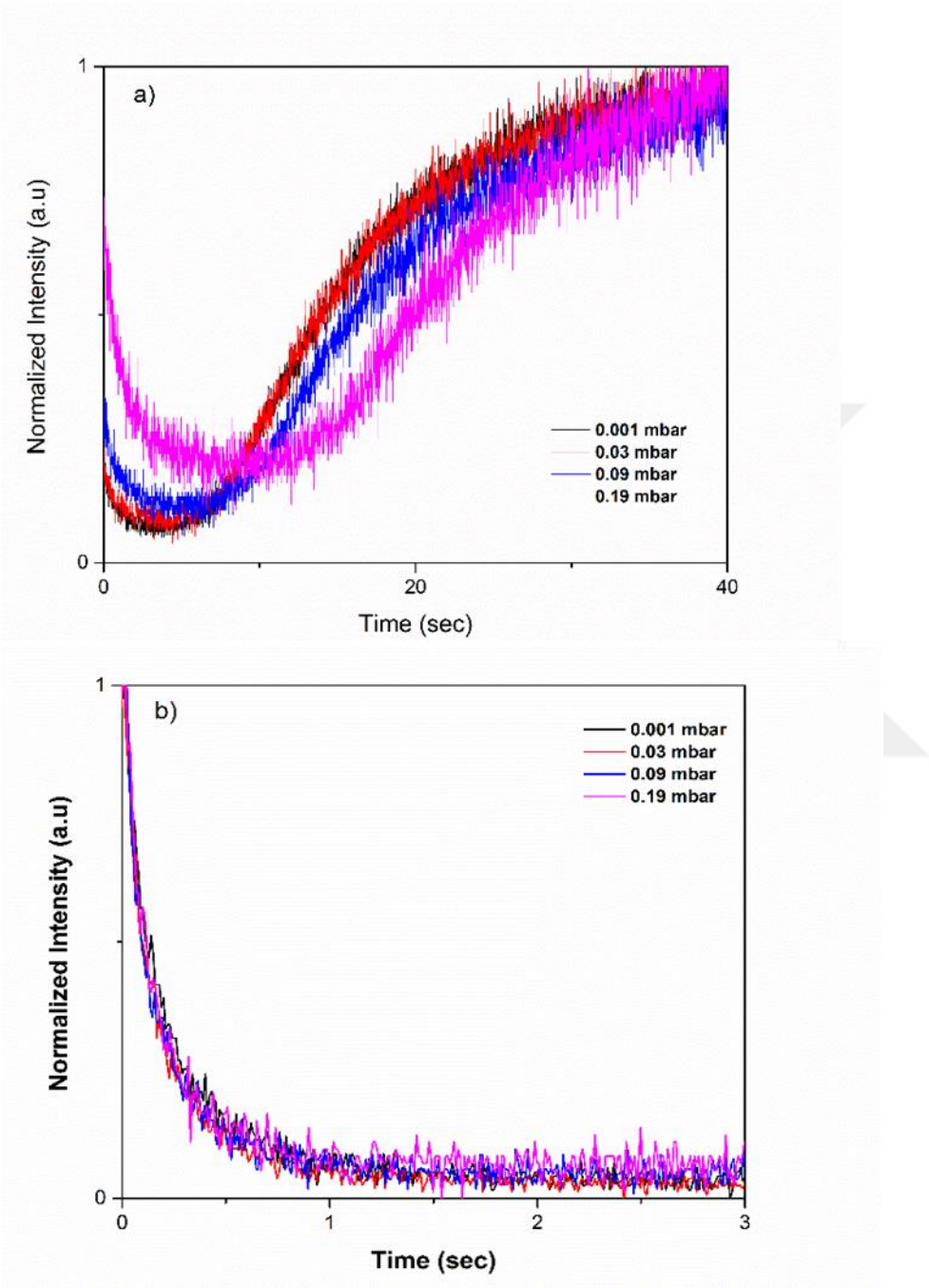

Figure 5.32 : a) Rise and b) decay patterns of 5% per mole Yb^{3+} doped yttrium silicate nanopowder depending on pressure.

The rise patterns of the white light from 5% per mole Yb^{3+} doped sample were found to be sensitive to pressure; however, the decay patterns have no significant dependences on pressure. Figure 5.33 indicates the normalized intensity versus

emission wavelengths of all samples at 3.38 W power value under 0.01 mbar pressure. While the main peak of undoped and 1% Yb^{3+} doped samples were ~715 nm and ~710 nm, respectively, the position of the peak of white light shifts to lower wavelengths of ~695 nm for 2% Yb^{3+} and ~680 nm for 10% and 20% Yb^{3+} doped samples. The increase of Yb^{3+}concentration causes a shift of the peak of white light to a high-energy region. The white light was seen in 10% and 20% Yb^{3+} doped samples even at atmospheric pressure. For 20% Yb^{3+} doped yttrium silicate sample, we could not obtain blue, green or red upconversion emission at low power values under 0.01 mbar.

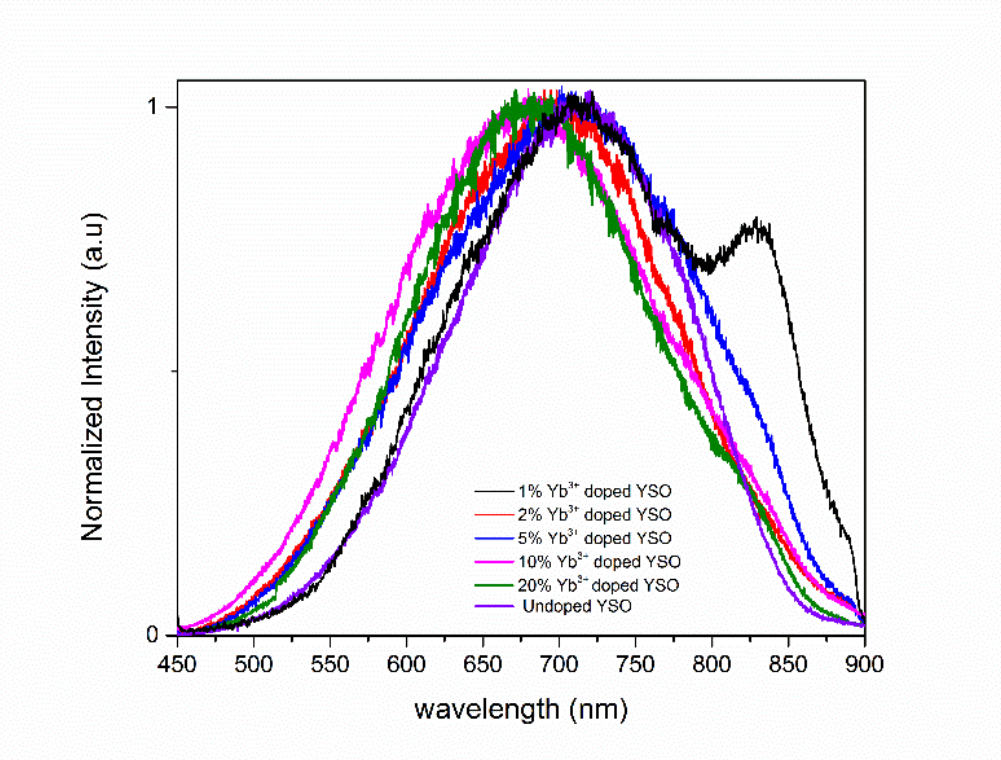

Figure 5.33 : Normalized white light spectra of all samples at 3.38 W power and under 0.01 mbar pressure.

The slopes of white light intensity dependence on excitation powers for all samples were shown in Figure 5.34. The white light was obtained when the pumping power is at least ~3.38 W, ~2.21 W, ~1.38 W, ~1.19 W, ~0.92 W and ~1.45 W for 1%, 2%, 5%, 10%, 20% and undoped yttrium silicates sequentially. The slope values for undoped and 1%, 2%, 5%, 10%, 20% Yb^{3+} doped yttrium silicate nanopowders of the linear fit on graph of white light intensity versus power in log-log scale indicate that there are two regions for the slopes except undoped and 1% Yb^{3+} doped samples and there are multiphonon absorption processes in the systems.

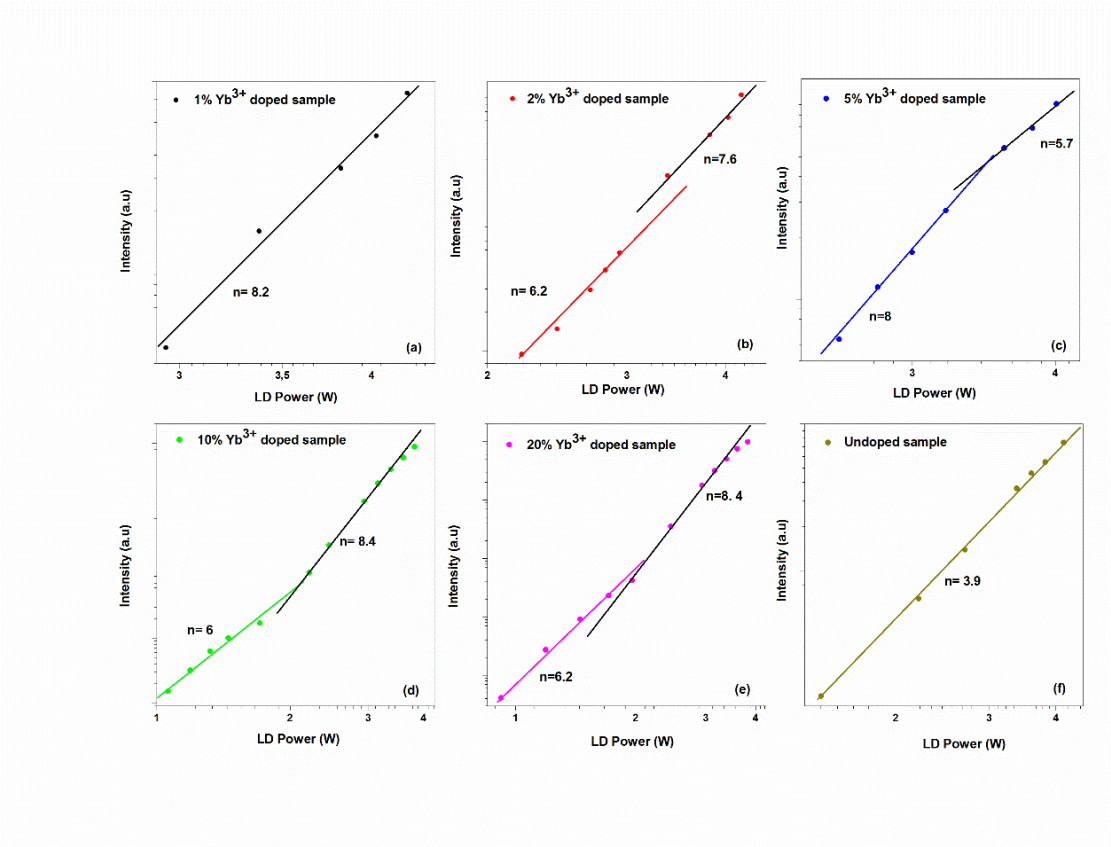

Figure 5.34 : The intensities of white light dependence on power (log-log scale) for a) 1% b) 2% c) 5%, d) 10%, e) 20% per mole Yb^{3+} doped and f) undoped $Y_2Si_2O_7$ nanophosphors.

Figure 5.35 shows the results of the normalized intensity of emissions versus pressure for all samples. 10% and 20% Yb^{3+} doped yttrium silicate nanopowders emitted white light even at high pressures. We did not obtain white light for 1% and 2% samples at higher pressure values at ~4 mbar and ~5 mbar, respectively. It is shown when the pressure is increased, the intensity of white light is decreased. For a certain laser light excitation, the intensity of white light increases with decreasing pressure in the dewar chamber where the powder resides. The pressure dependence shows that the thermal effects involve in broadband white light emission. Decreasing the pressure may decrease the thermal conductivity, favoring the heating of the powder, hence raising its temperature and seemingly indicating the thermal nature of the process responsible for the white light production. At intermediate pressure values, the emission due to $^4I_{15/2} \rightarrow {}^4I_{9/2}$ transition of Er^{3+}impurities were very strong for 2% Yb^{3+} doped sample (~840nm) comparing with that of the 5% and 10% per mole Yb^{3+} doped samples. The process of converting the near infrared photons into white light photons is nonlinear

behavior due to the conservation of energy and is found to be so in the measured nonlinearity of white light intensity versus excitation power.

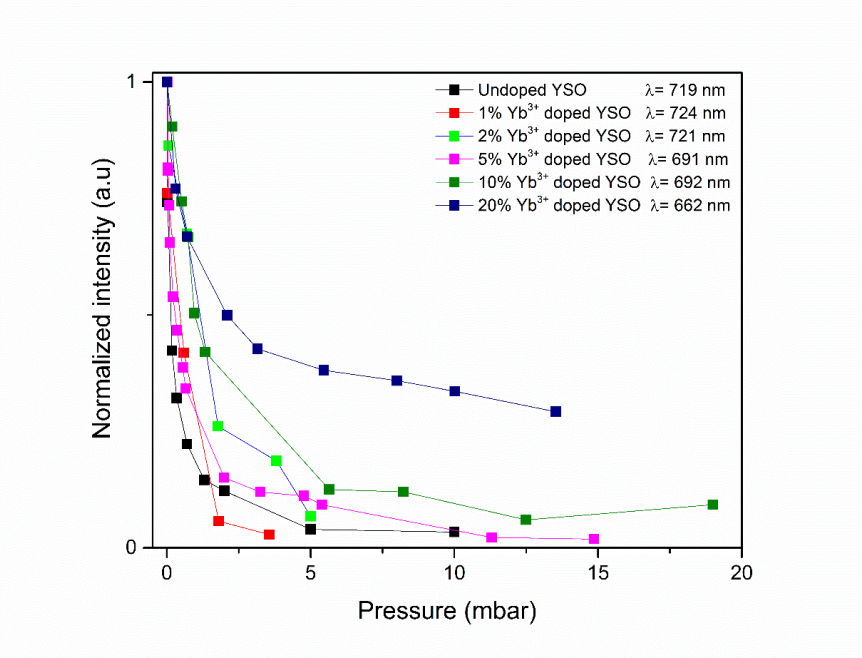

Figure 5.35 : The normalized maximum peak intensities of white light dependence on pressure at 300 K and 3.38 W pumping power with 975 nm excitation.

The surface effects of the nanocrystalline powders also may play an important role in white light production since the nanopowders have a larger ratio of surface area to its volume concerning to their bulk form. Figure 5.36 shows the minimum power required to obtain white light depending on Yb^{3+} concentration.

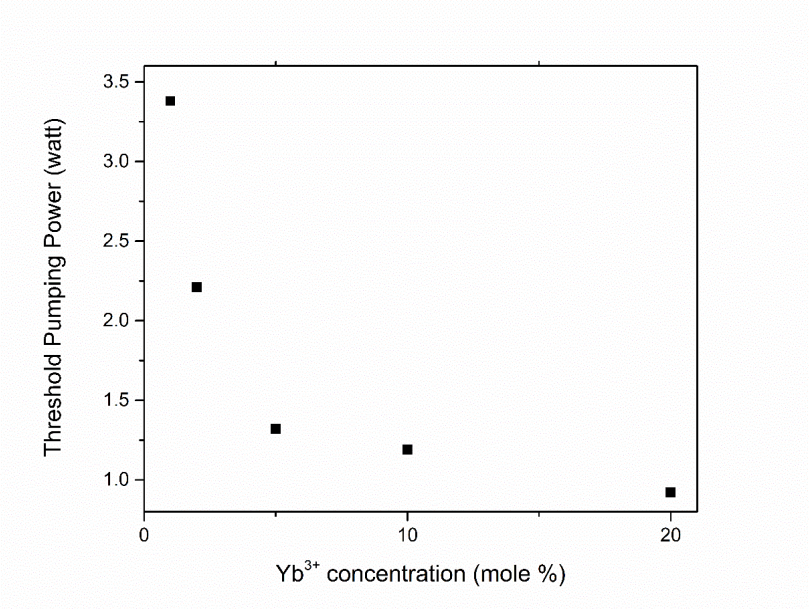

Figure 5.36 : Yb^{3+} concentration dependence of the threshold pumping powers.

The threshold power to obtain white light spectra decreased by increasing Yb^{3+} concentration and the generation of white light is strongly dependent on Yb^{3+} concentration. Figure 5.37 shows the summary of the UC emission spectra of the 1%, 2%, 5% and 10% Yb^{3+} doped nanopowders at 975 nm laser excitation under 0.01 mbar. The power values were 1.45 W for 1% and 2% Yb^{3+} doped samples and 0.52 W for 5% and 10% Yb^{3+} doped samples.

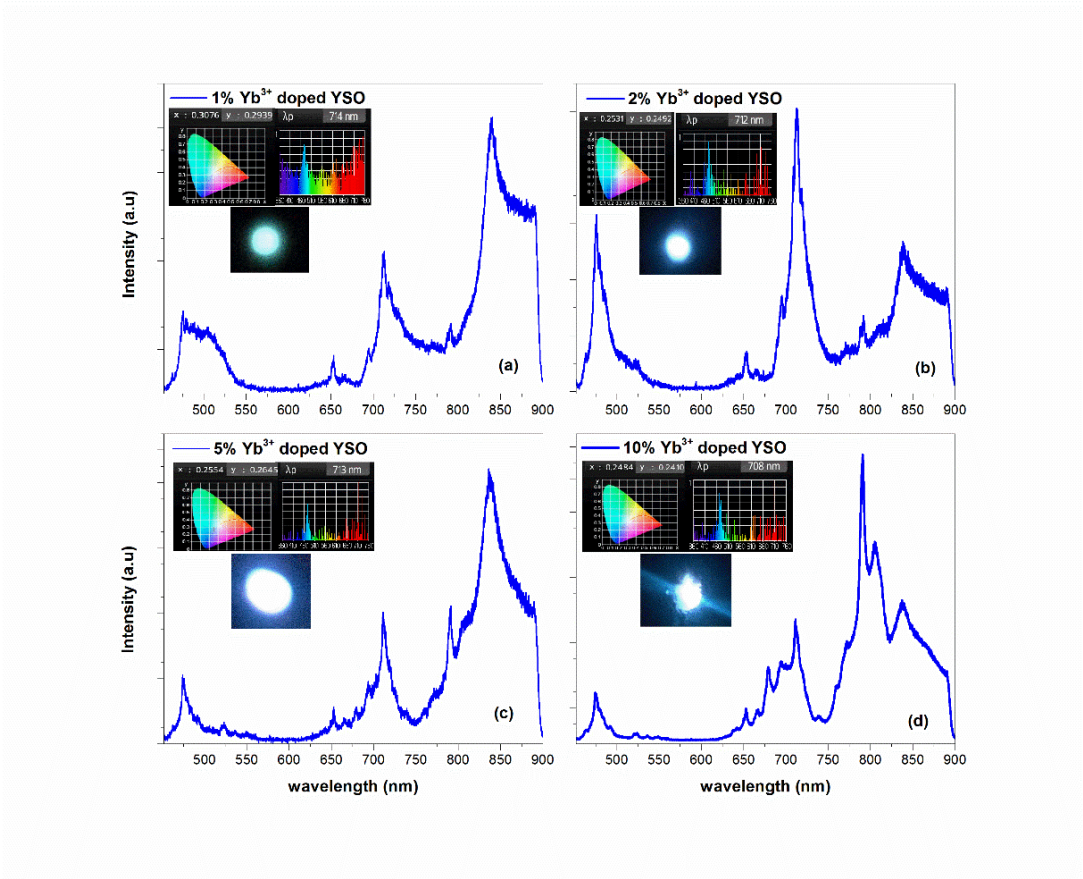

Figure 5.37 : UC spectra of a) 1%, b) 2% per mole Yb^{3+} doped yttrium silicate powders at 1.45 W and c) 5% and d) 10% per mole Yb^{3+} doped yttrium silicate powders at 0.52 W.

The samples exhibit a luminescence emission in the blue-green region and red domain of the visible spectra under the 975 nm excitation. In the experiments, the blue-green emission is very visible to our naked eyes even at low power value (0.38 watt). The blue emission is a cooperative emission corresponding to the simultaneous radiative relaxation of $Yb^{3+} \rightarrow Yb^{3+}$ ion pairs around ~475 nm; the green and red emission are due to $^4I_{15/2} \rightarrow (^2H_{11/2}, ^4S_{3/2})$ at ~523 nm and $^4I_{15/2} \rightarrow ^4F_{9/2}$ at ~653 nm energy transitions of unwanted Er^{3+} impurities under the excitation wavelength 975 nm, respectively. The $^4I_{15/2} \rightarrow ^4I_{9/2}$ energy transition of Er^{3+} impurities around 835 nm becomes weak

when the pumping power is increased. It disappears when the white light spectra are obtained at high pumping powers. At high pumping powers, red emission is spreading and the spectra begin to turn to thermal white light spectra. The blue light emission was very strong for 10% Yb^{3+} doped yttrium silicate sample at low pumping power even at atmospheric pressure by comparing the 1%, 2% and 5% Yb^{3+} doped nanopowders when we looked by naked eyes.

The chromaticity coordinates were given for all nanopowders samples in the white region of the 1931 Commission International I' Eclairage (CIE) diagram in Table 5.5.

Table 5.5 : The CIE 1931 (x, y) dependences on the doping concentration of Yb^{3+} for white light at 3.82 W under 0.01 mbar pressure for all samples.

White Light			
Yb^{3+} concentration (per mole)	CIE 1931 Coordinates (x, y)	CCT(K)	CRI
0 %	(0.3373, 0.3031)	5197	83
1%	(0.3390, 0.3024)	5097	82
2%	(0.3502, 0.3096)	4549	83
5%	(0.4221, 0.3726)	2991	93
10%	(0.4673, 0.4073)	2574	98
20%	(0.4779, 0.4127)	2481	99

Figure 5.38 shows the n-shape-like power dependence of the UC emission intensity for 1%, 2%, 5% and 10% Yb^{3+} doped samples. The all blue emission measurement results obey the quadratic power law behavior ($I \sim P^n$) with n=0.9, 1.35, 1.65 and 1.1 for samples %10, 5%, 2% and 1% Yb^{3+} doped samples, respectively. The blue-green UC intensity concerning to the emission wavelength has P^n shape behavior as expected for the nonlinear phenomenon of one and two photon absorption processes.

In conclusion, white light spectra were observed for all samples under vacuum conditions. The high concentration of Yb^{3+} ion doped (10% and 20% per mole) yttrium silicate nanopowders emitted very intense white light even at atmospheric pressure.

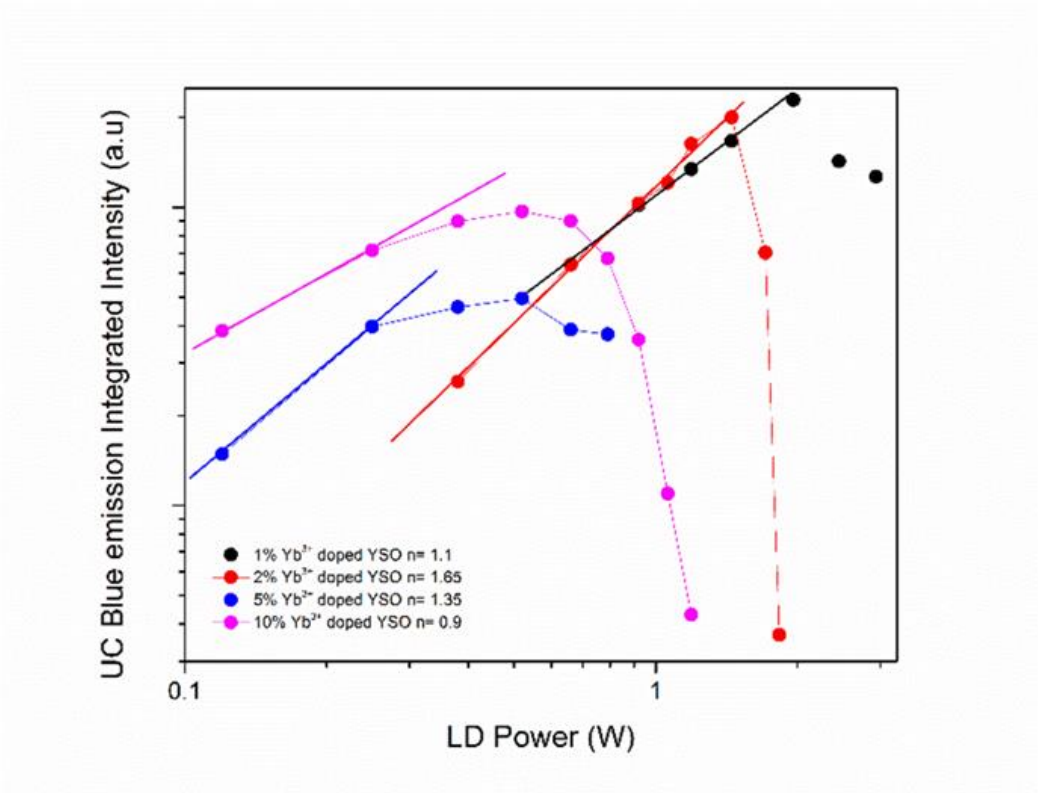

Figure 5.38 : Integrated intensities of blue light dependence on power (log-log scale) for samples.

The threshold power is also decreased under vacuum to obtain white light. The experimental results show that the Yb^{3+} doped samples should be a promising material for novel white light sources for optical applications.

6. STRUCTURAL AND LUMINESCENCE PROPERTIES OF RARE EARTH CODOPED YTTRIUM SILICATE (Y_2O_3:SiO_2) NANO PHOSPHORS

6.1 Nd^{3+}/ Yb^{3+} Codoped Yttrium Silicate Nanopowders

As mentioned before, Yb^{3+} ion has a simple electronic configuration and its energy levels (only two levels of $^2F_{7/2}$ and $^2F_{5/2}$) are at ~1.30 eV-1.13 eV in near infrared region. Yb^{3+} ion is generally used as the sensitizer to obtain high emissions from other rare earth ions by using ~980 nm laser since its great absorption cross section at ~980 nm and the near infrared photon energy can be transferred from Yb^{3+} to other ions. Besides the Nd^{3+} ion has a large absorption cross section about 800 nm so; Nd^{3+} doped materials can be excited by using a laser at this wavelength. Efficient energy transfers between Nd^{3+} and Yb^{3+} ions have been investigated in different systems [93, 94]. Nd^{3+} ions have very complex energy transfers according to the Dieke diagram and NIR laser (~ 800 nm) may excite the Nd^{3+} ions.

In this part of the thesis, 1% Nd^{3+} /10% Yb^{3+} codoped yttrium silicate nanophosphor was synthesized by the sol-gel method and Y_2O_3/SiO_2 ratio was at 1.127 as described in our previous work [61]. Nd $(NO_3)_3.6H_2O$ and Yb $(NO_3)_3.5H_2O$ and tetraethyl orthosilicate (TEOS- 99.9%), all having a purity of 99.9% were purchased from the Sigma Aldrich. The luminescence properties of Nd^{3+}/Yb^{3+} codoped nanopowder were investigated with 975 nm and 808 nm diode laser excitations. The emission properties and spectral changes were analyzed at atmospheric pressure and vacuum conditions. The decay and rise patterns were carried out under vacuum (0.01 mbar) and atmospheric pressures.

6.1.1 Structural analyses

Figure 6.1 shows the XRD patterns of the Nd^{3+}/Yb^{3+} codoped Y_2O_3-SiO_2 sample. The diffraction patterns of the codoped sample were mainly in good accordance with α-$Y_2Si_2O_7$ structure according to the JCPDS card number of 38-0223.

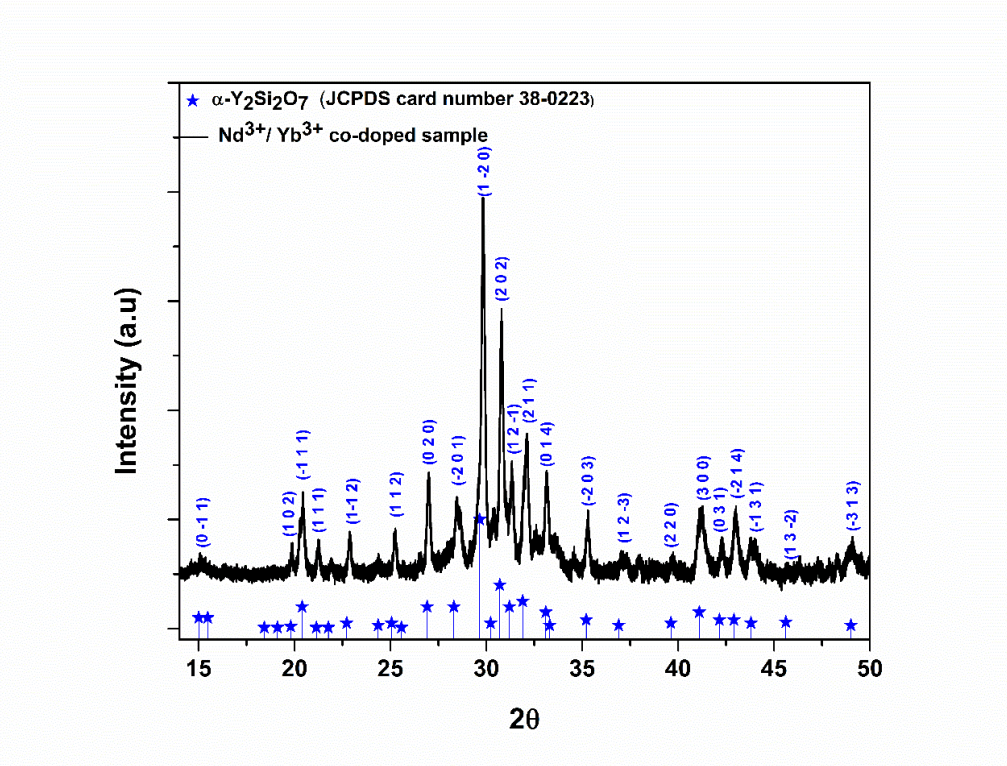

Figure 6.1 : XRD patterns of 1% Nd^{3+}/10%Yb^{3+} codoped α-$Y_2Si_2O_7$ nanopowder.

The structure of the sample, phase, and its average crystalline size were determined with X-Ray Diffraction (XRD) measurements by Bruker D2 Phaser Model (Cu-Kα radiation) diffractometer in the 2θ range from 10^0 to 50^0. The measurement has been done in a very detailed scan with the steps of 0.002^0. The crystal system was triclinic (anorthic) and space group P-1(2) for Nd^{3+}/Yb^{3+} codoped powder and the average particle size was calculated to be about 60 nm by using Scherer equation [50]. We observed that the sample has mostly a single phase as α-$Y_2Si_2O_7$. The $Y_2Si_2O_7$ shows different polymorphs (α, β, ɣ, δ, y) and obtaining a single pure phase is extremely difficult. The atomic radii of RE ions (Yb^{3+} and Nd^{3+}) are similar to Y^{3+} ions in the host material and substitute Y^{3+}sites randomly. The possible substitution may be between the Yb^{3+} or Nd^{3+} and Y^{3+} ions in host due to their similar ionic radius 0.925 Å, 0.983 Å, and 0.96 Å, respectively [95]. Hence, some modification in the structures of co-doped (Yb^{3+} and Nd^{3+}) yttrium silicate powder is possible due to the high concentration of Yb^{3+} (10%) and may not be distributed homogeneously in the host matrix.

6.1.2 Luminescence properties at 975 nm excitation

The luminescence spectra of the Yb^{3+}/Nd^{3+} codoped yttrium silicate at atmospheric pressure with the excitation of 975 nm were shown in Figure 6.2.

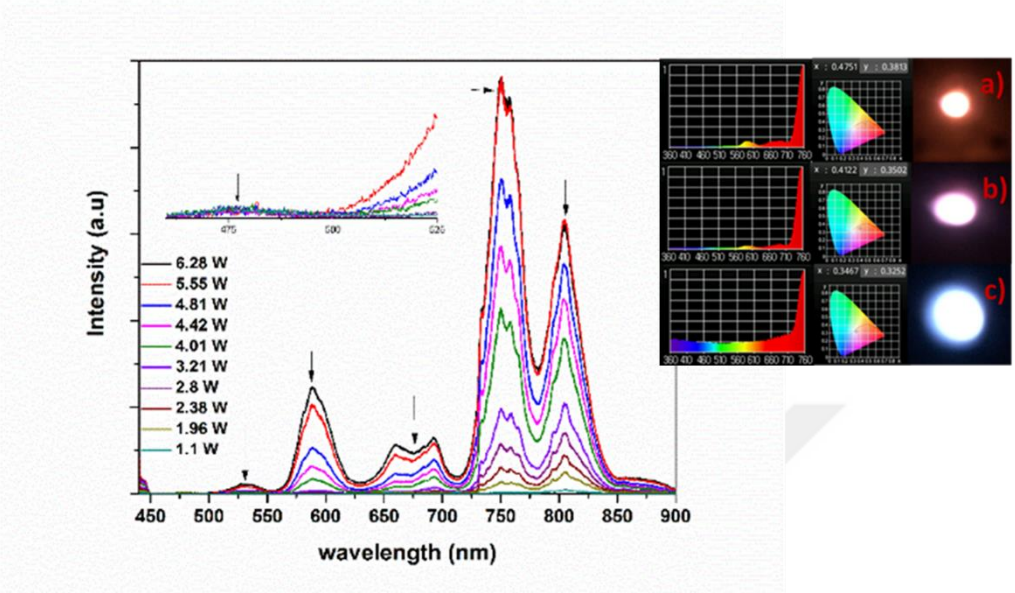

Figure 6.2 : Luminescence spectra of 1% Nd^{3+}-10% Yb^{3+} codoped yttrium silicate nanopowder at atmospheric conditions under 975 nm diode laser excitation. Illuminance meter results and photos at a) 5.55 W, b) 3.21 W and c) 1.54 W.

The observed slight blue emission band centered at ~477 nm for output laser power below 3W may be overlapping of the cooperative emission of two Yb^{3+} ions and $^2G_{9/2} \rightarrow {}^4I_{9/2}$ transition of the Nd^{3+} ion. The emissions at ~533 nm and ~589 nm may be due to the $^2G_{7/2} \rightarrow {}^4I_{9/2}$ and the $^2G_{5/2} \rightarrow {}^4I_{9/2}$ energy transitions of Nd^{3+} ions, respectively. The broader emissions centered at ~660 and 692 nm may be the superposition of $^4F_{9/2} \rightarrow {}^4I_{9/2}$ and $^4F_{7/2} + {}^4S_{3/2} \rightarrow {}^4I_{9/2}$ transitions of the Nd^{3+} ions. The observed sharp emission between 714 nm and 775 nm (~748) may be due to $^4F_{5/2} + {}^4S_{3/2} \rightarrow {}^4I_{9/2}$ transition of Nd^{3+} ions for all power values. The emission at ~ 804 nm may be the $^2H_{5/2} \rightarrow {}^4I_{9/2}$ energy transition of Nd^{3+}. Nd^{3+} ions could not be excited with diode laser of 975 nm according to Dieke diagram; however, Yb^{3+} ions can transfer energy to Nd^{3+} ions. Luminescence properties of Nd^{3+}/Yb^{3+} codoped yttrium silicate nanopowder were studied at vacuum conditions (0.01 mbar). In Figure 6.3, we can see the white light generation with the energy transitions of the Nd^{3+} ion. The broad shoulder at ~541 nm in the spectra above 1.9 W can be assigned to $^2G_{7/2} \rightarrow {}^4I_{9/2}$ energy transition of the Nd^{3+} and the strongest peak at ~597 nm in the spectra can be assigned the $^2G_{5/2} \rightarrow {}^4I_{9/2}$

transition. The emission at ~650 nm and 747 nm may be due to the $^4F_{9/2} \rightarrow {}^4I_{9/2}$ and $^4F_{5/2}+{}^4S_{3/2} \rightarrow {}^4I_{9/2}$ transitions of Nd^{3+} ions, respectively.

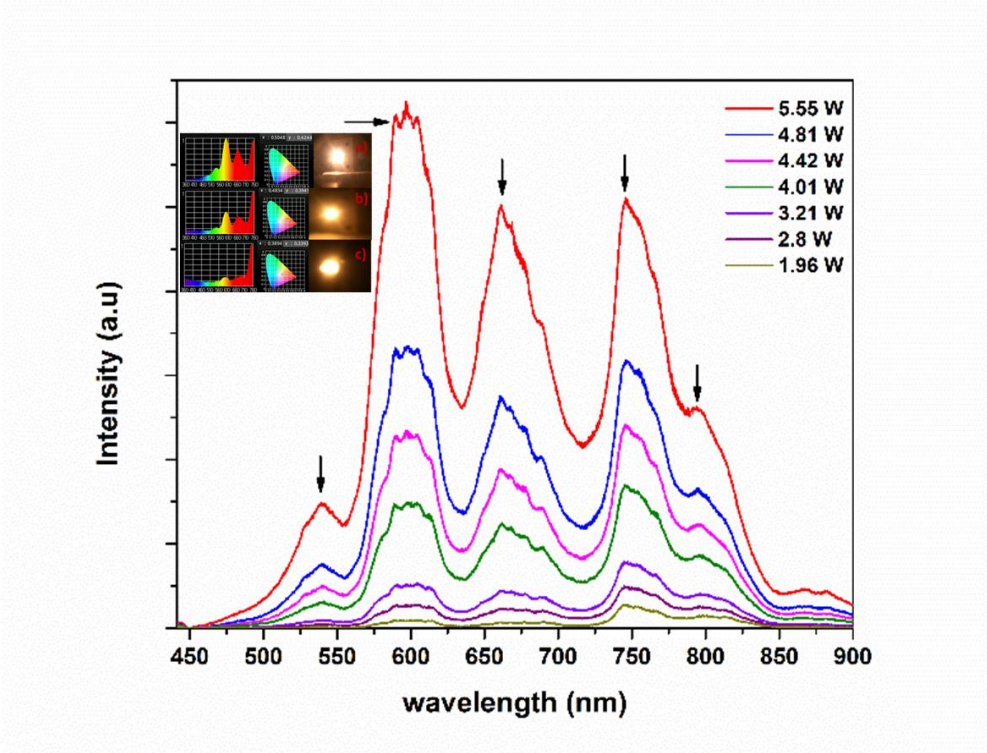

Figure 6.3 : Luminescence spectra of 1% Nd^{3+}/10% Yb^{3+} codoped yttrium silicate nanopowder at 975 nm diode laser excitation under vacuum. Illuminance meter results and photos are at a) 5.55 W, b) 3.21 W and c) 1.54 W.

The decay and rise patterns measurements were carried out at atmospheric pressure and vacuum conditions, as shown in Figures 6.4 and Figure 6.5, respectively. The decay and rise patterns were measured at 595 nm following the sudden turning on and shutting off the laser light, respectively, at atmospheric conditions (Figure 6.4a and Figure 6.4b). It is shown that decay patterns seemed to be independent increasing of the output power of the laser. However, the rise patterns are shorter for high output powers than those observed at low output powers (Figure 4b). These measurements were performed to observe the luminescence dynamics of the powder in the vacuum (Figure 6.5). The decay profiles at atmospheric pressure are not dependent on power and they take several milliseconds. The rise patterns indicate that rising takes several seconds and it is dependent on pumping power. The decay patterns showed similar behavior at 610 nm under vacuum as in the atmospheric conditions and were not strongly dependent on the output powers of the laser. However, the rise patterns as a function of the output power of the laser showed the power dependency (Figure 6.5b).

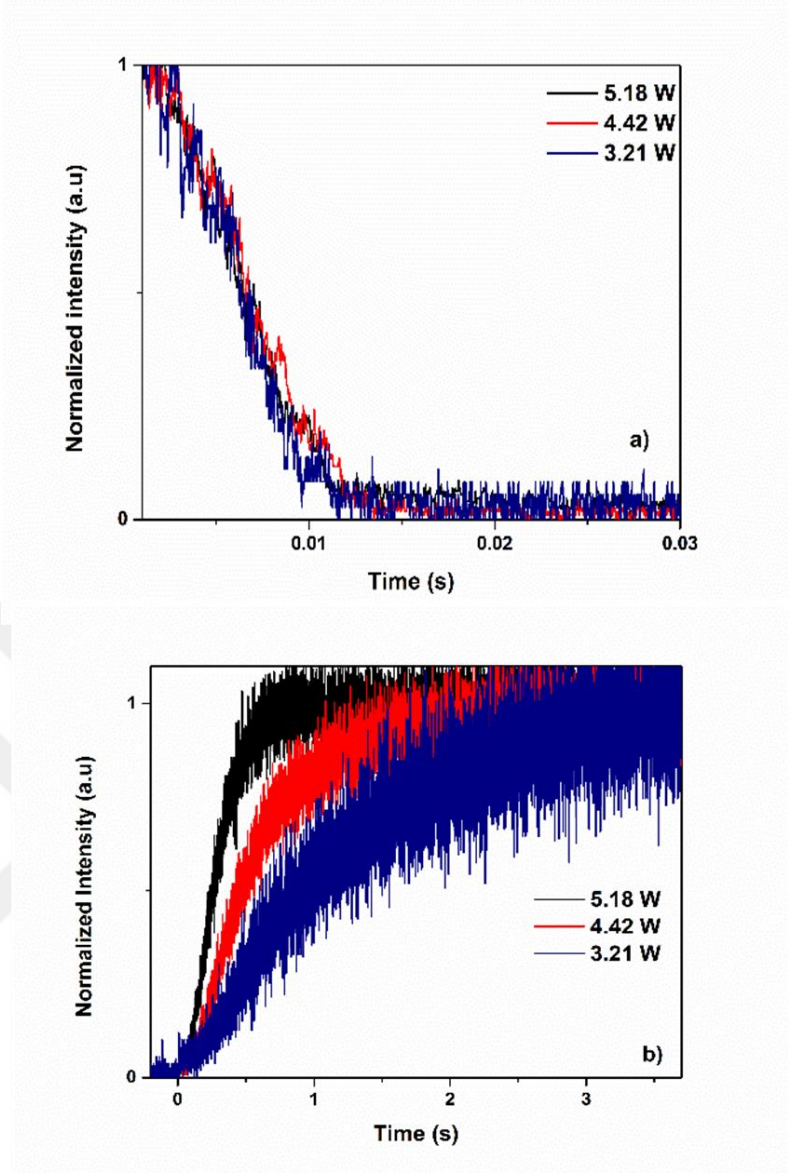

Figure 6.4 : Decay and rise patterns of 1% Nd^{3+}/10% Yb^{3+} codoped yttrium silicate sample at 595 nm under atmospheric pressure.

The rise patterns at 610 nm are shorter with increasing the output power of the laser. We see from the Figure 6.4a and Figure 6.5a, the longer rise times in atmospheric condition indicated that the thermal processes were effective at atmospheric pressure. In Figure 6.5, we see the decay and rise patterns at vacuum condition and decay patterns are longer than that are in atmospheric pressure measurements.

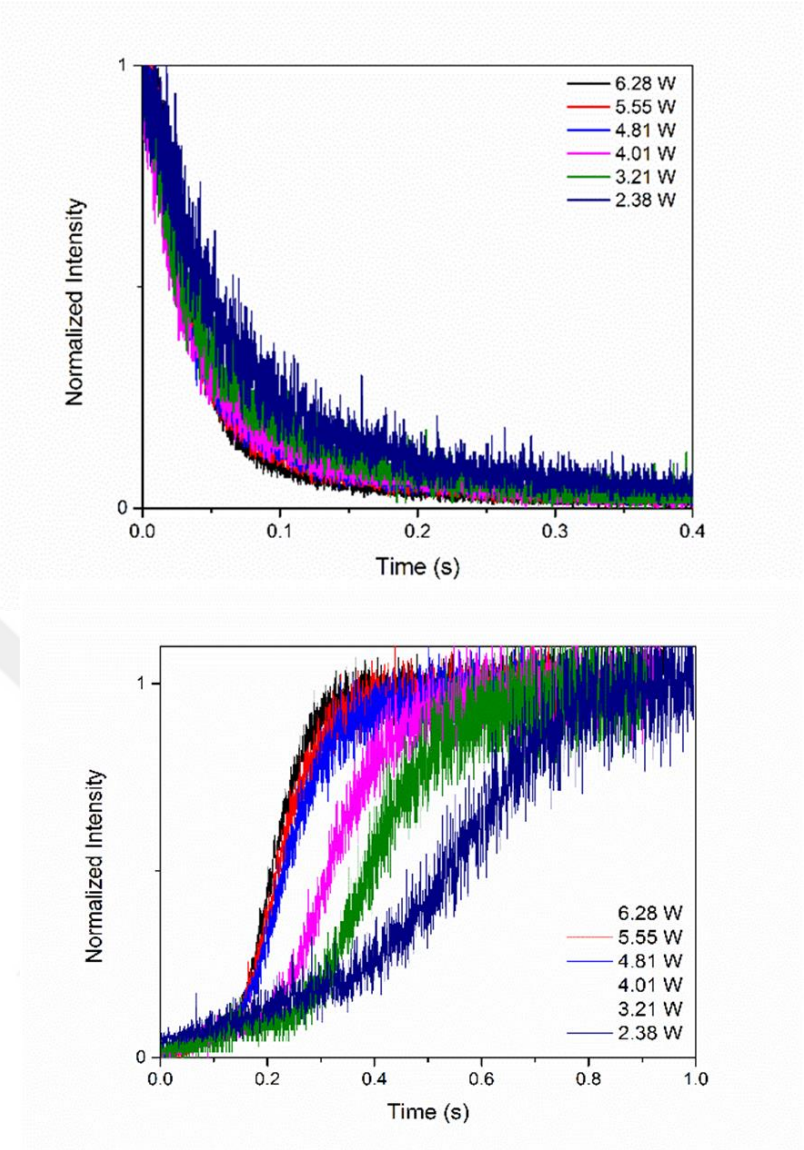

Figure 6.5 : Decay and rise patterns of 1% Nd^{3+}/ 10%Yb^{3+} codoped yttrium silicate sample at 610 nm under vacuum.

In addition, vacuum condition decay times are dependent on pumping power. Rising times at vacuum are shorter than that are in atmospheric pressure measurements and they are dependent on pumping power. We observed several emission bands due to energy levels of Nd^{3+} at low powers for the sample. The thermal white light spectra were obtained especially at high powers both at atmospheric and low pressures. The number of photons that are required for emission was found by using pump power dependence for 1% Nd^{3+}/10% Yb^{3+} codoped sample for atmospheric pressure and vacuum measurements (Figure 6.6 and 6.7). It is well known that the Nd^{3+} ions cannot be excited at 975 nm excitation; however, Yb^{3+} ions can transfer their energy to Nd^{3+} ions at this excitation energy.

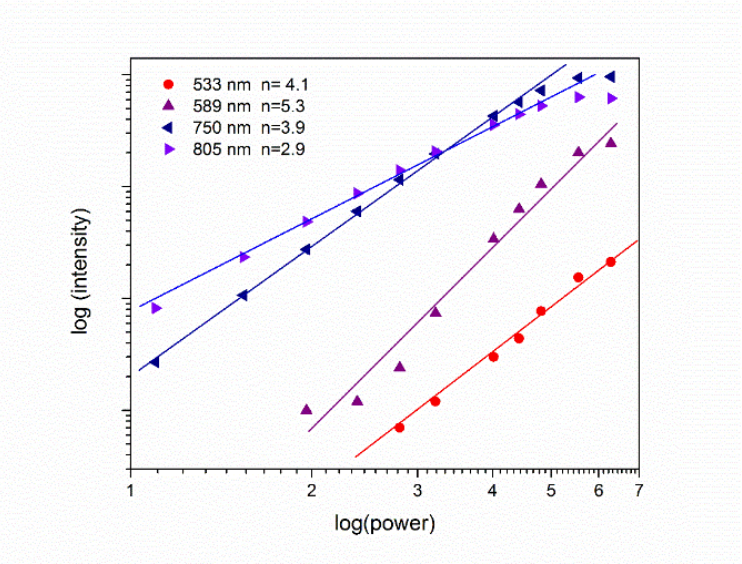

Figure 6.6 : Double logarithmic plot of Intensity-versus Power for white light spectra from 1% Nd^{3+}/ 10% Yb^{3+} codoped yttrium silicate sample at atmospheric pressure.

Since the Yb^{3+} ions have not emission in the range of 440 nm- 900 nm, the observed emission bands are due to energy transitions of Nd^{3+}ions. When the output powers of the laser were increased, the upconversion emission starts to become thermal emission with Nd^{3+} energy transitions. The yttrium silicate compound doping with Nd^{3+} and Yb^{3+} ions could be a light source for usage in many applications and this can lead to the development of the field of use.

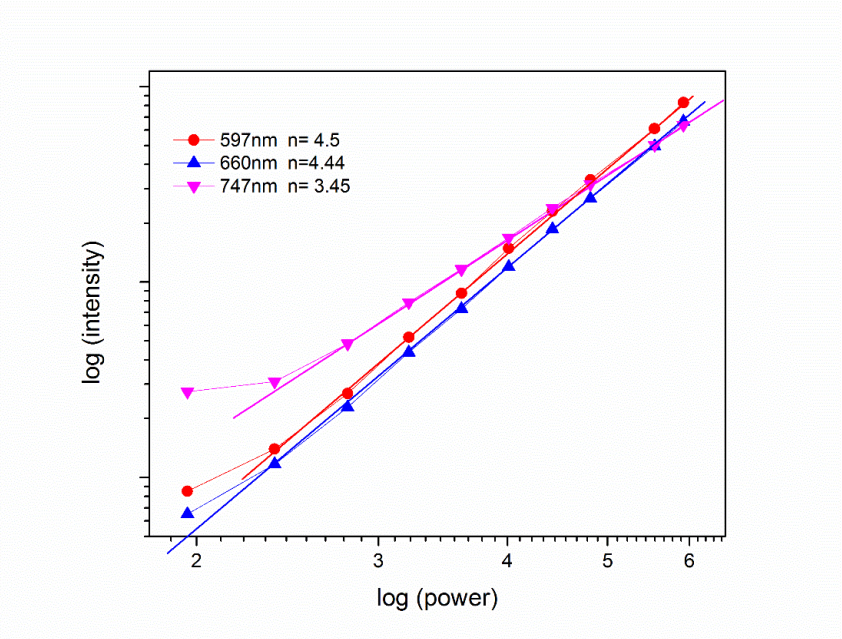

Figure 6.7 : Double logarithmic plot of Intensity-versus power for white light spectra from 1% Nd^{3+}/ 10% Yb^{3+} codoped yttrium silicate sample at vacuum.

6.1.3 Luminescence properties at 808 nm excitation

The luminescence measurements of 1% Nd^{3+}/ 10% Yb^{3+} codoped yttrium silicate (Y_2O_3:SiO_2) nanopowder were also performed with the near infrared (808 nm) laser diode excitation at atmospheric pressure and vacuum (0.01 mbar). The emission was observed with the wide bands corresponding to the energy transitions of Nd^{3+} ions and the energy transfer between Nd^{3+} and Yb^{3+} at various excitation power densities. For 808 nm excitation, the spectral changes were raised at atmospheric conditions in the case of different focusing arrangements. The luminescence profile of the sample was changed and s- shape pump power dependence was observed at vacuum condition. The structure of rare earth doped systems such as the distance between the dopant ions, atomic interactions between host and dopant ions, and the type of ions surrounding the dopant ion are very important parameters for the luminescence characteristics. UC emission efficiency depends strongly on host phonon energy and multi-photon relaxation processes are depressed and efficiency enhanced in low phonon energy hosts. Because of their excellent chemical and thermal stability, the similarity in ionic radius of Y^{3+} in yttrium silicate and rare earth ions, and their low phonon energy, the yttrium silicates are well-suited host materials [19,96].

Yb^{3+} ions are generally used as sensitizer by using ~970 nm excitation since its great absorption cross-section and the near infrared photon energy can be transferred from Yb^{3+} to other rare earth ions. The energy level $^4F_{3/2}$ of Nd^{3+} is a little higher than the $^2F_{5/2}$ level of Yb^{3+}, so pumping the Nd^{3+} doped material with an 808 nm laser diode excitation may provide energy transfer from Nd^{3+} to Yb^{3+} ion and also sensitization of Nd^{3+} ion by Yb^{3+}. Efficient energy transfers between Nd^{3+} and Yb^{3+} ions have been observed in different systems at various wavelengths [93, 94]. Due to the key role of the UC mechanism for the emission characteristics, it will be of great interest to gain a complete understanding of the UC mechanism in co-doped systems. The photon avalanche (PA) is a kind of UC process and it has feedback, or 'looping', the cycle of excited-state absorption (ESA) or energy transfer (ET) followed by cross relaxation (CR). All of these mechanisms lead to strong UC emission due to the population of a reservoir level of the rare-earth ions. There are some necessary conditions for this process to appear, such as the existence of a long lifetime intermediate state and some efficient CR processes [72]. However, in some cases, the photon avalanche mechanism could not be completely explained in the traditional sense and a new energy transfer

was demonstrated. Thus, the hetero-looping energy transfer that is a kind of avalanche UC process for the green and red emissions could be observed and reported simultaneously in some studies [97, 98]. Figures 6.8 and 6.9 show the emission spectra of Nd^{3+}/ Yb^{3+} codoped sample measured at atmospheric conditions at different scales of power densities. The focusing of the laser light, which varied the excitation power density, is a very important parameter for the measurements since the spectral profiles of the upconversion luminescence were affected. The changes of the spectral profiles were occurred for the low and high excitation power densities and could be adjusted by the tightness of focusing. The luminescence spectra at atmospheric conditions showed that up-conversion white light is dominant at low excitation power densities between 19.8 W/cm^2 and 98.6 W/cm^2. For the excitation power densities between 98.6 W/cm^2 and 570.7 W/cm^2, the up-conversion luminescence spectra could not be recorded due to the restrictions on the experimental setup used. However, the measurements were performed for the excitation power densities between 570.7 W/cm^2 and 935 W/cm^2 which can be called as strong focusing case. The spectral profiles were different from those measured between 19.8 W/cm^2 and 98.6 W/cm^2. Thus, the measurements were performed at both ranges of power densities for atmospheric conditions (Figure 6.8 and Figure 6.9). Figure 6.8 shows the visible UC luminescence in yttrium silicate doped with 10% Yb^{3+} and 1% Nd^{3+} ions with the energy transitions of Nd^{3+} under 808 nm excitation in the case of the low excitation power densities at a weak focusing case.

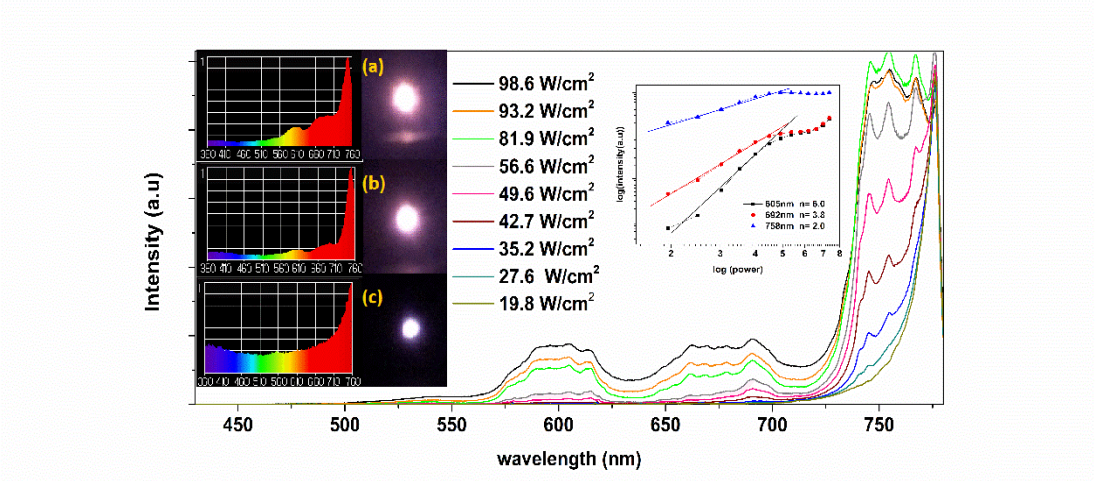

Figure 6.8 : Emission spectra of 1% Nd^{3+} and 10% Yb^{3+} co-doped yttrium silicate depending on power densities at atmospheric condition . The spectra and corresponding photos of the sample are given at (a) 98.6 W/cm^2, (b) 81.9 W/cm^2 and (c) 11.8 W/cm^2.

The inset figure in Figure 6.8 shows the double log representation of intensity versus laser power densities for measurements. The observed slight emission centered at ~542 nm arises from the intra-4f electronic transition $^4G_{7/2} \rightarrow {}^4I_{9/2}$ of Nd^{3+} ions. The other transitions of Nd^{3+} ions at ~605 nm, ~692 nm, and ~758 nm due to $^2G_{7/2}+{}^4G_{5/2} \rightarrow {}^4I_{9/2}$, $^4F_{7/2}+{}^4S_{3/2} \rightarrow {}^4I_{9/2}$, $^2H_{9/2}+{}^4F_{5/2} \rightarrow {}^4I_{9/2}$, respectively, were shown in Figure 6.8. It is well known that the number of the required photons for upper state emission can be found by using the relation $I \alpha P^n$ where I is the luminescence intensity, P is the pump laser power and n is the number of the photons involved in the process. The shapes of the slopes in red emissions of intensity versus power dependence at ~605 nm, ~692 nm, and ~758 nm were nearly identical and this behavior may indicate that the same intermediate state reservoir is involved in all upconversion processes [72].

Figure 6.9 shows the dominant thermal white light for high power densities at a strong focusing case. The broad emission at ~568 may be due to the $^4G_{5/2} \rightarrow {}^4I_{9/2}$ and this emission was observed at 570.7 W/cm^2.

The power density of 570.7 W/cm^2 is a threshold power to be able to record the emission from the sample at atmospheric conditions in a strong focusing case. We obtained the thermal white light for the excitation power densities above 570.7 W/cm^2 while the upconverted white emission was a dominant mechanism for the low excitation power densities below 98.6 W/cm^2.

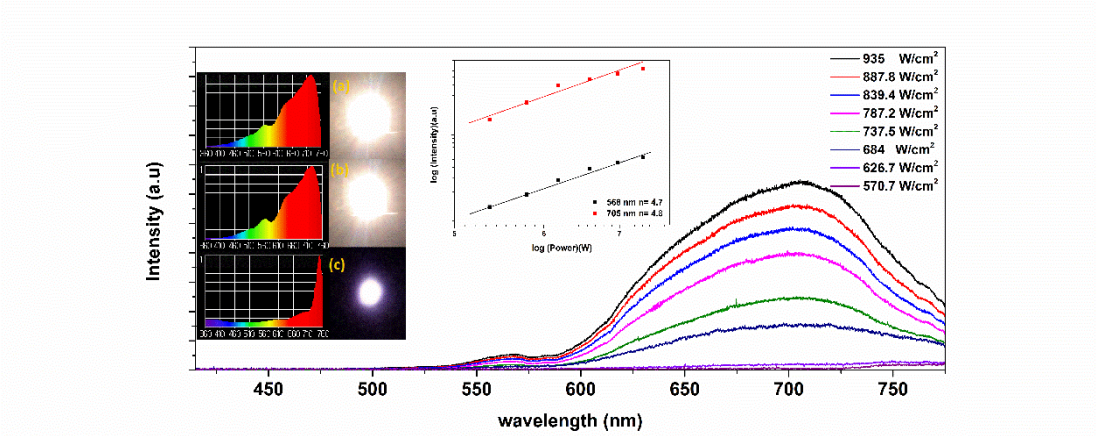

Figure 6.9 : Emission spectra of 1% Nd^{3+} and 10% Yb^{3+} co-doped yttrium silicate under atmospheric condition under 808 nm excitation at high power densities from 935 W/cm^2 to 570.7 W/cm^2. The emission spectra and the corresponding photos are given at (a) 887.8 W/cm^2, (b) 737.5 W/cm^2 and (c) 570.7 W/cm^2.

The similar luminescent behavior was observed for both Nd^{3+} and Nd^{3+}/Yb^{3+} the codoped samples for atmospheric conditions, however, in codoped case, we could not

obtain the upconversion white light and thermal white light together with increasing powers. For co-doped sample at atmospheric conditions, we obtained the up conversion white and thermal white light separately at different focusing cases, namely at various excitation power densities [18, 61]. When we compare the measurements of high and low power densities at strong and weak focusing cases, while the spectra of strong focusing are thermal white light, the other one is upconverted white light and both of them have strong emissions. The thermal white light may be due to the effects of high-intensity laser irradiation. The high power densities may cause the sample heating and can lead to generating broadband white emission with recombination of charge carriers [82]. The upconversion mechanism may be supposed to be very challenging for Nd^{3+}/Yb^{3+} codoped sample. The 808 nm laser diode excites Nd^{3+} into its $^4F_{5/2}$ state, and then a non-radiative relaxation may occur to the $^4F_{3/2}$ level of Nd^{3+}. This may be followed by emissions of Nd^{3+} due to $^4F_{3/2} \rightarrow {}^4I_{11/2}$, $^4I_{9/2}$ transitions. The energy could also be transferred from Nd^{3+} to Yb^{3+} and this may increase the population of the $^2F_{5/2}$ state of Yb^{3+} [18, 82]. The much larger slope values than n=2 indicate that a positively closed hetero-looping enhanced energy transfer upconversion mechanism that is a kind of photon avalanche (PA) between the Nd^{3+} and Yb^{3+} ions may be present. The possible energy level diagram of Nd^{3+} and Yb^{3+} ions in the co-doped yttrium silicate sample is shown in Figure 6.10.

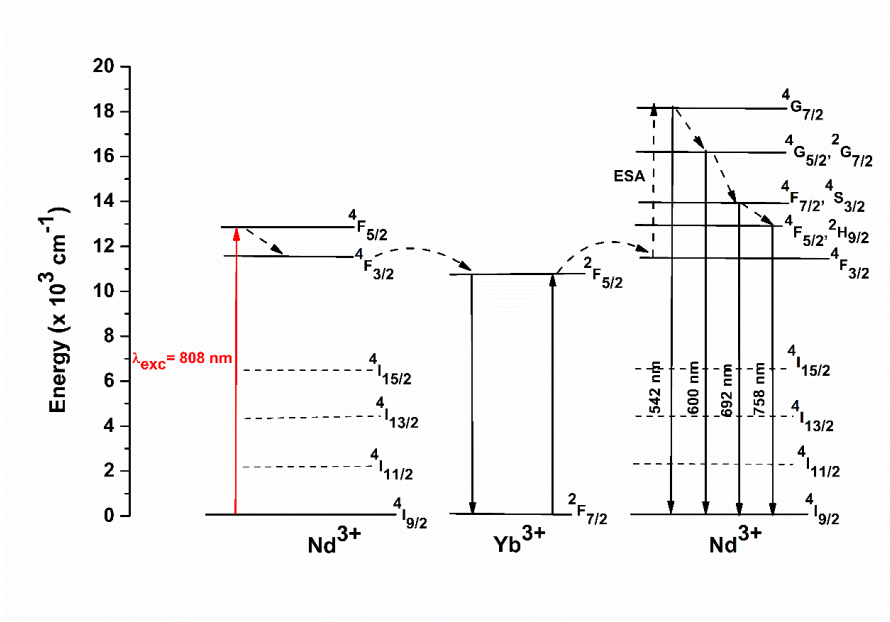

Figure 6.10 : The possible energy level diagram of Nd^{3+} and Yb^{3+} ions in co-doped yttrium silicate nanopowder.

In Figure 6.11, we see the emission spectra of Nd^{3+} and Yb^{3+} codoped yttrium silicate nanopowder with energy transition peaks of Nd^{3+} at vacuum conditions. The peak centered at ~483 nm due to the $^4G_{9/2} \rightarrow {}^4I_{9/2}$ electronic transition of Nd^{3+} was in the shape of a shoulder. The transitions at ~538 nm, ~600 nm, 661 nm and ~747 nm corresponding to $^4G_{7/2} \rightarrow {}^4I_{9/2}$, $^4G_{5/2} + {}^2G_{7/2} \rightarrow {}^4I_{9/2}$, $^4F_{9/2} \rightarrow {}^4I_{9/2}$ and $^4S_{3/2} + {}^4F_{5/2} \rightarrow {}^4I_{9/2}$ transitions of Nd^{3+}, respectively, were observed under vacuum conditions.

The number of photons that are required for emission was found by using pump laser power dependence relation for 1%Nd^{3+} and 10% Yb^{3+} codoped sample for vacuum measurements (Figure 6.12). Unexpectedly, the behavior of power dependency has an s-like shape with different three slopes. As illustrated in Figure 6.12, the shape of slopes and much larger n values above ~3 watts of excitation power, n ~4 or 6 may be referred to as a closed positive hetero-looping upconversion mechanism that is a kind of the conventional avalanche process [72]. In the vacuum, at high excitation power densities, n values may be lower than the exact photon numbers due to increasing competition between the decay and upconverted rate of intermediate states, which is called as saturation effect [99,100]. If upconversion dominates over linear decay for the depletion of intermediate excited states, the slope of luminescence from the upper state n is almost linear [100].

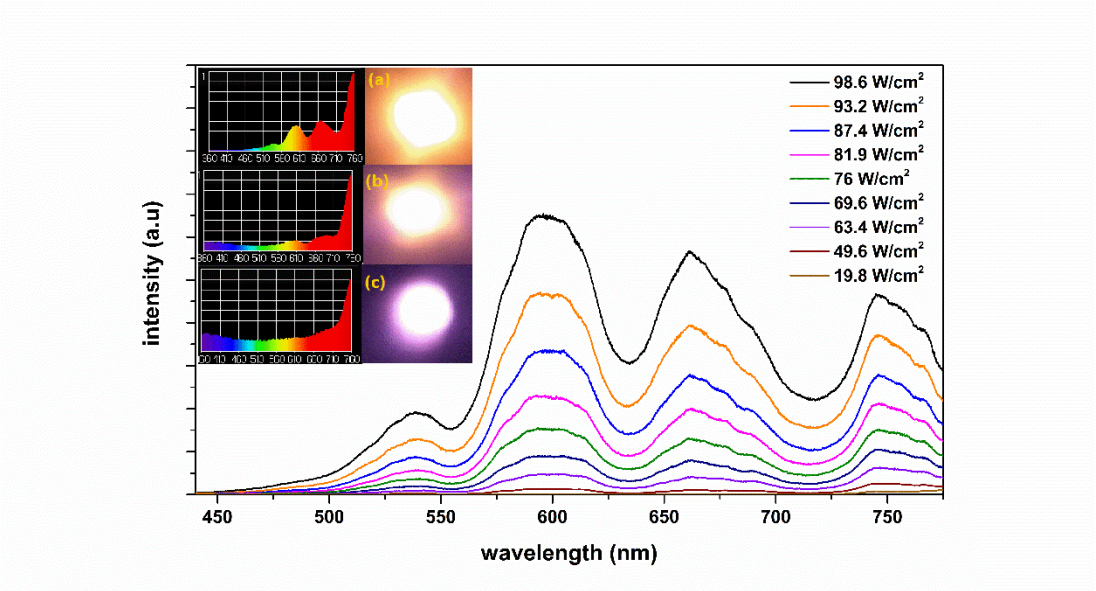

Figure 6.11 : White light generation of 10% Yb^{3+} and 1%Nd^{3+} doped yttrium silicate at 0.01 mbar under 808 nm excitation. The emission spectra and the corresponding photos of the sample are given at (a) 98.6 W/cm^2, (b) 35.2 W/cm^2 and (c) 11.8 W/cm^2.

In Figure 6.12, the slope of the double log plot of nanophosphor shows a decrease due to reaching saturation of the upconversion (above approximately 19.8 W/cm^2). For higher excitation power densities (between 935 W/cm^2 and 570.7 W/cm^2), the white light emission due to the thermal processes becomes dominant and the thermal process would introduce the much steeper growth after the saturation has begun to appear. The number of photons to obtain red emissions at 692 nm and 758 nm are n=3.8 and n=2 respectively, and those are lower than for the emission at 605 nm at atmospheric pressure. The separate regions for n values are characteristics of the photon avalanche process. Below the threshold, upconverted intensity is generally weak, above, the intensity increases by orders of magnitude, the pump light is strongly absorbed, and thermal processes play an effective role to obtain emission. The emission intensity of $^4G_{5/2}+^2G_{7/2}\rightarrow{}^4I_{9/2}$ transition at 605 nm is increasing faster than the red band at 758 nm for atmospheric pressure by increasing powers as seen in Figure 6.8.

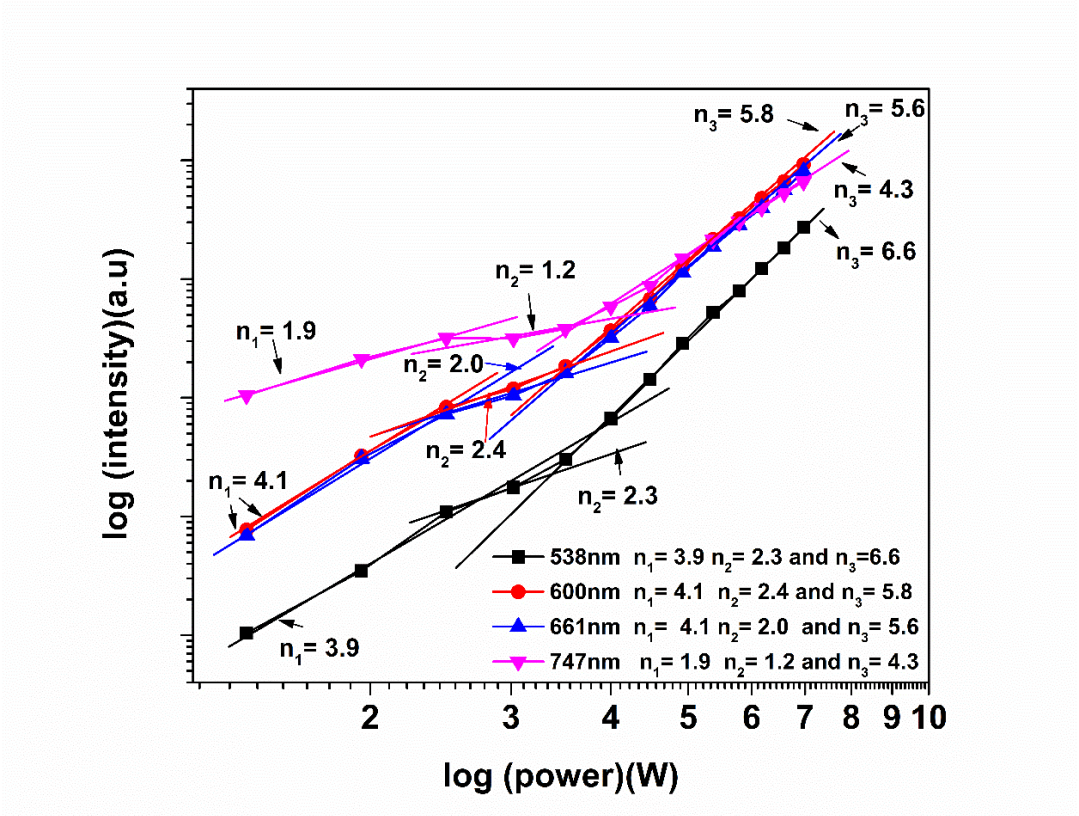

Figure 6.12 : Double log plot for 1% Nd^{3+} and 10% Yb^{3+} co-doped yttrium silicate sample at 0.01 mbar.

The increase in $^4G_{5/2}+^2G_{7/2}\rightarrow{}^4I_{9/2}$ transition at 605 nm is bigger than $^4F_{7/2}+^4S_{3/2}\rightarrow{}^4I_{9/2}$ transition at 692 nm. The cross relaxation processes between excited Yb^{3+} and Nd^{3+} ions in $^4F_{3/2}$ level may become one of the dominant processes causing an increase of

the UC emission at 605 nm. Then, increasing the excitation power causes thermal heating, which may increase the non-radiative transitions from upper level of emission centered at 692 nm and 758 nm to lower lying $^4F_{3/2}$ level of Nd^{3+} ions. As a result, the decrease of these emission intensities compared to emission at 605 nm is observed. At low pressure, the emission intensity of $^4G_{7/2} \rightarrow {}^4I_{9/2}$ at 538 nm is a little higher than that is in $^4G_{5/2} + {}^2G_{7/2} \rightarrow {}^4I_{9/2}$ at 600 nm. The other red band intensity centered at 661 nm is nearly the same with the strong orange emission at 605 nm. When the $^4F_{5/2} + {}^4S_{3/2} \rightarrow {}^4I_{9/2}$ transition of Nd^{3+} ion at 747 nm is increasing, the orange band emission at 600 nm is decreasing with power.

The results of illuminance meter measurements for Nd^{3+}/Yb^{3+} codoped sample at both atmospheric and low pressures were presented in Figure 6.13a, b, and c.

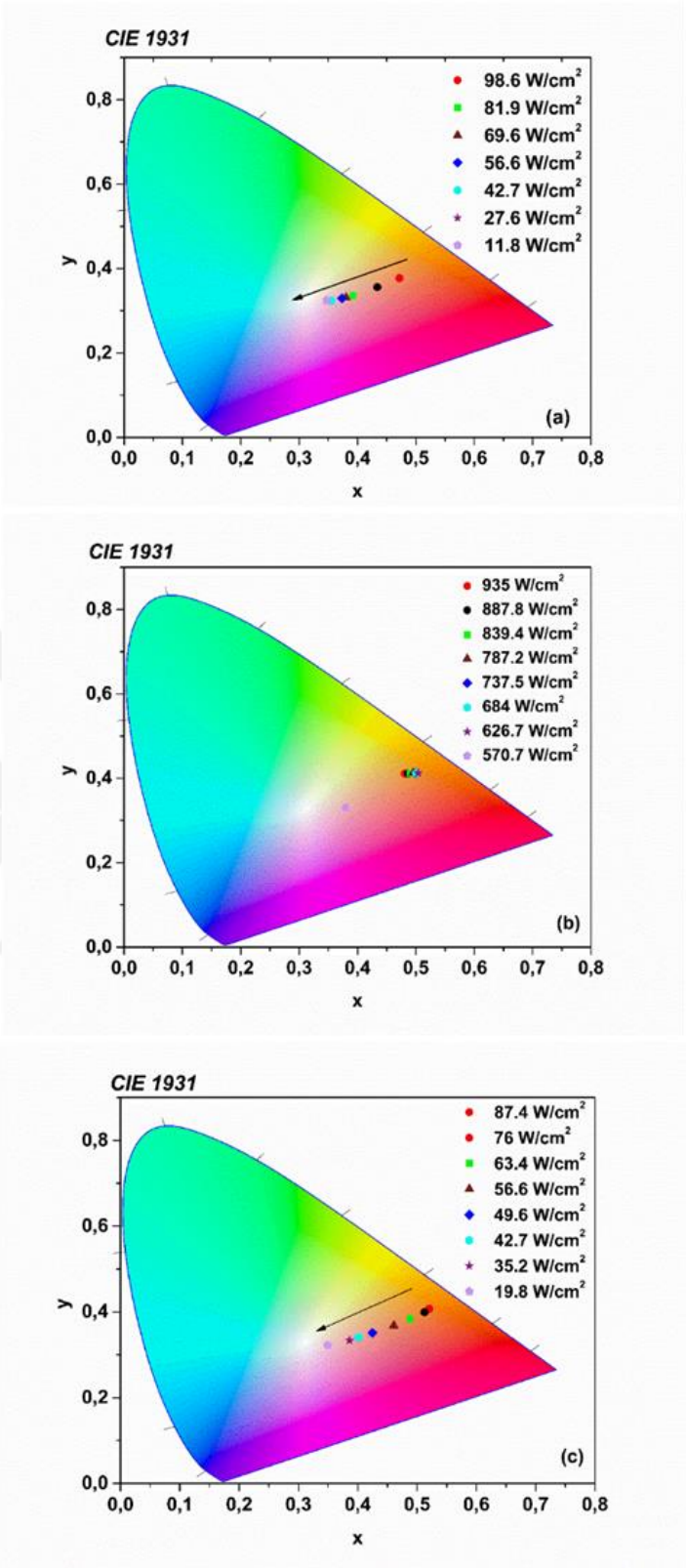

Figure 6.13 : The CIE 1931 (x, y) coordinates for 1% Nd^{3+} and 10% Yb^{3+} co-doped sample at 808 nm excitation (a) Case 1. Weak focusing with low power densities at atmospheric condition (b) Case 2. Strong focusing with high power densities at atmospheric condition (c) Case 3. Vacuum condition (0.01 mbar).

Chromaticity coordinates (x, y) were near to white light coordinates (0.33, 0.33) for measurements of atmospheric pressure with higher x, y values for high power densities. Color Rendering Index was generally higher for high power and small for low power densities at atmospheric pressure. The chromaticity values gave the different Correlated Color Temperature values for the sample between ~2100 K and ~4800 K for atmospheric and vacuum conditions. The emission was white at ~570 W/cm^2 and the color was shifted to the orange-red region like a candlelight with increasing pumping power. We get the emission 'like a candle white light' as in our previous work about Nd^{3+} single doped sample [18].

The decay and rise patterns were measured to observe the luminescence dynamics of the sample in atmospheric and vacuum conditions (Figure 6.14 and 6.15).

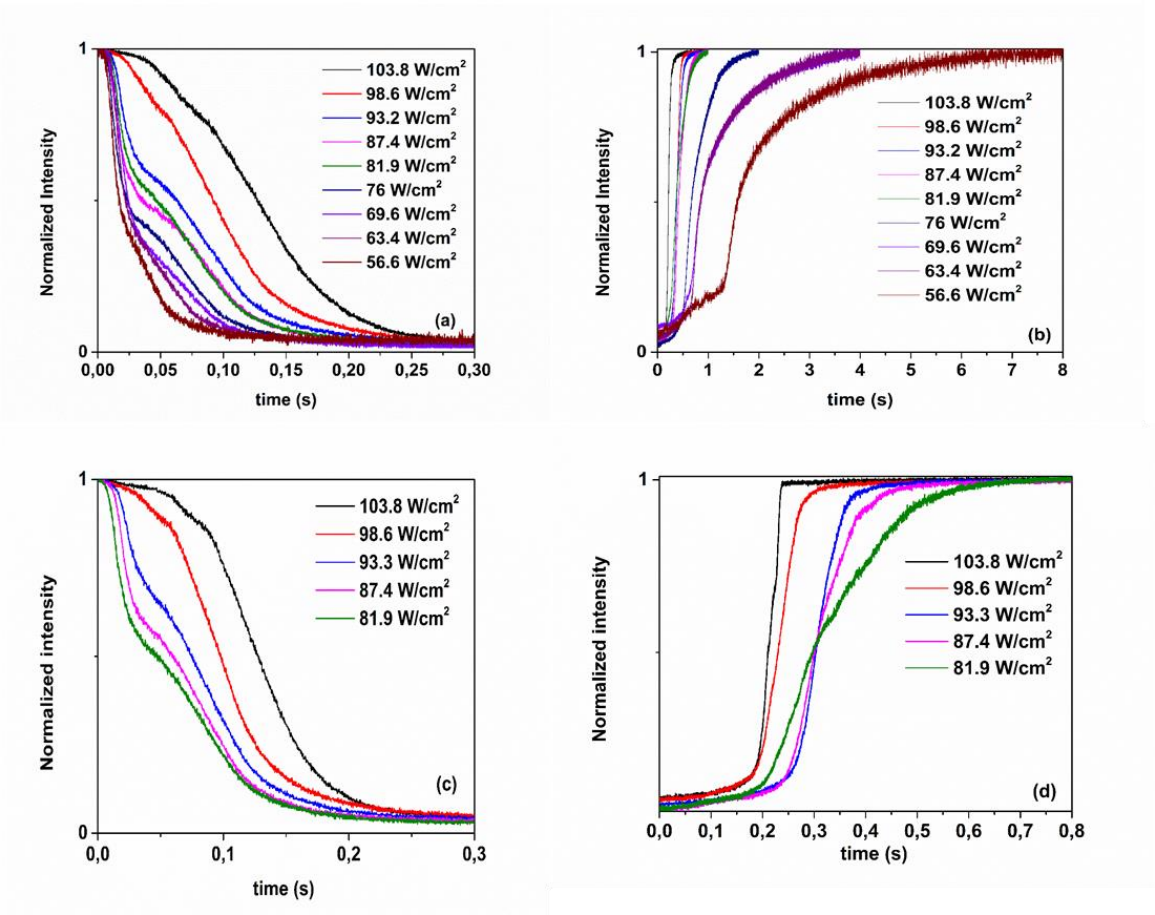

Figure 6.14 : a) Decay; b) rise patterns at 675 nm and c) decay d) rise patterns at 750 nm for 1% Nd^{3+} and 10% Yb^{3+} codoped yttrium silicate nanopowder depending on power densities at atmospheric conditions (in case of weak focusing).

The decay and rise curves were smoother at vacuum conditions. However, some variation in the intensities indicating some deviations from the single exponential

behavior of rising and decay curves were observed under atmospheric conditions. This may be due to the thermal conductivity of the air captured in the powder samples. The decay patterns at 675 and 750 nm (Figure 6.14 a, c) were nearly the same shapes, the strong laser absorption may occur, and thermal effects were generated in the sample. The rising times at 675 nm were longer than those at 750 nm (Figure 6.14 b, d), so it is indicated that the thermal effects are more effective at 675 nm and upconversion emission is dominant at 750 nm. In other words, the slow rise times show that the thermal effects are dominant for producing broadband white emission. The longer time at vacuum indicated that the existence of a long lifetime intermediate state and some efficient CR processes in the system (Figure 6.15). In Figure 6.14, it is seen from the rising and decay patterns that the emission intensity is not stable at atmospheric conditions. In contrast, the stability of emission at the vacuum is extremely high and that is in good agreement with the luminescence behaviors. It is well known that the thermal conductivity of air decreases with decreased pressure. The threshold power to obtain white light at vacuum is lower than that at atmospheric pressure due to the insulating effect of vacuum.

As a summary, the Nd^{3+}/Yb^{3+} codoped yttrium silicate sample was synthesized using the sol-gel method. The annealed powder sample was structurally characterized by using the X-ray diffraction analysis and the results indicate that nanostructure was successfully obtained. We observed different emission bands due to energy levels of Nd^{3+} at low power densities for atmospheric pressure and vacuum for 808 nm laser diode excitation. The UC mechanism, in fact, is more complex than the experimental emission profiles seem to suggest. At atmospheric conditions, we observed the different spectral behaviors under weak and strong focusing arrangements. We reported an interesting photon avalanche process based on the observation of anomalous s-shape pump power dependence of UC green and red radiations at vacuum. Under weak excitation conditions at atmospheric pressure, UC-assisted white light was observed for excitation power densities below ~99 W/cm^2 and white light due to the thermal effects was observed for excitation power densities higher than ~570 W/cm^2 at atmospheric conditions. At vacuum (0.01 mbar), however, the white light due to UC processes and the thermal effects were generated above ~20 W/cm^2 which is much lower than that measured for atmospheric conditions for low excitation cases.

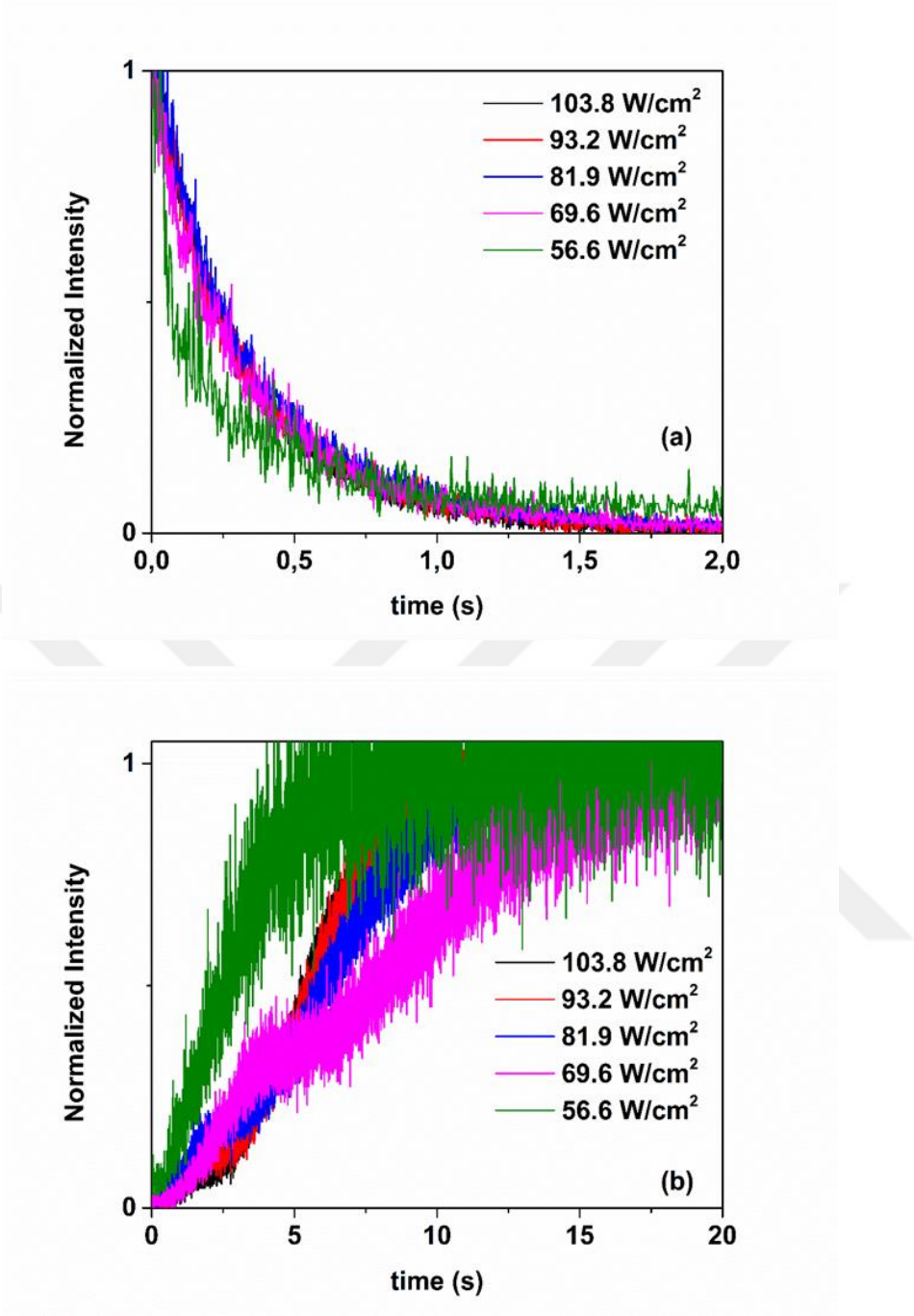

Figure 6.15 : a) Decay; b) rise patterns at 600 nm for 1% Nd^{3+} and 10% Yb^{3+} co-doped yttrium silicate nanopowder depending on power densities at 0.01 mbar.

The emitted light intensity was not stable at atmospheric pressure while it was more stable at 0.01 mbar. It was seen that the thermal effects due to the laser absorption, duration of the measurement and focusing arrangements play a more important role in the luminescence behavior at atmospheric pressure. We report the anomalous "s"-shape pump power dependence of the up-converted green and red emissions obtained under vacuum (0.01mbar). We have also investigated the luminescence dynamics of these emissions by analyzing the rise and decay patterns. The threshold power to obtain

very bright white light was decreased under vacuum condition and the color quality parameters were analyzed for all the experimental conditions.

We obtained the thermal white light from the undoped host, only Yb^{3+} doped host, and single Nd^{3+} doped host as indicated in our previous chapters [18, 61]. The white emission may be due to the host, Yb^{3+} ions or Nd^{3+} ions and due to the interactions between them. The obtained conclusions here may be applied to other single doped or codoped nanocrystals. The studies and further efforts in the development of fabrication and optical performance of upconversion (UC) materials can lead to improving their UC efficiency and may also reduce the production costs.

6.2 Nd^{3+}/ Tm^{3+} Codoped Yttrium Silicate Nanopowders

The upconverted materials that emit different colors play an important role in photonics. Blue light emitted solid-state systems have also attracted a great deal of interest by the researchers due to their potential use in photonic devices. For example, they are used for light emitting diodes, drug delivery, biological labels, and sensors, etc. [101–104]. To achieve a blue emission, trivalent ytterbium (Yb^{3+}) can be used as a near infrared sensitizer under ~980 nm excitation. The excited Yb^{3+} ions can transfer their energy to Tm^{3+} ions so, a strong blue upconversion emission may occur [105,106] or a blue emission can be occurred by cooperative emission of Yb^{3+}-Yb^{3+} couple [19]. It is also possible to obtain blue light from the Tm^{3+} doped yttrium silicate sample as mentioned in Chapter 5. The blue upconversion emission of Tm^{3+} ion is appeared by populating states $^1G_4$ (~21000 cm^{-1}) and $^1D_2$ (~28000 cm^{-1}) and thus $^1D_2 \rightarrow {}^3F_4$ and $^1G_4 \rightarrow {}^3H_6$ transitions peaked at ~450 nm and ~480 nm, respectively. The trivalent Neodymium (Nd^{3+}) is another near infrared sensitizer pumping around ~800 nm.

In this part, upconversion properties of Tm^{3+} and Nd^{3+} codoped yttrium silicate samples were investigated at atmospheric pressure and vacuum by using a continuous wave laser operating at 808 nm. We used Nd^{3+} as a sensitizer to observe the characteristics of light and mainly investigated the effects of pressure difference and pumping power on luminescence behavior. The gel formed sample was grinded at agate mortar after annealing at 1250 ^0C for 12 h. The sol-gel process allowed us to obtain single phase and homogeneous nanomaterial with desired elemental composition. The emission profile of the Tm^{3+} doped sample is dramatically influenced

by the presence of Nd^{3+} ions when we compare the spectrum of the codoped system with the single Tm^{3+} doped system.

6.2.1 Structural analyses

The X-ray diffraction patterns of Y_2O_3-SiO_2: 1% Nd^{3+}/ 0.5Tm^{3+} are shown in Figure 6.16. We can see from the figure that positions and relative intensities are most well suited to the α-$Y_2Si_2O_7$ structure with card number 38-0223 according to JCPDS.

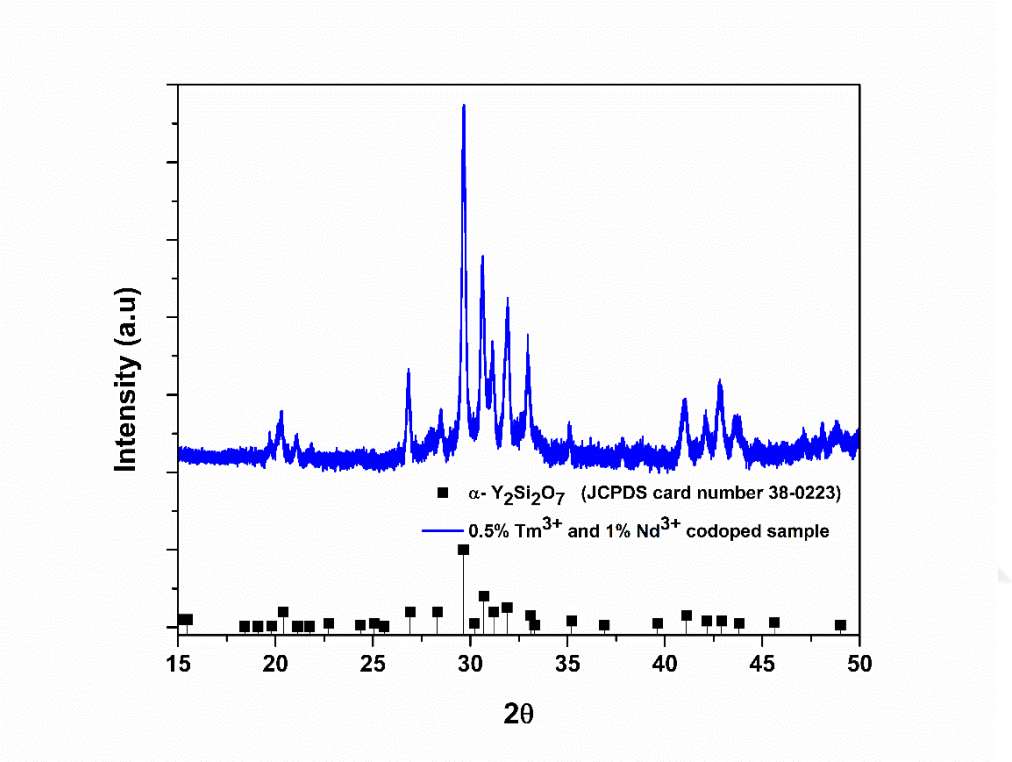

Figure 6.16 : XRD spectra of 1%Nd^{3+} and 0.5%Tm^{3+} doped yttrium silicate nanopowders.

The main phase is α-$Y_2Si_2O_7$ (triclinic, P-1(2) space group) and the strongest peak is detected at 2θ~29.60 with the plane (1 -2 0). There are very little impurities that can be neglected and it confirms that Nd^{3+} and Tm^{3+} ions were successfully located in the matrix. The average grain size was estimated as ~90 nm, by using the Scherer equation [50].

6.2.2 Luminescence properties of Tm^{3+}/Nd^{3+} codoped yttrium silicate at atmospheric conditions

The luminescence measurements of Tm^{3+} and Nd^{3+} doped yttrium silicate nanopowders were performed at atmospheric conditions under 808 nm laser excitation. Figure 6.17 shows the spectra and emissions can be attributed to the energy transition

of Tm^{3+} and Nd^{3+} ions. When the Tm^{3+} singly doped and Nd^{3+}/ Tm^{3+} codoped samples were exposed to the same excitation wavelength, the luminescence characteristics are extremely different. When we compare 0.5%Tm^{3+}/ 1% Nd^{3+} codoped sample with the 0.5% Tm^{3+} single doped sample (Chapter 5.1), it is clearly seen that the emission profile depends on dopant ions.

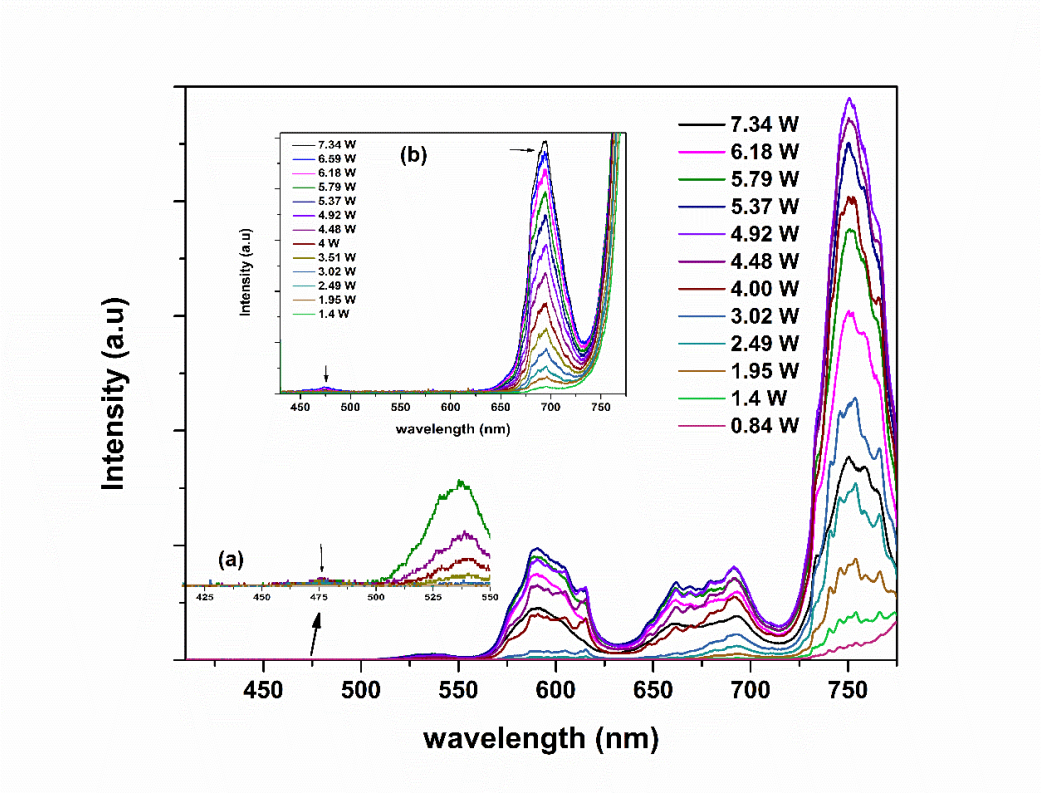

Figure 6.17 : Spectra of 1% Nd^{3+} and 0.5% Tm^{3+} doped yttrium silicate at atmospheric conditions under 808 nm excitation. The inset figures show a) blue region of the spectra in detail b) the spectra of Tm^{3+} single doped sample at atmospheric conditions at 808 nm to see the difference adding the Nd^{3+}.

The emission spectrum of the Tm^{3+}: $Y_2Si_2O_7$ has $^1G_4 \rightarrow {}^3H_6$ transition of about 475 nm while this emission has almost diminished in the Tm^{3+}/ Nd^{3+} codoped sample. Namely, $^1G_4 \rightarrow {}^3H_6$ energy transition is considerably quenched for the codoped sample and additional energy transitions of $^2G_{7/2} \rightarrow {}^4I_{9/2}$ at 536 nm, $^2G_{5/2}+{}^2H_{11/2} \rightarrow {}^4I_{9/2}$ at 590 nm due to Nd^{3+} ion appeared in spectra (Figure 6.17). The emission between 650-700 nm can be due to both Nd^{3+} and Tm^{3+} ions. We said that a sharp peak centered about 695 nm for a single Tm^{3+} doped sample can be due to the ($^3F_2$, $^3F_3$) $\rightarrow {}^3H_6$ of Tm^{3+} as mentioned in Chapter 5. In this case, when we add Nd^{3+} ion to the system, the sharp peak centered about 695 nm for single Tm^{3+} doped sample become broad emission and the peak shifts to 691 nm. It is understood that adding Nd^{3+} to the system causes

shifting of spectra to the blue region (Figure 6.18) and this behavior was observed by Rakov and Maciel before [106, 107]. The additional broad peak about 661 nm for the codoped samples may be due to $^4F_{9/2} \rightarrow {}^4I_{9/2}$ of Nd^{3+} ions. The emission centered at 750 nm may be due to $^4F_{5/2}+{}^4S_{3/2} \rightarrow {}^4I_{9/2}$ transitions of Nd^{3+} ion. The emission spectrum of the Tm^{3+} doped sample is dramatically influenced by the presence of Nd^{3+} ions.

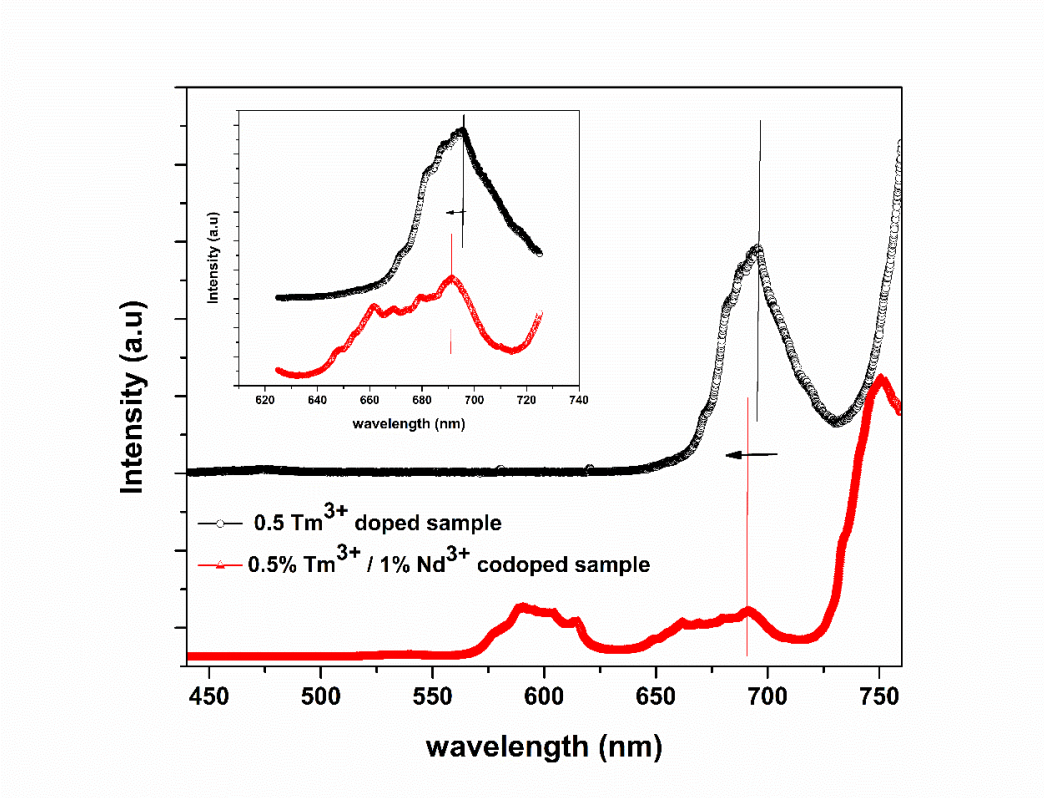

Figure 6.18 : The comparison of the UC luminescence spectrum ofTm^{3+} single doped and Tm^{3+}/ Nd^{3+} codoped samples at the atmospheric condition with an excitation wavelength of 808 nm pumping by 4.92 W.

The experimental data measured at various excitation powers for the emission bands of single Tm^{3+} doped and Tm^{3+}/ Nd^{3+} codoped samples have been fitted with a straight line. The double log representation of the intensity versus pumping power is shown in Figure 6.19.

The numbers of the photons involved in the processes have been found as n= ~5, ~5, ~3 and ~2 at 536 nm, 590 nm, 695 nm, and 750 nm, respectively, as seen in Figure 6.19. It is noticed that the photon number involved in the process at 695 nm is increased from ~2 to ~3 by adding Nd^{3+} to the Tm^{3+} doped yttrium silicate. We could not strongly detect the blue emission at 475 nm for the codoped sample (see Figure 5.13).

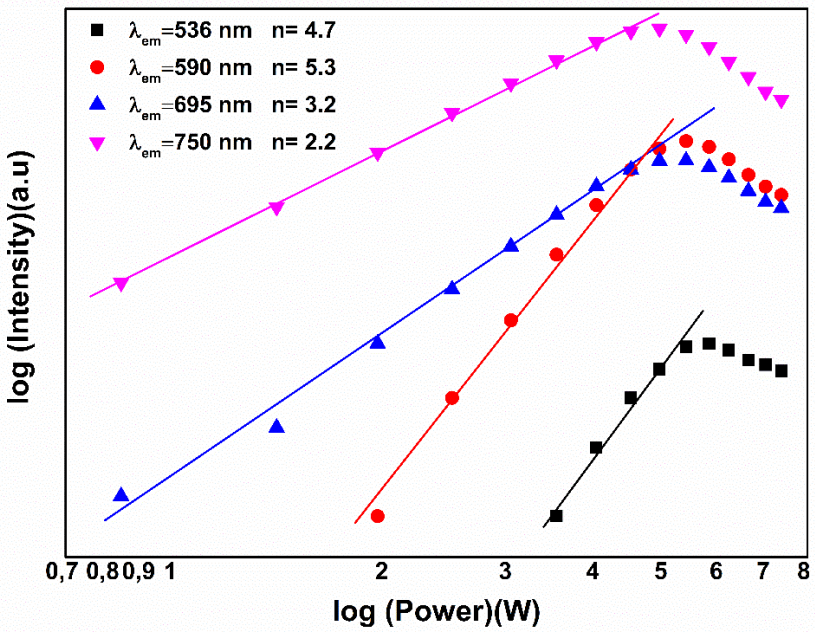

Figure 6.19 : Log-log plot of the 0.5% Tm^{3+}/1% Nd^{3+} codoped sample at the atmospheric condition with the excitation wavelength of 808 nm.

The CCT, CRI, CIE coordinates and the corresponding photo of the sample were given in Table 6.1 depending on pumping powers. The color quality coordinates (CIE-1931) were found to be (0.4777, 0.3680) and (0.3255, 0.2965) for 7.34 W and 0.84 W respectively, at atmospheric pressure. The color temperatures were measured as 2148 K and 5928 K at 7.34 W and 0.84 W, respectively, at atmospheric conditions. It has corresponded well with the emission turns to incandescent warm white light at high pumping powers.

Table 6.1 : HNT1_1250 (1% Nd^{3+} / 0.5% Tm^{3+} codoped Yttrium Silicate nanophosphor) at 808 nm excitation under atmospheric conditions.

Output Power (W)	CCT(K)	CRI (Ra)	CIE coordinates	Spectrum	Photo of the emission
7.34	2148	76	(0.4777, 0.3680)	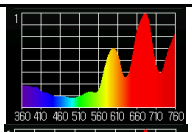	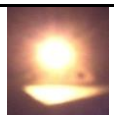
6.59	1940	69	(0.5072, 0.3784)	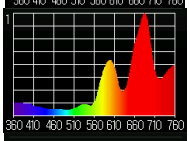	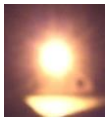
5.79	1857	64	(0.5204, 0.3822)	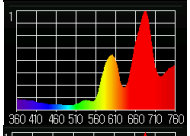	
4	1797	65	(0.5173, 0.3687)	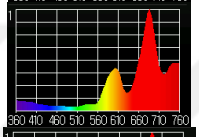	
3.02	2244	82	(0.4450, 0.3324)	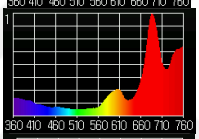	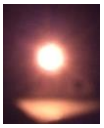
1.95	4453	78	(0.3505, 0.3001)	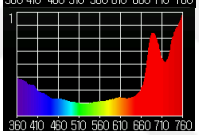	
0.84	5928	82	(0.3255, 0.2965)	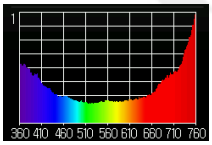	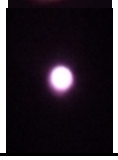

6.2.3 Luminescence properties of Tm^{3+}/ Nd^{3+} codoped yttrium silicate at vacuum

The luminescence spectra of Tm^{3+} and Nd^{3+} codoped yttrium silicate nanopowder at vacuum (0.01 mbar) under 808 nm laser excitation is shown in Figure 6.20. The inset figure belongs to 0.5 Tm^{3+} doped sample and it is clearly seen that spectra shifts to the blue region when Nd^{3+} ion is added to the system as in the case of the atmospheric condition. The red emission centered at 682 nm corresponding to ($^3F_2$, $^3F_3$) $\rightarrow ^3H_6$ of Tm^{3+}. The number of emission bands is increased by adding the Nd^{3+} ions to the system as expected. The other wideband transitions at 536 nm, 590 nm, 687 nm, and 748 nm are the same as those are in atmospheric pressure.

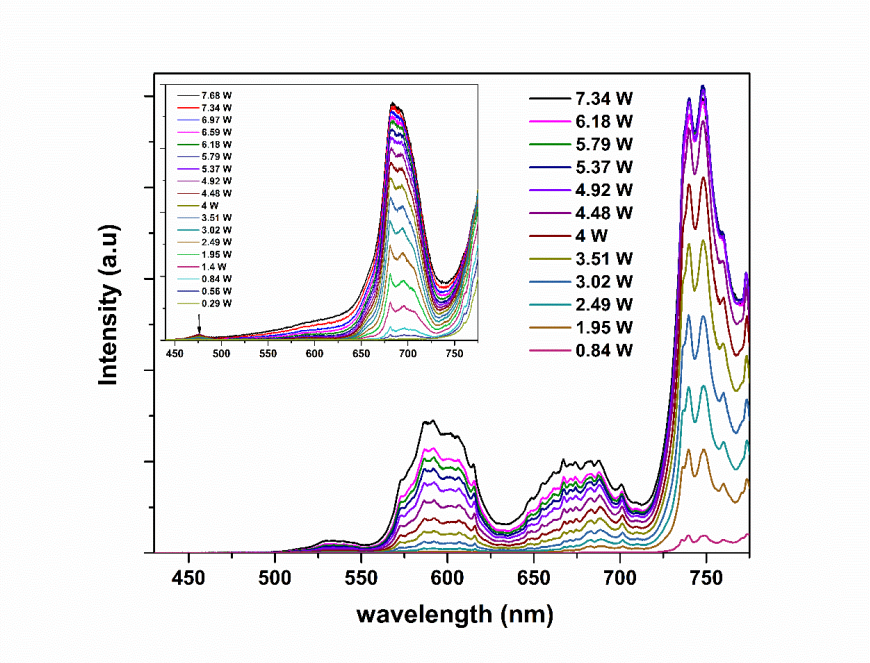

Figure 6.20 : Spectra of 1% Nd^{3+} and 0.5% Tm^{3+} doped yttrium silicate nanopowder depending on power at 0.01 mbar under 808 nm excitation. The inset figure shows the spectra of the single Tm^{3+} doped sample under vacuum for comparison.

Figure 6.21 shows intensity dependence on pumping power at vacuum conditions. The number of photons involved in energy transfer processes are decreased by comparing with the measurements at atmospheric pressure.

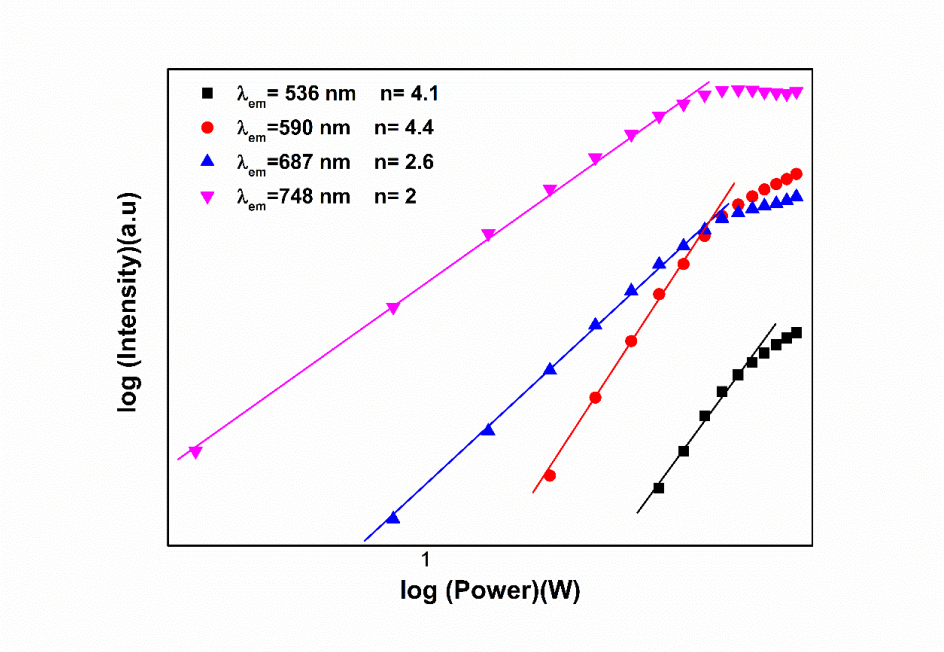

Figure 6.21 : Log log plot of the 0.5% Tm^{3+}/ 1% Nd^{3+} codoped sample at 0.01 mbar under 808 nm.

In addition, positions of the peaks at 695 nm and 750 nm attributed to $^3F_3 \rightarrow {}^3H_6$ and $^4F_{5/2}+{}^2H_{9/2} \rightarrow {}^4I_{9/2}$ respectively at atmospheric pressure are shifted to lower wavelengths at vacuum. The illuminance meter results and corresponding photos of the sample at vacuum are shown in Table 6.2.

Table 6.2 : HNT1_1250 (1% Nd^{3+} / 0.5% Tm^{3+} codoped Yttrium Silicate nanophosphor) at 808 nm excitation under vacuum conditions.

Output Power (W)	CCT(K)	CRI (Ra)	CIE coordinates	Spectra	Photo of the emission
7.34	1960	58	(0.5354, 0.4184)	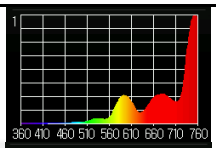	
6.59	1936	56	(0.5367, 0.4161)	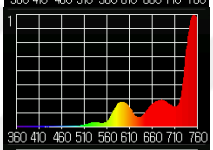	
5.79	1921	54	(0.5371, 0.4139)	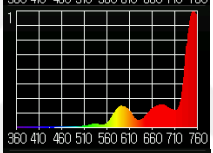	
4.92	1894	49	(0.5409, 0.4143)	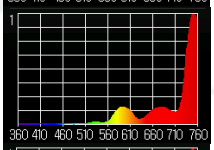	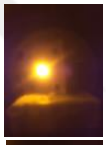
4	1851	45	(0.5483, 0.4161)	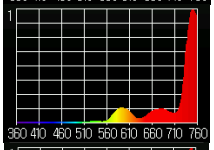	
3.02	1825	47	(0.5463, 0.4091)	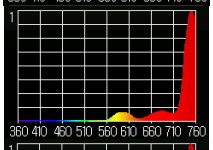	
1.95	2014	66	(0.5036, 0.3847)	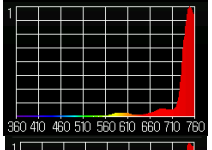	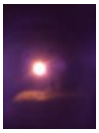
0.84	3608	89	(0.3829, 0.3406)	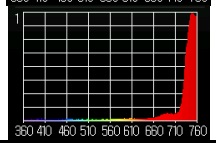	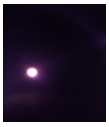

Color rendering index is the highest value (89%) at vacuum condition at 0.84 W. The CIE coordinates (x, y) values are higher at vacuum than that is in atmospheric pressure, for example, (0.5354, 0.4184) at 7.34 W. At vacuum, CCT values are less than the obtained results at atmospheric conditions.

Further characterization of the luminescence dynamics was carried out with performing the rise and decay patterns under atmospheric and vacuum conditions. The decay and rise patterns of the Nd^{3+}/ Tm^{3+} codoped system are shown in Figure 6.22. It is clearly seen that both decay and rise times are strongly dependent on pumping power. The decay patterns are shorter for low powers and increasing with the increased powers. We had measured decay and rise patterns of sample doped with single Nd^{3+} at vacuum before. We noticed that decay patterns were noticeably longer for the Nd^{3+} single doped sample. This may indicate that the dominant mechanism of energy transfer processes for the codoped sample is nonradiative energy transfer between Nd^{3+} and Tm^{3+} ions.

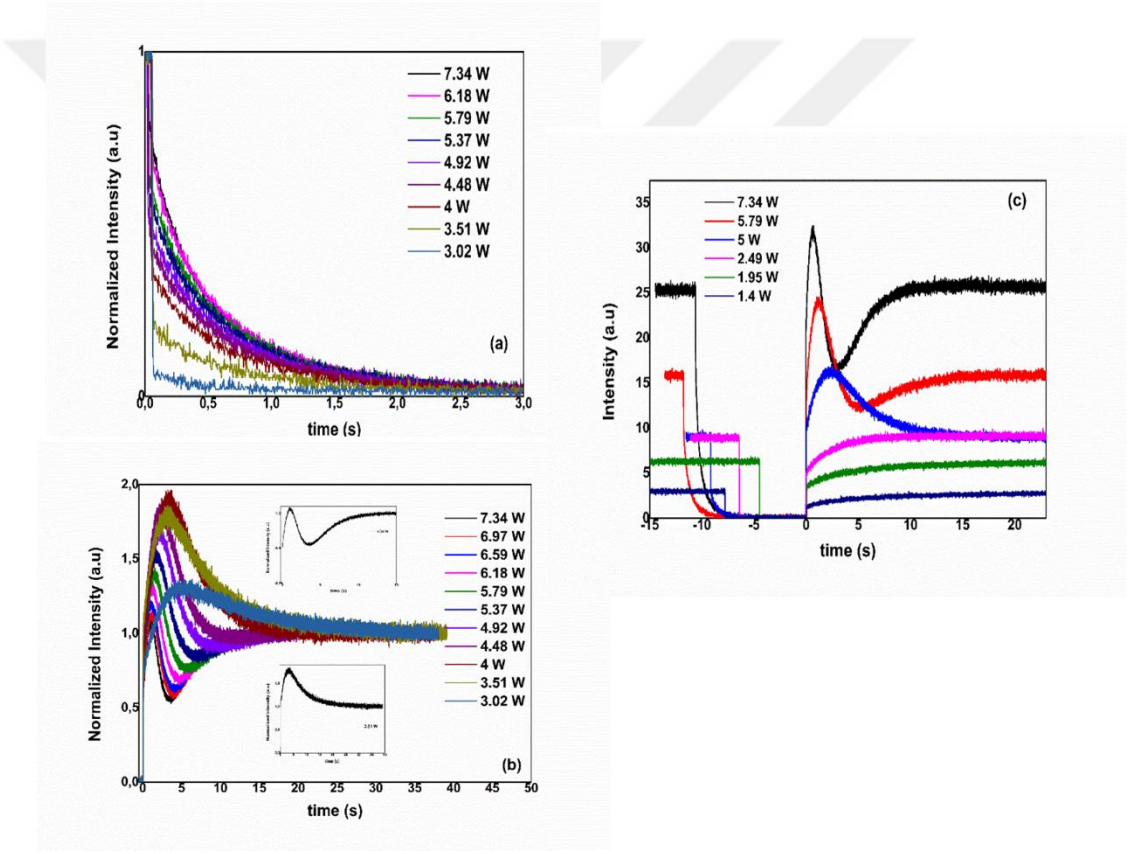

Figure 6.22 : Luminescence dynamics of the 0.5% Tm^{3+}/ 1 % Nd^{3+} co-doped sample a) decay patterns b) rise patterns and c) the whole picture of the decay and rise patterns detected together under 0.01 mbar.

In the same manner, the rise patterns are shorter for the codoped sample. The lifetime measurements are necessary to investigate which mechanism is responsible for the energy transfer mechanism of samples, but we have not an opportunity to get the lifetime measurements. However, decay and rise patterns can give us an idea about it.

6.3 Tm^{3+}/ Yb^{3+} Codoped Yttrium Silicate Nanopowders

Trivalent thulium ion has widely studied due to its near infrared and visible emissions properties. It has technological importance for applications such as developing medical laser technologies, optical fiber [108-110]. We know that the trivalent Ytterbium ion has the simple energy level, large absorption and emission cross section, long lifetime, and usually used as a sensitizer. There are some studies about the Tm^{3+} / Yb^{3+} codoped systems such as fluoride crystals [111], lanthanum aluminum germanate glasses [112], fluorophosphate glasses [113] etc. For yttrium silicate host material, the dopant ions (Tm^{3+}, Nd^{3+}, and Yb^{3+}) are replaced by the Y^{3+} ions randomly since they have similar size and same valence state.

The excited Yb^{3+}at 975 nm can transfer its energy to Tm^{3+} ion by phonons via energy transfer processes. Similarly, the excited Tm^{3+} ion at 808 nm can also gain energy for Yb^{3+}. The selection of the host matrix is very important at this point. High phonon energy increases the nonradiative processes. Yttrium silicates hosts have low phonon energy and suitable for obtaining efficient luminescence results. So, we used yttrium silicate as host and synthesized %0.5Tm^{3+}/10% Yb^{3+}(HTY1_1250), %0.25 Tm^{3+}/10% Yb^{3+}(HTY2_1250) and %1.0 Tm^{3+}/10% Yb^{3+} (HTY3_1250) codoped nanophosphors via sol-gel method. The luminescence properties of the samples were investigated at atmospheric conditions by 808 and 975 nm excitations. The emission properties of HTY1_1250 sample were also studied at vacuum conditions. Color quality parameters and decay rise patterns were determined experimentally.

6.3.1 Structural analysis

To obtain information on crystal structure such as phase and purity for the samples, XRD measurement was performed in the range of $2\theta=15^0$ and 50^0 with the step of 0.02. According to JCPDS, the resultant patterns are presented Figure 6.23 together with a reference pattern for α-$Y_2Si_2O_7$ (triclinic, P-1(2) space group) (JCPDS card number: 38-0223.)

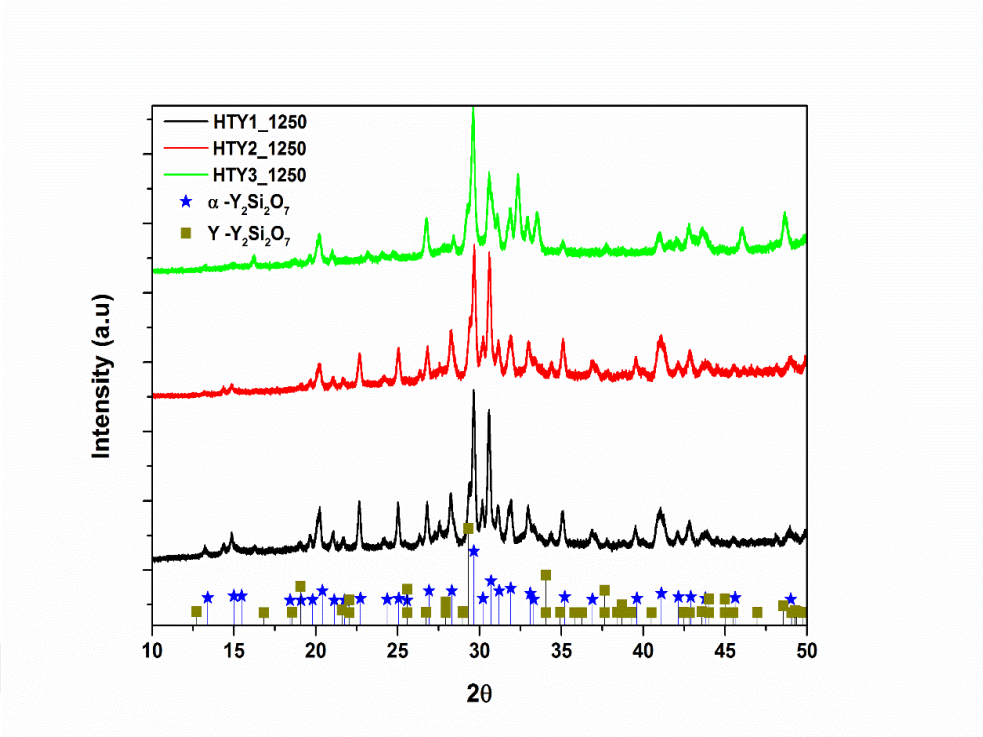

Figure 6.23 : XRD patterns of the Tm^{3+}/Yb^{3+} doped Y_2O_3-SiO_2 samples.

The doping ytterbium (10% Yb^{3+}) may cause additional peaks due to Y-$Y_2Si_2O_7$ phase with card number 74-1994. The grain sizes of the samples HTY1_1250, HTY2_1250 and HTY3_1250 are found as ~79 nm, ~68 nm and ~61 nm, respectively, by using Scherrer equation.

6.3.2 Luminescence properties of Tm^{3+}/Yb^{3+} codoped nanophosphors at 975 nm

Luminescence emission properties in Tm^{3+}/Yb^{3+} codoped yttrium silicate samples have been studied at atmospheric conditions (Figure 6.24) and vacuum (Figure 6.25) with 975 nm excitation. The excitation wavelength of 975 nm is coincident with the ground state absorption of Yb^{3+} ions. The Yb^{3+} ions were excited with 975 nm diode laser and then transferred its energy to Tm^{3+} ions, which results in characteristic emission bands of Tm^{3+} at ~475 nm, ~700 nm, ~ 800 nm. In Figure 6.24, the slight blue peak about 475 nm corresponds to the $^1G_4 \rightarrow {}^3H_6$ energy transfer of Tm^{3+} or cooperative emission of Yb^{3+} and near infrared peak about 800 nm corresponds to the $^3H_4 \rightarrow {}^3H_6$ transition of Tm^{3+}. Both levels are populated through the $^2F_{5/2}$ level of Yb^{3+} [114]. The band centered about the 700 nm may be due to $^3F_3 \rightarrow {}^3H_6$ energy transfer of trivalent Thulium(III) ion.

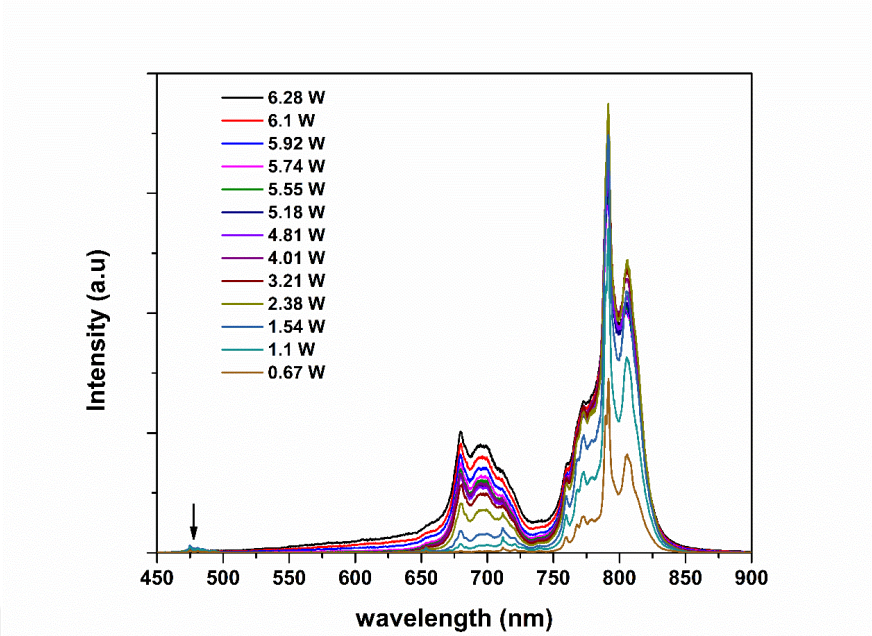

Figure 6.24 : Luminescence spectra of 0.5%Tm^{3+} and 10%Yb^{3+} doped yttrium silicate sample (HTY1_1250) depending on pumping powers at atmospheric conditions, excitation of 975 nm.

The vacuum results of the luminescence measurements were demonstrated at Figure 6.25 for the codoped sample.

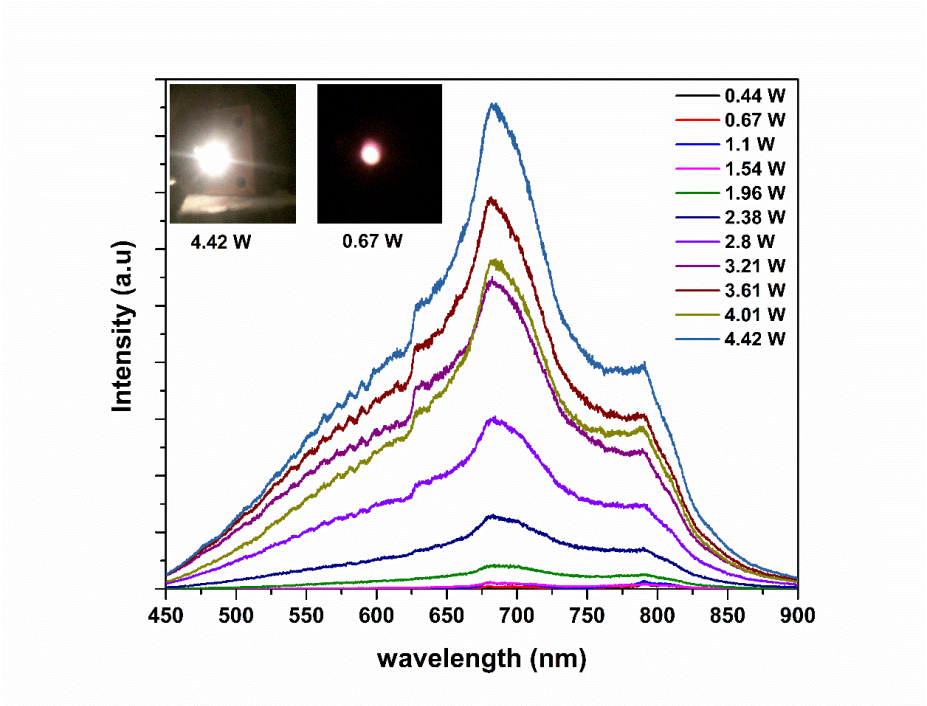

Figure 6.25 : Luminescence spectra of 0.5%Tm^{3+} and 10%Yb^{3+} doped yttrium silicate sample (HTY1_1250) depending on pumping powers at vacuum, excitation of 975 nm.

It was seen that upconversion peaks of Tm^{3+} ion became to turn into thermal white emission with increased pumping powers. However, the $^3F_3 \rightarrow {}^3H_6$ transition about 700 nm was dominant with thermal white emission at vacuum. The luminescence spectra of %0.25 Tm^{3+}/10% Yb^{3+} (HTY2_1250) and %1 Tm^{3+}/10% Yb^{3+}(HTY3_1250) codoped nanophosphors at atmospheric conditions with 975 nm excitation were similar to spectra of 0.5%Tm^{3+}/10% Yb^{3+} codoped yttrium silicate sample as seen in Figure 6.26 and 6.27.

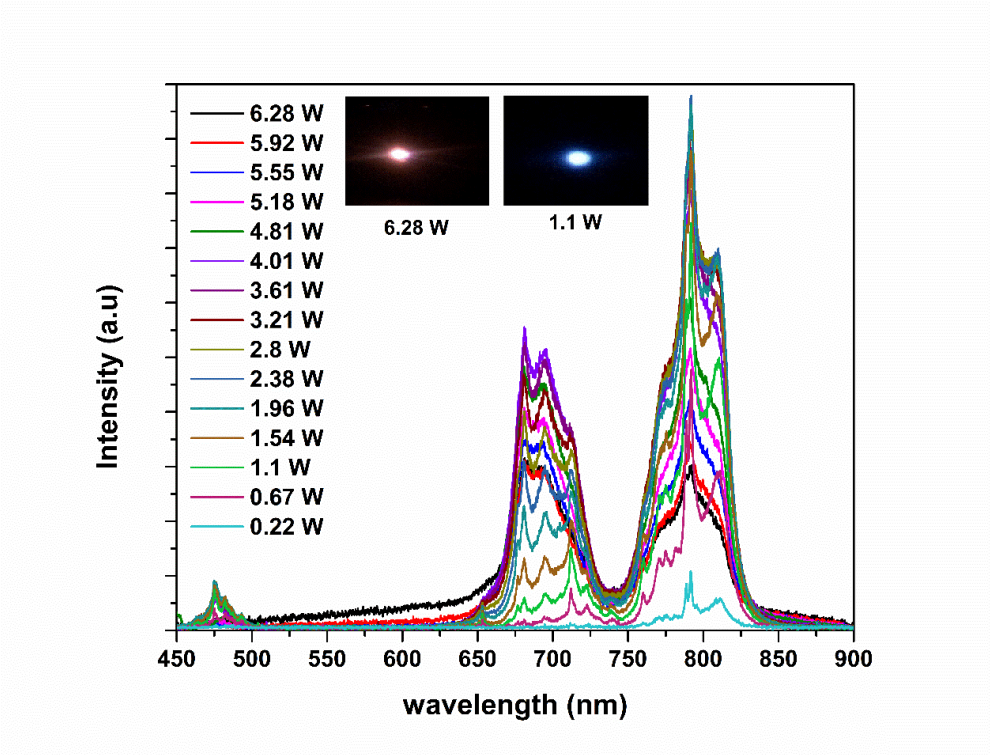

Figure 6.26 : Luminescence spectra of 0.25%Tm^{3+} and 10% Yb^{3+} doped yttrium silicate sample (HTY2_1250) depending on pumping powers at atmospheric conditions, excitation of 975 nm.

The near infrared emission of about 790 nm is very intense in the spectra comparing with blue and red emissions. The blue upconverted emission can be easily saturated at low pumping powers. The vibrational energy or phonon energy of the host is very important. It must be low to prevent multiphonon assisted quenching and also it must be large enough to provide multiphonon relaxation of energy transfer from excited states to lower states [115, 116, 117].

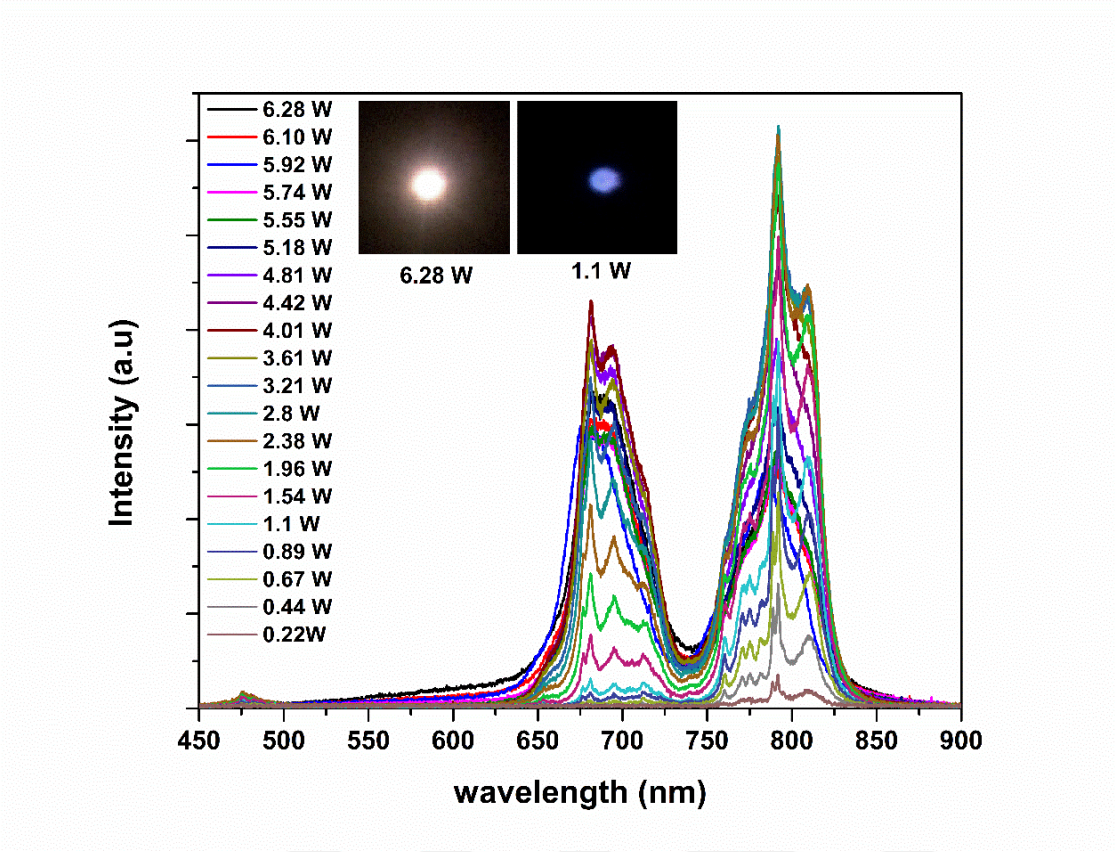

Figure 6.27 : Luminescence spectra of 1.0 %Tm^{3+} and 10% Yb^{3+} doped yttrium silicate sample (HTY3_1250) depending on pumping powers at atmospheric conditions, excitation of 975 nm.

6.3.3 Luminescence properties of Tm^{3+}/Yb^{3+} codoped nanophosphors at 808 nm

The luminescence spectra of the 0.5%Tm^{3+} and 10% Yb^{3+} doped yttrium silicate sample were measured at a diode laser of 808 nm excitation at atmospheric pressure and vacuum. The results from atmospheric pressure were shown in Figure 6.28 and vacuum in Figure 6.29. The artificial peaks between 550 nm and 650 nm are due to the scattering of laser light in the system. In Figure 6.28, we see very slight blue emission and the strong band about 700 nm corresponded to the $^3F_3 \rightarrow {}^3H_6$ transition of Tm^{3+}. The results of vacuum measurements with increasing pumping powers were shown in Figure 6.29a and 6.29 b. We can say that the spectra below ~4.9 W are similar to the results of atmospheric conditions (Figure 6.29a). When the pumping powers increased, the spectra became to a thermal white emission with the peak of $^3F_3 \rightarrow 3H_6$ transition of thulium (III) (Figure 6.29 b).

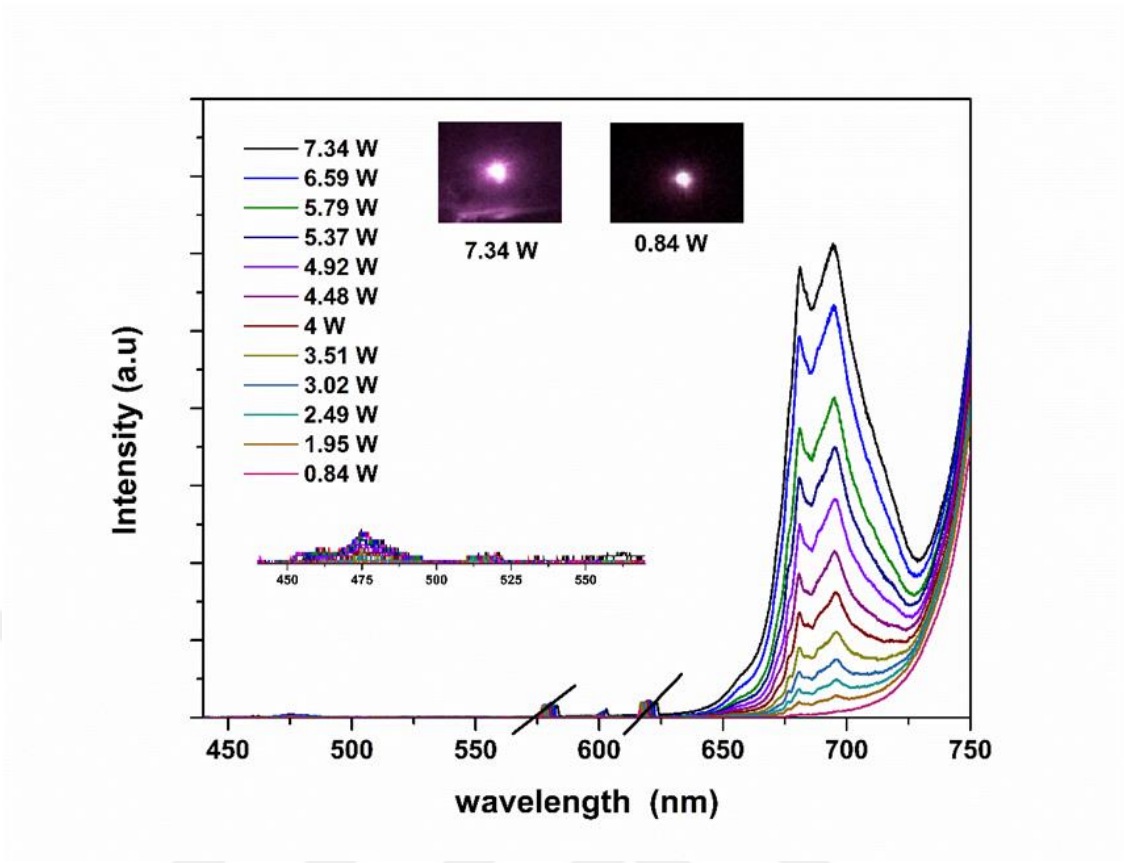

Figure 6.28 : Luminescence spectra of 0.5%Tm^{3+} and 10% Yb^{3+} doped yttrium silicate sample depending on pumping powers at atmospheric conditions, excitation of 808 nm.

The luminescence spectra of %0.25 Tm^{3+}/ 10% Yb^{3+} and %1.0 Tm^{3+}/ 10% Yb^{3+} co-doped nanophosphors were again similar to the 0.5%Tm^{3+}/ 10% Yb^{3+} codoped sample at 808 nm excitation as seen in Figure 6.29 and 6.30.

The blue emission from the samples is stronger at atmospheric pressure than that is in the vacuum. The spectra are broader in the vacuum instead of having sharp peaks of emissions.

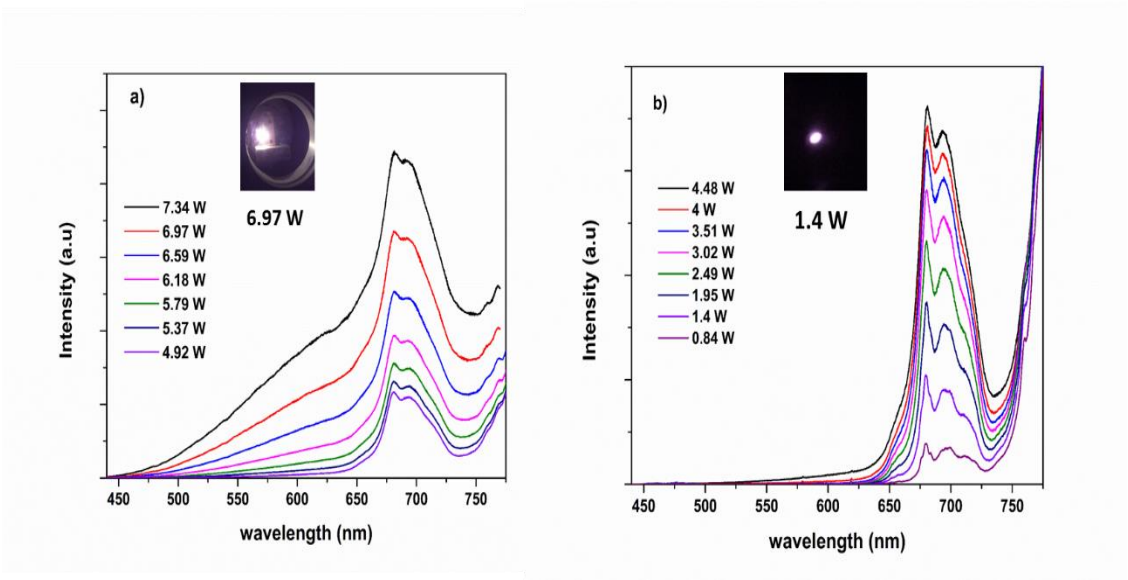

Figure 6.29 : Luminescence spectra of 0.5%Tm^{3+} and 10%Yb^{3+} doped yttrium silicate sample (HTY1_1250) depending on pumping powers at vacuum, excitation of 808 nm.

As indicated in Figure 6.31, there are no important differences between atmospheric pressure cases at both 975 nm or 808 nm excitation. However, the chromaticity values are extremely different for HTY1_1250 (0.5 Tm^{3+}/10% Yb^{3+} codoped sample) at vacuum case under 975 nm or 808 nm excitations.

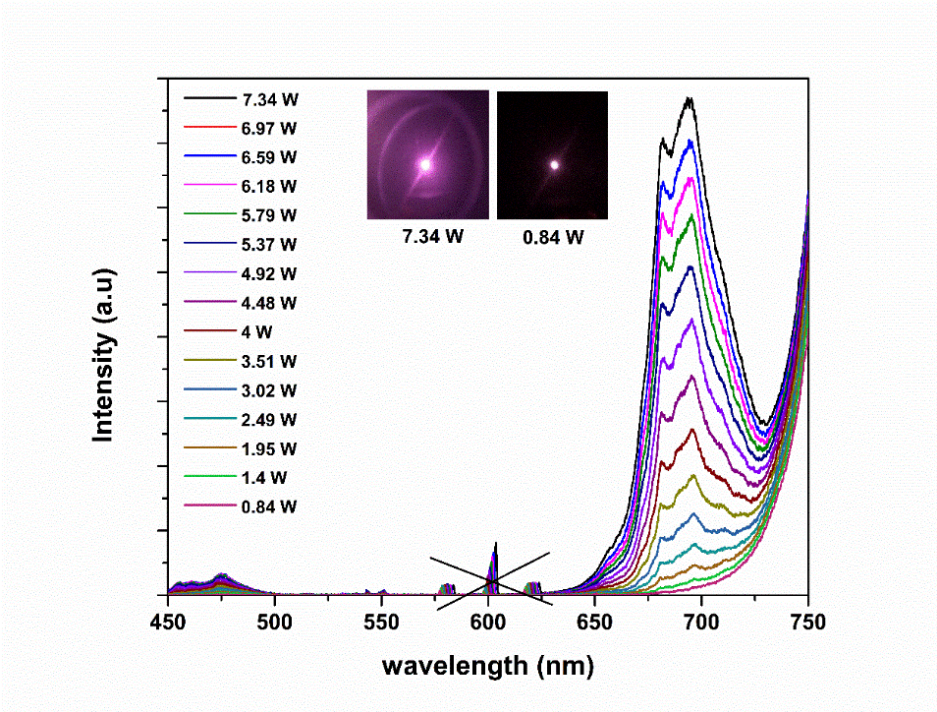

Figure 6.30 : Luminescence spectra of 0.25%Tm^{3+} and 10%Yb^{3+} doped yttrium silicate sample (HTY2_1250) depending on pumping powers at atmospheric conditions, excitation of 808 nm.

We see the CIE 1931 coordinates of HTY1_1250 codoped yttrium silicate nanophosphor in Figure 6.32 as a function of excitation powers at excitation of 975 nm / 808 nm under atmospheric conditions.

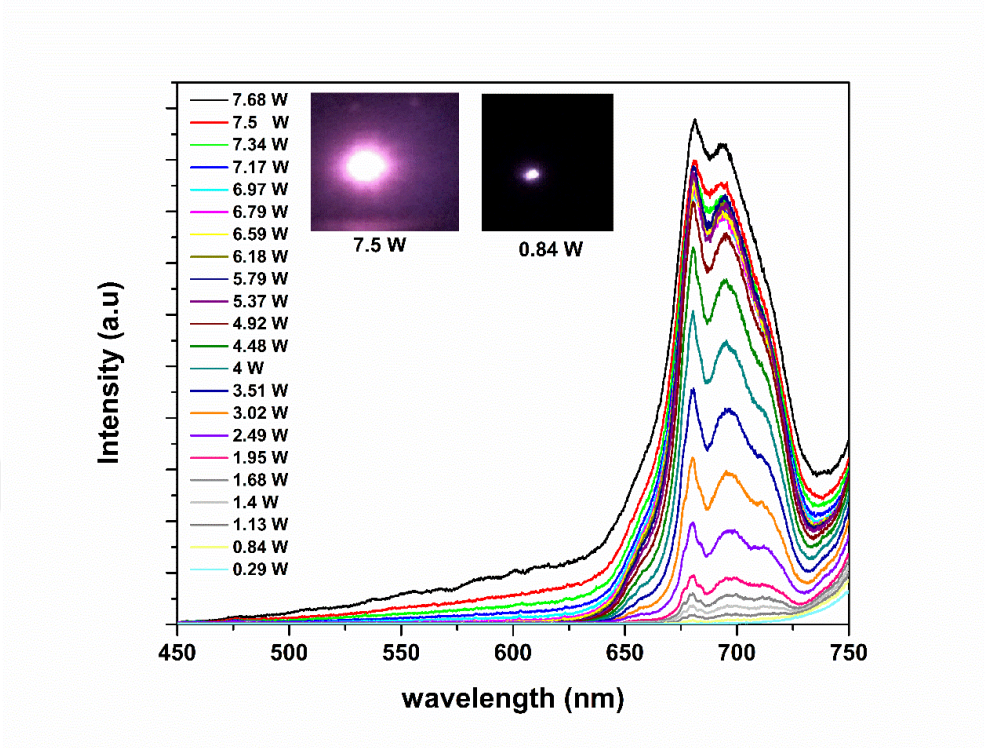

Figure 6.31 : Luminescence spectra of 1.0 %Tm^{3+} and 10% Yb^{3+} doped yttrium silicate sample (HTY3_1250) depending on pumping powers at atmospheric conditions, excitation of 808 nm.

The CIE 1931 coordinates of the Tm^{3+}/ Yb^{3+} codoped samples were shown in Figure 6.32, Figure 6.33, and Figure 6.34 at 975nm or 808 nm excitations under atmospheric conditions and vacuum.

In Figure 6.32, we see the CIE 1931 coordinates of the HTY1_1250 sample as a function of excitation powers at a) atmospheric conditions and b) vacuum at excitations of 808 nm and c) atmospheric conditions and d) vacuum at 975 nm. In Figure 6.33 and Figure 6.34, we see the CIE 1931 coordinates of HTY2_1250 and HTY3_1250 samples as a function of excitation powers under atmospheric conditions at excitation of a) 975 nm and b) 808 nm.

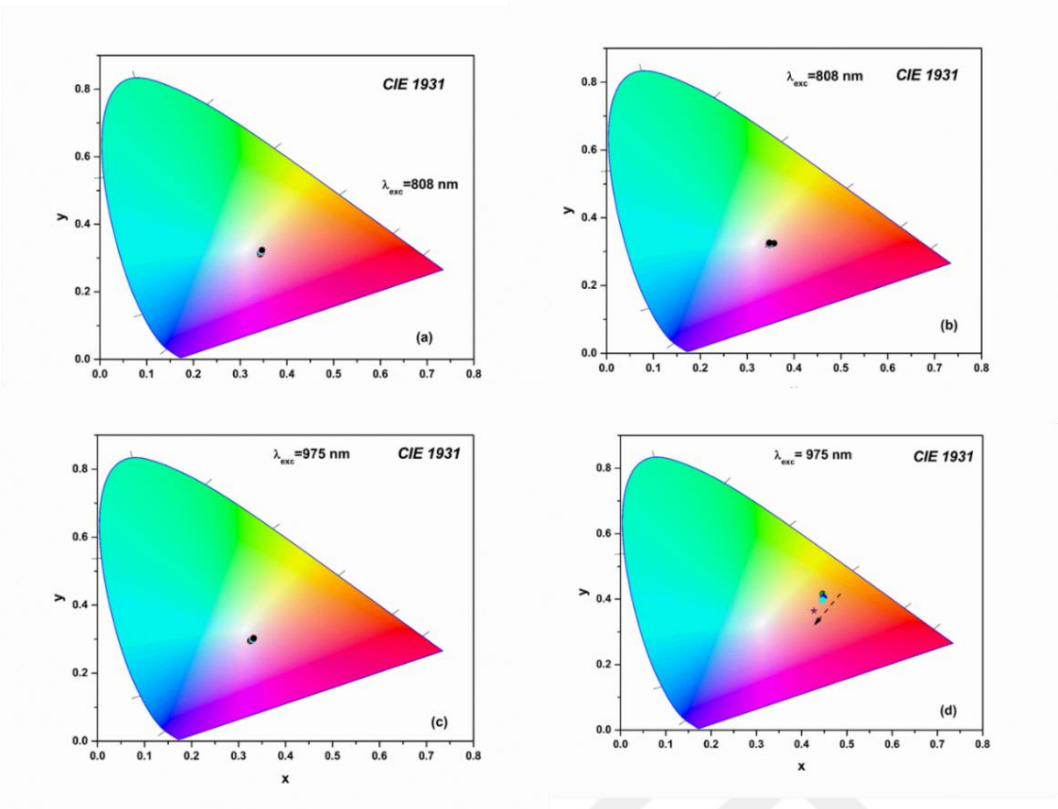

Figure 6.32 : CIE 1931 coordinates of Tm^{3+}/Yb^{3+} co-doped yttrium silicate (HTY1_1250) as a function of excitation powers a) atmospheric conditions at 808 nm b) vacuum at 808 nm c) atmospheric conditions at 975 nm d) vacuum at 975 nm.

In summary, upconversion emission properties in Tm^{3+} and Yb^{3+} codoped yttrium silicates nanophosphors with the various concentration of Tm^{3+} ions were investigated depending on excitation wavelengths, pumping powers and pressure. We obtain blue, orange, yellow and red emission in different cases.

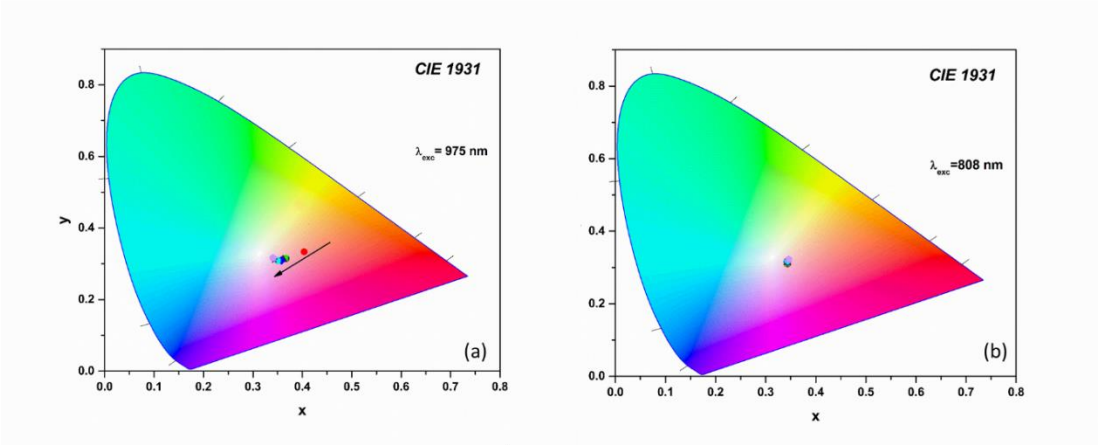

Figure 6.33 : CIE 1931 coordinates of Tm^{3+}/ Yb^{3+} co-doped yttrium silicate nanophosphor (HTY2_1250) as a function of excitation powers a) atmospheric conditions at 975 nm b) atmospheric conditions at 808 nm.

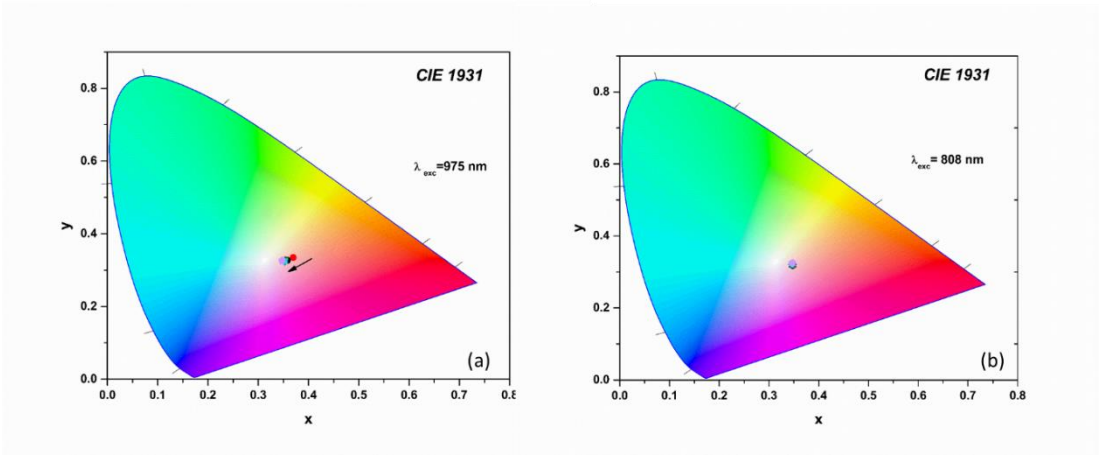

Figure 6.34 : CIE 1931 coordinates of Tm^{3+}/ Yb^{3+} co-doped yttrium silicate nnanophosphor (HTY3_1250) as a function of excitation powers a) atmospheric conditions at 975 nm b) atmospheric conditions at 808 nm.

7. STRUCTURAL AND LUMINESCENCE PROPERTIES OF RARE EARTH TRIPLY (Nd^{3+}/ Tm^{3+}/ Yb^{3+}) DOPED YTTRIUM SILICATE (Y_2O_3: SiO_2) NANO PHOSPHORS

The great interest in literature is to obtain white light by mixing the light of red, green and blue colors in some proportions. The rare earth ions can emit these basic three colors as we know and white light can be generated by the way of upconversion processes using these ions. The systems doped with rare earth ions to mix the blue, green and red can be used in the photonic industry and various optical applications [118-120]. In literature, there are some studies Nd^{3+}/ Tm^{3+}/ Yb^{3+} triply doped glasses and ceramics [121-123]. However, there is no reported study about tunable multicolor and bright white UC on yttrium silicate host doped with these rare earth ions.

In this time, we will present luminescence properties of Nd^{3+}/Tm^{3+}/Yb^{3+} triply doped yttrium silicate samples in different concentrations of ions at 975 nm and 808 nm excitations. The luminescence studies indicated that there are efficient emissions of samples in the range of 450-900 nm and 450-780 nm at 975 nm and 808 nm excitations, respectively. This leads to intense upconversion processes with emissions of three basic colors: blue, green and red. There are some energy transfers among the sensitizers $Yb^{3+}$and Nd^{3+}, and Tm^{3+}dopants. The concentrations of triple doped nanophosphors are %10 Yb^{3+}, %1 Nd^{3+}, %0.5 Tm^{3+} (HNTY1), %10 Yb^{3+}, %0.5 Nd^{3+}, %0.25 Tm^{3+} (HNTY2), %2 Yb^{3+}, %0.25 Nd^{3+}, %0.5 Tm^{3+} (HNTY3), %2 Yb^{3+}, %0.5 Nd^{3+}, %0.25 Tm^{3+} (HNTY4) and %10 Yb^{3+}, %0.25 Nd^{3+}, %0.5 Tm^{3+} (HNTY5).

Firstly, bulk forms of Yb^{3+}/Nd^{3+}/Tm^{3+} triple doped yttrium silicates have been successfully prepared via the sol-gel method and powder forms were obtained by annealing process at 1250 ^{0}C for 12h. The luminescence spectroscopy technique was employed to measure luminescence spectra at excitation of 975 nm/ 808 nm depending on powers under atmospheric and vacuum conditions. The samples emitted blue (~475

nm), green (~530nm), yellow (~590 nm) and red (~693 nm and ~750 nm) colors at various physical conditions. The combination of blue, green and red emissions created the white light, which was visible by naked eyes.

Among the various sensitizers, Yb^{3+} ion was used to sensitize the system since it is excited effectively under the NIR pumping source. Nd^{3+} is used to obtain red and green colors and Tm^{3+} is for blue light. In addition, white emission was also obtained by the way of thermal processes. The CIE coordinates indicated that $Yb^{3+}/Nd^{3+}/Tm^{3+}$ triple doped yttrium silicate samples emitted the light close to the white region (0.33, 0.33) at some special physical conditions. Power dependence of each emission intensity was investigated and the possible upconversion mechanisms were discussed. The results showed that the samples might have potential applications for the industrial and photonics areas.

7.1 Structural Analyses

Yttrium silicate host shows different polymorphs (α, β, ɣ, δ, y) and obtaining a single pure phase is extremely difficult. A representative example of XRD patterns of the triply doped samples is shown in Figure 7.1.

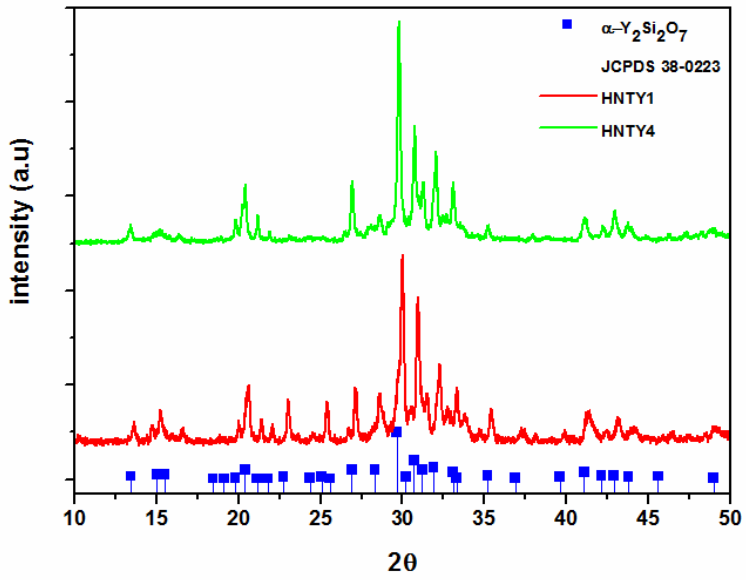

Figure 7.1 : XRD patterns of the triply doped samples.

The structures of all samples were found to be mainly as α-$Y_2Si_2O_7$ with card number 38-0223 according to JCPDS (Joint Committee for Powder Diffraction Data). The

additional Y-$Y_2Si_2O_7$ impurity phase with card number 74-1994 was also observed for samples that include a high concentration of Yb^{3+} (10% per mole). The XRD patterns indicate that annealed powders contain mainly triclinic (anorthic) crystalline phase and P-1(2) space group. It is observed that the samples have mainly a single phase without obvious changes by substitution of rare earth ions thus confirming successful synthesis. In Figure 7.2 and Figure 7.3, representative examples of Scanning Electron Microscopy images of triple samples are shown.

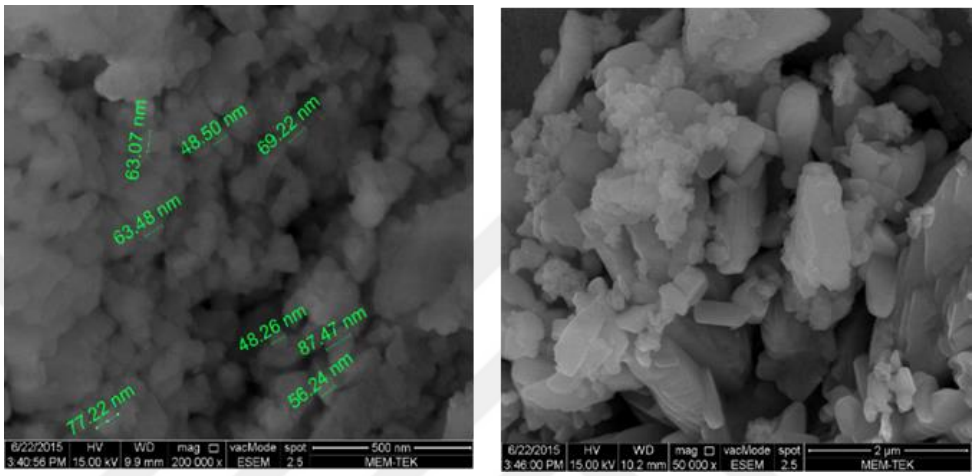

Figure 7.2 : The SEM images of the HNTY1 (10%Yb^{3+}, 1%Nd^{3+}, 0.5 % Tm^{3+} doped sample annealed at 1250 ^{0}C).

The SEM measurements exhibited the information about the particle distribution and particle size and it is in good agreement with XRD results.

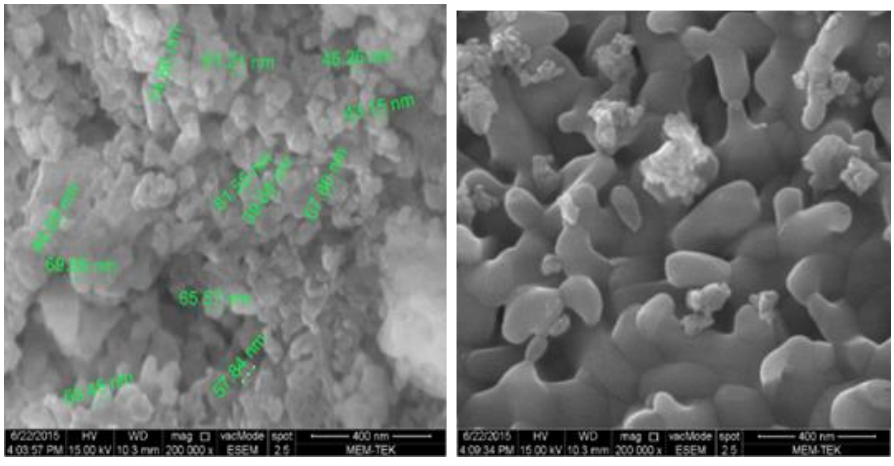

Figure 7.3 : The SEM images of the HNTY4 (2%Yb^{3+}, 0.5%Nd^{3+}, 0.25%Tm^{3+} doped sample annealed at 1250 ^{0}C).

SEM observations of the samples are investigated at low (50000×) and high magnification (200000×). The agglomeration is shown for triply doped samples in Figure 7.2 and Figure 7.3.

7.2 Luminescence Properties of Triply Doped Samples

It is worthwhile to realize that upconversion luminescence and generation of white emission can be controlled by adjusting the concentration of rare earth ions. Therefore, the concentration of Yb^{3+} and Tm^{3+} ions were adjusted and luminescence properties were analyzed depending on various physical parameters such as pressure difference, pumping power, excitation source, etc. Based on the decay and rise patterns, some information about the luminescence dynamics was examined at the vacuum condition. Also, the chromaticity properties of each measurement were determined by taking the illuminance meter images. The luminescence spectra, corresponding photos and illuminace meter results of 1% Nd^{3+}, 0.5% Tm^{3+}, 10% Yb^{3+} triple doped sample (HNTY1_1250) were shown in Figure 7.4.

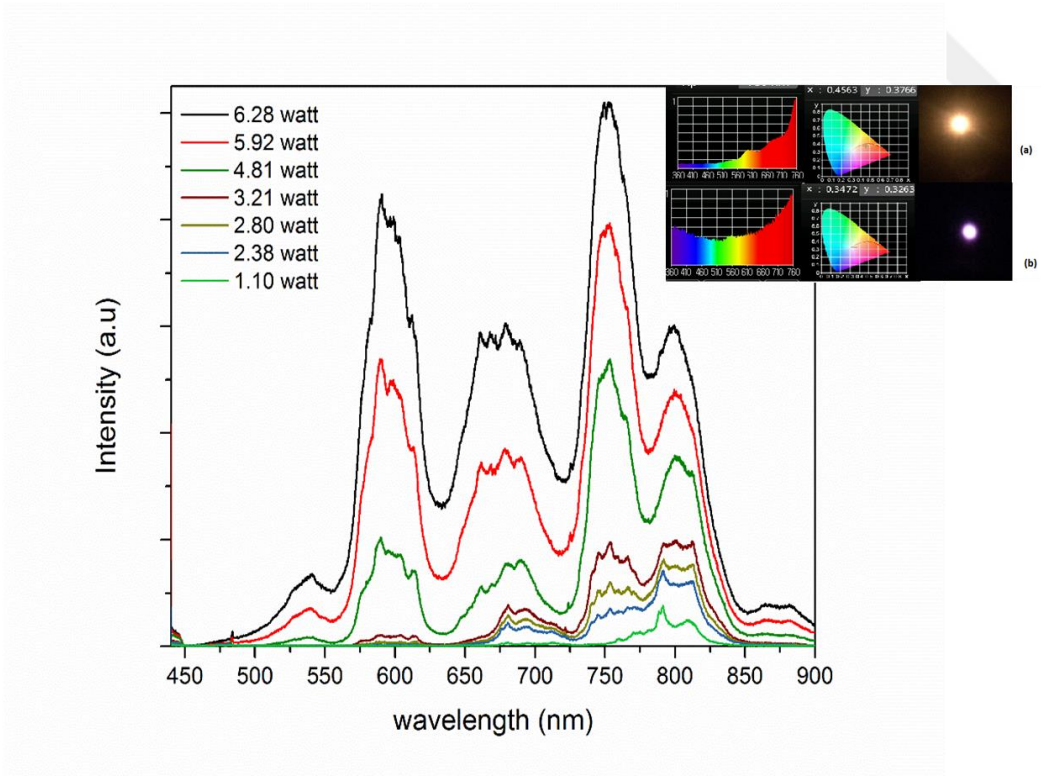

Figure 7.4 : Luminescence spectra of 1% Nd^{3+}, 0.5% Tm^{3+},10% Yb^{3+} (HNTY1_1250) triply doped yttrium silicate at atmospheric pressure, illuminance meter results at a) 5.92 W and b) 0.67 W.

We obtained from luminescence measurements that a high concentration of Yb^{3+} (10%) causes to be thermal processes more effective than upconversion processes. Upconverted white light due to blue, green, red emissions was dominant at atmospheric conditions. At lower pumping powers below ~2.8 W, blue emission was visible however; the intensity of blue emission was decreased with enhancing of the pumping power. The white emission was observed that has resulted from thermal processes with emission peaks of Nd^{3+} or Tm^{3+} ions at vacuum (Figure 7.5). The threshold power to obtain white light at the vacuum condition was less than that it is in atmospheric pressure as we expected.

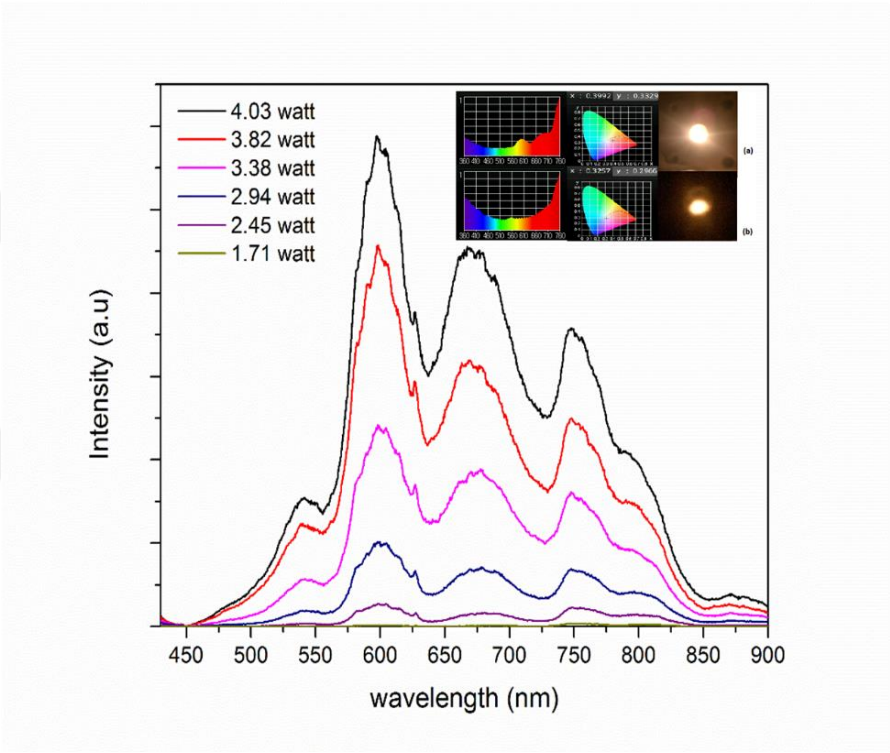

Figure 7.5 : Luminescence spectra of 1% Nd^{3+}, 0.5% Tm^{3+},10% Yb^{3+} (HNTY1_1250) triply doped yttrium silicate at vacuum (0.01 mbar), illuminance meter results at a) 3.16W b) 1.45W.

The number of the required laser photons (n) for an upconversion emission can be found by using the relation of $I\alpha P^n$, where I is the luminescent intensity, P is the pump laser power. When we compare the slope of the double logarithm plot of intensity versus output power for atmospheric pressure and vacuum, atmospheric condition values are less than vacuum for HNTY1_1250 (Figure 7.6 and 7.7).

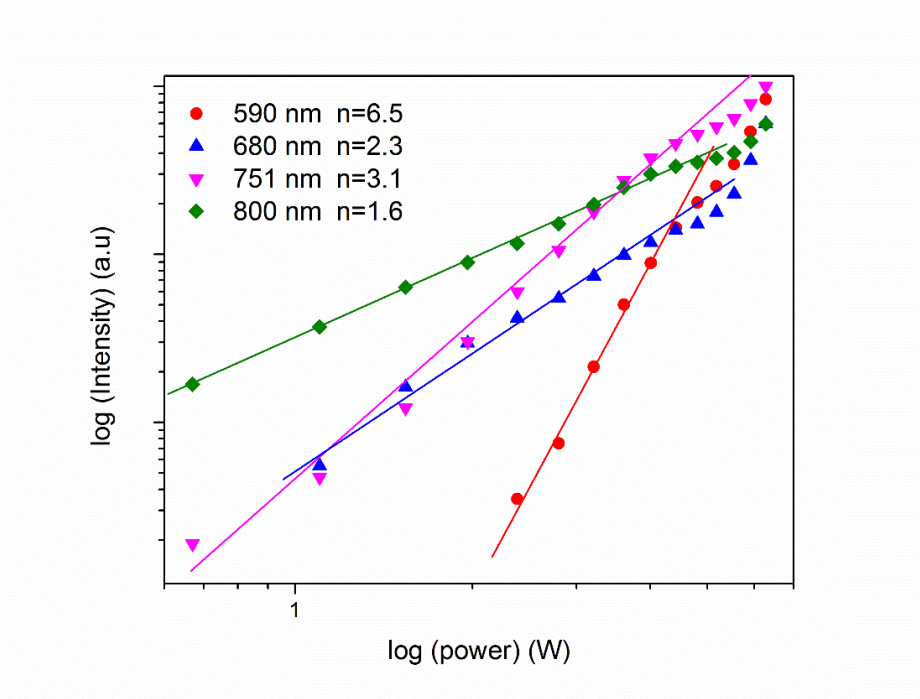

Figure 7.6 : Log-log plot of 1% Nd^{3+}, 0.5% Tm^{3+}, 10% Yb^{3+} (HNTY1_1250) triply doped yttrium silicate at atmospheric pressure.

It indicates that the thermal processes are more effective at vacuum conditions to generate white light. Upconversion processes were dominant at atmospheric pressure.

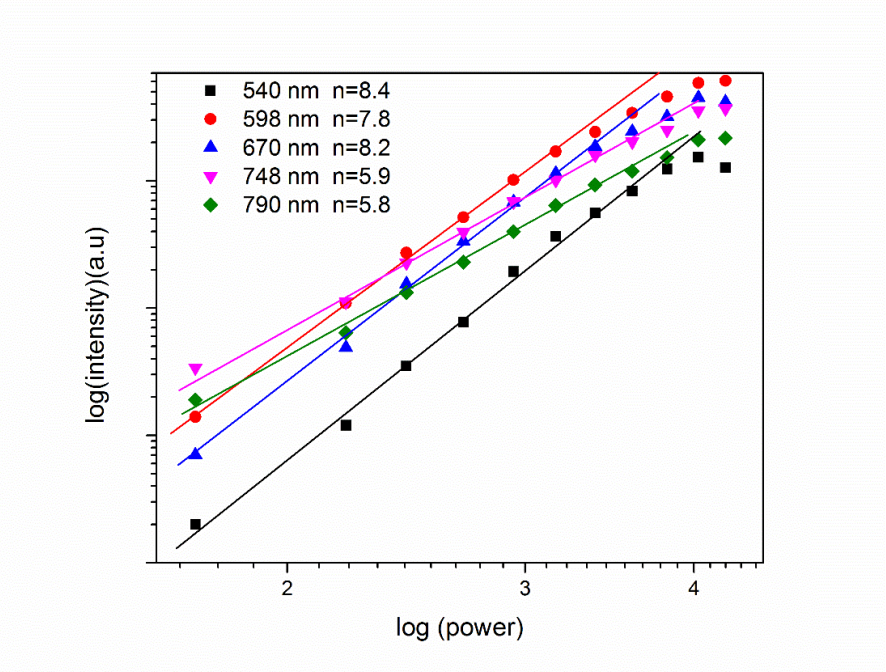

Figure 7.7 : Log-log plot of 1% Nd^{3+}, 0.5% Tm^{3+}, 10% Yb^{3+}(HNTY1_1250) triply doped yttrium silicate at vacuum.

For 0.5% Nd^{3+}, 0.25% Tm^{3+}, 10% Yb^{3+} (HNTY2_1250) triple doped yttrium silicate, we see the luminescence behavior at 975 nm excitation under atmospheric conditions depending on pumping powers (Figure 7.8). The blue, green and red emissions are shown in the figure.

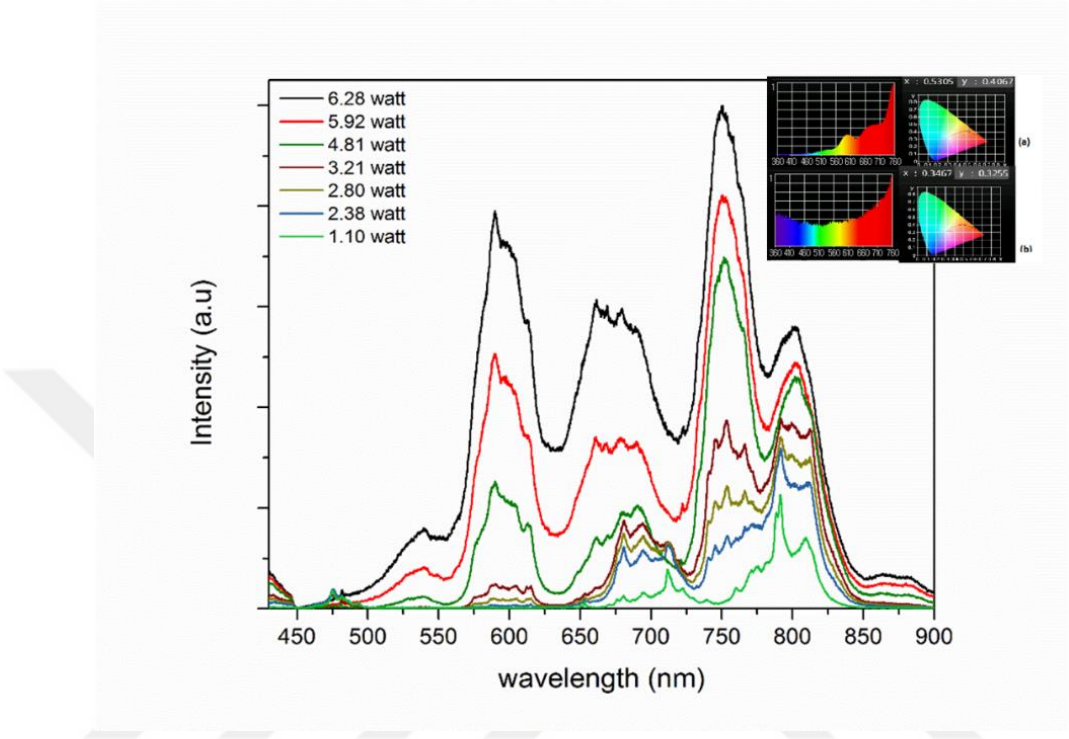

Figure 7.8 : Luminescence spectra of 0.5% Nd^{3+}, 0.25% Tm^{3+}, 10% Yb^{3+} triple doped yttrium silicate (HNTY2_1250) at atmospheric conditions, illuminance meter results at a) 5.92 W and b) 0.67 W.

Figure 7.9 shows the log-log plot of intensity versus power for sample HNTY2_1250. The results of emission measurements obey quadratic power law behavior ($I \sim P^n$) with n=5.6, 1.9, 2.8 and 1.3 for 590 nm, 680 nm, 751 nm, and 800 nm, respectively.

The decay patterns and rise patterns behaviors are shown in Figures 7.10. It indicates that the decay patterns of the triple doped sample haven't strong dependence on pumping power, however, the rising patterns are more sensitive to the pumping powers. As seen in Figure 7.10, the decay pattern is very fast at high powers. The rise time patterns are affected by both pumping power and a high concentration of Yb^{3+} ions.

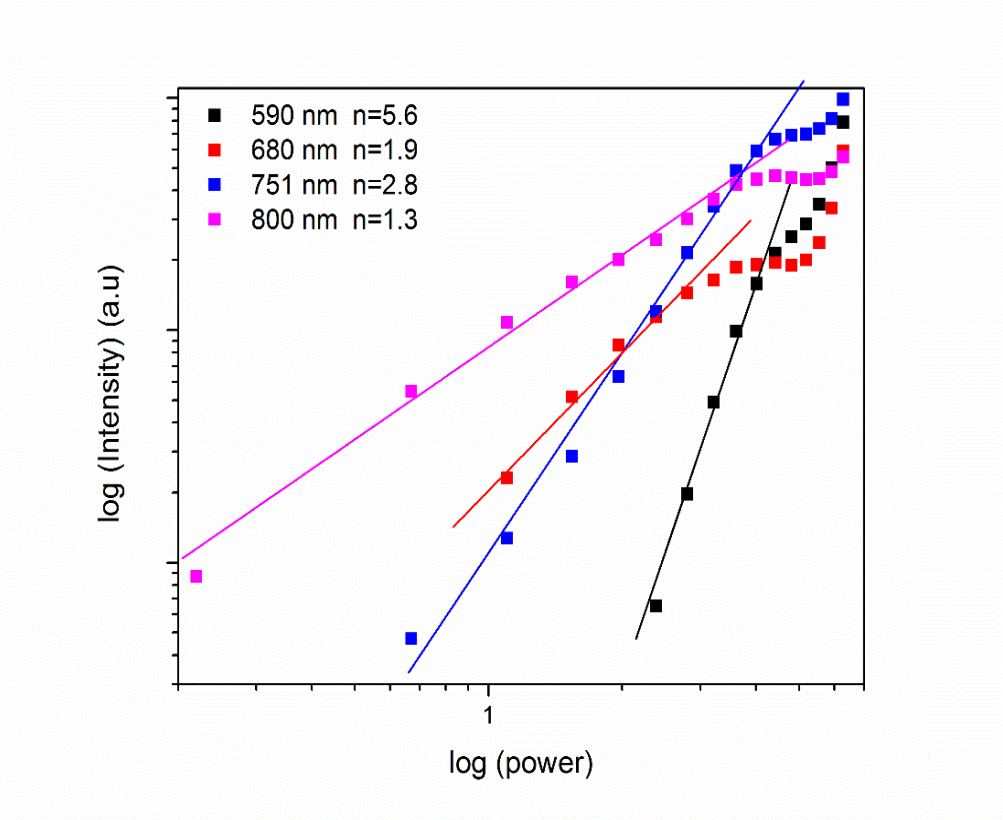

Figure 7.9 : Log-log plot of Intensity versus power of 0.5% Nd^{3+}, 0.25% Tm^{3+}, 10% Yb^{3+} triple doped yttrium silicate (HNTY2_1250) at atmospheric conditions.

For the 0.25%Nd^{3+}, 0.5%Tm^{3+}, 2%Yb^{3+} doped yttrium silicate sample (HNTY3_1250), the sharp lines due to the emission from rare earth ions were shown in Figure 7.11. The white light was obtained when the pumping power is at least ~4W for 0.25% Nd^{3+}, 0.5% Tm^{3+}, 2% Yb^{3+} triple doped sample. The spectra show that a low concentration of Yb^{3+} (2%) supported the upconverted white light instead of thermal processes. When Yb^{3+} concentration is decreased to 2% from 10%, the intensity of blue emission was increased. In other words, the high concentration of Yb^{3+} can cause to decrease in blue emission, which may attribute to Yb^{3+} induced luminescence quenching [124-126].

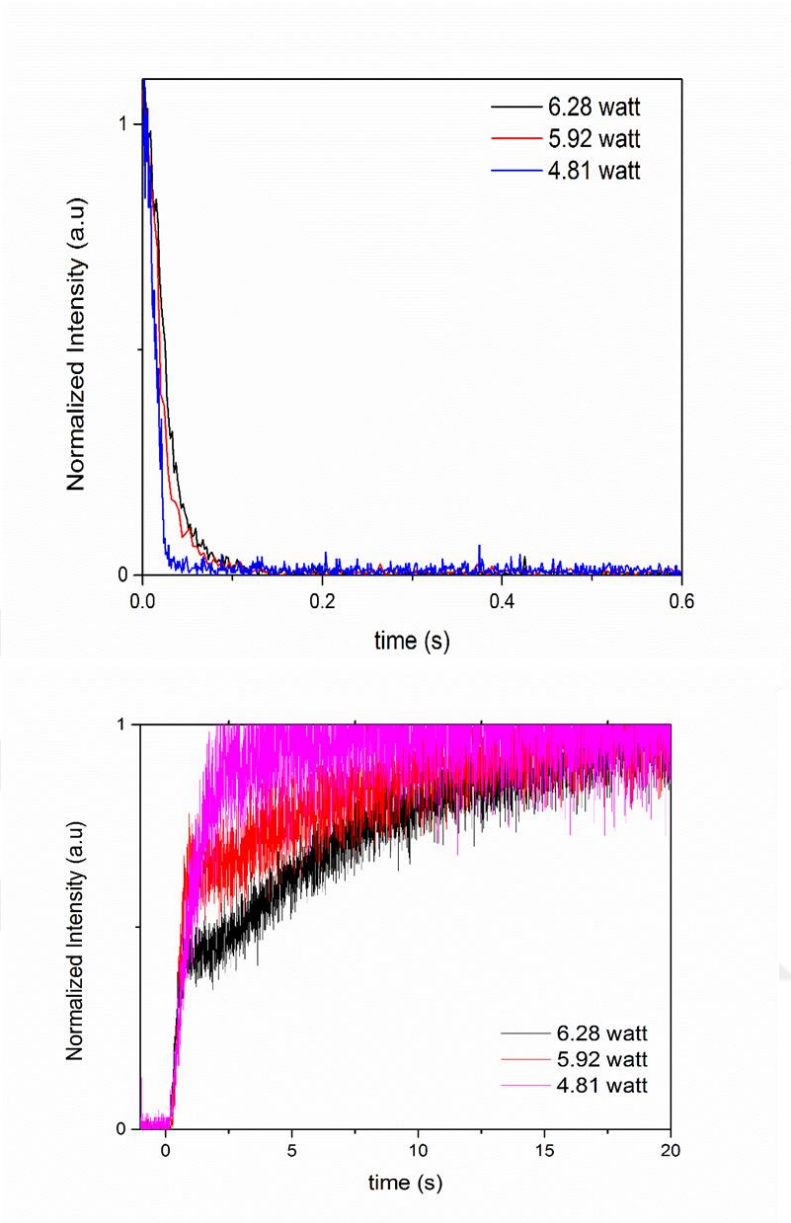

Figure 7.10 : a) Decay and b) rise patterns of 0.5% Nd^{3+}, 0.25% Tm^{3+}, 10% Yb^{3+} doped sample under atmospheric pressure at 590 nm.

The blue emission centered at ~474 nm may be due to the $^1G_4 \rightarrow {}^3H_6$ transition of Tm^{3+} or cooperative emission of Yb^{3+} ions. The green band centered at ~531 nm, the yellow band centered at ~590 nm, red bands centered at ~693 nm and ~750 nm may be due to $^2G_{7/2} \rightarrow {}^4I_{9/2}$, $^2G_{5/2} + {}^2H_{11/2} \rightarrow {}^4I_{9/2}$, $^4F_{7/2} + {}^4S_{3/2} \rightarrow {}^4I_{9/2}$ and $^4F_{5/2} + {}^4S_{3/2} \rightarrow {}^4I_{9/2}$ energy transitions of Nd^{3+}, respectively. The energy transfers between the ions and thermal processes were effective to obtain white light for triply doped samples. White light as a combination of blue, green and red colors based on UC emissions of Tm^{3+} and Nd^{3+} was obtained at atmospheric pressure for 975 nm diode laser excitation.

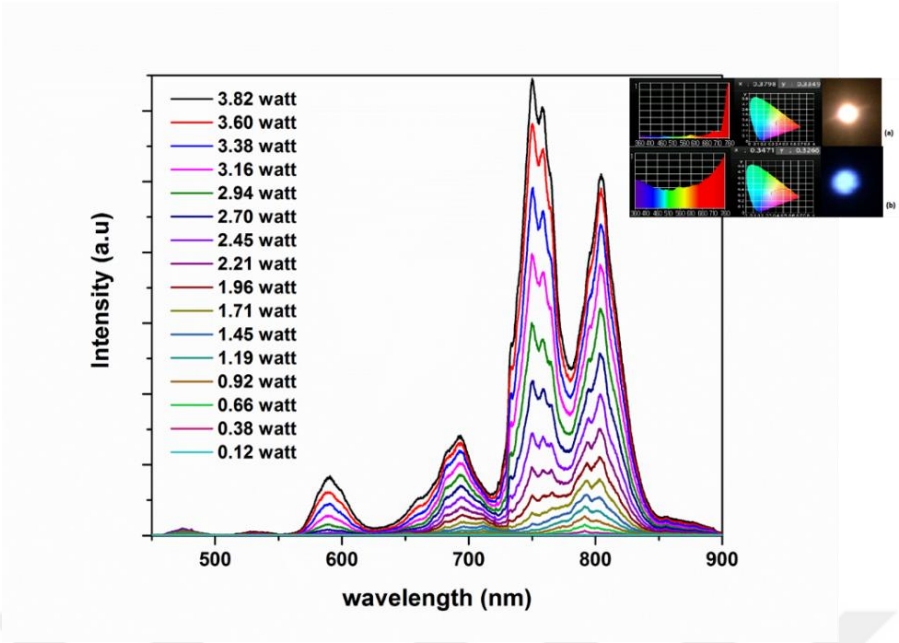

Figure 7.11 : Luminescence spectra of 0.25% Nd^{3+}, 0.5% Tm^{3+}, 2% Yb^{3+} triple doped yttrium silicate (HNTY3_1250) at atmospheric pressure under 975 nm excitation, illuminance meter results at a) 5.92 W and b) 0.67 W.

The intensity versus power in double log representation of the triply doped sample is shown in Figure 7.12 for atmospheric measurements. As seen in Figure 7.12, power dependencies of the emission intensities indicate that there are two, three, four and seven photons absorptions.

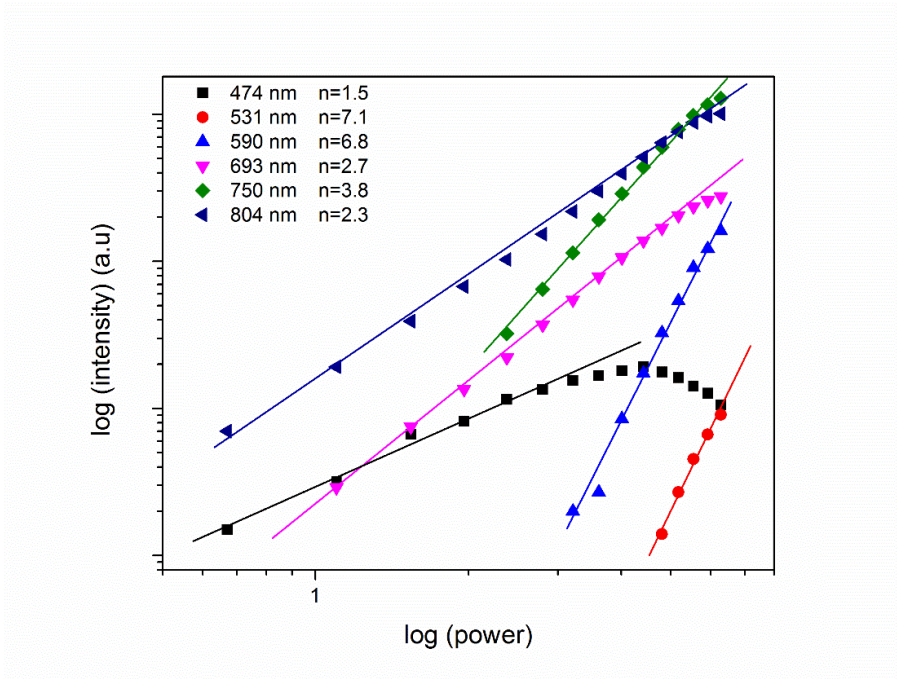

Figure 7.12 : Log-log plot of Intensity versus power of 0.25% Nd^{3+}, 5% Tm^{3+}, 2% Yb^{3+} triple doped yttrium silicate (HNTY3_1250) at atmospheric pressure.

The broad bands are possibly affected by a photon avalanche population process because of cross-relaxation processes provided that the excitation power is high. As a result, it may indicate that photon avalanche mechanisms present together with thermal processes. From Figure 7.12, it was determined that blue, green, yellow, orange and red bands require ~2, ~7, ~7, ~3, ~4 and ~2 photon absorptions at atmospheric pressure, respectively. We see the spectra of 0.5% Nd^{3+}, 0.25% Tm^{3+}, 2% Yb^{3+} triple doped sample (HNTY4) in Figure 7.13. Upconversion and thermal white light were obtained from the sample. This indicates both the energy transfers between the ions and thermal processes were effective to obtain white light for triply doped samples.

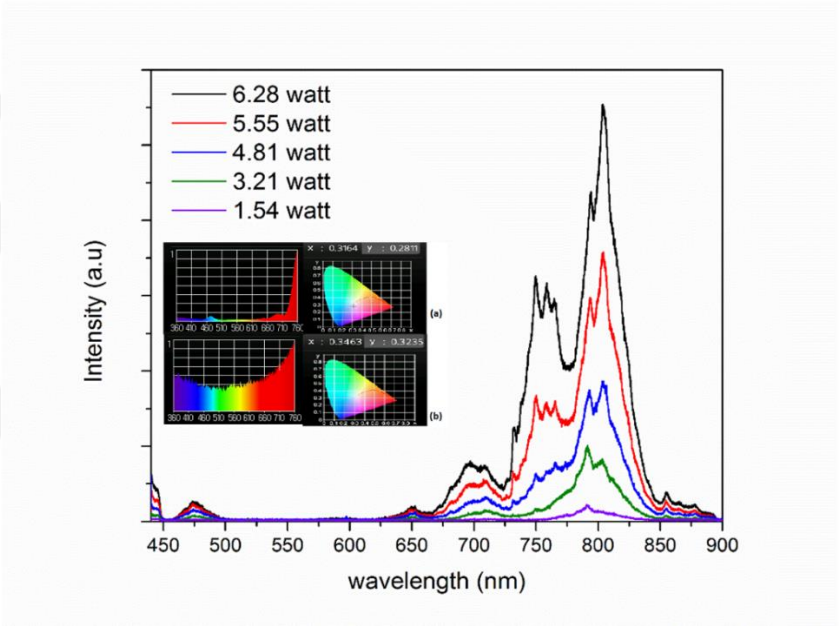

Figure 7.13 : Luminescence spectra of 0.5% Nd^{3+}, 0.25% Tm^{3+}, 2% Yb^{3+} triple doped yttrium silicate (HNTY4_1250) at atmospheric pressure, illuminance meter results at a) 5.92 W and b) 0.67 W.

Moreover, the concentration of Yb^{3+} also important for white light emission. Thermal processes are more effective for the high concentration of Yb^{3+}. The number of photons involved upconversion processes for each emission peaks were given in Figure 7.14. The higher value of the n than expected one indicates that there are some thermal processes and avalanche effects about 750 nm.

The luminescence spectra and the double log plot of the intensity versus pumping power of the 0.25% Nd^{3+}, 0.5% Tm^{3+}, 10% Yb^{3+} triple doped sample (HNTY5) are shown Figure 7.15 and Figure 7.16, respectively.

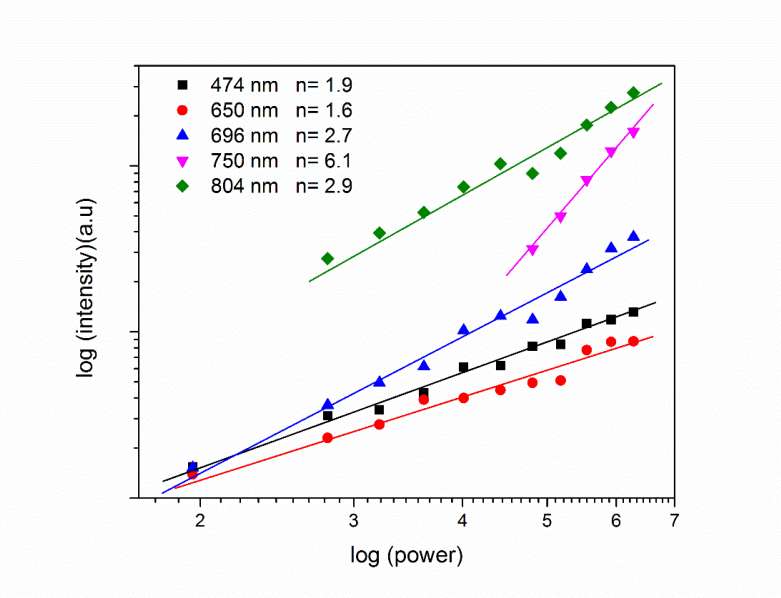

Figure 7.14 : Log-log plot of Intensity versus power of 0.5% Nd^{3+}, 0.25% Tm^{3+}, 2% Yb^{3+} triple doped yttrium silicate (HNTY4_1250) at atmospheric pressure.

The emission intensities and the shape of the spectra strongly depend on the pumping powers. Nd^{3+} and Tm^{3+} ions can be excited by using ~800 nm diode laser excitation while 975 nm diode laser can excite Yb^{3+} ion. For the triply doped samples, we used 975 nm excitation and Yb^{3+} may transfer energy to the other ions. It is well known that Yb^{3+} ion generally leads to being a bridge for energy transition between the ions.

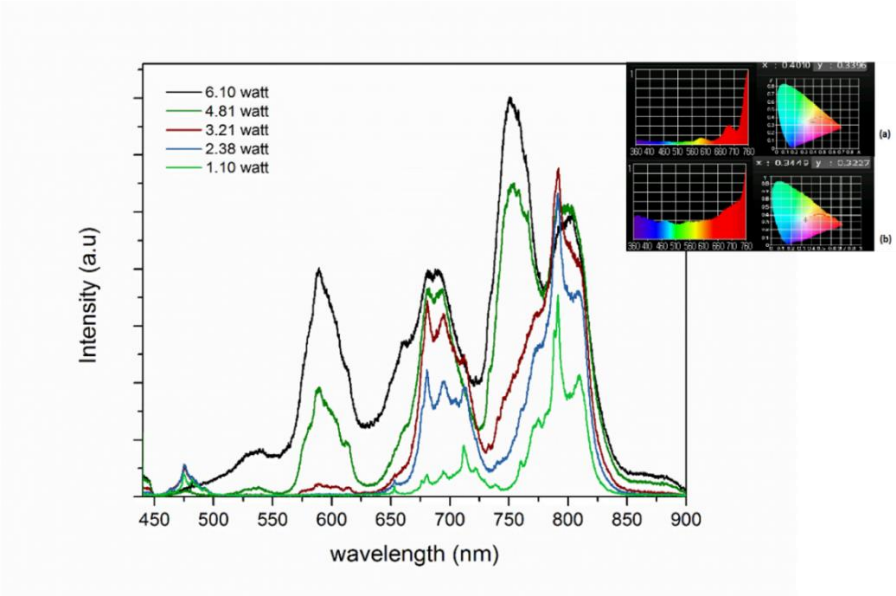

Figure 7.15 : Luminescence spectra of 0.25% Nd^{3+}, 0.5% Tm^{3+}, 10% Yb^{3+} triple doped yttrium silicate (HNTY5_1250) at atmospheric pressure, illuminance meter results at a) 5.92 W and b) 1.1 W.

The color temperatures of the samples measured by illuminance meter indicate that emitted light was close to the white region with chromaticity coordinates x=0.33, y=0.33 according to CIE 1931 at all excitation powers. The emitted white light was like cool white for powers between ~6.2 W and ~4.8. The white light was like daylight below ~4 W at atmospheric conditions as given in Table 7.1. In addition, a large range of tunability of multi-colored emission was observed from the samples by changing ambient pressure and pumping powers.

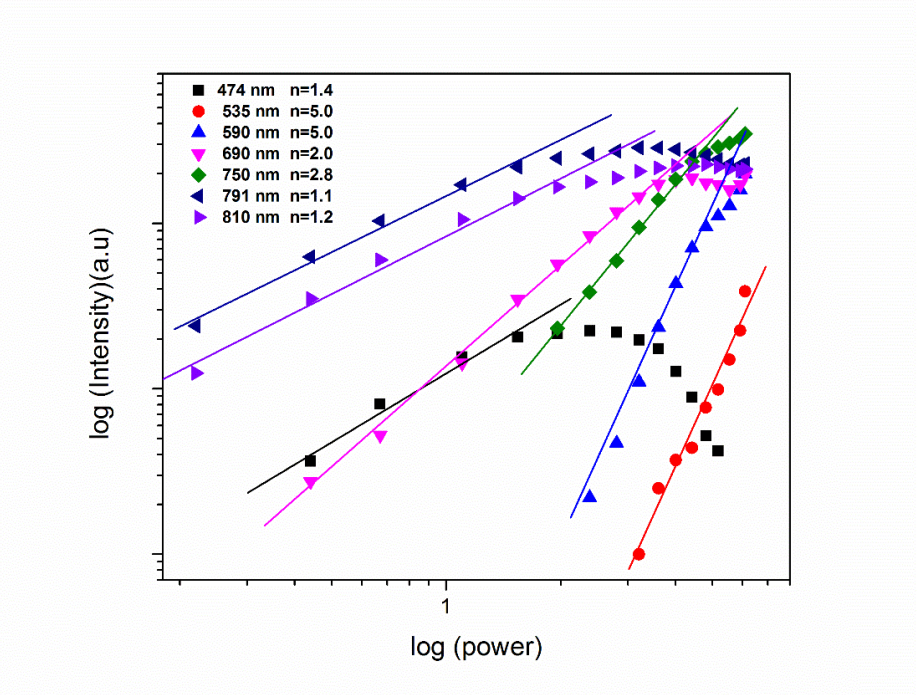

Figure 7.16 : Log-log plot of Intensity versus power of 0.25% Nd^{3+}, 0.5% Tm^{3+},10% Yb^{3+} triple doped yttrium silicate(HNTY5_1250) at atmospheric pressure.

In summary, Nd^{3+} and Tm^{3+} ions can be excited by using ~800 nm diode laser excitation while 975 nm diode laser can excite Yb^{3+} ion. For triply doped samples, we used 975 nm excitation and Yb^{3+} may transfer energy to the other ions. Upconversion and thermal white light were obtained from the $Nd^{3+}/Tm^{3+}/Yb^{3+}$ doped samples. This indicates both the energy transfers between ions and thermal processes were effective to obtain white light for triply doped samples. Moreover, the concentrations of dopants are important for the quality of emitted white light. Thermal processes are more effective for the high concentration of Yb^{3+}. Vacuum condition leads to generate white light easier than that it is in atmospheric pressure.

Table 7.1 : Color quality parameters for the white light measured at various output powers of laser for HNTY5_1250.

Output Power (W)	CCT(K)	CRI(Ra)	CIE coordinates(x, y)
6.28	3385	91	(0.3902, 0.3392)
5.55	3862	91	(0.3718, 0.3307)
4.81	4420	89	(0.3556, 0.3238)
4.01	4777	87	(0.3470, 0.3204)
2.8	4918	88	(0.3441, 0.3217)
1.96	4876	89	(0.3452, 0.3231)
1.1	4812	89	(0.3468, 0.3251)
0.67	4809	90	(0.3471, 0.3266)

The results obtained from different concentrations of rare earth ions, various pumping power and pressure will contribute to design new kinds of materials to generate white light for physical and industrial applications.

8. WHITE LIGHT FROM 20% PER MOLE Yb^{3+} DOPED YTTRIUM SILICATE BULK SAMPLE

So far, we said that white emission is due to upconversion mechanisms among the rare earth ions or thermal processes among them or host lattice. There are some strategies to develop nanocrystalline lanthanide-doped powders using various synthesis techniques [127-129]. White light generation due to upconversion or thermal processes requires complex mixing or doping schemes. From a conceptual point of view, optical characteristics of rare earth doped materials depend on the energy levels of rare earth ions and host material properties depending on the size, of course, annealing of the sample. The nanosize so large surface to volume ratio also causes to dominate surface states and decreases the band edge emission. Thus, very broad white emission occurs [130].

In this part, we demonstrate the luminescence properties of the sol-gel synthesized unannealed (bulk) 20% Yb^{3+} doped Y_2O_3:SiO_2 sample at excitation of 975 nm under atmospheric conditions. We have observed the broad white emission from the bulk samples. It is found that the sample is a promising white emitting source without complex doping or heating procedures.

8.1 Luminescence Properties of the Bulk Sample

We know that the crystals and ceramics in powder form samples doped with rare earth ions can emit white light. The upconversion process consists of some other sub-processes such as excited state absorption, energy transfer, cooperative emission, and photon avalanche processes. As we mentioned in Chapter 4, we obtain white emission from a single Nd^{+3} doped sample in both ways of upconversion and thermally. In literature, there are lots of studies about the white light generation from various materials such as powder, glass or ceramic form of compounds [131-136]. According

to our knowledge, there is a very limited study about white emitting from a bulk sample at room temperature and atmospheric pressure [137].

Luminescence measurements of 20% Yb^{3+} doped Y_2O_3:SiO_2 sample in bulk form were performed between 0.67 W and 6.28 W with a laser diode pumping at 975 nm. At lower powers, blue emission may be due to cooperative emission of Yb^{3+}-Yb^{3+} ions and other peaks may belong to unwanted Er^{3+} impurities as mentioned before. The main reasons to obtain white emission from the bulk sample may be the effects of energy migration, photon avalanche, and charge-transfer luminescence processes. In addition, any changes in host material affect the luminescence properties and dynamics of the dopants. When laser light exposed to the sample, the sample emitted a very bright, intense white light.

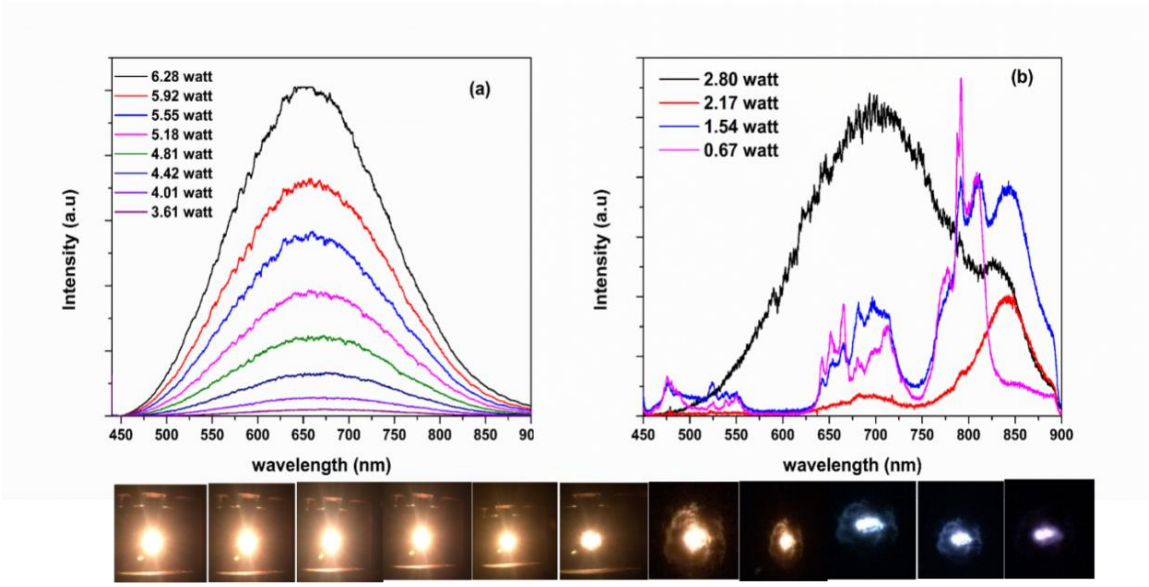

Figure 8.1 : Luminescence spectra and corresponding photos of the 20% per mol Yb^{3+} doped bulk sample.

As seen in the Figure 8.1a and 8.1b, we applied various pumping powers of a diode laser to bulk sample and obtained upconversion processes at lower powers due to cooperative emission of Yb^{3+}-Yb^{3+} and presence of Er^{3+} impurities. Above 2.17 W, the spectrum turns to broadband thermal anti-Stokes white emission and the additional peaks were disappearing completely just above 2.8 W. In other words, a threshold pumping power is necessary to form a broadband thermal white light. Besides, the double log representation of emission intensity as a function of excitation power is shown in Figure 8.2 and n value is approximately eight. These observations indicate that there may be a photon avalanche effect in the luminescence process.

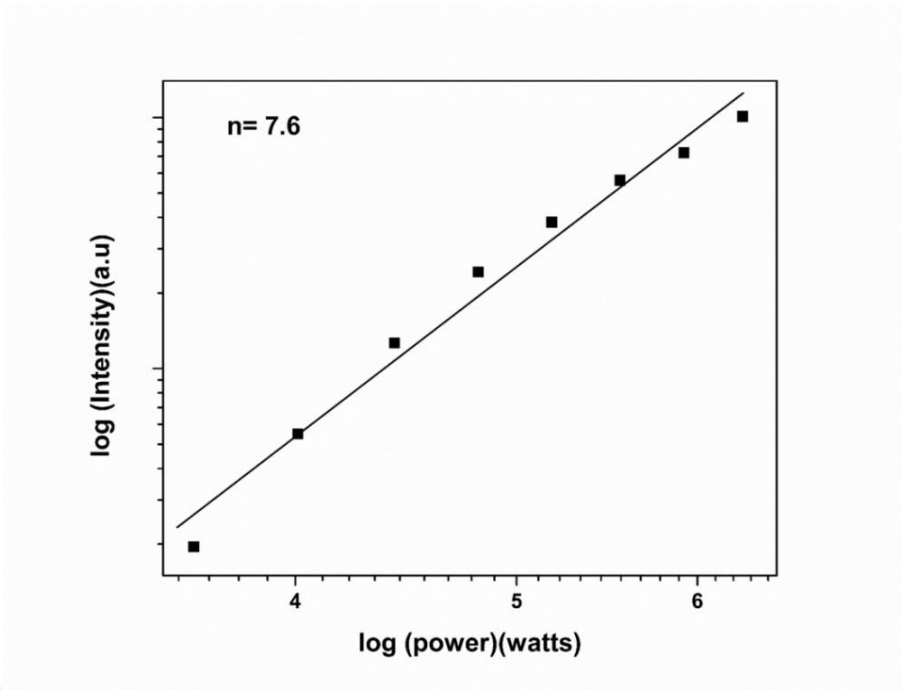

Figure 8.2 : Log-log plot of the 20% per mol Yb^{3+} doped bulk sample.

Below 2.17 W, in unsaturated UC case, the emission intensity is proportional to the excitation powers ($I \approx P^n$). This relation generally holds for lower excitation powers. If we measure the luminescence at high powers, the upconversion process will saturate. Upconversion is a nonlinear process and energy should be conserved, however, this behavior cannot be continuos to infinite excitation. Therefore, the power dependence would not in the same shape, and it will change at higher pumping powers. We obtain the slopes from the log-log plot of intensity versus excitation powers deviated from the expected values at high powers.

Figure 8.3 shows the chromaticity values of the bulk sample on the diagram. When the pumping powers decrease, the color was shifted to the white region. At high powers, the sample emitted orange- red like a light. The high-intensity laser can cause sample heating and a broadband emission with the recombination of charge carriers [82, 138]. The slow rising times means the thermal effects are again significant in producing broadband emission. The decay and rise patterns of 20% Yb^{3+} doped bulk sample depending on pumping powers were seen in Figure 8.4. The decay patterns are not strongly dependent on power while rising patterns more dependent on power. In addition, the time scale values of rise patterns are about sixty times of decay patterns.

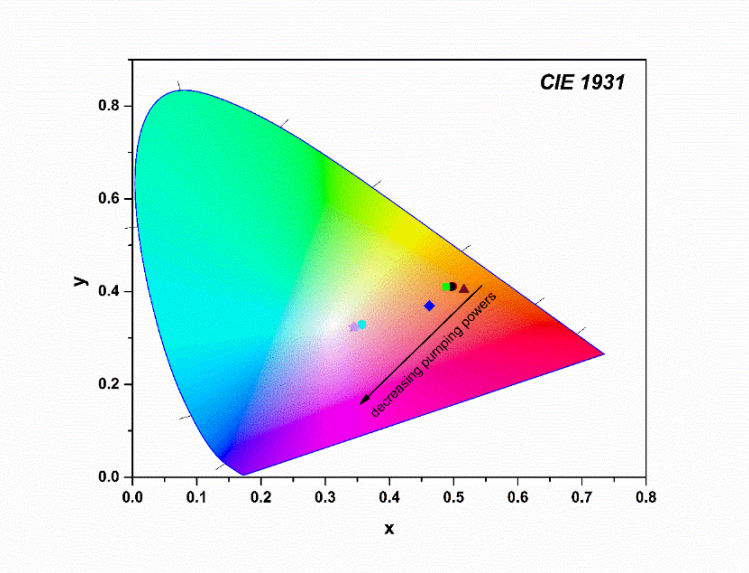

Figure 8.3 : The CIE 1931 chromaticity diagram of the 20% Yb^{3+} doped bulk sample at 975 nm excitation with various pumping powers.

The long times of rise patterns indicate that thermal processes are effective on the luminescence mechanism.

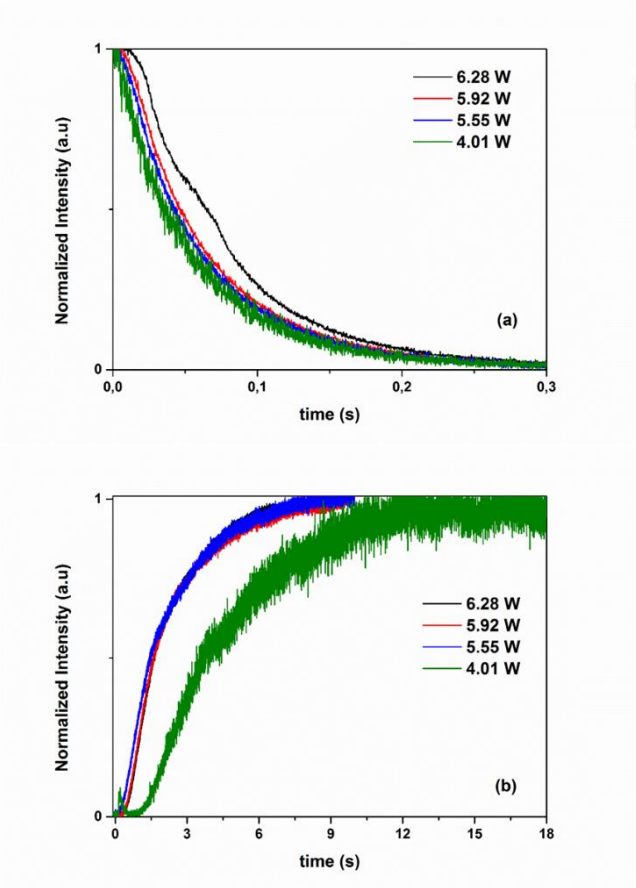

Figure 8.4 : The a) decay and b) rise patterns of the 20% Yb^{3+} doped bulk sample at 975 nm excitation depending on excitation power.

9. TEMPERATURE DEPENDENCE OF WHITE LIGHT EMISSION

Trivalent rare earth doped materials are very interesting for a wide range of applications due to their unique optical properties like sharp emission bands, strong absorbance, being effective as luminescence centers and having the similar atomic size in host lattices.

The experimental data of this thesis showed that efficient luminescence emissions were observed from RE doped yttrium silicates. The white emission observed was based on thermal effects and upconversion processes. Besides various physical parameters such as doping concentration, pressure, excitation wavelength, etc. temperature sensitivity of rare earth doped samples affects the luminescence properties. In literature, there are very few studies about the temperature dependence of upconverted color or white emission [139-141]. In this part of the thesis, we have investigated temperature-dependent luminescence properties of sol-gel synthesized/ annealed undoped and 20% Yb^{3+} doped yttrium silicate nanophosphors. In addition, the spectra at a certain temperature were investigated as a function of pumping powers.

The measurements show that the temperature-dependent luminescence spectrum of a sample is a characteristic property [142]. In some situations, when temperature increased, the peak of emission can be shifted to lower energy (longer wavelength), the emission band can broaden, the intensity of emission can quench at some temperature values since the temperature changes affect all electron-phonon interaction, the ground and excited states of them [142-143].

9.1 Pressure- Temperature Calibration

The measurements of the temperature dependence of luminescence properties were performed in a wide range from 780K to 4K. Firstly, we should explain how the temperature-dependent measurements were performed since the experimental set up

required some modifications to take measurements truely. The study about the experimental set up will also lead us to discuss the origin of pressure versus temperature dependence and to consider how to keep both parameters constant during emission measurements.

During the temperature dependence measurements, at least two physical parameters that are pressure, temperature and pumping powers should be constant because of taking the true data. Of course, we could not take experimental data when two parameters were changing at the same time. Moreover, we know that luminescence properties are very sensitive to pressure and pumping powers. According to Ideal gas law, when the temperature goes down, pressure also goes down. To keep the pressure as a constant value, either the number of particles must be kept stable or change the volume by using a sensitive valve.

For our system, firstly, the changes in pressure with temperature are determined as shown in Figure 9.1 without any modification.

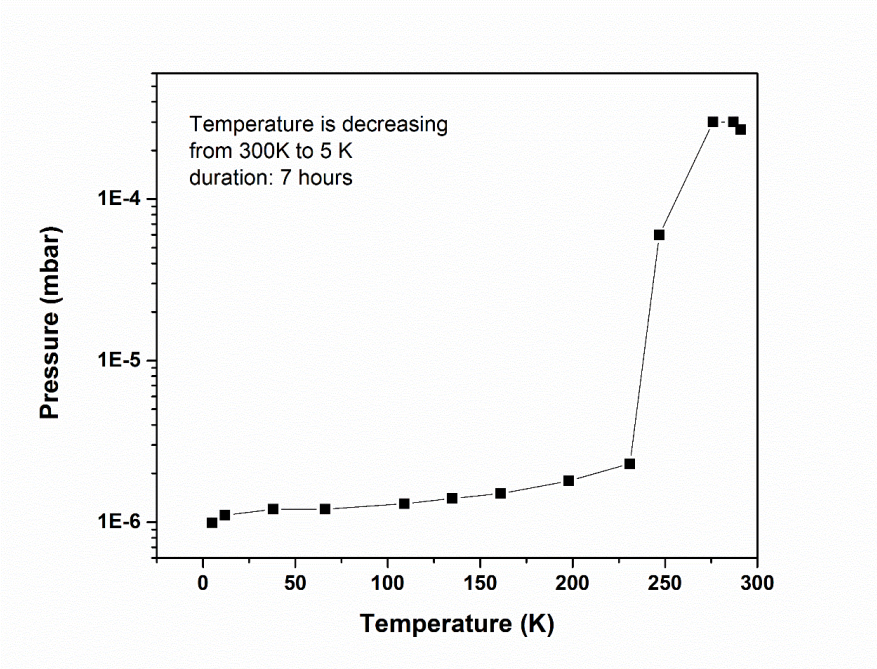

Figure 9.1 : Temperature-Pressure calibration.

It is shown in Figure 9.1; the pressure depends strongly on temperature changes. Below about 250K, the dependence can be seen as if it is very little, however, even those little changes affect the intensity of white emission very much due to strong dependence of white light on pressure. Therefore, to keep the pressure at a constant value with various temperatures, a modification was needed in the system and we used a special valve

like a needle. Thanks to this special valve, the pressure value of the system was kept constant for each temperature value during measurements by inserting air very very slowly to the vacuum area. For example, if the temperature goes down, the pressure was also down, if we want to increase the pressure of the system without change the temperature, the valve needs to open and vacuum the system should be decreased. Besides this approach, the threshold value of pressure was also determined at some low-temperature values of the system. For example, to obtain 4K from the system, the pressure inside must be at least 10^{-4} mbar.

9.2 Temperature Dependence of White Light Intensity for Undoped Yttrium Silicate Nanophosphors

In Figure 9.2, we see temperature-dependent luminescent spectra of undoped yttrium silicate sample. Based on our previous works [58, 61], we have observed the broadband thermal bright white emission from undoped sample at either 975 nm or 808 nm excitations. For the undoped sample, the temperature dependence of white light intensity at a definite power was investigated (see Figure 9.2 and 9.3). There is a breakpoint about room temperature. Above 300 K, white light intensity was increasing with the ambient temperature but it could not continuous. The result is related to non-radiative recombination. The activation of non-radiative recombination centers was enhanced with increasing temperature. As shown in Figure 9.2, the luminescence intensity decreases rapidly with increasing temperature below room temperature. This may be caused thermal quenching process, which could be due to either a multiple phonon relaxation processes or thermal ionization of ions in the host, which was a part of the trapping mechanism that produced long persistence. Without the photoionization process, multiphonon processes are generally regarded as the cause of nonradiative processes that induced thermal quenching. Smaller lattice phonon energy is then better to reduce such a quenching process [144, 145].

The measurements depending on temperature were carried out at 5.5 W, between 4K and 550 K. The lowest temperature was obtained as 4K for the experimental setup but 20K was recorded due to the effect of laser heating. The slits were at 0.2 mm, and the excitation wavelength was 975 nm during the measurements. Also, blueshift and broadening of emission spectra with increasing temperatures were obtained for the sample. This indicates that there are some temperature-dependent electron-phonon

interactions in the system. In nanometer materials, electron-phonon interaction becomes much stronger than that in the bulk form.

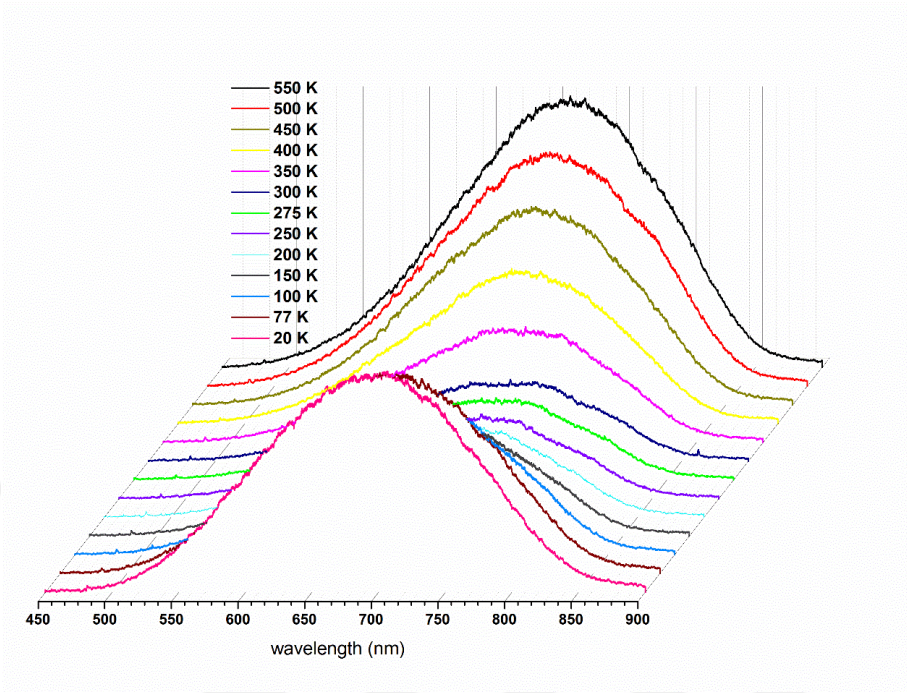

Figure 9.2 : Temperature effects on the luminescence spectra for undoped yttrium silicate sample. (Pressure: between 2- $3x10^{-4}$mbar).

FWHM values of emission spectra of undoped sample increase by increasing temperature above 300 K. Below the 550 K, the emission intensity is thermally quenched until 300 K, however, below 300K the intensity of white emission became to increase with decreasing temperature. The increasing of FWHM and decreasing emission intensity with increasing temperature mean that there may be thermal quenching at a configurational coordinate diagram [147]. However, FWHM values were increased with decreasing temperatures below 300K. When the luminescent center is excited, it is thermally activated through phonon interaction. After that, it thermally released through the crossing point between excited and ground states in the configurational diagram. This process is strongly dependent on temperature and results from a decrease in emission intensity [142]. At high temperatures, the population of phonons increases, electron-phonon interaction is dominant and so FWHM of the spectra is broadened. The position of the peak of the emission is shifted to the red region above 300K with increasing temperature and is shifted to the blue region below 300 K with decreasing temperature.

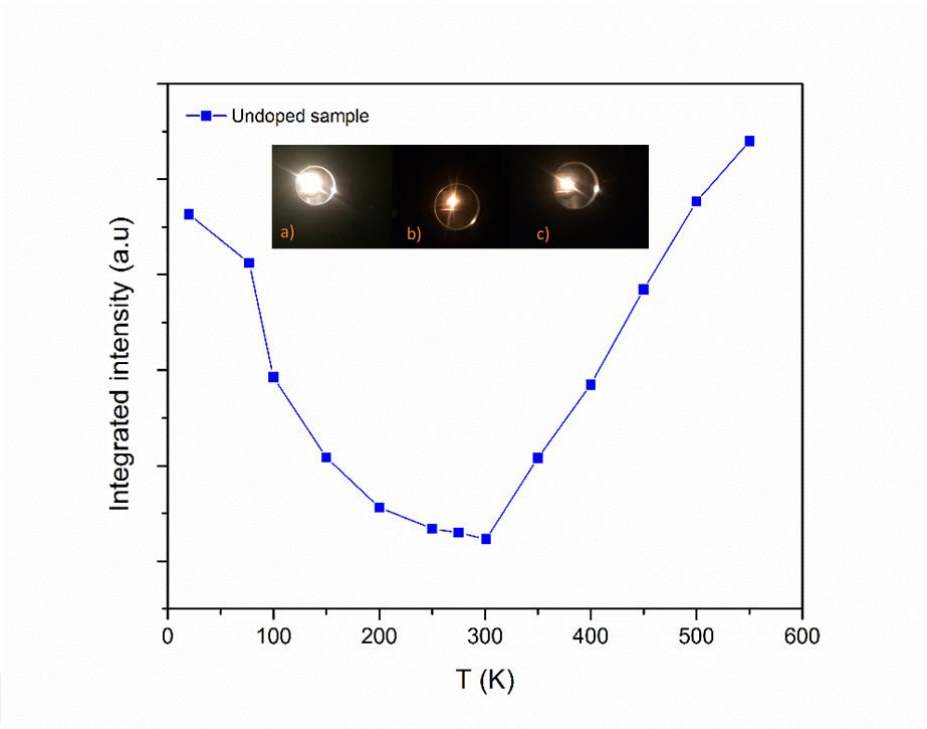

Figure 9.3 : Temperature dependence of the luminescence intensity for undoped yttrium silicate sample. The photos of the sample at a) 550K b) 300K and c) 20K.

This behavior can be explained by the Varshini equation for temperature dependence;

$$E(T) = E_0 - \frac{aT^2}{T+b} \tag{9.1}$$

where E(T) is the energy difference between the excited and ground states at T, E_0 is the energy difference at 0K, and a and b fitting parameters. At high temperatures, crystal field is decreased due to increasing of bond length between the luminescent center and its ligand ions. The symmetry of the luminescent center is distorted and it causes split excited or ground states. These processes cause to decrease of the transition energy and emission peak is shifted to lower energy with increasing temperature [142].

The emission intensity of most luminescent materials usually decreases with increased temperature due to the increase in nonradiative transition probabilities of high temperatures. However, in our case, the intensity increases with increasing temperature above 300K. For persistent phosphors, activators are expected to be ionized by one photon to produce trapped electrons. Sometimes when the electronically excited state is below the conduction band, the electrons need thermal energy to be ionized. This process thermal ionization and needs the electron energy level to be close to the host conduction band. If there is a thermal ionization in the

system, thermal quenching plays an important role due to the trapping of many electrons. In addition, the thermal quenching is not effective at very high temperatures even 550K. We understand that the host material has excellent thermal stability [139].

9.3 Temperature Dependence of the White Light Intensity for 20% Yb^{3+} Doped Yttrium Silicate Nanophosphor

The intensity of white light of undoped and 20% Yb^{3+} doped samples was affected by temperature changes of ambient. At very low temperature (below 150K) and powers, the Yb^{3+} doped sample gave the cooperative emission Yb^{3+}-Yb^{3+} ions and emission peaks of unwanted Er^{3+} impurities.

In Figure 9.4, we see the temperature dependence measurements at constant pumping power (3.21 W), and constant pressure (P= 1.10^{-4}mbar) for 20% Yb^{3+} doped yttrium silicate sample. It can be seen that with the increase of temperature from 10K to 200K, the intensity of white light is decreased due to the temperature quenching [139].

In general, there may be temperature dependence of electron-phonon interactions in luminescence center and thermally activated photoionization of rare earth ions for the occurance of thermal quenching. Moreover, these accepted mechanisms are strongly related to the crystal structure of the host matrix, the crystallinity of phosphors and quenching rates [139,144]. According to the Boltzmann distribution,

$$N_n \alpha \exp(-E_n/\mathrm{kT}) \tag{9.2}$$

where N_n is the number of molecules in the excited state, k is the Boltzmann constant, n is the vibrational quantum number of the excited state molecules. The increase of temperature will cause the redistribution of excited state molecules; will not bring up the number of molecules in the ground state to transition to the excited state [141]. When temperature increases, the number of molecules in the excited state will increase. In Figure 9.5 the luminescence intensity decreased above 300K while it increased above 200K. This may be possible due to the partial energy transfer of unwanted Er^{3+} impurity ions. As the temperature increases, the intensity of the emission decreases for 20% Yb^{3+} doped sample. The reason can be an increased number of phonons in the matrix with increasing temperature.

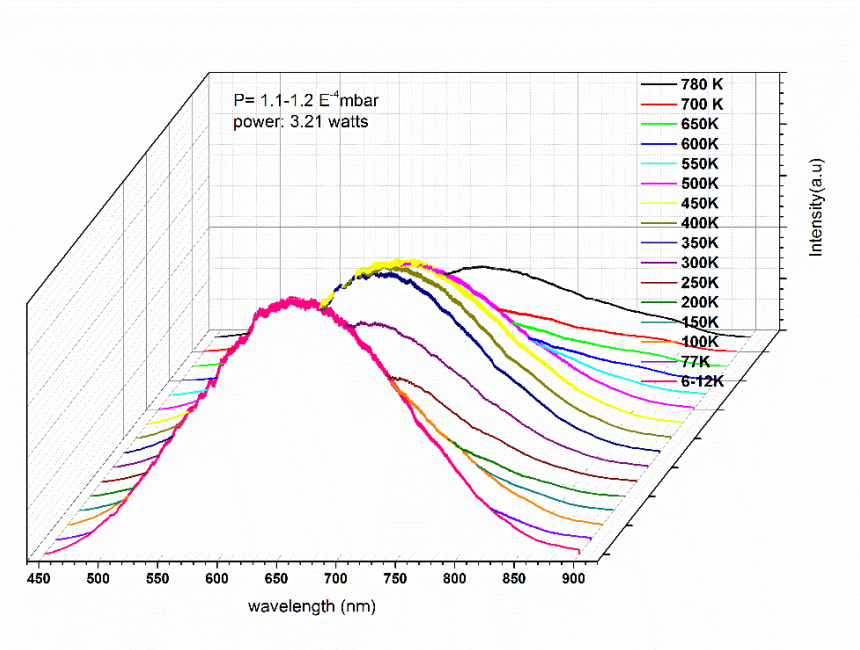

Figure 9.4 : Temperature dependence of the luminescence intensity of 20% Yb^{3+} doped sample at pressure $1x10^{-4}$mbar at 3.21 W.

In Figure 9.5, firstly the intensity of the emission increased from 700K to 350K, and decreased from 350K to 200K.

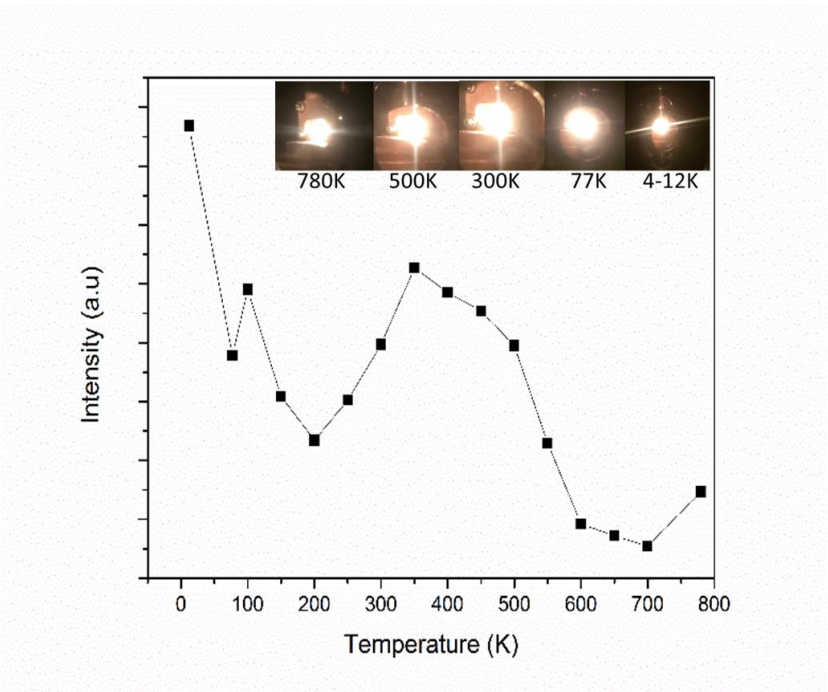

Figure 9.5 : Double log figure of 20% Yb^{3+} doped sample at pressure $1x10^{-4}$mbar at 3.21 W.

Below 200K, the emission increased again and the reason for these different behaviors may be the difference in crystal-field levels for the sample. In other words, the

phenomena can be explained by the interaction between the electrons and thermally active phonons.

9.4 Power Dependence of White Light Intensity for 20% Yb^{3+} Doped Yttrium Silicate Nanophosphors at Definite Temperatures (8K, 77K, 200K, 450K, and 780K)

Luminescence measurements were carried out to determine the power dependence of the emissions at definite temperature values for 20% Yb^{3+} doped sample. Figure 9.6 shows the luminescence spectra at 8K depending on pumping powers, however, the laser causes heating and the temperature reached 18 K during the measurement.

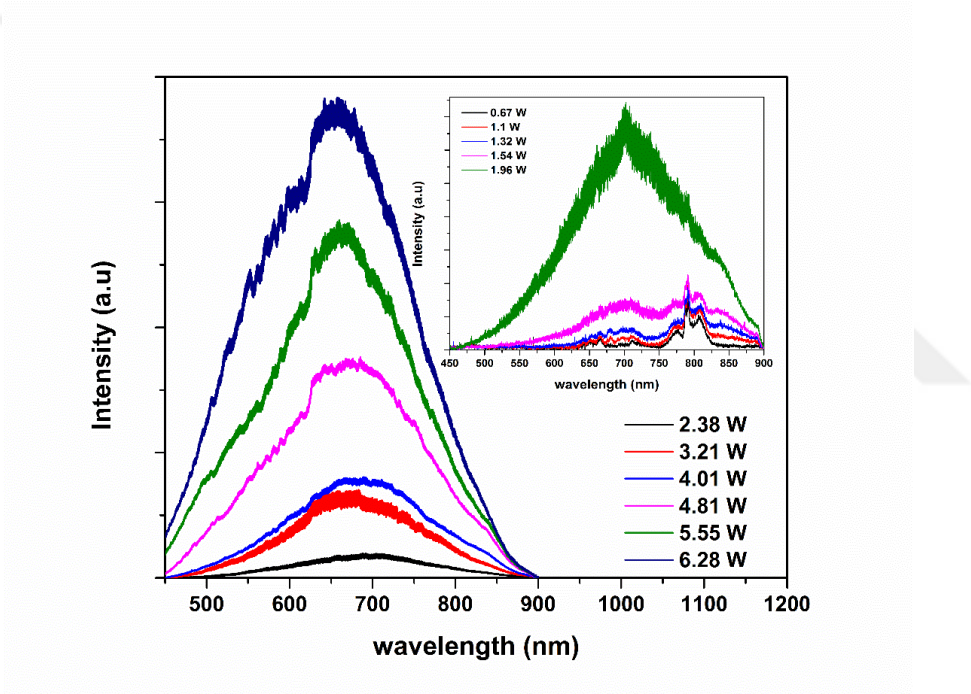

Figure 9.6 : Power dependence of the luminescence spectra of 20% Yb^{3+} doped sample at constant pressure (10^{-7}) mbar and temperature (8K).

To take the temperature measurements, firstly, the system was cooled until to reach 4K temperature and then measurement was started. It is determined from the experimental results; the power dependence of the emission is stronger than the temperature dependence. In other words, the most effective physical parameters on emission intensity are pressure, power, and temperature, sequentially. The intensity of white light of 20% Yb^{3+} doped yttrium silicate powders was affected by the temperature changes. It was observed that if the temperature was decreased, obtaining white light was more difficult.

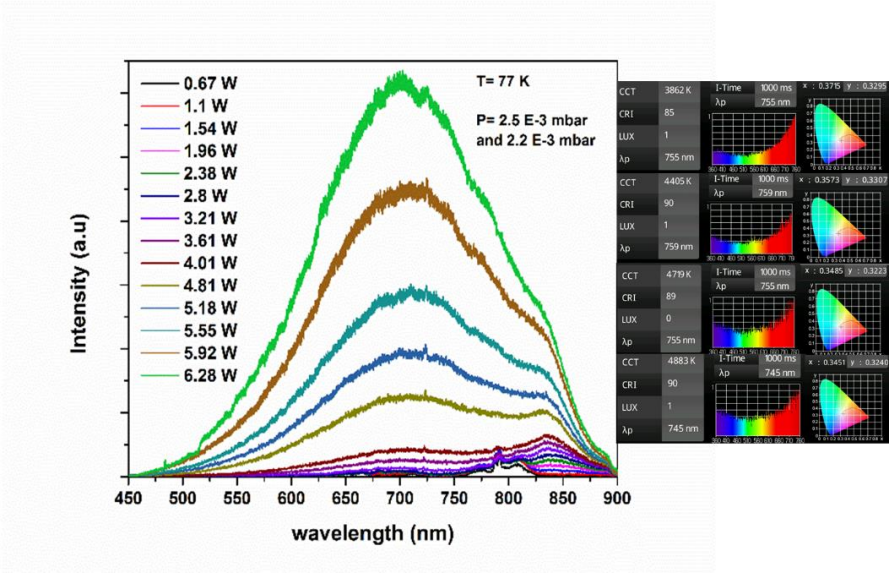

Figure 9.7 : Power dependence of the luminescence spectra of 20% Yb^{3+} doped sample at constant pressure $2x10^{-3}$ mbar and temperature 77K.

At temperature 77K, the emission intensity of 20%Yb^{3+} doped samples were increasing with the increasing pumping powers and n~6 value indicates that the photon avalanche was effective for the system. (Figure 9.7 and 9.8, respectively)

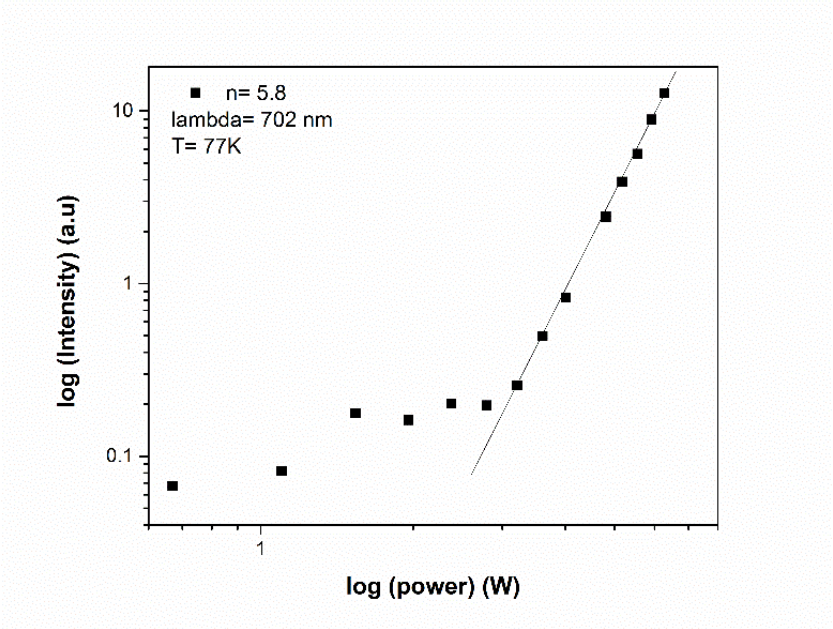

Figure 9.8 : Double log plot of 20% Yb^{3+} doped sample at constant pressure $2x10^{-3}$ mbar and temperature 77K.

The luminescence results for 200K and 8K showed that the similar behavior was obtained from the sample with increasing pumping powers. (Figure 9.9, 9.10, 9.11 and 9.12)

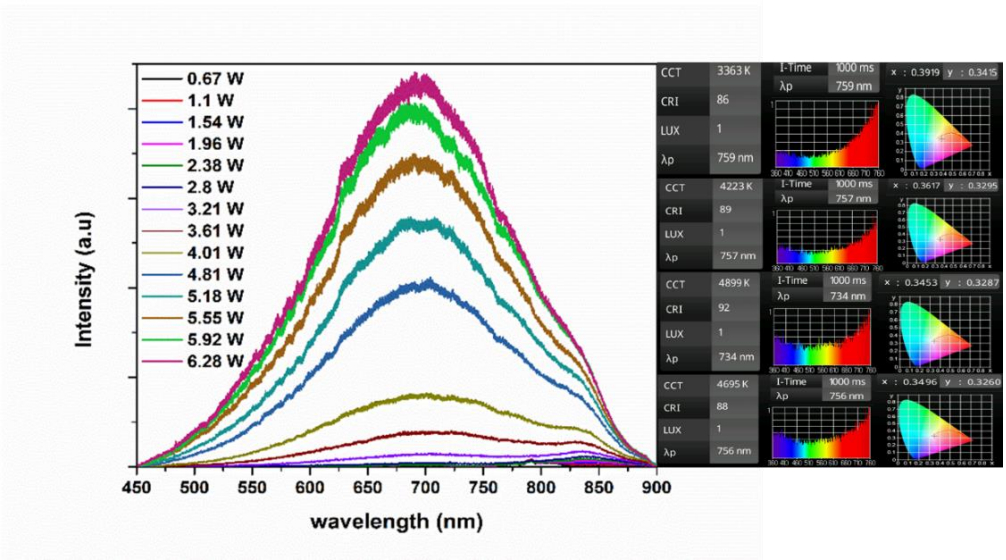

Figure 9.9 : Power dependence of the luminescence spectra of 20% Yb^{3+} doped sample at constant pressure $2x10^{-3}$ mbar and temperature 200K.

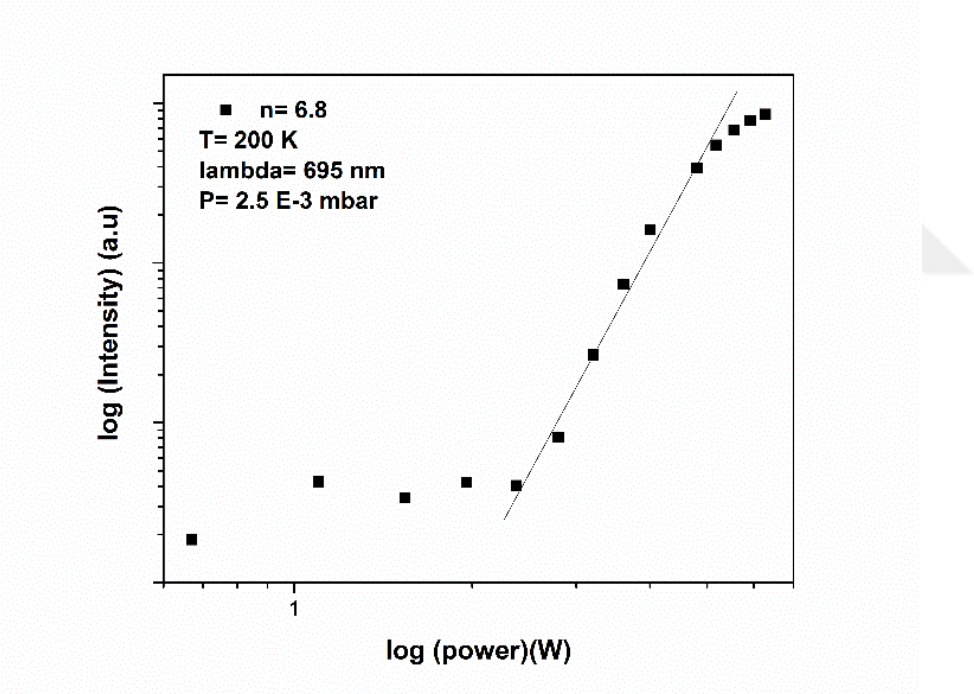

Figure 9.10 : Double log plot of 20% Yb^{3+} doped sample at pressure $2x10^{-3}$mbar and temperature 200K.

The power dependence of white light intensity at a definite pressure and temperature values were observed. The intensity of white light of 20% Yb^{3+} doped yttrium silicate powder was affected by the temperature changes. It was observed that if we decrease the temperature, obtaining white light is more difficult.

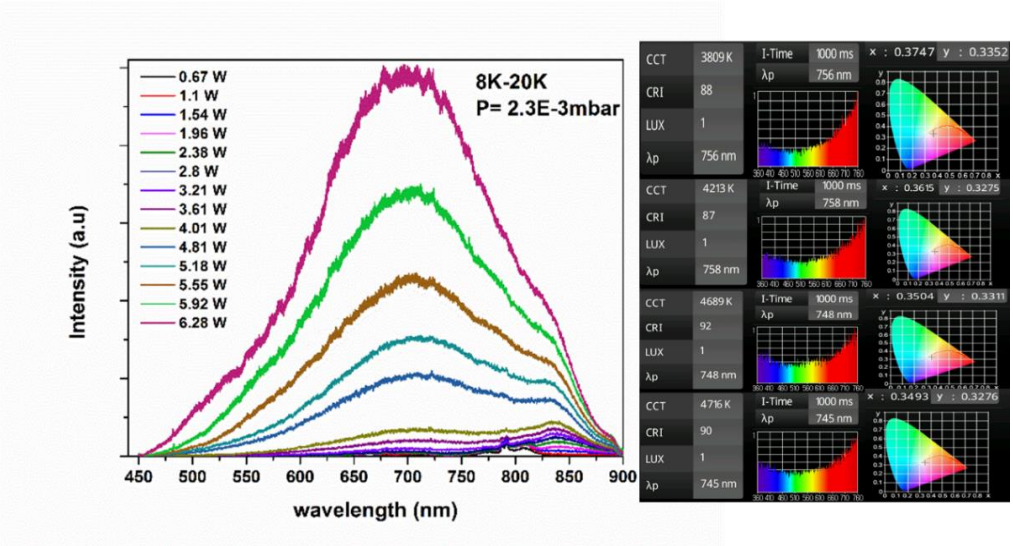

Figure 9.11 : Power dependence of the luminescence spectra of 20% Yb^{3+} doped sample at pressure $2x10^{-3}$ mbar and temperature 8K.

At very low temperatures and powers, the sample gave luminescence emission of Er^{3+} impurities instead of white light spectra. The integrated intensity values will be calculated for power dependence at different temperatures.

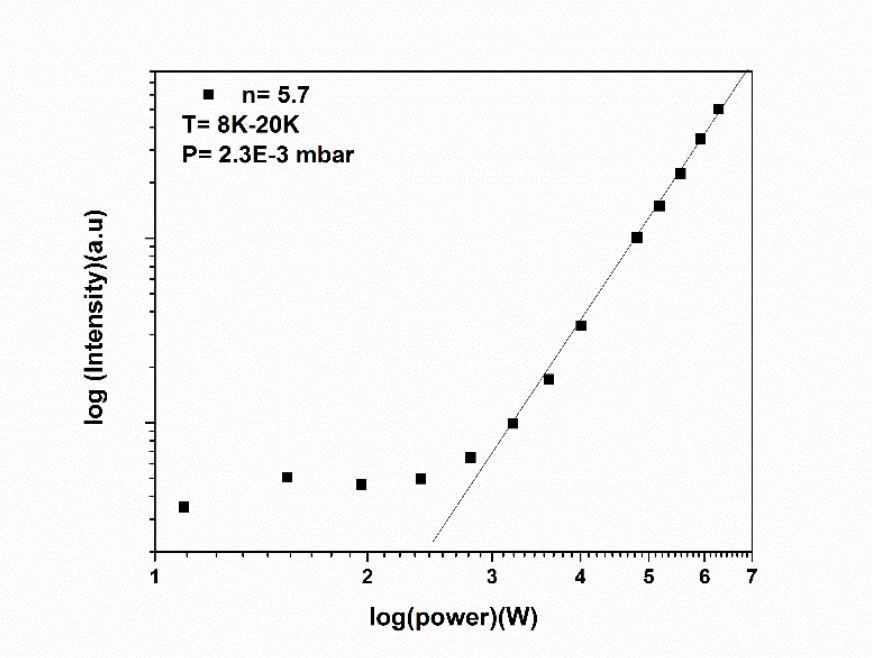

Figure 9.12 : Double log plot of 20% Yb^{3+} doped sample at $2x10^{-3}$mbar and temperature 8K.

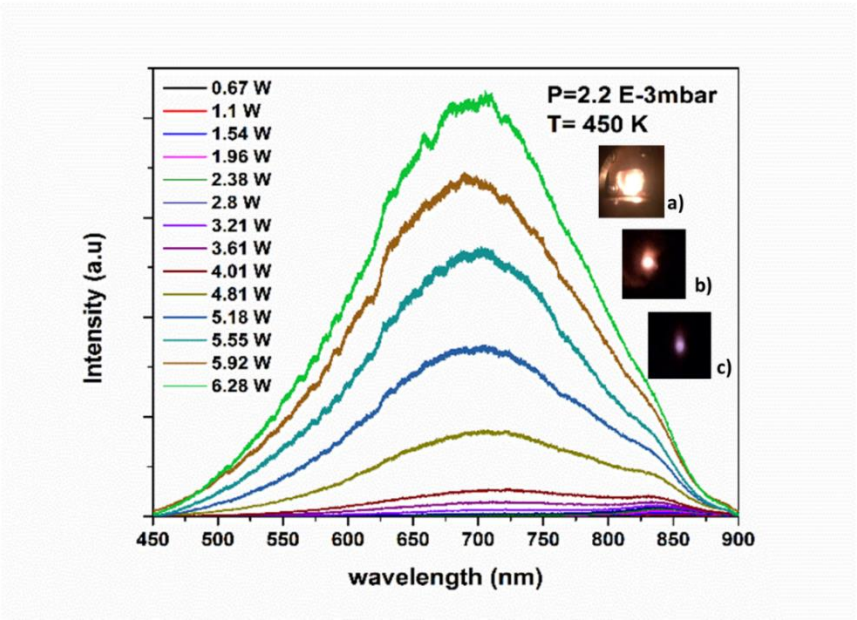

Figure 9.13 : Pumping power dependence of the luminescence intensity of 20% Yb^{3+} doped sample at pressure $2x10^{-3}$mbar at 450K. The photos of the sample at a)6.28 W, b) 4.01 W and c)1.54 W.

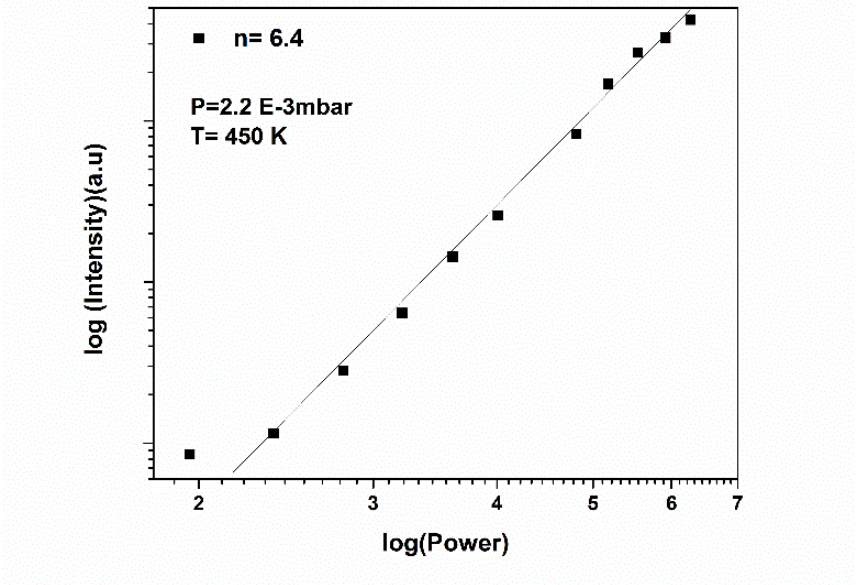

Figure 9.14 : Double log figure of 20% Yb^{3+} doped sample at pressure $2x10^{-3}$mbar and temperature 450K.

The temperature dependence of white light intensity at a definite power was investigated. The idea is that different pressures values may give different spectral behavior with the temperature changes.

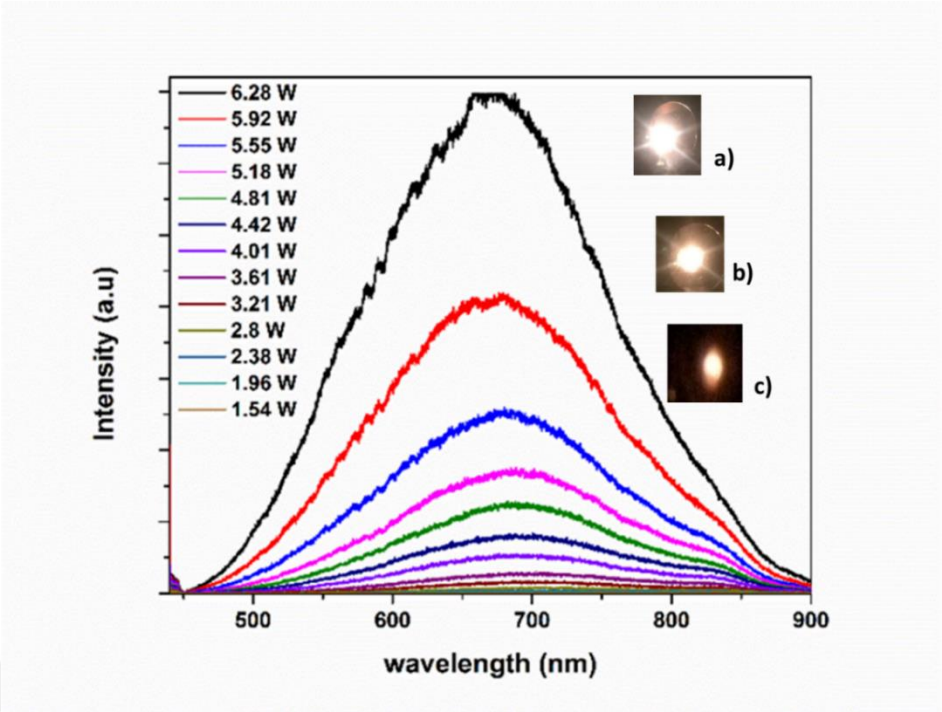

Figure 9.15 : Power dependence of the luminescence intensity of 20% Yb^{3+} doped sample at pressure $2x10^{-3}$mbar at 780K. The photos of the sample at a) 6.28 W b) 3.21W and c) 0.67 W.

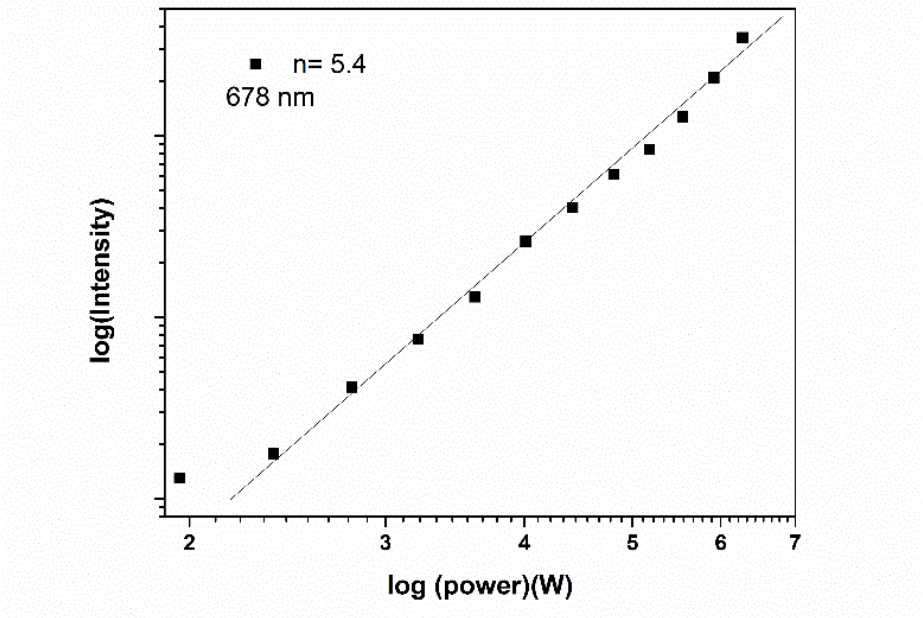

Figure 9.16 : Double log figure of 20% Yb^{3+} doped sample at pressure $2x10^{-3}$ mbar at 780K.

10. WHITE EMISSION SPECTRA OF NANOPHOSPHORS AT VARIOUS PRESSURES

As we know, the generation of white emission and the intensity of it depend strongly on pressure and pumping powers. The emission intensity increases exponentially with a decrease in pressure. The dependence of white emission intensity on the ambient pressure within the thermal case is given by the relation [82]:

$$I_{em} = I_0 \exp(-P/P_0) \quad (10.1)$$

where P_0 is the critical ambient pressure of sample and I_{em} is the quenching emission intensity except saturation case due to higher pumping powers.

The present study focuses upon the dependence of white emission on the pressure also pumping powers. Pressure and power dependences have been investigated for 20% Yb^{3+} doped yttrium silicate annealed at 1150 ^{0}C. We reported the luminescence behavior of the sample at atmospheric conditions, at 1 mbar and 10^{-3} mbar pressures depending on powers by using 975 nm excitation. The output power dependence of the emission is examined at each pressure value. We know from our experimental results that there is a threshold pressure value to obtain white light if the generation of white emission is thermal.

Figure 10.1 shows the luminescence spectra of the sample at atmospheric conditions and the chromaticity pictures of it at various powers. The unwanted Er^{3+} ions were obtained as in the other Yb^{3+} doped samples at low output powers of the laser. When the output powers increase, the UC spectra and peaks of transitions of Er^{3+} impurities became to disappear and the spectra turn to broadband thermal white light. The result is similar to Yb^{3+} doped samples as explained in Chapter 5. When the sample was at vacuum conditions, it is expected that the threshold power to obtain white light should be decreased. Meanwhile, the white emission at 1 mbar pressure was obtained easier than that was in atmospheric conditions. The emission spectra were shown in Figure

10.2 for the 1 mbar. Very bright and intense white emission is obtained at 1 mbar with increasing output powers of the laser (Figure 10.2).

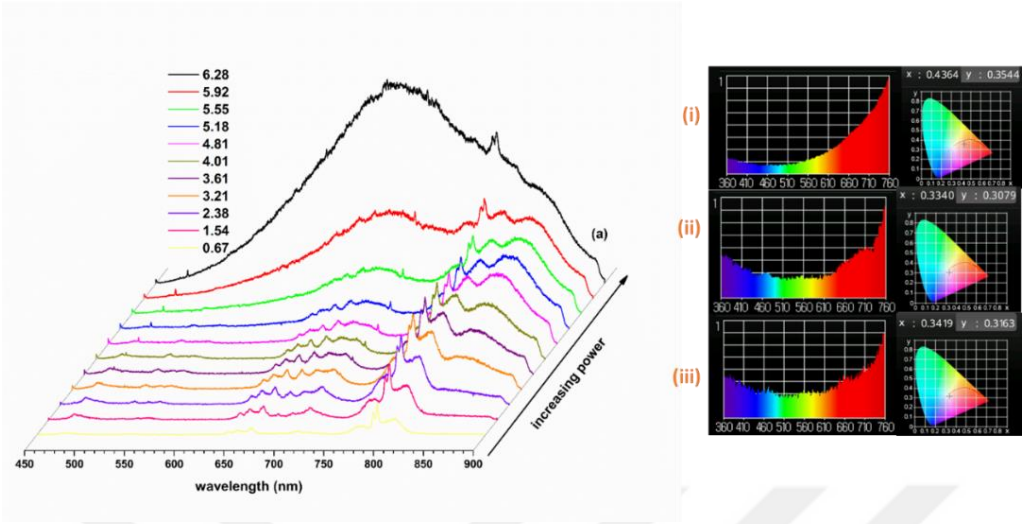

Figure 10.1 : Luminescence spectra of the 20%Yb^{3+} doped yttrium silicate nanophosphor annealed at 1150 ^{0}C as a function of excitation powers at atmospheric pressure, illuminance meter images at i) 6.28 W, ii) 4.01 W, and iii) 1.54 W.

Similarly, in Figure 10.3, the threshold pumping power is again decreased at 10^{-3} mbar and white emission was obtained easiest from the sample at that pressure value. In addition to this observation, the pressure dependence of white emission is stronger than the power dependence of it. In the same manner, the white emission was also investigated at 10^{-3} mbar and the intensity of the emission was increased much more than that was in 1 mbar case. The result was shown in Figure 10.3. The obtained emission was very strong and energetic due to shifting the peak to the blue region.

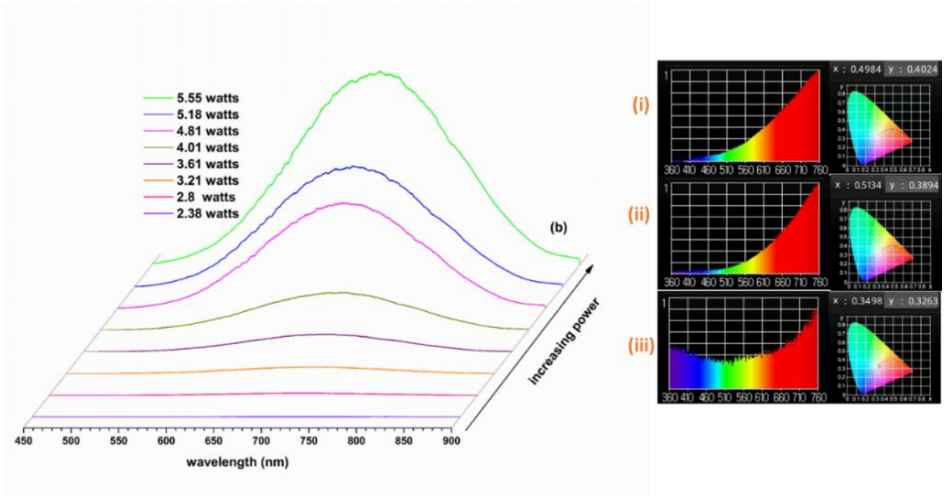

Figure 10.2 : Luminescence spectra of the 20% Yb^{3+} doped yttrium silicate nanophosphor annealed at 1150 ^{0}C as a function of excitation powers about 1 mbar, illuminencemeter images at i) 6.28 W, ii) 4.01 W, and iii) 1.54 W.

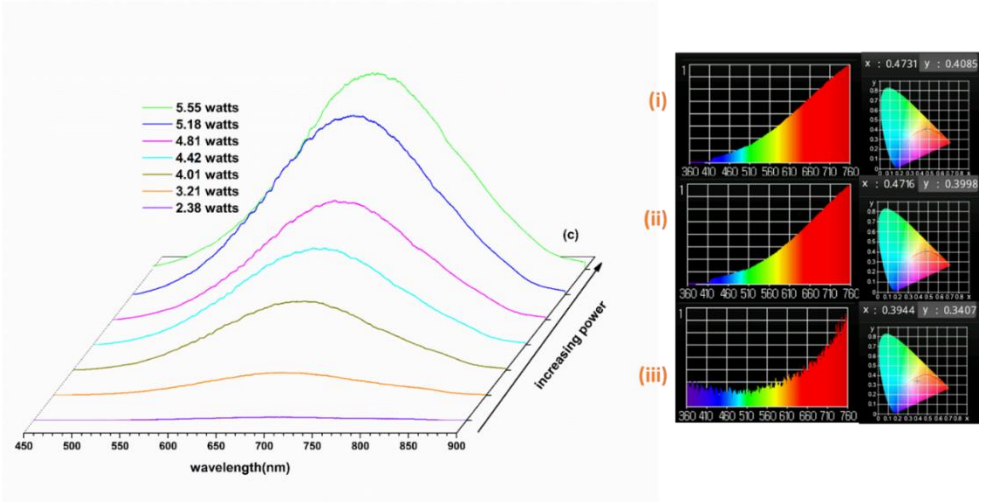

Figure 10.3 : Luminescence spectra of the 20% Yb^{3+} doped yttrium silicate nanophosphor annealed at 1150 ^{0}C as a function of excitation powers about 10^{-3} mbar, illuminance meter images at i) 6.28 W, ii) 4.01 W, and iii) 1.54 W.

Figure 10.4 shows a summary of three values of pressures for white light generation. It can be seen from Figure 10.4 that there is a blue shift, a more energetic region with decreasing the pressure and the intensity of emission is also increasing with decreased pressure. The increase in relative intensities of the shift is highest at 10^{-3} mbar pressure. This behavior also proves that the emission intensity is very sensitive to pressure changes for powder samples.

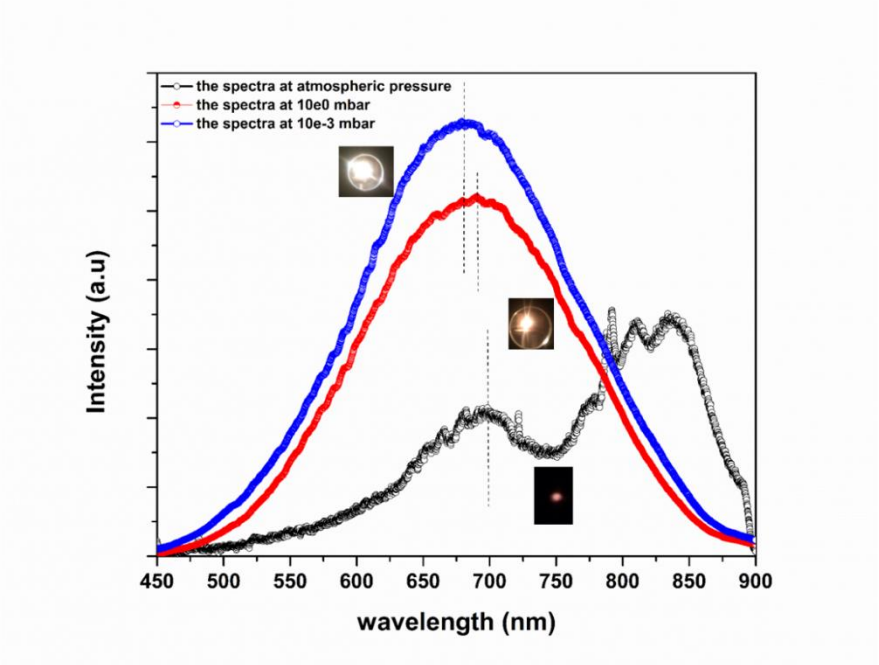

Figure 10.4 : The comparison of the luminescence spectrum of 20% Yb^{3+} doped yttrium silicate nanophosphor annealed at 1150 ^{0}C at various ambient pressures with the constant pumping power of 5.55 W.

Figure 10.5 gives information about the dependence of intensity versus powers in each pressure value. The numbers of photons involved in the processes are ~9, ~7, ~5 with decreasing pressures, respectively. This demonstrated that the number of photons is proportional to decreasing pressure.

The CIE coordinates were determined to measure the color of visible emission and the summary of chromaticity coordinates at various pressures depending on pumping powers were given in Table 10.1. The obtained color-rendering index from 79 to 98 indicates that there is a large range for the quality of observed emission at different pressure cases.

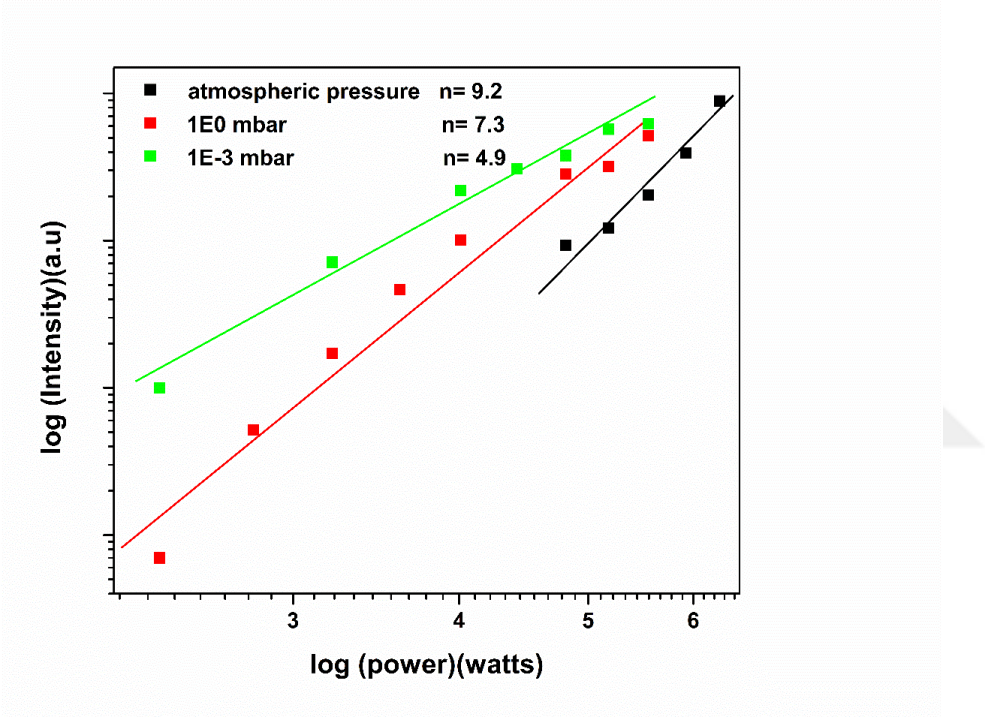

Figure 10.5 : Log-log plot of the 20% Yb^{3+} doped yttrium silicate nanophosphor annealed at 1150 ^{0}C.

The CIE coordinates were measured for the sample at each condition to characterize emissions in terms of lightning performance as seen in Table 10.1.

Table 10.1 : The illuminance meter results of 20% Yb^{3+} doped yttrium silicate sample unnealed at 1150 ^{0}C under various pressure depending on pumping power.

Atmospheric Pressure			
Power	**CIE1931 Coordinates (x, y)**	**CCT (K)**	**CRI**
6.28 W	(0.4364, 0.3544)	3863	79
4.01 W	(0.2217, 0.4598)	5391	80
3.21 W	(0.2220, 0.4610)	5320	82
2.38 W	(0.2228, 0.4616)	5237	81
1.54 W	(0.2237, 0.4657)	5004	85
0.67 W	(0.2231, 0.4684)	4942	87
Pressure: 1 mbar			
Power	**CIE1931 Coordinates (x, y)**	**CCT (K)**	**CRI**
6.28 W	(0.2978, 0.5310)	2009	97
4.01 W	(0.3090, 0.5273)	1959	94
3.21 W	(0.2791, 0.5027)	2448	86
2.38 W	(0.2284, 0.4743)	4461	88
1.54 W	(0.2251, 0.4724)	4688	90
0.67 W	(0.2236, 0.4734)	4739	89
Pressure: 10^{-3} mbar			
Power	**CIE1931 Coordinates (x, y)**	**CCT (K)**	**CRI**
6.28 W	(0.2709, 0.5273)	2534	98
4.01 W	(0.2752, 0.5250)	2461	96
3.21 W	(0.2849, 0.5246)	2297	95
2.38 W	(0.2940, 0.5224)	2161	93
1.54 W	(0.2505, 0.4867)	3286	86
0.67 W	(0.2252, 0.4706)	4739	90

In conclusion, the vacuum environment provides to make white emission more intense than atmospheric pressure as we expected. The threshold power to generate white emission is also decreased in the vacuum. The peak position of white emission was shifted to the blue region when the pressure decreased.

11. CONCLUSIONS AND RECOMMENDATIONS

All the samples in this thesis were synthesized by the sol-gel method since the method has many advantages such as minimizing defects and decompositions, low working temperature and easy control of the processes. After the heat treatment, the structural analyses of samples were carried out in various techniques. XRD, SEM, TEM, EDS and FTIR methods were performed the structural and morphological properties of the samples. XRD patterns gave information about the phase structure and average grain sizes of the samples. The main structure was mostly α-$Y_2Si_2O_7$ for samples with some exceptions. An additional Y-$Y_2Si_2O_7$ phase was seen in the XRD results of samples that contain Yb^{3+} ions. When the concentration of Yb^{3+} increased from 10% to 20% per mole, both phases X_2-Y_2SiO_5 and $Y_2Si_2O_7$ appeared in the spectrum. The agglomeration in SEM results supported the XRD result for a high concentration of Yb^{3+}. Single Nd^{3+} doped yttrium silicate sample has both X_1-Y_2SiO_5 and X_2- Y_2SiO_5 phases. According to the phase diagram of Y_2O_3-SiO_2, Y_2SiO_5 has polymorphic structure and can be in X_1- or X_2- type at different synthesis temperatures.

The luminescence properties of undoped yttrium silicate samples as functions of pumping powers were investigated in Chapter 4 both at 975/808 nm excitation wavelengths under atmospheric pressure and vacuum. Unexpectedly, the undoped sample emitted the white light at all physical conditions. The source of white emission in the undoped sample may be due to defects in the sample. The high number of photons involved in the emission process with n= ~22 and n= ~14 at 975 nm and 808 nm, respectively, showed us the thermal processes were very effective and avalanche mechanism occurred at atmospheric pressure. The long rising and decaying patterns were evidence for thermal processes. The threshold pumping power to observe white emission was decreased at vacuum. The luminescence behaviors of single Nd^{3+}, Tm^{3+} and Yb^{3+} doped samples were analyzed in Chapter 5. Nd^{3+} doped sample showed very challenge emission characteristics depending on pumping powers. The spectra of Nd^{3+} doped sample turned to thermal white light above ~5.7 W, while it emitted upconverted

white light of blue, green and red emissions below it at atmospheric pressure. The anamolous behavior in decay and rise times of Nd^{3+} doped sample can be due to being together of photon avalanche UC processes and thermal effects together. At vacuum, below ~3.5 W, UC processes were dominant while the thermal processes become stronger above ~3.5 W. This behavior was seen easily in two different regions at double log representation of intensity versus power. The samples in various low concentrations of Tm^{3+} emitted the blue and red light in similar characteristics. The $^1G_4 \rightarrow {}^3H_6$ and $^3F_3 \rightarrow {}^3H_6$ transitions of Tm^{3+} ions were observed in power dependent spectra at 475 nm and 695 nm, respectively. It is not expected to observe visible light from Yb^{3+} ions due to the electronic transition property of Yb^{3+}. Only cooperative emission of two Yb^{3+} makes possible to obtain blue light in the visible spectrum. However, some transitions were observed in spectra due to Er^{3+} impurities in raw chemicals. The luminescence properties were investigated for various concentrations of Yb^{3+} from 1% to 20% in samples. We observed the cooperative blue UC emission of about 475 nm. When the power was increased, the spectrum becomes to turn thermal white light. The peaks of the spectra were also shifted to a high energy region with increasing pumping power and Yb^{3+} concentration. The threshold power to obtain white emission was also decreased with increasing dopant concentrations. While the rise patterns were very sensitive to pumping powers, the decay patterns were not strongly dependent on power. 20% Yb^{3+} doped sample was the brightest one among all the samples.

In Chapter 6, codoped samples were investigated with the excitations of 975 and/or 808 nm at atmospheric pressure and vacuum conditions. Since both Nd^{3+} and Yb^{3+} show a sensitizer characteristics, the Nd^{3+}/Yb^{3+} codoped sample had extremely different emission behavior at 808 nm excitation. The sudden changes were observed in spectral profiles for low and high excitation power densities. The transitions in spectra were due to Nd^{3+} energy transitions. The shapes of slopes in the double log graph were nearly identical and this may indicate the involving all UC processes in the same intermediate state. The comparison of the low and high power cases showed us the thermal white emission may be due to the effects of high intensity laser irradiation and heterolooping energy transfer could be observed. At vacuum, the log-log plot of the Nd^{3+}/Yb^{3+} codoped sample showed s-shape power dependence instead of n- shape. The emitted light was more stable under vacuum conditions and 975 nm excitations

depending on the output power of the laser diode. The luminescence measurements for Nd^{3+}/ Tm^{3+} codoped sample were performed at 808 nm since Nd^{3+} or Tm^{3+} ions could not be excited at excitation of 975 nm. When we compared the codoped sample with the Tm^{3+} single doped sample, adding Nd^{3+} ions to the Tm^{3+} system caused the transition of Tm^{3+} to blue (high energy) region. The spectrum of Tm^{3+} doped sample was dramatically affected by adding Nd^{3+} to the system. The emission centered between 650 nm and 700 nm were the superposition of ($^3F_2$, $^3F_3$)$\rightarrow$$^3H_6$ of Tm^{3+} and $^4F_{9/2}\rightarrow$ $^4I_{9/2}$ of Nd^{3+}. The Tm^{3+}/ Yb^{3+} codoped yttrium silicate samples in various concentrations gave similar characteristics at 975 nm excitation. The intensity of emission at 808 nm was weaker than it is at 975 nm. The energy transfer from Yb^{3+} to Tm^{3+} is easier than that is the case from Tm^{3+} to Yb^{3+} ions. At vacuum, the spectra again turned to thermal white light with the transition of $^3F_3\rightarrow$$^3H_6$ of Tm^{3+}.

In Chapter 7, dynamical and characteristic properties of triple Nd^{3+}/ Tm^{3+}/Yb^{3+} doped yttrium silicate samples were introduced in various physical conditions. White light based on upconversion emission of rare earth ions was observed at lower pumping powers of diode lasers and containing low concentration of Yb^{3+} (2% per mole) doped samples. When the power increased and concentration of Yb^{3+} increased from 2% to 10%, the emitted light becomes to thermal white light with the energy transition of Tm^{3+} and Nd^{3+} ions, also cooperative emission of Yb^{3+} pairs.

It is explained that obtaining white emission is possible for a bulk sample of 20% Yb^{3+} doped yttrium silicate in Chapter 8. The result was important due to its avoiding complex doping procedures to obtain white emission for some applications. Below ~2.8W, the sample emitted the blue emission due to the cooperative UC of Yb^{3+}. The other emissions in green, yellow and red regions in visible range were attributed to unwanted Er^{3+} impurities.

The temperature dependence measurements of white light were carried out for the undoped and 20% Yb^{3+} doped samples from 550 K to 4K- 20K and from 780K to 4K-20K, respectively and the results were discussed in Chapter 9. The results showed that the temperature dependence of white light is a characteristic property for a sample. The intensity of white emission from undoped sample was increased below and above 300K. In other words, 300 K was a breakpoint for two regions. The intensity of white light was increased below 700K and it decreased after ~300K. Below 150K, the intensity started again to increase. In addition, the comparison of the pumping power

dependence and temperature dependence of white light was explained in Chapter 9 by analyzing the power dependence of the emission at some definite temperatures such as 8K, 77K, 200 K, 450K and 780 K.

The effects of pressure changes on white emission were investigated in Chapter 10 for the 20% Yb^{3+} doped sample. The power dependence measurements were performed at atmospheric pressure, 1 mbar and 0.001 mbar. One of the most important results is the peak of the thermal white emission was shifted to a more energetic region (blue side) with decreasing pressure. The number of photons involved in the process was decreased with decreasing pressure.

We have studied the luminescence characteristics and the white emission of the mentioned yttrium silicate samples depending on many physical parameters. However, one can be improved the study in light of the information and results of this dissertation. We can list the prospects for future works:

- The different synthesis techniques can be used to fabricate these samples and it can be studied how the various synthesis techniques affect the luminescence and white light properties.
- The temperature dependence of all samples can be investigated at various power values and temperature sensing properties can be carried out.
- Unusual decay rise patterns from some samples, for example, Nd^{3+}/ Tm^{3+} codoped sample, can be investigated in detail.
- The polarization or dielectric properties of the samples can be investigated depending on temperature.
- In the thesis, we have studied the various concentration of Tm^{3+} and Yb^{3+} ions in single doped, codoped or triply doped yttrium silicates. The results of the Nd^{3+} doped samples were interesting in our study. Therefore, the concentration of Nd^{3+} ions may be changed and the luminescence properties may be examined at various physical conditions.

Even if the actual origin of the white light generation is still unknown, several important points to product white emission were discussed in the thesis. The experimental results will lead to future works about luminescent material, upconversion processes, and white light generation. The originality of the measured

warm or cold WL emission can be due to host, doped with rare earth ions (single, codoped or triply doped) by the ways of upconversion or thermal processes. To obtain the white emission from only the host provides us to avoid the complexity of the synthesis and doping of RE ions procedures. It can overcome the critical issues of color balance and thermal stability. A very large of tunable color emissions or combinations of them to white emission were observed and vacuum conditions supported to generate it. For the photonics and optical applications, luminescent properties of the samples reported for the usage of them as WL sources.

REFERENCES

[1] **Rakov, N., & Maciel, G. S.** (2012). Three-photon upconversion and optical thermometry characterization of Er^{3+}: Yb^{3+} co-doped yttrium silicate powders. *Sensors and Actuators B: Chemical*, *164*(1), 96-100.

[2] **Rakov, N., Maciel, G. S., Guimarães, R. B., & Carvalho, I. C. S.** (2010). Upconversion emission from Tm^{3+}: Yb^{3+} and Tm^{3+}: Er^{3+}: Yb^{3+} doped Y_2SiO_5 powders prepared by combustion synthesis. *Materials Chemistry and Physics*, *123*(1), 199-202.

[3] **Hemmer, E., Venkatachalam, N., Hyodo, H., Hattori, A., Ebina, Y., Kishimoto, H., & Soga, K.** (2013). Upconverting and NIR emitting rare earth based nanostructures for NIR-bioimaging. *Nanoscale*, *5*(23), 11339-11361.

[4] **Enrichi, F., Riccò, R., Parma, A., Riello, P., & Benedetti, A.** (2008). Synthesis and characterization of monodisperse Eu-doped luminescent silica nanospheres for biological applications. In *Biophotonics: Photonic Solutions for Better Health Care*, *6991*, 69912E. International Society for Optics and Photonics.

[5] **Chatterjee, D. K., Rufaihah, A. J., & Zhang, Y.** (2008). Upconversion fluorescence imaging of cells and small animals using lanthanide doped nanocrystals. *Biomaterials*, *29*(7), 937-943.

[6] **Li, C., & Lin, J.** (2010). Rare earth fluoride nano-/microcrystals: synthesis, surface modification and application. *Journal of Materials Chemistry*, *20*(33), 6831-6847.

[7] **Escudero, A., Carrillo-Carrión, C., Zyuzin, M. V., & Parak, W. J.** (2016). Luminescent rare-earth-based nanoparticles: a summarized overview of their synthesis, functionalization, and applications. *Topics in Current Chemistry*, *374*(4), 48.

[8] **Jianbei, Q. I. U., Qing, J. I. A. O., Dacheng, Z. H. O. U., & Zhengwen, Y. A. N. G.** (2016). Recent progress on upconversion luminescence enhancement in rare-earth doped transparent glass-ceramics. *Journal of Rare Earths*, *34*(4), 341-367.

[9] **Janek, J., Sołtys, M., Żur, L., Pietrasik, E., Pisarska, J., & Pisarski, W. A.** (2016). Luminescence investigations of rare earth doped lead-free borate glasses modified by MO (M= Ca, Sr, Ba). *Materials Chemistry and Physics*, *180*, 237-243.

[10] **Dolan, M. D., Harlan, B., White, J. S., Hall, M., Misture, S. T., Bancheri, S. C., & Bewlay, B.** (2008). Structures and anisotropic thermal expansion of the α, β, γ, and δ polymorphs of $Y_2Si_2O_7$. *Powder Diffraction*, *23*(1), 20-25.

[11] **Luo, Y., Wang, J., Li, J., Hu, Z., & Wang, J.** (2015). Theoretical study on crystal structures, elastic stiffness, and intrinsic thermal conductivities of β-, γ-, and δ-$Y_2Si_2O_7$. *Journal of Materials Research*, *30*(4), 493-502.

[12] **Saha, S., Chowdhury, P. S., & Patra, A.** (2005). Luminescence of Ce^{3+} in Y_2SiO_5 nanocrystals: Role of crystal structure and crystal size. *The Journal of Physical Chemistry B*, *109*(7), 2699-2702.

[13] **Campos, S., Denoyer, A., Jandl, S., Viana, B., Vivien, D., Loiseau, P., & Ferrand, B.** (2004). Spectroscopic studies of Yb^{3+}-doped rare earth orthosilicate crystals. *Journal of Physics: Condensed Matter*, *16*(25), 4579.

[14] **Sun, Z., Zhou, Y., & Li, M.** (2006). Low-temperature synthesis and sintering of γ-$Y_2Si_2O_7$. *Journal of Materials Research*, *21*(6), 1443-1450.

[15] **Shang, M., Li, C., & Lin, J.** (2014). How to produce white light in a single-phase host?. *Chemical Society Reviews*, *43*(5), 1372-1386.

[16] **Stefanski, M., Lukaszewicz, M., Hreniak, D., & Strek, W.** (2017). Broadband laser induced white emission observed from Nd^{3+} doped Sr_2CeO_4 nanocrystals. *Journal of Luminescence*, *192*, 243-249.

[17] **Bilir, G., Ozen, G., Collins, J., Cesaria, M., & Di Bartolo, B.** (2014). Unconventional Production of Bright White Light Emission by Nd-Doped and Nominally Un-Doped Y_2O_3 Nano-Powders. *IEEE Photonics Journal*, *6*(4), 1-17.

[18] **Cinkaya, H., Eryurek, G., & Di Bartolo, B.** (2018). White light emission based on both upconversion and thermal processes from Nd^{3+} doped yttrium silicate. *Ceramics International*, *44*(4), 3541-3547.

[19] **Eryurek, G., Cinkaya, H., Erdem, M., & Bilir, G.** (2016). Blue cooperative upconversion and white light emission from $Y_2Si_2O_7$: Yb^{3+} nanopowders due to 975-nm infrared excitation. *Journal of Nanophotonics*, *10*(2), 026022.

[20] **Erdem, M., Eryurek, G., & Di Bartolo, B.** (2015). Change of spectral output with pressure and white light generation in nanoscale Yb^{3+}: $Y_2Si_2O_7$. *Optical Materials*, *49*, 90-93.

[21] **Erdem, M., Erguzel, O., Ekmekci, M. K., Orucu, H., Cinkaya, H., Genc, S., Mergen, A., Eryurek, G., & Di Bartolo, B.** (2015). Bright white up-conversion emission from sol–gel derived $Yb^{3+}/Er^{3+}/Tm^{3+}$: Y_2SiO_5 nanocrystalline powders. *Ceramics International*, *41*(10), 12805-12810.

[22] **Xia, H., Lei, L., Xia, J., Hua, Y., Deng, D., & Xu, S.** (2019). Yb/Er/Tm tri-doped Na3ZrF7 upconversion nanocrystals for high performance temperature sensing. *Journal of Luminescence*, 209, 8-13.

[23] **Wang, J., Wang, F., Wang, C., Liu, Z., & Liu, X.** (2011). Single-band upconversion emission in lanthanide-doped $KMnF_3$ nanocrystals. *Angewandte Chemie International Edition*, *50*(44), 10369-10372.

[24] **Liu, P., Wang, F., Yang, B., & Chen, X. (2019).** Color-tunable and upconversion luminescence of Gd_2O_2S:Er, Tm phosphor: experimental investigations and first-principles calculation. *Applied Physics A*, *125*(1), 11.

[25] **Balda, R., Hömmerich, U., Nyein, E. E., Arriandiaga, M. A., & Fernández, J.** (2006). Spectroscopy and frequency upconversion in KPb_2Br_5: Nd^{3+} crystal. In *Optical Components and Materials III*, *6116*, 61160D. International Society for Optics and Photonics.

[26] **Lei, Y., Song, H., Yang, L., Yu, L., Liu, Z., Pan, G., & Fan, L.** (2005). Upconversion luminescence, intensity saturation effect, and thermal effect in Gd_2O_3:Er^{3+},Yb^{3+} nanowires. *The Journal of Chemical Physics*, *123*(17), 174710.

[27] **Marvin J. Weber** (2018). *Handbook of optical materials*. CRC Press, Berkeley, California.

[28] **Ronda, C. R.** (Ed.). (2007). *Luminescence: from theory to applications*. John Wiley & Sons.

[29] **Kitai, A. H.** (Ed.). (2012). *Solid state luminescence: Theory, materials and devices*. Springer Science & Business Media.

[30] **Xie, L., Wang, Y., & Zhang, H.** (2009). Near-infrared quantum cutting in YPO_4:Yb^{3+}, Tm^{3+} via cooperative energy transfer. *Applied Physics Letters*, *94*(6), 061905.

[31] **Montoya, E., Espeso, O., & Bausa, L. E.** (2000). Cooperative luminescence in Yb^{3+}: $LiNbO_3$. *Journal of Luminescence*, *87*, 1036-1038.

[32] **Wang, F., Deng, R., Wang, J., Wang, Q., Han, Y., Zhu, H., ... & Liu, X.** (2011). Tuning upconversion through energy migration in core–shell nanoparticles. *Nature Materials*, *10*(12), 968.

[33] **Nadort, A., Zhao, J., & Goldys, E. M.** (2016). Lanthanide upconversion luminescence at the nanoscale: fundamentals and optical properties. *Nanoscale*, *8*(27), 13099-13130.

[34] **Boyer, D., & Derby, B.** (2003). Yttrium silicate powders produced by the sol–gel method, structural and thermal characterization. *Journal of the American Ceramic Society*, *86*(9), 1595-1597.

[35] **Muresan, L. E., Popovici, E.J., Bica, E, Cadis, A.I., Morar, M., & Indrea E.** (2010). Spectroscopic and Structural characterization of SiO_2 -Y_2O_3 based materials with luminescent properties, *Studia Universitatis Babes-Bolyai, Chemia*, XLV, 2, Tom II.

[36] **Diaz, M., Pecharroman, C., Del Monte, F., Sanz, J., Iglesias, J. E., Moya, J. S., Yamagata, C., & Mello-Castanho, S.** (2005). Synthesis, thermal evolution, and luminescence properties of yttrium disilicate host matrix. *Chemistry of Materials*, *17*(7), 1774-1782.

[37] **Chambers, J. J., & Parsons, G. N.** (2001). Physical and electrical characterization of ultrathin yttrium silicate insulators on silicon. *Journal of Applied Physics*, *90*(2), 918-933.

[38] **Balda, R., Fernández, J., Arriandiaga, M. A., & Fernández-Navarro, J. M.** (2007). Spectroscopy and frequency upconversion in Nd^{3+}-doped TeO_2–TiO_2–Nb_2O_5glass. *Journal of Physics: Condensed Matter*, *19*(8), 086223.

[39] **Dieke, G. H., Crosswhite, H. M., & Crosswhite, H.** (1968). *Spectra and energy levels of rare earth ions in crystals*, New York: Interscience Publishers.

[40] **F Fan, H., Gao, G., Wang, G., Hu, J., & Hu, L.** (2010). Tm^{3+} doped Bi_2O_3–GeO_2–Na_2O glasses for 1.8 μm fluorescence. *Optical Materials*, *32*(5), 627-631.

[41] **Barua, P., Sekiya, E. H., Saito, K., & Ikushima, A. J.** (2008). Influences of Yb^{3+} ion concentration on the spectroscopic properties of silica glass. *Journal of Non-Crystalline Solids*, *354*(42-44), 4760-4764.

[42] **Bunzli, J. C. G., & Pecharsky, V. K.** (2016). *Handbook on the Physics and Chemistry of Rare Earths: Including Actinides* (Vol. 50). Elsevier.

[43] **Lucas, J., Lucas, P., Le Mercier, T., Rollat, A., & Davenport, W. G.** (2015). *Rare Earths Electronic Structures and Trends in Properties.* Elsevier BV.

[44] **de Bettencourt-Dias, A. (Ed.).** (2014). *Luminescence of lanthanide ions in coordination compounds and nanomaterials*. John Wiley & Sons.

[45] **Url-1** http://hyperphysics.phy-astr.gsu.edu/hbase/vision/cie.html#c2, accessed: 09.08.2019

[46] **Kaminskii, A. A.** (2013). *Laser crystals: Their physics and properties* (Vol. 14). Springer.

[47] **Thornton, W. A.** (1971). Luminosity and color-rendering capability of white light. *JOSA*, *61*(9), 1155-1163.

[48] **Sokolnicki, J.** (2011). Upconversion luminescence from Er^{3+} in nanocrystalline $Y_2Si_2O_7$: Er^{3+} and $Y_2Si_2O_7$: Yb^{3+}, Er^{3+} phosphors. *Materials Chemistry and Physics*, *131*(1-2), 306-312.

[49] **Cannas, C., Mainas, M., Musinu, A., Piccaluga, G., Enzo, S., Bazzoni, M & Bettinelli, M.** (2007). Structural investigations and luminescence properties of nanocrystalline europium-doped yttrium silicates prepared by a sol–gel technique. *Optical Materials*, *29*(6), 585-592.

[50] **Scherer, P.** (1918). Bestimmung der inneren Struktur und der Größe von Kolloidteilchen mittels Röntgenstrahlen, *Nachrichten von der Gesellschaft der Wissenschaften zu Göttingen, Mathematisch-Physikalische Klasse, 1918*, 98-100.

[51] **Azumi, T., Gray, H. B., Humbs, W., Miki, H., Patterson, H. H., Miskowski, V. M., ... & Strasser, J.** (1997). *Electronic and vibronic spectra of transition metal complexes II* (Vol. 2). Springer Science & Business Media.

[52] **Ganem, J., & Bowman, S. R.** (2013). Use of thulium-sensitized rare earth-doped low phonon energy crystalline hosts for IR sources. *Nanoscale Research Letters*, *8*(1), 455.

[53] **Kahlenberg, V., Wertl, W., Többens, D. M., Kaindl, R., Schuster, P., & Schottenberger, H.** (2008). Rietveld Analysis and Raman Spectroscopic Investigations on α-$Y_2Si_2O_7$. *Zeitschrift für Anorganische und Allgemeine Chemie*, *634*(6-7), 1166-1172.

[54] **Muresan, L., Cadis, A., Perhaita, I., & Indrea, E.** (2014). Morpho-structural and luminescence investigations on yttrium silicate based phosphors prepared with different precipitating agents. *Open Chemistry*, *12*(10), 1023-1031.

[55] **Hofmeister, A. M., & Chopelas, A.** (1991). Vibrational spectroscopy of end-member silicate garnets. *Physics and Chemistry of Minerals*, *17*(6), 503-526.

[56] **Venyaminov, S. Y., & Prendergast, F. G.** (1997). Water (H2O and D2O) Molar Absorptivity in the 1000–4000 cm^{-1} Range and Quantitative Infrared Spectroscopy of Aqueous Solutions. *Analytical Biochemistry*, *248*(2), 234-245.

[57] **Cinkaya, H., Eryurek, G., & Di Bartolo, B.** (2019). The anomalous luminescent behaviors of the Nd^{3+}/Yb^{3+} co-doped yttrium silicate at different physical conditions. *Laser Physics*, *29*(6), 065701.

[58] **Cinkaya, H., Eryurek, G., Bilir, G., Erdem, M., & Di Bartolo, B.** (2017). Effect of pressure and temperature on the white light produced by Ytterbium (III) doped and undoped Yttrium Silicate nanopowders excited by a laser diode. *Journal of Luminescence*, *181*, 321-326.

[59] **Tabanli, S., Yilmaz, H. C., Bilir, G., Erdem, M., Eryurek, G., Di Bartolo, B., & Collins, J.** (2018). Broadband, white light emission from doped and undoped insulators. *ECS Journal of Solid State Science and Technology*, *7*(1), R3199-R3210.

[60] **Singh, A. K., Singh, S., Kumar, D., Rai, D. K., Rai, S. B., & Kumar, K.** (2012). Light-into-heat conversion in La_2O_3: Er^{3+}-Yb^{3+} phosphor: an incandescent emission. *Optics Letters*, *37*(5), 776-778.

[61] **Cinkaya, H., Eryurek, G., Bilir, G., Collins, J., & Di Bartolo, B.** (2017). Spectral characterization and white light generation by yttrium silicate nanopowders undoped and doped with Ytterbium (III) at different concentrations when excited by a laser diode at 975 nm. *Optical Materials*, *63*, 167-172.

[62] **Zhang, Z., Yu, C., Liu, L., Li, H., He, Y., Lü, X. & Jones, R. A.** (2016). Efficient near-infrared (NIR) luminescent PMMA-supported hybrid materials doped with tris-β-diketonate Ln^{3+} complex (Ln= Nd or Yb). *Journal of Photochemistry and Photobiology A: Chemistry*, *314*, 104-113.

[63] **Balda, R., Fernändez, J., Nyein, E. E., & Hömmerich, U.** (2006). Infrared to visible upconversion of Nd^{3+} ions in KPb_2Br_5 low phonon crystal. *Optics Express*, *14*(9), 3993-4004.

[64] **Elan, F., Falcão-Filho, E. L., Camilo, M. E., Garcia, J. A., Kassab, L. R., & de Araújo, C. B.** (2016). Upconversion photoluminescence in GeO_2-PbO glass codoped with Nd^{3+} and Yb^{3+}. *Optical Materials*, *60*, 313-317.

[65] **Nadaraia, L., Jalabadze, N., Chedia, R., Kukava, T., Mikeladze, A., & Khundadze, L.** (2009). Problems of manufacturing nanocrystalline yttrium silicate materials. *IEEE Transactions on Nuclear Science*, *56*(3), 972-976.

[66] **Qin, X., Ju, Y., Bernhard, S., & Yao, N.** (2007). Europium-doped yttrium silicate nanophosphors prepared by flame synthesis. *Materials research bulletin*, *42*(8), 1440-1449.

[67] **Hill, R. J. (1983).** Calculated X-ray powder diffraction data for phases encountered in lead/acid battery plates. *Journal of Power Sources*, *9*(1), 55-71.

[68] **Al-Jaroudi, S. S., Ul-Hamid, A., Mohammed, A. R. I., & Saner, S.** (2007). Use of X-ray powder diffraction for quantitative analysis of carbonate rock reservoir samples. *Powder Technology*, *175*(3), 115-121.

[69] **Sun, Z., Li, M., & Zhou, Y.** (2009). Thermal properties of single-phase Y_2SiO_5. *Journal of the European Ceramic Society*, *29*(4), 551-557.

[70] **Bilir, G., Kaya, A., Cinkaya, H., & Eryürek, G.** (2016). Spectroscopic investigation of zinc tellurite glasses doped with Yb^{3+} and Er^{3+} ions. *Spectrochimica Acta Part A: Molecular and Biomolecular Spectroscopy*, *165*, 183-190.

[71] **Chen, G. Y., Liang, H. J., Liu, H. C., Somesfalean, G., & Zhang, Z. G.** (2009). Anomalous power dependence of upconversion emissions in Gd_2O_3:Er^{3+} nanocrystals under diode laser excitation of 970 nm. *Journal of Applied Physics*, *105*(11), 114315.

[72] **Sivakumar, S., van Veggel, F. C. M., & May, P. S.** (2007). Near Infrared (NIR) to Red and Green Up-Conversion Emission from Silica Sol− Gel Thin Films Made with $La_{0.45}Yb_{0.50}Er_{0.05}F_3$ Nanoparticles, Hetero-Looping-Enhanced Energy Transfer (Hetero-LEET): A New Up-Conversion Process. *Journal of the American Chemical Society*, *129*(3), 620-625.

[73] **Silver, J., Martinez-Rubio, M. I., Ireland, T. G., Fern, G. R., & Withnall, R.** (2001). The effect of particle morphology and crystallite size on the upconversion luminescence properties of erbium and ytterbium co-doped yttrium oxide phosphors. *The Journal of Physical Chemistry B*, *105*(5), 948-953.

[74] **Zhu, Y., Cui, S., Liu, M., Liu, X., Lu, C., Xu, X., & Xu, W.** (2015). Observation of upconversion white light and ultrabroad infrared emission in YbAG: Ln^{3+} (Ln= Nd, Sm, Tb, Er). *Applied Physics Express*, *8*(7), 072602.

[75] **Zheng, J., Wang, X. F., He, W. Y., Bu, Y. Y., & Yan, X. H.** (2014). Seven-photon ultraviolet upconversion emission of Er^{3+} induced by 1,540-nm laser excitation. *Applied Physics B*, *115*(4), 443-449.

[76] **Rathaiah, M., Martín, I. R., Babu, P., Linganna, K., Jayasankar, C. K., Lavín, V., & Venkatramu, V.** (2015). Photon avalanche upconversion in Ho^{3+}-doped gallium nano-garnets. *Optical Materials, 39*, 16-20.

[77] **Wang, B., Zhan, Q., Zhao, Y., Wu, R., Liu, J., & He, S.** (2016). Visible-to-visible four-photon ultrahigh resolution microscopic imaging with 730-nm diode laser excited nanocrystals. *Optics Express*, *24*(2), A302-A311.

[78] **Maciel, G. S., & Rakov, N.** (2013). Anomalous up-conversion dynamics in rare earth doped yttrium oxide powders. *Journal of Materials Chemistry C*, *1*(22), 3563-3568.

[79] **Wang, J., Hao, J. H., & Tanner, P. A.** (2015). Persistent luminescence upconversion for Er_2O_3 under 975 nm excitation in vacuum. *Journal of Luminescence*, *164*, 116-122.

[80] **Ju, G., Hu, Y., Chen, L., & Wang, X.** (2012). Persistent luminescence and its mechanism of Ba_5 $(PO_4)_3$ Cl: Ce^{3+}, Eu^{2+}. *Journal of Applied Physics*, *111*(11), 113508.

[81] **Wang, J., Hao, J. H., & Tanner, P. A.** (2011). Upconversion luminescence of an insulator involving a band-to-band multiphoton excitation process. *Optics Express*, *19*(12), 11753-11758.

[82] **Wang, J., & Tanner, P. A.** (2009). Upconversion for white light generation by a single compound. *Journal of the American Chemical Society*, *132*(3), 947-949.

[83] **Antic-Fidancev, E., Hölsä, J., Lastusaari, M., & Lupei, A.** (2001). Dopant-host relationships in rare-earth oxides and garnets doped with trivalent rare-earth ions. *Physical Review B, 64*(19), 195108.

[84] **Hölsä, J., Antic-Fidancev, E., Lastusaari, M., & Lupei, A.** (2003). Local perturbations due to rare earth (R^{3+}) doping. *Journal of Solid State Chemistry*, *171*(1-2), 282-286.

[85] **Hua, H., & Vohra, Y. K.** (1997). Pressure-induced blueshift of Nd^{3+} fluorescence emission in $YAlO_3$: Near infrared pressure sensor. *Applied Physics Letters*, *71*(18), 2602-2604.

[86] **Bungenstock, C., Tröster, T., & Holzapfel, W. B.** (2000). Effect of pressure on free-ion and crystal-field parameters of Pr^{3+} in LOCl (L= L a, P r, Gd). *Physical Review B, 62*(12), 7945.

[87] **Hollis, D. B., Cruickshank, F. R., & Payne, M. J. P.** (2001). Structural influence of tellurite glasses on fluorescence of thulium near 1.86 μm. *Journal of Non-crystalline Solids, 293*, 422-429.

[88] **Braud, A., Tigreat, P. Y., Doualan, J. L., & Moncorgé, R.** (2001). Spectroscopy and cw operation of a 1.85 μm Tm: KY_3F_{10} laser. *Applied Physics B, 72*(8), 909-912.

[89] **Poirier, G., Jerez, V. A., de Araújo, C. B., Messaddeq, Y., Ribeiro, S. J., & Poulain, M.** (2003). Optical spectroscopy and frequency upconversion properties of Tm^{3+} doped tungstate fluorophosphate glasses. *Journal of Applied Physics, 93*(3), 1493-1497.

[90] **Poirier, G., Cassanjes, F. C., de Araújo, C. B., Jerez, V. A., Ribeiro, S. J., Messaddeq, Y., & Poulain, M.** (2003). Optical properties and frequency upconversion fluorescence in a Tm^{3+}-doped alkali niobium tellurite glass. *Journal of Applied Physics, 93*(6), 3259-3263.

[91] **Kir'yanov, A. V., Barmenkov, Y. O., Martinez, I. L., Kurkov, A. S., & Dianov, E. M.** (2006). Cooperative luminescence and absorption in Ytterbium-doped silica fiber and the fiber nonlinear transmission coefficient at λ= 980 nm with a regard to the Ytterbium ion-pairs' effect. *Optics Express, 14*(9), 3981-3992.

[92] **Hreniak, D., Strek, W., Opalińska, A., Nyk, M., Wołcyrz, M., Lojkowski, W., & Misiewicz, J.** (2004). Luminescence Properties of Tb-Doped Yttrium Disilicate Prepared by the Sol–Gel Method. *Journal of Sol-gel Science and Technology, 32*(1-3), 195-200.

[93] **Rakov, N., & Maciel, G. S.** (2016). An efficient energy transfer process in Nd^{3+}: Yb^{3+} co-doped SrF_2 powders containing A^{l3+} and prepared by the combustion synthesis technique. *Journal of Materials Chemistry C, 4*(23), 5442-5447.

[94] **Balda, R., Fernández, J., Iparraguirre, I., & Al-Saleh, M.** (2006). Spectroscopic study of Nd^{3+}/Yb^{3+} in disordered potassium bismuth molybdate laser crystals. *Optical Materials, 28*(11), 1247-1252.

[95] **Shannon, R. D.** (1976). Revised effective ionic radii and systematic studies of interatomie distances in halides and chaleogenides. *Acta Crystallogr. A, 32*(5), 751-767.

[96] **Marciniak, L., Hreniak, D., Strek, W., Piccinelli, F., Speghini, A., Bettinelli, M., & Priolo, F.** (2016). Spectroscopic and structural properties of polycrystalline $Y_2Si_2O_7$ doped with Er^{3+}. *Journal of Luminescence, 170*, 614-618.

[97] **Sivakumar, S., Boyer, J. C., Bovero, E., & van Veggel, F. C.** (2009). Up-conversion of 980 nm light into white light from sol-gel derived thin film made with new combinations of LaF_3: Ln^{3+} nanoparticles. *Journal of Materials Chemistry, 19*(16), 2392-2399.

[98] **Marciniak, L., Stefanski, M., Tomala, R., Hreniak, D., & Strek, W.** (2015). Synthesis and up-conversion luminescence of Er^{3+} and Yb^{3+} codoped nanocrystalline tetra-($KLaP_4O_{12}$) and pentaphosphates (LaP_5O_{14}). *The Journal of Chemical Physics, 143*(9), 094701.

[99] **Pollnau, M., Gamelin, D. R., Lüthi, S. R., Güdel, H. U., & Hehlen, M. P.** (2000). Power dependence of upconversion luminescence in lanthanide and transition-metal-ion systems. *Physical Review B, 61*(5), 3337.

[100] **Suyver, J. F., Aebischer, A., García-Revilla, S., Gerner, P., & Güdel, H. U.** (2005). Anomalous power dependence of sensitized upconversion luminescence. *Physical Review B, 71*(12), 125123.

[101] **Wang, Y. F., Liu, G. Y., Sun, L. D., Xiao, J. W., Zhou, J. C., & Yan, C. H.** (2013). Nd^{3+}-sensitized upconversion nanophosphors: efficient in vivo bioimaging probes with minimized heating effect. *ACS nano, 7*(8), 7200-7206.

[102] **Chen, P., Zhang, J., Xu, B., Sang, X., Chen, W., Liu, X. & Qiu, J.** (2014). Lanthanide doped nanoparticles as remote sensors for magnetic fields. *Nanoscale, 6*(19), 11002-11006.

[103] **Kumar, P., Dwivedi, J., & Gupta, B. K.** (2014). Highly luminescent dual mode rare-earth nanorod assisted multi-stage excitable security ink for anti-counterfeiting applications. *Journal of Materials Chemistry C, 2*(48), 10468-10475.

[104] **Yang, D., Hou, Z., Cheng, Z., Li, C., & Lin, J.** (2015). Current advances in lanthanide ion (Ln^{3+})-based upconversion nanomaterials for drug delivery. *Chemical Society Reviews, 44*(6), 1416-1448.

[105] **Chen, D., Wang, Y., Yu, Y., & Huang, P.** (2007). Intense ultraviolet upconversion luminescence from Tm^{3+}/ Yb^{3+}: β-YF_3 nanocrystals embedded glass ceramic. *Applied Physics Letters, 91*(5), 051920.

[106] **Rakov, N., & Maciel, G. S.** (2011). Blue shift of Tm^{3+} upconversion owing to Nd^{3+} in yttrium oxide powders pumped by pulsed red laser. *Chemical Physics Letters, 503*(1-3), 124-128.

[107] **Rakov, N., Gómez, L. A., Rátiva, D. J., & Maciel, G. S.** (2009). Blue upconversion emission from Tm^{3+} sensitized by Nd^{3+} in aluminum oxide crystalline ceramic powders. *Applied Physics B, 94*(2), 199-202.

[108] **Richards, B., Shen, S., & Jha, A.** (2006). Emission spectroscopy and energy transfer in Tm^{3+}, Tm^{3+}-Ho^{3+}, and Tm^{3+}-Yb^{3+} doped tellurite fibers. In *Lidar Technologies, Techniques, and Measurements for Atmospheric Remote Sensing II* (Vol. 6367, p. 63670G). International Society for Optics and Photonics.

[109] **Fan, W., Chen, S., Htein, L., & Han, W. T.** (2015). Enhanced broadband upconversion emission and 23 dB optical gain at 780 nm in Tm^{3+}/Nd^{3+} codoped optical fiber. *Journal of Luminescence, 162*, 164-167.

[110] **Peterka, P., Kasik, I., Dhar, A., Dussardier, B., & Blanc, W.** (2011). Theoretical modeling of fiber laser at 810 nm based on thulium-doped silica fibers with enhanced $^3H_4$ level lifetime. *Optics Express, 19*(3), 2773-2781.

[111] **Rapaport, A., Milliez, J., Bass, M., Cassanho, A., & Jenssen, H.** (2005). Numerical model of the temperature dependence of the up-conversion efficiency of fluoride crystals codoped with ytterbium and thulium. *Journal of Applied Physics, 97*(12), 123527.

[112] **Zhang, Q., Chen, G., Zhang, G., Qiu, J., & Chen, D.** (2010). Infrared luminescence of Tm^{3+}/Yb^{3+} codoped lanthanum aluminum germanate glasses. *Journal of Applied Physics, 107*(2), 023102.

[113] **Özen, G., Denis, J. P., Goldner, P., Wu, X., Genotelle, M., & Pellé, F.** (1993). Enhanced Tm^{3+} blue emission in Tm, Yb, co-doped fluorophosphate glasses due to back energy transfer processes. *Applied Physics Letters, 62*(9), 928-930.

[114] **Grzyb, T., & Tymiński, A.** (2016). Up-conversion luminescence of GdOF: Yb^{3+}, Ln^{3+} (Ln= Ho, Tm, Er) nanocrystals. *Journal of Alloys and Compounds, 660*, 235-243.

[115] **Pandey, A., Rai, V. K., Kumar, V., Kumar, V., & Swart, H. C.** (2015). Upconversion based temperature-sensing ability of Er^{3+}–Yb^{3+} codoped SrWO4: An optical heating phosphor. *Sensors and Actuators B: Chemical*, *209*, 352-358.

[116] **Song, H., Wang, C., Han, Q., Tang, X., Yan, W., Chen, Y., & Liu, T.** (2018). Highly sensitive Tm^{3+}/Yb^{3+} codoped $SrWO_4$ for optical thermometry. *Sensors and Actuators A: Physical*, *271*, 278-282.

[117] **Vetrone, F., Mahalingam, V., & Capobianco, J. A.** (2009). Near-infrared-to-blue upconversion in colloidal $BaYF_5$: Tm^{3+}, Yb^{3+} nanocrystals. *Chemistry of Materials*, *21*(9), 1847-1851.

[118] **Shen, J., Chen, G., Vu, A. M., Fan, W., Bilsel, O. S., Chang, C. C., & Han, G.** (2013). Engineering the upconversion nanoparticle excitation wavelength: cascade sensitization of tri-doped upconversion colloidal nanoparticles at 800 nm. *Advanced Optical Materials*, *1*(9), 644-650.

[119] **Zmojda, J., Kochanowicz, M., Miluski, P., Righini, G. C., Ferrari, M., & Dorosz, D.** (2016). Investigation of upconversion luminescence in Yb^{3+}/Tm^{3+}/Ho^{3+} triply doped antimony-germanate glass and double-clad optical fiber. *Optical Materials*, *58*, 279-284.

[120] **Chen, D., Wang, Y., Yu, Y., Liu, F., & Huang, P.** (2007). Sensitized thulium ultraviolet upconversion luminescence in Tm^{3+}/Yb^{3+}/Nd^{3+} triply doped nanoglass ceramics. *Optics Letters*, *32*(21), 3068-3070.

[121] **Gouveia-Neto, A. S., Da Costa, E. B., Dos Santos, P. V., Bueno, L. A., & Ribeiro, S. J. L.** (2003). Sensitized thulium blue upconversion emission in Nd^{3+}/Tm^{3+}/Yb^{3+} triply doped lead and cadmium germanate glass excited around 800 nm. *Journal of Applied Physics*, *94*(9), 5678-5681.

[122] **Courrol, L. C., Ranieri, I. M., Tarelho, L. V. G., Baldochi, S. L., Gomes, L., & Júnior, N. D. V.** (2005). Enhancement of blue upconversion mechanism in $YLiF_4$: Yb: Tm: Nd crystals. *Journal of Applied Physics*, *98*(11), 113504.

[123] **Courrol, L. C., Ranieri, I. M., Tarelho, L. V., Baldochi, S. L., Gomes, L., & Vieira Jr, N. D.** (2007). Study of optical properties of YLF: Nd: Yb: Tm crystals. *Journal of Luminescence*, *122*, 474-477.

[124] **Liu, S., Liu, S., Ming, H., Du, F., Peng, J., You, W., & Ye, X.** (2018). Tunable multicolor and bright white upconversion luminescence in Er^{3+}/Tm^{3+}/Yb^{3+} tri-doped SrLu2O4 phosphors. *Journal of Materials Science*, *53*(20), 14469-14484.

[125] **Zhang, C., Ma, P. A., Li, C., Li, G., Huang, S., Yang, D. & Lin, J.** (2011). Controllable and white upconversion luminescence in BaYF5: Ln^{3+} (Ln= Yb, Er, Tm) nanocrystals. *Journal of Materials Chemistry*, *21*(3), 717-723.

[126] **Li, Y., Zhang, J., Luo, Y., Zhang, X., Hao, Z., & Wang, X.** (2011). Color control and white light generation of upconversion luminescence by operating dopant concentrations and pump densities in Yb^{3+}, Er^{3+} and

Tm^{3+} tri-doped Lu_2O_3 nanocrystals. *Journal of Materials Chemistry*, *21*(9), 2895-2900.

[127] **Giri, N. K., Mishra, K., & Rai, S. B.** (2011). Upconversion based tunable white-light generation in Ln: Y_2O_3 nanocrystalline phosphor (Ln= Tm/Er/Yb). *Journal of Fluorescence*, *21*(5), 1951.

[128] **Maciel, G. S., & Rakov, N.** (2015). Photon conversion in lanthanide-doped powder phosphors: concepts and applications. *RSC Advances*, *5*(22), 17283-17295.

[129] **Da Silva, J. E. C., de Sa, G. F., & Santa-Cruz, P. A.** (2002). White light simulation by up-conversion in fluoride glass host. *Journal of Alloys and Compounds*, *344*(1-2), 260-263.

[130] **Ki, W., & Li, J.** (2008). A semiconductor bulk material that emits direct white light. *Journal of the American Chemical Society*, *130*(26), 8114-8115.

[131] **Chen, D., Wang, Y., Zheng, K., Guo, T., Yu, Y., & Huang, P.** (2007). Bright upconversion white light emission in transparent glass ceramic embedding Tm^{3+}/ Er^{3+}/ Yb^{3+}: β-YF_3 nanocrystals. *Applied Physics Letters*, *91*(25), 251903.

[132] **Wang, J., Hao, J. H., & Tanner, P. A.** (2010). Luminous and tunable white-light upconversion for YAG ($Yb_3Al_5O_{12}$) and (Yb, Y)$_2O_3$ nanopowders. *Optics Letters*, *35*(23), 3922-3924.

[133] **Strek, W., Marciniak, L., Gluchowski, P., & Hreniak, D.** (2013). Infrared laser stimulated broadband white emission of Yb^{3+}: YAG nanoceramics. *Optical Materials*, *35*(11).

[134] **Xu, X., Zhao, Z., Song, P., Jiang, B., Zhou, G., Xu, J., & Fulop, A.** (2005). Upconversion luminescence in Yb^{3+}-doped yttrium aluminum garnets. *Physica B: Condensed Matter*, *357*(3-4), 365-369.

[135] **Xiao, K., & Yang, Z.** (2006). Blue Cooperative Luminescence in Yb^{3+}-Doped Barium Gallogermanate Glass Excited at 976 nm. *Journal of Fluorescence*, *16*(6), 755-759.

[136] **Zhang, R., Lin, H., Yu, Y., Chen, D., Xu, J., & Wang, Y.** (2014). A new-generation color converter for high-power white LED: transparent Ce^{3+}: YAG phosphor-in-glass. *Laser & Photonics Reviews*, *8*(1), 158-164.

[137] **Zhu, S., Wang, C., Li, Z., Jiang, W., Wang, Y., Yin, H., & Zhang, G.** (2016). High-efficiency broadband anti-Stokes emission from Yb^{3+}-doped bulk crystals. *Optics Letters*, *41*(10), 2141-2144.

[138] **Zhou, S., Deng, K., Wei, X., Jiang, G., Duan, C., Chen, Y., & Yin, M.** (2013). Upconversion luminescence of $NaYF_4$: Yb^{3+}, Er^{3+} for temperature sensing. *Optics Communications*, *291*, 138-142.

[139] **Chen, J., Zhao, W., Wang, N., Meng, Y., Yi, S., He, J., & Zhang, X.** (2016). Energy transfer properties and temperature-dependent luminescence of $Ca_{14}Al_{10}Zn_6O_{35}$: Dy^{3+}, Mn^{4+} phosphors. *Journal of Materials Science*, *51*(9), 4201-4212.

[140] **Stefanski, M., Marciniak, L., Hreniak, D., & Strek, W.** (2016). Size and temperature dependence of optical properties of Eu^{3+}: Sr_2CeO_4

nanocrystals for their application in luminescence thermometry. *Materials Research Bulletin, 76,* 133-139.

[141] **Xu, Q., Li, Z., Wang, Y., & Li, H.** (2016). Temperature-dependent luminescence properties of lanthanide (III) β-diketonate complex-doped LAPONITE®. *Photochemical & Photobiological Sciences, 15*(3), 405-411.

[142] **Kim, J. S., Park, Y. H., Kim, S. M., Choi, J. C., & Park, H. L.** (2005). Temperature-dependent emission spectra of $M_2SiO_4:Eu^{2+}$ (M= Ca, Sr, Ba) phosphors for green and greenish white LEDs. *Solid-State Communications, 133*(7), 445-448.

[143] **Hsu, D., Skinner, J. L.** (1984). Nonperturbativetheoryof temperature-dependent optical dephasing in crystals. I.Acoustic or optical phonons. *The Journal of Chemical Physics, 81*(12), 5471-5479.

[144] **Mikhailik, V. B., Kraus, H., Wahl, D., Itoh, M., Koike, M., & Bailiff, I. K.** (2004). One-and two-photon excited luminescence and band-gap assignment in $CaWO_4$. *Physical Review B, 69*(20), 205110.

[145] **Van der Kolk, E., Dorenbos, P., De Haas, J. T. M., & Van Eijk, C. W. E.** (2005). Thermally stimulated electron delocalization and luminescence quenching of Ce impurities in $GdAlO_3$. *Physical Review B, 71*(4), 045121.

[146] **Shao, Q., Wang, L., Song, L., Dong, Y., Liang, C., He, J., & Jiang, J.** (2017). Temperature dependence of photoluminescence spectra and dynamics of the red-emitting K_2SiF_6: Mn^{4+} phosphor. *Journal of Alloys and Compounds, 695,* 221-226.

[147] **Shionoya, S., Yen, W. M., & Yamamoto, H. (Eds.).** (2018). Phosphor handbook. CRC press.

CURRICULUM VITAE

Name Surname **:** Hatun ÇINKAYA YILMAZ

Place and Date of Birth **:** Istanbul/ Beyoglu, 18.02.1982

E-Mail **:** cinkayahatun@itu.edu.tr
hatun.yilmaz@tubitak.gov.tr
hatuncinkaya@gmail.com

EDUCATION:

- **B.Sc.:** 2007, Izmir Institute of Technology, Faculty of Science, Department of Physics
- **M.Sc.:** 2011, Istanbul Technical University, Faculty of Science and Letters, Department of Physics Enginnering

PROFESSIONAL EXPERIENCE AND REWARDS:

- June 2019- cont. Senior Researcher at Tübitak-Bilgem
- February 2010- June 2019 Research Assistant at Istanbul Technical University, Department of Physics Engineering
- December 2015- December 2016 Visiting Scholar at Boston College, Department of Physics, Lab of Spectroscopy, Massachusetts, USA (TÜBİTAK 2214A)
- KOÇ Foundation- Education Fellowship (2012-2013 Academic year)
- TÜBİTAK 1002-Production and Characterization of White Light Based on Energy Upconversion Mechanisms in Yb^{3+}, Nd^{3+}, Tm^{3+} Rare Earth Ions Doped Y_2O_3-SiO_2 Nanophosphor Materials,
- İTÜ- BAP Project for PhD thesis- 'Yb^{+3}, Nd^{+3}, Tm^{+3} Nadir Toprak İyon Katkılı Nanofosfor Malzemelerde Üst Dönüşüm Mekanizmasına Dayalı Beyaz Işık Üretimi ve Karakterizasyonu'.
- Graduation from Izmir Institute of Technology with Honour Degree in B.S., Department of Physics, with the Highest Third Mark (Izmir Institute of Technology, Physics Department -2007).

PUBLICATIONS, PRESENTATIONS AND PATENTS ON THE THESIS:

ARTICLES:

- **Cinkaya, H.**, Eryurek, G., Di Bartolo, B. 2019. The anomalous luminescent behaviors of the Nd^{3+}/Yb^{3+} co-doped yttrium silicate at different physical conditions, *Laser Physics*, 29(6), 065701.
- Tabanli, S., **Yilmaz, H. C.**, Bilir, G., Erdem, M., Eryurek, G., Di Bartolo, B., Collins, J. 2018. Broadband, white light emission from doped and undoped insulators, *ECS Journal of Solid State Science and Technology*, 7(1), R3199-R3210.
- **Cinkaya, H.**, Eryurek, G., Di Bartolo, B. 2018. White light emission based on both upconversion and thermal processes from Nd^{3+} doped yttrium silicate, *Ceramics International*, 44(4), 3541-3547.
- **Cinkaya, H.**, Eryurek, G., Bilir, G., Collins, J., Di Bartolo, B. 2017. Spectral characterization and white light generation by yttrium silicate nanopowders undoped and doped with Ytterbium (III) at different concentrations when excited by a laser diode at 975 nm, *Optical Materials*, 63, 167-172.
- **Cinkaya, H.**, Eryurek, G., Bilir, G., Erdem, M., Di Bartolo, B. 2017. Effect of pressure and temperature on the white light produced by Ytterbium (III) doped and undoped Yttrium Silicate nanopowders excited by a laser diode, *Journal of Luminescence*, 181, 321-326.
- Eryurek, G., **Cinkaya, H.**, Erdem, M., Bilir, G. 2016. Blue cooperative upconversion and white light emission from $Y_2Si_2O_7:Yb^{3+}$ nanopowders due to 975-nm infrared excitation, *Journal of Nanophotonics*, 10(2), 026022.

FULL ARTICLE IN BOOK SERIES

- **Cinkaya, H.**, Bilir, G., Erdem, M., & Eryurek, G. 2017: Investigation of the Luminescence Spectral Profiles and the Efficiencies of Yb^{3+}, Nd^{3+}, Tm^{3+} Doped Y_2O_3-SiO_2 Nano-phosphors. *Nano-Optics: Principles Enabling Basic Research and Applications* (pp. 441-444). Springer, Dordrecht.

PROCEEDINGS

- **Cinkaya, H.**, Eryurek, G., Di Bartolo, B. 2016. Upconversion and White Light Generation Properties of Undoped and Yb^{3+} doped Yttrium Silicate Nano-Phosphors, *18th Annual Nanotech Conference& Expo- NanoTech 2016, Advanced Materials TechConnect Briefs 2016, Advanced Manufacturing, Electronics and Microsystems, Photonic Materials & Devices* Chapter 7, pp. 255-259.
- **Cinkaya, H.**, Eryurek, G., & Di Bartolo, B. 2018. Luminescence properties of Nd^{3+}/Yb^{3+} codoped yttrium silicate nanophosphors excited by at laser diode of 975 nm, *AIP Conference Proceedings* (Vol. 1935, No. 1, p. 120003). AIP Publishing.
- **Cinkaya, H.**, Eryurek, G., Di Bartolo, B. 2017. Upconversion white Light Luminescence from $Yb^{3+}/Nd^{3+}/Tm^{3+}$ Triple doped Yttrium Silicate

Nanophosphor, *International Porous and Powder Materials Symposium and Exhibition- PPM2017 Proceedings book*, page 285-289.

PRESENTATIONS

- **Cinkaya, H.**, Eryurek, G., Di Bartolo, B. 2017: Nd^{3+}/Yb^{3+} Katkılı Itriyum Silikat Nanofosfor Malzemelerin Luminesans Özellikleri. FOTONIK 2017,19. Ulusal Optik, Elektro-Optik ve Fotonik Çalıştayı, September 29, 2017 Koç University, İstanbul, Turkey.
- **Cinkaya, H.**, Eryurek, G., Di Bartolo, B. 2017: White light production from Nd^{3+} doped Yttrium Silicate Nanophosphor. Turkish Physical Society 33rd International Physics Congress-TPS33, September 6-10, 2017 Bodrum, Turkey.
- **Cinkaya, H.**, Eryurek, G., Di Bartolo B. 2017: Luminsecence properties of Nd^{3+}/Yb^{3+} codoped yttrium silicate nanophosphors excited by at a laser diode of 975 nm. Turkish Physical Society 33rd International Physics Congress-TPS33, September 6-10, 2017 Bodrum, Turkey.
- **Cinkaya**, **H.,** Eryurek, G., Di Bartolo, B. 2017: Temperature dependent luminescence Properties of Undoped Yttrium Silicate Nanopowder. Porous Powders Materials 2017- PPM2017, September 12-15, 2017 Kuşadası, Turkey.
- **Cinkaya**, **H.,** Eryurek, G., Di Bartolo, B. 2017: Upconversion white Light Luminescence from $Yb^{3+}/Nd^{3+}/Tm^{3+}$ Triple doped Yttrium Silicate Nanophosphor. Porous Powders Materials 2017-PPM2017, September 12-15, 2017 Kuşadası, Turkey.
- **Cinkaya, H.**, Eryurek, G., Erdem, M., Di Bartolo, B. 2017: Synthesis and Luminescence Properties of Thulium(III) doped and Thulium (III)/ Neodymium(III) codoped Yttrium Silicate Nanophosphors. Porous Powders Materials 2017-PPM2017, September 12-15, 2017 Kuşadası, Turkey.
- **Cinkaya**, **H.,** Eryurek, G., Di Bartolo, B. 2016: Upconversion and White Light Generation Properties of Undoped and Yb^{3+} doped Yttrium Silicate Nano-Phosphors. Tech Connect World Innovation 2016, May 2016 Washington DC. U.S.A.
- **Cinkaya**, **H.,** Eryurek, G., Kelly, C., Bilir, G., Erdem, M., Collins, J., Di Bartolo, B. 2016: On the pressure dependence of white light emitted by NIR-excited Ytterbium(III) -doped Yttrium Silicate nanopowders. American Physical Society (APS) New England Section Spring meeting, April 1, 2016 Wheaton College, Massachusetts U.S.A.
- **Cinkaya**, **H.,** Eryurek, G., Bilir, G., Collins, J., Di Bartolo, B. 2016: Properties of White Light generated by near infrared excitation of Yttrium silicates undoped and doped with Ytterbium. American Physical Society (APS) New England Section Spring meeting, April 2, 2016 Wheaton College, Massachusetts, U.S.A.
- **Cinkaya**, **H.,** Bilir, G., Erdem, M., Eryurek, G. 2015: Investigation of the Luminescence spectral profiles and the efficiencies of Yb^{3+}, Nd^{3+}, Tm^{3+} doped Y_2O_3-SiO_2 nano-phosphors. Ettore Majorana Foundation and Centre for Scientific Culture, International School of Atomic and Molecular

Spectroscopy, Nano-Optics: Principles Enabling Basic Research and Applications, NATO Advanced Study Institute, July 2015 Erice, Sicily, ITALY.

OTHER PUBLICATIONS, PRESENTATIONS AND PATENTS:

PUBLICATIONS

- Bilir, G., Kaya, A., **Cinkaya**, **H.,** G. Eryurek. 2016. Spectroscopic investigation of zinc tellurite glasses doped with Yb^{3+} and Er^{3+}ions, *Spectrochimica Acta Part A: Molecular and Biomolecular Spectroscopy*, 165, 183–190.
- Erdem, M., Erguzel, O., Ekmekci, M.K., Orucu, H., **Cinkaya**, **H.,** Genc, S., Mergen, A., Eryurek, G., Di Bartolo, B. 2015. Bright white up-conversion emission from sol – gel derived Yb^{3+} /Er^{3+}/Tm^{3+}: Y_2SiO_5 nanocrystalline powders', *Ceramics International*, 41, 12805-12810.
- **Cinkaya, H.** 2011. Hidrojen Bağlı Termotropik Yan Zincirli Sıvı Kristalik Polimerlerin Dielektrik Spektroskopisi, MSc thesis, Department of Physics Engineering, Istanbul Technical University, Istanbul, Turkey.

PRESENTATIONS

- Erdem, M., Erguzel, O., Ekmekci, M. K., **Cinkaya**, **H.,** Orucu, H., Mergen, A., G. Eryürek, B. Di Bartolo. 2015: White upconversion emission fromYb^{3+}/Er^{3+}/Tm^{3+}: Y_2SiO_5 nano powders. International Porous and Powder Materials Symposium and Exhibition 2015- PPM2015, 15-18 September 2015 İzmir-Turkey
- Salehli, F., Bilici, C., **Cinkaya**, **H.,** Okay, O. 2012: Uzun Alkil yan zincirli çaprazbağlı polimerlerde (sulu ve kuru durumlar) molekül dinamiği ve faz geçişleri. 16. Ulusal Sıvıhal Fiziği Sempozyumu, December 21-22, 2012 Baltalimanı, İstanbul, Turkey.
- **Cinkaya**, **H.,** Gursel, Y. H., Salehli, F. 2012: Dielectric Spectroscopy of hydrogen bonded Thermotropic Liquid Crystalline polymer with six methylene units in the side chain. BDS 2012- Broadband Dielectric Spectroscopy Congress, September 3-7 2012 Leipzig, Germany.